Non-Markovian Dynamics of Open Bose-Einstein Condensates

Dissertation
zur
Erlangung des Doktorgrades (Dr. rer. nat.)
der
Mathematisch-Naturwissenschaftlichen Fakultät
der
Rheinischen Friedrich-Wilhelms-Universität Bonn

von
Tim Lappe
aus
Düsseldorf

Bonn, 12.10.2020

Dieser Forschungsbericht wurde als Dissertation von der Mathematisch-Naturwissenschaftlichen Fakultät der Universität Bonn angenommen und ist auf dem Publikationsserver der ULB Bonn https://nbn-resolving.org/urn:nbn:de:hbz:5-61354 elektronisch publiziert.

1. Gutachter:	Prof. Dr. Johann Kroha
2. Gutachterin:	Prof. Dr. Corinna Kollath
Tag der Promotion:	22.02.2021
Erscheinungsjahr:	2021

Abstract

Quantum many-body systems coupling photonic and matter degrees of freedom are ideal for the realization of driven open quantum dynamics at the intersection of quantum optics and condensed matter. They offer the possibility to address unresolved issues regarding a variety of non-equilibrium phenomena. In such open systems, the substructure of the reservoir then introduces further timescales that may enter into competition with rapid system processes, raising long-standing questions about the influence of non-Markovian effects on dynamics and equilibration out of equilibrium.

The central result of this thesis is a general pseudo-particle technique that can be applied to a large class of models of interacting light and matter and allows for realistic and efficient simulations of the full non-equilibrium dynamics of these systems. Since organic molecules, as used in experiments with photon condensates, which provide the main area of application for this thesis, possess an electronic transition coupled to vibrational phonon modes, we construct a representation where an auxiliary boson is assigned to each vibrational state of the molecule. An operator constraint then enforces single occupation across all of these states. We emphasize that we implement the operator constraint exactly and that we are the first to apply a faithful auxiliary-boson representation to open quantum systems.

As a contribution to bridging the gap between well-understood equilibrium and less explored non-equilibrium phenomena, we investigate photon condensates as they are driven away from equilibrium. The earliest signs of the non-equilibrium character of the driven-dissipative photon gas do not manifest in the spectrally resolved intensity distribution but in the time dependence of the intensity fluctuations. The energy flow through the system renders it non-Hermitian and induces a novel driven-dissipative transition in the second-order correlations characterized by the appearance of exceptional points. If only the static intensity spectrum is monitored, this transition remains unnoticed, as does the fact that the system is not truly in equilibrium. Non-Markovian effects due to the non-separability of system and reservoir timescales are shown to become important far away from equilibrium. Furthermore, we derive a novel photon-condensate Gross-Pitaevskii equation, which is capable of describing photo-molecular coherence. Such effects cannot be captured by existing theories and hence serve as a validation of our auxiliary-boson method. These results provide a building block to understanding the properties of the photon condensates in stationary operation where they act as fluctuating light sources. In the future, lattice systems of coupled photon condensates may lead to the appearance of novel driven-dissipative phases of light.

Zusammenfassung

Quanten-Vielteilchensysteme, die photonische und Materie-Freiheitsgrade koppeln, sind ideal für die Realisierung einer getriebenen offenen Quantendynamik am Schnittpunkt von Quantenoptik und kondensierter Materie. Sie bieten die Möglichkeit, ungelöste Fragen zu einer Vielzahl von Nichtgleichgewichtsphänomenen anzugehen. In solch offenen Systemen kann die Substruktur des Reservoirs dann weitere Zeitskalen einführen, die in Konkurrenz zu schnellen Systemprozessen treten, was seit langem bestehende Fragen nach dem Einfluss nicht-Markov'scher Effekte auf Dynamik und Equilibration außerhalb des Gleichgewichts aufwirft.

Das zentrale Ergebnis dieser Arbeit ist eine allgemeine Pseudoteilchen-Methode, die auf eine große Klasse von Modellen der Wechselwirkung von Licht und Materie angewendet werden kann und realistische und effiziente Simulationen der vollständigen Nichtgleichgewichtsdynamik dieser Systeme ermöglicht. Da organische Moleküle, wie sie in Experimenten mit Photonenkondensaten verwendet werden, die das Hauptanwendungsgebiet dieser Arbeit darstellen, einen elektronischen Übergang besitzen, der an Vibrationsmoden gekoppelt ist, konstruieren wir eine Darstellung, bei der jedem Vibrationszustand des Moleküls ein Hilfsboson zugeordnet wird. Ein Operator-Zwangsbedingung setzt dann die einfache Besetzung über alle diese Zustände hinweg durch. Wir betonen, dass wir die Operator-Zwangsbedingung exakt implementieren und dass wir die ersten sind, die eine solche getreue Hilfsbosonendarstellung auf offene Quantensysteme anwenden.

Als Beitrag zur Überbrückung der Lücke zwischen gut verstandenen Gleichgewichts- und weniger erforschten Nichtgleichgewichtsphänomenen untersuchen wir Photonenkondensate, die aus dem Gleichgewicht getrieben werden. Die frühesten Anzeichen für Nichtgleichgewicht im getrieben-dissipativen Photonengas zeigen sich dabei nicht in der spektral aufgelösten Intensitätsverteilung, sondern in der Zeitabhängigkeit der Intensitätsfluktuationen. Der Energiefluss durch das System macht es nicht-hermitesch und induziert einen neuartigen getrieben-dissipativen Übergang in den Korrelationen zweiter Ordnung, die durch das Auftreten von sogenannten *exceptional points* gekennzeichnet sind. Wenn nur das statische Intensitätsspektrum betrachtet wird, bleibt dieser Übergang ebenso unbemerkt wie die Tatsache, dass sich das System nicht im Gleichgewicht befindet. Es zeigt sich, dass nicht-Markov'sche Effekte aufgrund der Nicht-Separierbarkeit von System- und Reservoirzeitskalen weit entfernt vom Gleichgewicht wichtig werden. Darüber hinaus leiten wir eine neuartige Gross-Pitaevskii-Gleichung ab, die in der Lage ist, die photo-molekulare Kohärenz zu beschreiben. Solche Effekte können durch bestehende Theorien nicht erfasst werden und dienen daher als Validierung unserer Hilfsbosonenmethode. Diese Ergebnisse liefern einen Baustein zum Verständnis der Eigenschaften der Photonenkondensate im stationären Zustand, wo sie als fluktuierende Lichtquellen wirken. In der Zukunft könnten Gittersysteme aus gekoppelten Photonenkondensaten zur Erscheinung neuartiger getrieben-dissipativer Lichtphasen führen.

Preface

Experimental platforms coupling a set of cavity modes to a collection of two-level systems with local vibrational degrees of freedom, such as a wide variety of organic molecules [1], are relevant for applications ranging from Bose-Einstein condensation of photons [2–6], exciton-polaritons [7, 8] and plasmonic lattices [9] to single-photon sources for quantum information [10]. These platforms are ideal for the realization of driven open quantum systems at the intersection of quantum optics and condensed matter that pose a variety of intriguing questions regarding non-equilibrium stationary states and dynamics [11]. For example, what are the effects of drive and dissipation on Bose-Einstein condensation?

In open systems, the substructure of the reservoir introduces further timescales that may compete with both incoherent and coherent system processes such as cavity loss and quantum tunneling, respectively. Driving the system strongly out of equilibrium, one enters a regime where the full dynamical description of the reservoir becomes necessary and established approximate models based on the separation of system and reservoir timescales begin to break down. As experiments with photon Bose-Einstein condensates, for instance, move in a direction where fast Josephson oscillations become relevant that can approach the timescale of reservoir relaxation processes [12], the influence of non-Markovian memory effects [10, 13] on the dynamics and equilibration of the system moves into focus.

The theoretical treatment of the systems in question is complicated by several technical difficulties. For one thing, the large number of matter constituents precludes employing numerically exact methods, where even advanced techniques cannot go beyond rather small systems [14]. In the quantum-optical framework of the master equation, the usual Born-Markov approximation does allow for a description of large systems in terms of rate equations [15–19] that even feature a frequency dependence of the incoherent light-matter coupling. However, these equations are invariably semi-classical since they are based on assuming a classical distribution for photon and matter excitations. Thus, coherence effects are neglected. The non-Markovian case is also difficult to treat in a quantum Langevin approach because of the non-linearity inherent to the non-canonical spin operators, which for this reason were approximated as bosons in Ref. [20].

In this thesis, our central result is a general pseudo-particle technique that can be applied to a large class of models where light and matter are coherently coupled, such as the Holstein-Tavis-Cummings Hamiltonian or indeed arbitrary spins or multi-level atoms inside a cavity, as long as the correlations between individual matter constituents can be neglected. This is equivalent to working with an effective single-impurity problem.

The technique of using canonical operators to represent (impurity) spins goes back to Abrikosov [21]. The basic idea is to express operators that do not have canonical commutation relations

in terms of operators that do and are thus amenable to standard field-theory techniques. In a two-level system, for example, either the ground or excited state must always be occupied. If each state is represented by a fermionic operator, the trouble arises that unphysical degrees of freedom are introduced by the doubly occupied and unoccupied states. This must be counteracted by an operator constraint that excludes these unphysical states. In the context of the infinite-U Anderson model [22], a combination of fermions and auxiliary bosons has been introduced [23–27] which project out the unphysical states by satisfying one holonomic operator constraint. These techniques are valid in equilibrium field theory. The extension to non-equilibrium has been given in [28–31]. A more recent exposition in non-equilibrium may also be found in [32]. One has to distinguish this approach from others where the operator constraint is satisfied on average [33, 34].

The microscopic model of organic molecules comprises an electronic transition coupled to vibrational phonon modes and hence invites a representation in terms of auxiliary bosons only: each vibrational state of the molecule will be described by a pair of bosonic creation and destruction operators. The operator constraint then enforces single occupation across all of these states. We emphasize that we implement the operator constraint exactly and that approximations enter only via the diagrammatic expansion, which can be adjusted depending on the problem at hand. Furthermore, quantum coherence between light and matter can be preserved, which is also true of the full memory of the system. The method is presented to make it easily accessible for use in novel applications to this field. To our knowledge, we are also the first to apply a faithful representation of the operator constraint to open quantum systems.

This thesis is organized as follows. In **Chp. 1** we set out with a brief historical introduction to Bose-Einstein condensation, complemented by a theoretical discussion of the ideal Bose gas in two and three dimensions. Subsequently, we recapitulate the fact that for black-body radiation, Bose-Einstein condensation does not occur, before giving a first presentation of the main topic of this thesis: photon Bose-Einstein condensates. Because the latter are driven-dissipative systems, we conclude this Chp. by introducing a number of theoretical tools that can be applied to model both classical and quantum systems coupled to external reservoirs: stochastic differential equations, path integrals, the Fokker-Planck and finally the quantum master equation.

While the quantum master equation is the most frequently employed tool in *quantum optics*, the photon condensate is perhaps the best example of a system situated right at the intersection of quantum optics and *condensed matter*. The method of choice for describing open condensed-matter systems, however, is non-equilibrium quantum field theory, which we introduce in **Chp. 2** by first discussing the Schwinger-Keldysh formalism as it applies to open systems. A comparison with the Martin-Siggia-Rose path integral and the Wigner representation will then help us to form a proper understanding of the formalism. Diagrammatic expansions are the bread and butter of field theory, for which reason we introduce the two-particle-irreducible effective action as a useful tool to construct self-consistent perturbation theory. Since the ensuing equations of Kadanoff-Baym type need to be solved at the end of the day, this Chp. is concluded by a presentation of Adams-Bashforth-Moulton predictor-corrector methods. To demonstrate the accuracy of our implementation of these methods, we provide benchmark results from an application to the analytically solvable problem of Brownian motion.

Chp. 3 discusses atomic Bose-Einstein condensates and is hence slightly out of the main line of this thesis. It may be skipped by readers who are only interested in photon condensates. Consisting

of two parts, this Chp. first gives a detailed account of how to use non-equilibrium quantum field theory in Keldysh representation in the presence of a symmetry-broken order parameter. The physics we can understand in this way concerns the growth and depletion of macroscopic matter waves. In the second part, we present our quantitative results on the influence of the trap geometries employed in cold-atom experiments on the dynamical stability of the condensates. Note that this part is based on our publication [35]. Closely related to this is the detailed review of the frequently used two-mode approximation in App. C.

With **Chp. 4** we begin our investigation of photon Bose-Einstein condensates by analyzing its established microscopic model. We then pursue the derivation of the quantum master equation which follows when the molecular vibrational degrees of freedom are integrated out via the Born-Markov approximation. From the master equation, we obtain the rate equations for the photon occupation and molecular excitation numbers which describe the system well as long as there is the above-mentioned separation of timescales. The rate equations provide the foundation for our study of second-order correlations functions in the system. They can be rederived by making an incoherent ansatz for the density matrix that reduces the problem to the dynamics of a classical probability distribution, which in turn enables a well-defined truncation scheme for the expectation-value hierarchy. The latter is needed to calculate the initial values of the second-order correlation dynamics, which we prove via quantum regression to obey the same dynamics as small fluctuations around the steady state. We find that the second-order coherence of the photon condensate can exist in two distinct regimes: whereas very close to equilibrium, the intensity-intensity correlations decay *bi-exponentially*, as described by two different relaxation rates, they follow a *damped-oscillating* relaxation when the system is driven more strongly. The transition between these two dynamical regimes is marked by an exceptional point in the spectrum of the second-order coherence. As a function of the cavity dissipation and the external driving, this results in a phase diagram in which the two regimes are separated by a continuous boundary. The question of the global shape of the boundary delimiting the damped-oscillating regime remains open at this point. Finally, we show that these theoretical findings are confirmed by experiment. The Chp. is based on publication [36]. The experimental verification of the theoretically found exceptional point is presented in Ref. [37].

The rate equations employed up to this point suffer from two drawbacks: neither can they treat coherence between photons and molecules nor is it possible to have system timescales such as the inverse cavity loss grow independently of the reservoir relaxation. To address both of these difficulties, in **Chp. 5** we extend the microscopic model of the photon condensate by explicitly including the relaxation processes of the molecular vibrations and introduce a pseudo-particle representation that allows us to apply a well-defined perturbative expansion in the photo-molecular coupling. We then derive the modified diagrammatic rules that enable one to enforce the pseudo-particle operator constraint in the non-equilibrium case. A resummation technique of the photon T-matrix is introduced to map the many-molecule system to an effective single-impurity problem. A novel result of this thesis is the application of the pseudo-particle technique to the open-system dynamics induced by the Lindblad operators describing the vibrational relaxation. Having established the method in this way, we proceed to present a variety of benchmark dynamics with an eye to both verification and illustration. The step toward realistic systems then necessitates the introduction of a memory-truncation scheme to keep the numerics feasible. Before harness-

ing this to obtain physical results, we take a step back to prove that our method reproduces the preceding rate equations in the appropriate limit. An interlude is dedicated to another novel result, the photon-condensate Gross-Pitaevskii equation, which follows from our theory naturally because of its ability to handle the photo-molecular coherence. Instead of pursuing this route to its conclusion, however, we return to our previous topic regarding the dynamical regimes of the photonic second-order coherence. First, we highlight that our theory is capable of producing realistic molecular spectra which, in particular, satisfy the Kennard-Stepanov relation around the so-called zero-phonon line. Second, we demonstrate that the damped-oscillating regime is indeed bounded and acquires quantitative corrections for large cavity loss which are not captured by the rate equations. The results of this Chp. form the basis for Ref. [38].

This is the place to thank my supervisor Hans Kroha for his support and advice, for giving me the opportunity to grow, and for being patient when things got stuck. Special thanks are also due to: Michael Kajan, who worked out the auxiliary-boson field theory in equilibrium and always understood what I was grasping to say about field theory; Francisco Meirinhos for sharp comments on numerical methods and for good times in Cologne; Christopher Lietmeyer, who has taken up the development of the Gross-Pitaevskii equation derived in Chp. 5; and Fahri Öztürk, who performed the experiments with the photon condensates that grew into an important stimulus to this thesis. I would also like to thank Ammar Nejati, Bastian Havers, Zhong Yuan Lai, Marvin Lenk, my office mate Qiu Haixin, my collaborator Anna Posazhennikova, and Corinna Kollath for being on my thesis committee.

Further thanks go to Martin Weitz and all of my collaborators in his group. I am especially grateful to Frank Vewinger for arranging my stay in London, where I had a good and productive time for which I would also like to thank Florian Mintert, Rob Nyman and Himadri Dhar.

Many thanks are due to everyone who enabled and kept going the SFB/TR 185 “OSCAR”, in particular Dieter Meschede and Michael Fleischhauer, Ruth Bischoff, Petra Weiß and Patricia Zündorf. The SFB has supported me from the very beginning in more ways than I can say. In this spirit, I would also like to thank my friends and colleagues from Kaiserslautern, notably Lukas Wawer, Maximilian Kiefer-Emmanouilidis, Enrico Stein and Milan Radonjić. For many stimulating discussions, I also thank James Anglin and Axel Pelster.

This thesis would not exist but for the love of my family, who set the foundation for everything, and the support of my old friends from Zürich: Marcel Bräutigam, Michael Pircher, Cedric Klinkert, Richard Senner and Maximilian Seyrich. You are the best.

Finally, I would like to dedicate this work to my fiancée Svenja: there is as much of your energy in it as there is of mine. I could not have done it without you.

Contents

CHAPTER 1

Introduction

Bosons occur everywhere in natural systems. All of the known force-carrying particles are bosons, most notably the photon. Protons, neutrons and electrons, however, are fermions of spin $1/2$. Yet any composite, integer-spin particle consisting of an even number of fermions is in turn a boson. This is the reason why in atoms that are not ionized, i.e. where for every proton in the nucleus there is an electron in one of the atom's shells, the number of neutrons determines the total spin. A good example to illustrate this fact are the isotopes of helium: while helium-3 possesses a single neutron and hence is a fermion, helium-4 contains two neutrons and is accordingly a boson. This constitutes a fundamental difference between the two isotopes. While the exclusion principle states that no two fermions may possess the exactly same quantum numbers, such a restriction does not exist for bosons: in sharp contrast to fermions, any quantum state can be occupied by arbitrarily many of them.

The simplest collection of bosons is the so-called *ideal Bose gas*, which we discuss in Sec. 1.1. At low temperatures (or high densities), it gives rise to the famous *Bose-Einstein condensate* (BEC), where the difference to fermions is most pronounced as a macroscopic fraction of the gas particles aggregates in the ground state. The first experimental verification of this phenomenon was achieved with rubidium-87 [39], which contains 50 neutrons and hence is indeed a boson. To properly understand the physical background for the greater part of this thesis, which is a BEC of *photons* as opposed to cold atoms, it is necessary to first discuss the problem of black-body radiation, for which a BEC notably does not occur. This is the subject of Sec. 1.2. With the photon BEC entering the stage in Sec. 1.3, our focus gradually moves from equilibrium phenomena such as the ideal Bose gas and black-body radiation to the wide field of non-equilibrium physics. The photon BEC is still close to equilibrium, for which reason it can attain a Bose-Einstein spectrum for a finite time, yet ultimately it is an *open system* that must be driven externally to compensate for the unavoidable effects of dissipation (cf. Chp. 4). For Bose gases coupled to environments, technically the description is similar to that of classical stochastic systems. It is worthwhile to review these techniques in Sec. 1.4 because it helps to build a deeper conceptual understanding of all of the methods involved in describing both quantum optical and bosonic condensed-matter systems. This topic is finally taken up in Sec. 1.5, where we introduce open quantum systems.

1.1 Ideal Bose Gas

The main idea behind the central physical theme of this thesis, *Bose-Einstein condensation*, follows most naturally from the historical context of its conception in 1924. As discussed at length by Bach [40], the accurate history of what we now call Bose-Einstein *statistics* is long and slightly involved. Bach makes the argument that it was first mentioned by Boltzmann as early as 1868, and again in 1877. Its first *consequential* appearance for physics was certainly in 1900, when Planck tried to find a derivation for his formula interpolating between the Wien and Rayleigh-Jeans limits in the problem of black-body radiation, and ended up introducing light quanta. Incidentally, this was also the inception of quantum theory. Why then are the names of Bose and Einstein, instead of Boltzmann and Planck, attached to our topic? While Planck was concerned with the statistics of *radiation*, in 1924 Einstein applied the new statistics to an ideal gas of *atoms*. This step, inspired by the analogy with radiation which, under certain circumstances, can itself be described as a gas of particles, went beyond what was known at the time. Bose, in turn, was a yet unknown physicist from India who sent his derivation of the statistics to Einstein after it had been rejected by the *Philosophical Magazine*.[1] Einstein translated Bose's work and arranged for its publication. Subsequently, Einstein developed the idea into the quantum theory of the ideal (Bose) gas in several articles of his own [42, 43].

In the 19th century, Boltzmann had given a statistical foundation to thermodynamics, aptly summarized in Einstein's formula [44] relating the entropy S to the number of configurations W of a gas,

$$W = \mathrm{e}^{S/k_B} \,. \tag{1.1}$$

In a certain sense, much of the technical work in this thesis will be about more sophisticated ways of using variants of this formula, which via the *large-deviation principle* [45] is intimately related to the effective-action techniques that are going to be of great relevance in later parts. Boltzmann's ideas relate the macroscopic equilibrium state, i.e. the state of maximum entropy, to that state of the system which has the most microscopic realizations. In this picture, a gas is in its most probable state most of the time. Since for systems with a large number of constituents,[2] one macrostate is overwhelmingly more probable than all others, we rarely observe deviations from equilibrium. Seen through Boltzmann's lense, however, such fluctuations constantly occur.

Both Planck, in his derivation of the black-body spectrum [40], and Einstein followed the intellectual tradition founded by Boltzmann around the idea of atomicity. Einstein's work on Brownian motion was indeed decisive in bringing the molecular concept into the mainstream of science. This happened not least because Brownian motion, the perpetual random jiggling of, for instance, pollen suspended in water, is the best example where the above-mentioned fluctuations around the most probable macrostate, usually imperceptible, become visible to the bare eye.[3]

Thus in 1924, the accepted description of the ideal gas was *Maxwell-Boltzmann* statistics.

[1] Cf. Chp. 23 of Ref. [41].

[2] A gas indeed has a very great number of particles, as exemplified by the Avogadro number $6 \cdot 10^{23}$.

[3] The mathematical description of Brownian motion will be of importance below. It provides helpful insights for the stochastic description of physical systems (cf. Sec. 1.4).

The key assumption behind this form of statistics is the uniform distribution of microstates (or *configurations* in Bach's terminology [40]). Combined with an energy and particle-number constraint, and the principle of maximum entropy, this leads directly to the well-known *Boltzmann factor* $\exp\left\{\left(E_i - E_j\right)/k_B T\right\}$ expressing the ratio of the probabilistic frequencies with which two states of energies E_i and E_j will be occupied. For Bose-Einstein statistics, on the contrary, the uniform distribution of microstates is replaced by the uniform distribution of occupation numbers [40].

The significance of this break with the assumptions of classical Maxwell-Boltzmann statistics is illustrated vividly by a short episode from the Schrödinger-Einstein correspondence of 1925 [46]. Although like Boltzmann from the Vienna school, Schrödinger had difficulties in grasping the new way of distributing the particles over the microstates which distinguished the novel Bose-Einstein from the established classical statistics. Schrödinger even thought that Einstein might have made a mistake.[4] In his reply, Einstein explains the matter clearly with the help of Tab. 1.1, which shows an illustration of the two kinds of statistics for the exemplary case of two particles distributed over two states or cells. The left part corresponds to Bose-Einstein statistics: three different cases are possible. On the right, we see the Maxwell-Boltzmann way of counting: this results in four different cases. For the thermodynamics, however, not the absolute but only the relative frequencies of the different cases are important. By treating the second and third of Boltzmann's cases as a single one (2. case on the left), the relative importance of the two cases where both particles occupy the same state is increased. This is sometimes referred to as "statistical attraction". In Einstein's words: "Nach Bose hocken die Moleküle relativ häufiger zusammen als nach der Hypothese der statistischen Unabhängigkeit der Moleküle."[5] Schrödinger's difficulties with the subject[6] are echoed even today, as the precise interpretation of the two types of statistics is still a matter of debate [47–49]. Their difference is usually summarized by saying that classical particles are "distinguishable", while quantum particles are "indistinguishable". Ref. [48] argues that either both types of particle are distinguishable, or both are indistinguishable. Ref. [49] summarizes the different definitions of these notions to be found in the literature. A thorough discussion of these subtleties is, however, besides the point of this thesis.

In present-day thermodynamics, the partition function of the grand canonical ensemble is given by the sum over all possible total particle numbers N. The relative weights of the different momentum states $\mathbf{k}_i$ are given by the Boltzmann factors $\exp\left\{-\beta\left(\varepsilon_{\mathbf{k}_i} - \mu\right)\right\}$, where $\beta = 1/k_B T$

[4] Letter 011†, p. 101 of Ref. [46].

[5] Translation by the author: "According to Bose, the molecules relatively huddle together more often than under the hypothesis of statistical independence of the molecules."

[6] Schrödinger's reply to Einstein's clarification: "Sie hatten schon vor längerer Zeit... die Güte, mir einen recht dummen Einwand gegen Ihre erste Entartungsarbeit in liebenswürdigster Weise und so zu beantworten, daß mir die Sache sofort klar war. Erst durch Ihren Brief ging mir das Eigenartige und Neue Ihrer statistischen Behandlungsweise auf, die ich vorher gar nicht verstanden hatte..."

Translation by the author: "A while ago you had the kindness to answer a rather stupid objection of mine to your first degeneracy work most amiably and in such a way that the matter was immediately clear to me. It was only through your letter that I realized the peculiarity and novelty of your statistical treatment, which I had not at all understood before."

	Bose statistics			Independent molecules	
	1. cell	2. cell		1. cell	2. cell
1. case	••	-	1. case	I II	-
2. case	•	•	2. case	I	II
3. case	-	••	3. case	II	I
			4. case	-	I II

Table 1.1: Reproduction of the table from the Schrödinger-Einstein correspondence [46].

and μ is the chemical potential. Then the classical grand partition function reads [50]

$$\begin{aligned}\mathcal{Z} &= \sum_{n_{\mathbf{k}_1}, n_{\mathbf{k}_2}, \dots} \left[\frac{1}{n_{\mathbf{k}_1}!} \left(\mathrm{e}^{-\beta\left(\varepsilon_{\mathbf{k}_1} - \mu\right)} \right)^{n_{\mathbf{k}_1}} \frac{1}{n_{\mathbf{k}_2}!} \left(\mathrm{e}^{-\beta\left(\varepsilon_{\mathbf{k}_2} - \mu\right)} \right)^{n_{\mathbf{k}_2}} \dots \right] \\ &= \sum_{N=0}^{\infty} \frac{1}{N!} \left\{ \sum_{\mathbf{k}} \mathrm{e}^{-\beta(\varepsilon_{\mathbf{k}} - \mu)} \right\}^N = \exp\left\{ \sum_{\mathbf{k}} \mathrm{e}^{-\beta(\varepsilon_{\mathbf{k}} - \mu)} \right\}\end{aligned} \tag{1.2}$$

where $n_{\mathbf{k}_i} \in \mathbb{N}_0$ and the momentum sums run over all allowed $\mathbf{k}$. For the example from Tab. 1.1, we have $N = 2$ and only two different $\mathbf{k}$ vectors. The corresponding summand in Eq. (1.2) is hence

$$\frac{1}{2} \left\{ \mathrm{e}^{-\beta\left(\varepsilon_{\mathbf{k}_1} - \mu\right)} + \mathrm{e}^{-\beta\left(\varepsilon_{\mathbf{k}_2} - \mu\right)} \right\}^2 = \frac{\mathrm{e}^{2\beta\mu}}{2} \left\{ \mathrm{e}^{-2\beta\varepsilon_{\mathbf{k}_1}} + 2\,\mathrm{e}^{-\beta\left(\varepsilon_{\mathbf{k}_1} + \varepsilon_{\mathbf{k}_2}\right)} + \mathrm{e}^{-2\beta\varepsilon_{\mathbf{k}_2}} \right\}. \tag{1.3}$$

The factor of 2 in front of the second term on the right-hand side shows that the second and third case from the right half of Tab. 1.1 are indeed counted separately. According to Einstein, this stems from the *statistical independence* of the classical particles: after the first particle is placed, the second particle has two states it can go to; whither it goes is not influenced by the already determined state of the first particle.

As indicated above, for the quantum case, the situation is different [47]. In his letter to Schrödinger, Einstein also emphasizes that as the density of the particles is increased, statistical independence breaks down. The location of the second particle is now influenced by that of the first: they tend to cluster together. In seemingly innocent distinction to Eq. (1.2), the *quantum* grand partition function reads [50]

$$\begin{aligned}\mathcal{Z} &= \sum_{n_{\mathbf{k}_1}, n_{\mathbf{k}_2}, \dots} \left[\left(\mathrm{e}^{-\beta\left(\varepsilon_{\mathbf{k}_1} - \mu\right)} \right)^{n_{\mathbf{k}_1}} \left(\mathrm{e}^{-\beta\left(\varepsilon_{\mathbf{k}_2} - \mu\right)} \right)^{n_{\mathbf{k}_2}} \dots \right] \\ &= \prod_{\mathbf{k}} \sum_{n_{\mathbf{k}}=0}^{\infty} \left\{ \mathrm{e}^{-\beta(\varepsilon_{\mathbf{k}} - \mu)} \right\}^{n_{\mathbf{k}}} = \prod_{\mathbf{k}} \frac{1}{1 - \mathrm{e}^{-\beta(\varepsilon_{\mathbf{k}} - \mu)}}.\end{aligned} \tag{1.4}$$

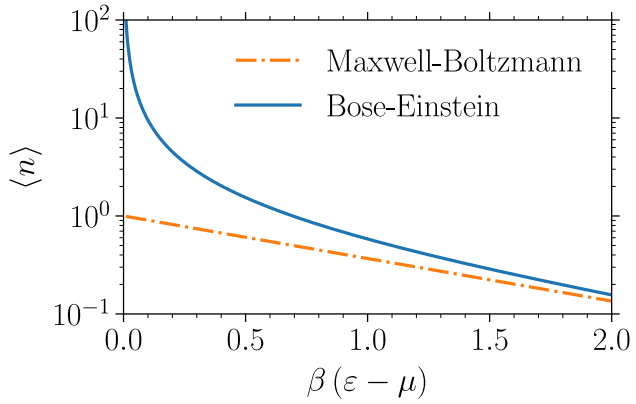

Figure 1.1: Comparison of Maxwell-Boltzmann and Bose-Einstein statistics. The average occupation number $\langle n \rangle$ diverges as $\varepsilon - \mu \to 0$. In the classical limit $\beta(\varepsilon - \mu) \to \infty$, Bose-Einstein approaches Maxwell-Boltzmann statistics.

Once more, for the example from Tab. 1.1 we find as contributions to $\mathcal{Z}$ the terms

$$\mathrm{e}^{2\beta\mu}\left\{\mathrm{e}^{-2\beta\varepsilon_{\mathbf{k}_1}} + \mathrm{e}^{-\beta\left(\varepsilon_{\mathbf{k}_1}+\varepsilon_{\mathbf{k}_2}\right)} + \mathrm{e}^{-2\beta\varepsilon_{\mathbf{k}_2}}\right\}, \tag{1.5}$$

where now the cases where both cells are occupied once is no longer counted twice. As one can see comparing Eqs. (1.2) and (1.4), mathematically the difference between classical and Bose statistics amounts to the difference between summing an exponential and a geometric series.

1.1.1 Average Occupation

The grand partition function $\mathcal{Z}$ allows the calculation of statistical average quantities by taking derivatives. The occupation of mode $\mathbf{k}$ is found to be

$$\langle n_{\mathbf{k}} \rangle = -\frac{1}{\beta}\frac{\partial}{\partial \varepsilon_{\mathbf{k}}} \ln \mathcal{Z} = \frac{1}{\mathrm{e}^{\beta(\varepsilon_{\mathbf{k}}-\mu)} - 1} = \frac{\mathrm{e}^{-\beta(\varepsilon_{\mathbf{k}}-\mu)}}{1 - \mathrm{e}^{-\beta(\varepsilon_{\mathbf{k}}-\mu)}}. \tag{1.6}$$

The average occupation serves well to illustrate the connection between classical and quantum statistics. In the limit where $(\varepsilon_{\mathbf{k}} - \mu) \gg k_B T$, one has

$$\frac{1}{\mathrm{e}^{\beta(\varepsilon_{\mathbf{k}}-\mu)} - 1} \approx \mathrm{e}^{-\beta(\varepsilon_{\mathbf{k}}-\mu)}, \tag{1.7}$$

which is again the classical Boltzmann factor. Thus we understand that quantum effects become important when the system energy is on the order of $k_B T$. Deep in the quantum regime, that is, usually for very low temperatures, the different way of counting states that led to a geometric series instead of an exponential one has rather dramatic consequences: when $\varepsilon_{\mathbf{k}} \approx \mu$, we have $\langle n_{\mathbf{k}} \rangle \to \infty$ and the particle number diverges, which is illustrated in Fig. 1.1.

Since, in reality, the particle number cannot diverge, we impose the total particle number N as a

boundary condition to fix the chemical potential:

$$N = \sum_{\mathbf{k}} \frac{1}{\mathrm{e}^{\beta(\varepsilon_{\mathbf{k}}-\mu)}-1} \approx \left(\frac{L}{2\pi}\right)^D \int \mathrm{d}\Omega \int_0^\infty \mathrm{d}k\, k^{D-1} \frac{1}{\mathrm{e}^{\beta(\varepsilon_k-\mu)}-1}, \tag{1.8}$$

where the approximation of the sum as an integral does not take into account the contribution from the ground state $\mathbf{k} = 0$.

1.1.2 Densities of States

In the following, we will only consider the ideal Bose gas in dimensions $D = 3$ and $D = 2$, as these are the relevant cases for this thesis. The densities of states in these cases may be written as

$$\begin{aligned} g(\varepsilon) &= \sum_{\mathbf{k}} \delta(\varepsilon - \varepsilon_{\mathbf{k}}) \approx \left(\frac{L}{2\pi}\right)^D \int \mathrm{d}\Omega \int_0^\infty \mathrm{d}k\, k^{D-1} \delta(\varepsilon - \varepsilon_k) \\ &= \left(\frac{L}{2\pi}\right)^D \int \mathrm{d}\Omega\, \frac{1}{2} \left(\frac{2m}{\hbar^2}\right)^{D/2} \int_0^\infty \mathrm{d}\varepsilon_k\, \varepsilon_k^{(D-2)/2} \delta(\varepsilon - \varepsilon_k) \\ &= \begin{cases} \varepsilon^{1/2}(L^3/4\pi^2)(2m/\hbar^2)^{3/2}, & D = 3, \\ (L^2/2\pi)m/\hbar^2, & D = 2, \end{cases} \end{aligned} \tag{1.9}$$

where we have substituted $k = \pm\sqrt{2m\varepsilon_k/\hbar^2}$. We have found the typical square-root behavior of the density of states in three dimensions, as well as the well-known energy-independent result in $D = 2$. This difference in the exponents with which the energy appears in the density of states results in the distinct physical behavior of the respective Bose gases.

1.1.3 Three-Dimensional Bose Gas

For the ideal Bose gas in $D = 3$, our previous calculation leading to $g(\varepsilon) \sim \varepsilon^{1/2}$ has profound consequences. From Eq. (1.8), the total particle number involves the integral

$$\int_0^\infty \mathrm{d}\varepsilon_k \frac{\varepsilon_k^{1/2}}{\mathrm{e}^{\beta(\varepsilon_k-\mu)}-1} = \beta^{-3/2} \int_0^\infty \mathrm{d}x \frac{x^{1/2}}{\mathrm{e}^{-\beta\mu}\,\mathrm{e}^x - 1} = \beta^{-3/2}\Gamma(3/2)\mathrm{Li}_{3/2}(\mathrm{e}^{\beta\mu}), \tag{1.10}$$

where we have introduced the Gamma function and the polylogarithm

$$\mathrm{Li}_s(z) = \frac{1}{\Gamma(s)} \int_0^\infty \mathrm{d}x \frac{x^{s-1}}{z^{-1}\,\mathrm{e}^x - 1}, \tag{1.11}$$

which converges only for $\mathrm{Re}\, s > 0$ and $|z| < 1$, $z \in \mathbb{C}$. When z approaches unity from below on the real axis, it becomes the Riemann zeta function, $\mathrm{Li}_s(z) \xrightarrow{z\nearrow 1} \zeta(s)$. Thus we find

$$\mu \leq \varepsilon_0 = 0 \tag{1.12}$$

for the chemical potential of the ideal Bose gas in three dimensions. For a given temperature T, the critical density of particles in the states with $k > 0$ is then[7]

$$\rho_c(T) = \frac{N_c}{V} = \frac{1}{4\pi^2}\left(\frac{2mk_BT}{\hbar^2}\right)^{3/2}\Gamma(3/2)\zeta(3/2) = \lambda_T^{-3}\zeta(3/2) \approx 2.6 \cdot \lambda_T^{-3}. \tag{1.13}$$

Conversely, for a given density ρ, the critical temperature is

$$T_c(\rho) = \frac{2\pi\hbar^2}{mk_B}\left(\frac{\rho}{\zeta(3/2)}\right)^{2/3}. \tag{1.14}$$

The obvious question to ask now is: For a given T and a particle density $\rho < \rho_c$, what happens when further particles are added to the system by slowly increasing the chemical potential μ until $\rho > \rho_c$? As long as the density is not saturated, the system still lowers its free energy ($\mu < 0$) by accepting more particles into the states $k > 0$. But as the saturation threshold is approached and $\mu \nearrow 0$, this is less and less advantageous. At some point, it becomes energetically more favorable to accept additional particles into the ground state $k = 0$. In thermodynamic language, one says that they "condense" into the ground state. This means that the true particle density must be written

$$\rho = \frac{N}{V} = \rho_0(T) + \rho_c(T), \tag{1.15}$$

where $\rho_0(T)$ is the condensate density. Evidently, for a fixed density ρ, one may just as well lower the temperature below T_c to achieve the same effect. While this is employed in condensating ultracold gases where the number of atoms cannot be increased but the temperature can be lowered by techniques such as evaporative cooling [39], in the case of the photon BEC condensation is indeed achieved by adding more photons to a system at constant temperature.[8]

1.1.4 (Trapped) Two-Dimensional Bose Gas

In two dimensions at $T > 0$, condensation has been proven to be impossible for homogeneous systems [51]. The integral analogous to Eq. (1.10),

$$\int_0^\infty \mathrm{d}\varepsilon_k \, \frac{1}{\mathrm{e}^{\beta(\varepsilon_k-\mu)}-1} = -k_BT\ln\left(1-\mathrm{e}^{\beta\mu}\right), \tag{1.16}$$

[7] The thermal de Broglie wavelength is defined as $\lambda_T = \sqrt{2\pi\hbar^2/mk_BT}$ and $\Gamma(3/2) = \sqrt{\pi}/2$.

[8] The photon BEC is not, however, a three-dimensional condensate (s. discussion below).

is evidently infrared divergent when $\mu \nearrow 0$. There is no upper bound to the number of particles that may be absorbed into the states with $k > 0$. Therefore, Bose-Einstein condensation *cannot* occur for homogeneous systems in two dimensions.

On the contrary, for a two-dimensional Bose gas in a power-law potential

$$U(r) = U_0 \left(\frac{r}{a}\right)^{\eta}, \tag{1.17}$$

where $\eta > 0$, condensation is possible [52, 53]. This point will be of great importance for the photon Bose-Einstein condensate to be discussed in Sec. 1.3. Before doing so, however, we turn to the classic problem of black-body radiation, which will help us to appreciate the intricate combination of conditions that enables the photon BEC.

1.2 Black-Body Radiation

As mentioned above, the problem of black-body radiation was the first where the idea of Bose statistics achieved recognition. Both black-body radiation and ideal Bose gases are large assemblies of bosonic particles. What then differentiates photonic radiation from a dilute gas of atoms with integer spin?

In the present context, the first important difference is the *chemical potential*: for the latter, it is fixed to some finite value by the total number of atoms in the gas, while for the former, the particle number is not conserved and the chemical potential is zero. Through absorption by and emission from the walls of the cavity with which the radiation is in equilibrium, the photon number is constantly adjusted to the value prescribed by the temperature of the black body. The second difference is the *dispersion relation*: instead of $\varepsilon_{\mathbf{k}} = \hbar^2 k^2/2m$ as for massive bosons, *in vacuo* photons have a *linear* dispersion $\omega_{\mathbf{k}} = c\,|\mathbf{k}|$, where c is the speed of light.

The first model that comes to mind here is the one-dimensional quantum harmonic oscillator [50]. The eigenenergies are $E_n = \hbar\Omega(n + 1/2)$, $n \in \mathbb{N}_0$, and the grand canonical partition function becomes

$$\mathcal{Z} = \mathrm{e}^{-\beta\hbar\Omega/2} \sum_{n=0}^{\infty} \mathrm{e}^{-\beta\hbar\Omega n} = \frac{\mathrm{e}^{-\beta\hbar\Omega/2}}{1 - \mathrm{e}^{-\beta\hbar\Omega}} = \frac{1}{2\sinh\left(\beta\hbar\Omega/2\right)}. \tag{1.18}$$

For the average occupation number, one finds

$$2\langle n\rangle + 1 = -\frac{1}{\hbar\Omega}\frac{\partial}{\partial\beta} \ln \mathcal{Z} = \coth\left(\beta\hbar\Omega/2\right). \tag{1.19}$$

This is our first encounter with an instance of the *fluctuation-dissipation* theorem connecting correlation and response functions [11].

Going over to a more realistic description in terms of a collection of electromagnetic modes

confined to a box in three dimensions, we obtain for the partition function

$$\mathcal{Z} = \prod_{\mathbf{k}} \left(\frac{\mathrm{e}^{-\beta\hbar\omega_{\mathbf{k}}/2}}{1-\mathrm{e}^{-\beta\hbar\omega_{\mathbf{k}}}} \right)^2, \tag{1.20}$$

where the square comes from taking into account the polarization. Analogous to before, the total photon number is

$$n(\beta) = 2\sum_{\mathbf{k}} \frac{1}{\mathrm{e}^{\beta\hbar\omega_{\mathbf{k}}}-1}, \tag{1.21}$$

and the density of states now reads

$$D(\omega) = 2\sum_{\mathbf{k}} \delta(\omega-\omega_{\mathbf{k}}) \approx 2\frac{V}{(2\pi)^3} 4\pi \int_0^\infty \mathrm{d}k\; k^2 \delta(\omega-\omega_k) = \frac{V}{\pi^2}\frac{\omega^2}{c^3}. \tag{1.22}$$

which results in

$$\frac{n(T)}{V} = \frac{1}{\pi^2 c^3}\int_0^\infty \mathrm{d}\omega\; \frac{\omega^2}{\mathrm{e}^{\beta\hbar\omega}-1} = \frac{T^3}{\pi^2}\left(\frac{k_B}{\hbar c}\right)^3 \Gamma(3)\zeta(3). \tag{1.23}$$

This is finite, yet without a chemical potential, the photon density of black-body radiation vanishes like T^3 as the temperature goes to zero: no Bose-Einstein condensation takes place.

1.3 Photon Bose-Einstein Condensate

Can Bose-Einstein condensation still be achieved for photons? From what we have explored so far, three things are clear: there needs to be a mechanism to thermalize the photons, that is, a heat bath absorbing and emitting photons at frequencies such that a Bose-Einstein distribution results; a chemical potential must be introduced to fix the photon number independently of the temperature; and the dispersion relation has to be such that condensation can occur (unlike for the free two-dimensional Bose gas). It turns out that all of these requirements can be met by trapping the photons in an optical microcavity filled with a fluorescent medium [2, 53].

1.3.1 Thermalization Mechanism

The thermalization mechanism for the photons can be obtained by filling a cavity with a solution of fluorescent dye molecules at room temperature ($T \approx 300$ K). A sketch of this set-up is given in Fig. 1.2. The physics of such vibrating molecules is governed by the Franck-Condon principle [1]. In a simplified picture, a dye molecule may change both its electronic and its vibrational state upon absorption of a photon. The reason is that for a many-atom molecule, the equilibrium bond length between the atoms depends on the electronic state. Imagine a molecule is both in its electronic and

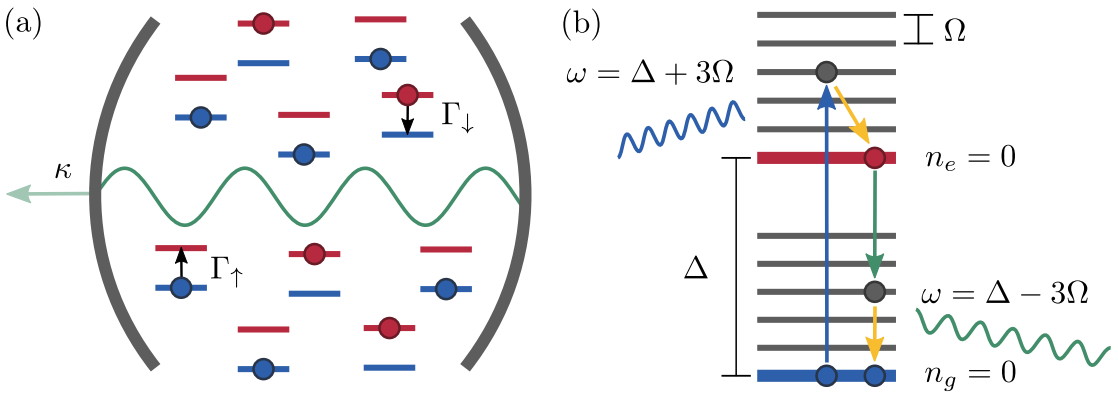

Figure 1.2: The dye-filled cavity is depicted schematically in panel (a) together with a standing wave of the electromagnetic field. A number of driven-dissipative processes, i.e. the cavity loss κ, the external optical pumping $\Gamma_\uparrow$, and the non-radiative decay $\Gamma_\downarrow$ are also shown, although we ignore them in this introduction (for a discussion, cf. Chp. 4). In panel (b), we present a sketch of the substructure of the dye molecules as described in the main text. The vibrational relaxation processes are indicated by the short (yellow) arrows.

vibrational ground state, i.e. the constituent atoms do not oscillate.[9] When a photon is absorbed, the electronic state changes, while the atoms remain in their former equilibrium positions. In the new electronic state, however, these positions correspond to a non-equilibrium (Franck-Condon) state, such that the atoms start to vibrate around the displaced equilibrium. The photon has provided the energy for both the electronic transition and the phononic excitation of the molecular vibration. Because of the fast thermalization, the new vibrational ground state is reached quickly after the absorption event (Kasha's rule). From this state, the molecule then decays back to the electronic ground state by emission of a photon (up to imperfections due to limited quantum efficiency). The equilibrium positions change again during this emission, the atoms oscillate for a short time, and then relax back to the original ground state.

The transitions are most likely to happen when the wave functions of the initial and final states have a large overlap at the atomic positions in the instant of absorption. This creates a symmetry between absorption and emission, where the initial and final vibrational state are interchanged. As depicted in Fig. 1.2 (b), if upon absorption the molecule is most likely to end up in the third excited state of the phononic oscillator, then after the relaxation to the vibrational ground state (while still being in the *electronic* excited state), the preferred final state of emission will be the electronic ground state combined with the third exited state of the phononic oscillator. Denoting the electronic transition frequency (also called the *zero-phonon line*) by Δ and the phononic frequency by Ω, the to-be-absorbed photon of frequency ω must provide the energy $\hbar\,(\Delta + 3\Omega)$, while the emitted photon will have the energy $\hbar\,(\Delta - 3\Omega)$. This is an example of the *Stokes shift*: emission happens at lower frequencies (larger wavelengths) than absorption). This may also be expressed

[9] Actually, since the molecules are in contact with a solvent heat bath, the vibrations are thermally occupied via a thermalization process that happens on very short picosecond timescales.

generally as a sum rule for the involved frequencies,

$$\omega + n_g \Omega = \Delta + n_e \Omega, \tag{1.24}$$

where $n_{g,\,e}$ denotes the phonon number in the electronic ground and excited state, respectively. As a function of the frequency, the thermal occupation numbers of the phonons in the ground and excited states are then connected by a Boltzmann factor [53],

$$\frac{n_g}{n_e} = \mathrm{e}^{\beta\hbar(\omega-\Delta)}, \tag{1.25}$$

where we have made the simplifying assumption that the phonon frequency is the same for the electronic ground and excited states.[10] Assuming detailed balance, one finds for the Einstein coefficients of absorption and stimulated emission

$$\frac{B_{12}(\omega)}{B_{21}(\omega)} = \mathrm{e}^{\beta\hbar(\omega-\Delta)}\,. \tag{1.26}$$

Since together with spontaneous emission, this will determine the distribution of the photons over the frequencies via the Einstein rate equations, the fact that we have found a Boltzmann factor is crucial for obtaining a proper equilibrium photon spectrum. Eq. (1.26) is known as the *Kennard-Stepanov relation*.

1.3.2 Chemical Potential and Critical Photon Number

The photon chemical potential is also introduced via the dye molecules. Idealizing these as two-level systems which may absorb and emit single photons, at temperature T the relative occupation of the excited and ground states will be given by a Boltzmann factor

$$M_\uparrow / M_\downarrow = \mathrm{e}^{-\beta\hbar\Delta}, \tag{1.27}$$

where $M_\uparrow$ ($M_\downarrow$) is the excited (ground) state occupation and Δ again the (electronic) transition frequency. If $\beta^{-1} = k_B T \ll \hbar\Delta$, practically all molecules are in the ground state. Of course, this also means no photons will be in the cavity. Importantly though, it is possible to introduce molecular excitations by optical pumping. If the cavity mirrors are very good (high reflectivity) and the quantum efficiency of the dye is close to one, the sum of photons and excited molecules is (approximately) conserved,

$$n + M_\uparrow = M_\downarrow. \tag{1.28}$$

[10] $\sum_l \mathrm{e}^{-\beta\hbar\Omega_g l} \,/\, \sum_l \mathrm{e}^{-\beta\hbar\Omega_e l} = 1.$

The amount of dye excitations converted into photons may be incorporated into Eq. (1.27) by means of a *photon* chemical potential μ_γ, such that

$$M_\uparrow / M_\downarrow = \mathrm{e}^{-\beta\left(\hbar\Delta - \mu_\gamma\right)} . \tag{1.29}$$

The real situation is slightly more complicated since neither the dye efficiency nor the mirror reflectivity are perfect. Hence, the system is really *open*, and both the mirror and the quantum loss have to be taken into account in a full description [16]. These issues will be addressed in Chp. 4.

The dispersion relation of a microresonator with cylindrical symmetry is [53]

$$\omega_{\mathbf{k}} = \frac{c}{n}\sqrt{k_r^2 + k_z^2(r)}, \tag{1.30}$$

where n is the refractive index of the cavity medium and $k_z(r) = \pi q / D(r)$. The longitudinal mode number is denoted by q, while $D(r)$ describes the distance between the two mirror surfaces as a function of the distance to the optical axis z. A symmetric, spherical cavity with curvature radius R is described by $D(r) = D(0) - 2\left(R - \sqrt{R^2 - r^2}\right)$. In paraxial approximation, i.e. for $R \gg r$ and $k_z(r) \gg k_r$, the dispersion may be approximated as[11]

$$\begin{aligned} \hbar\omega_{\mathbf{k}} &= \frac{\hbar c}{n}\frac{\pi q}{D_0}\left(1 + \frac{r^2}{D_0 R}\right) + \frac{\hbar c k_r^2}{2n\pi q}\left(D_0 - \frac{r^2}{R}\right) \\ &\approx \underbrace{\frac{\hbar\pi q n}{D_0 c}}_{m}\left(\frac{c}{n}\right)^2 + \frac{m}{2}\underbrace{\frac{2c}{D_0 R n}}_{\Omega^2} r^2 + \frac{\hbar^2 k_r^2}{2m}, \end{aligned} \tag{1.31}$$

where we have introduced an effective photon mass m and an effective harmonic frequency Ω, and neglected the last term of the first line. In this approximation, the photons obtain a dispersion relation equivalent to that of *massive* bosons trapped in a two-dimensional harmonic potential. The linear dispersion relation of black-body radiation is thus avoided. Taking the ground state of the two-dimensional oscillator as the zero of energy, the eigenfrequencies read

$$\omega_{l_x, l_y} = \Omega\left(l_x + l_y\right), \tag{1.32}$$

where $l_{x,y} \in \mathbb{N}_0$. The photon number as a function of frequency then becomes

$$n(\omega) = \frac{g(\omega)}{\mathrm{e}^{\beta\left(\hbar\omega - \mu_\gamma\right)} - 1}, \tag{1.33}$$

where $g(\omega) = 2\left(\omega/\Omega + 1\right)$, as explained in Tab. 1.2. Summing over all states except the ground state, we find the number of photons in the excited states of the photon gas. Similar to what we did

[11] This is true for very weakly curved mirrors brought extremely close together. One finds $D(r) \approx D_0 - 2R\left(1 - \left(1 - r^2/2R^2\right)\right) = D_0 - r^2/R$ and $k_z(r) = \frac{\pi q}{D_0 - r^2/R} \approx \frac{\pi q}{D_0}\left(1 + \frac{r^2}{D_0 R}\right)$.

	$\omega = \Omega$		$\omega = 2\Omega$		
l_x	1	0	2	0	1
l_y	0	1	0	2	1

Table 1.2: Degeneracy of eigenfrequencies for the two-dimensional harmonic oscillator. There are two ways to distribute a single quantum, and three ways to distribute two quanta. Including the polarization, for l quanta one finds $g(l) = 2\,(l+1)$.

above for the ideal Bose gas confined to a box, for temperatures large compared to the oscillator frequency, $\hbar\Omega \ll k_B T$, the sum can be approximated by an integral,

$$n_c = \sum_{l=1}^{\infty} n(l\Omega) \approx 2\left(\frac{k_B T}{\hbar\Omega}\right)^2 \int_0^\infty \mathrm{d}x\, \frac{x}{\mathrm{e}^x - 1} = 2\left(\frac{k_B T}{\hbar\Omega}\right)^2 \Gamma(2)\zeta(2) = \left(\frac{k_B T}{\hbar\Omega}\right)^2 \frac{\pi^2}{3}. \tag{1.34}$$

This is finite as for the three-dimensional Bose gas or the trapped two-dimensional Bose gas. Since we now have a chemical potential $\mu_\gamma \leq 0$, it is possible to add further particles beyond n_c to the system by letting $\mu_\gamma \nearrow 0$. These additional particles will then condense to the ground state $l_x = l_y = 0$ of the harmonic potential.

With an eye to parameters, the trap frequency quoted in Ref. [53] is $\Omega = 2\pi \cdot 4.1 \cdot 10^{10}$ Hz. At $T = 300$ K this results in a critical particle number of $n_c \approx 77068$. The refractive index is usually quoted as $n = 1.43$.

1.4 Classical Stochastic Systems

Before coming to the methods relevant for describing open *quantum* systems, the following Sec. will give a brief tour of the techniques used by physicists to model *classical stochastic systems*. The merit of reviewing these techniques is that they will help us to understand *non-equilibrium quantum field theory* (cf. Chp. 2) in a more intuitive way by contrasting those features of the latter that are genuinely quantum with those that merely follow from the effects of classical noise. The part about the classical path integral in 1.4.2 will be especially helpful in coming to grips with the Schwinger-Keldysh formalism (cf. 2.1). After completing the tour of classical stochastics, we discuss one of the essential methods to this thesis: we will derive the *quantum master equation* and explore its connection to other methods for describing open quantum systems in Sec. 1.5.

1.4.1 Stochastic Differential Equation

Brownian motion is the random motion of dissolved microscopic particles brought about by collisions with the submicroscopic molecules of the surrounding solvent. To the eye, this motion looks entirely erratic: the particles jump here and there without any apparent regularity. The mathematical description of Brownian motion is founded upon the insight that this intuitive picture

of randomness may be cast into a rigorous formal assumption. The equations of motion

$$\begin{aligned} \dot{q}(t) &= \frac{1}{m}p(t), \\ \dot{p}(t) &= -V'(q(t)) - \frac{\lambda}{m}p(t) + \sqrt{2\lambda kT}\xi(t) \end{aligned} \tag{1.35}$$

go over into Hamilton's equations of classical mechanics for $\lambda \to 0$. Yet for finite friction λ and temperature T they are conceptually different from the equations of classical mechanics. The reason for this is the "fluctuating force" $\xi(t)$. It describes the random shocks received by the microparticle from the collisions with the water molecules. In physical terms, the lack of "regularity" now means that there is no correlation between one perceptible jump of the microparticle and the next. Of course, this is an idealization that only holds if the timescale over which the experimentalist can measure the motion of the microparticle is by far larger than the typical timescale of the molecular motion. This idea can be expressed as

$$\langle \xi(t)\xi(t') \rangle = \delta(t - t'), \tag{1.36}$$

that is, the values of the fluctuating force at two different points in time are delta-correlated. This is equivalent to a so-called white noise

$$A(\omega) = \int_{-\infty}^{\infty} \mathrm{d}t \; \mathrm{e}^{\mathrm{i}\omega t} \langle \xi(t)\xi(0) \rangle = 1, \tag{1.37}$$

which is completely flat in frequency space. Again, in reality such a constant spectrum does not exist. Rather, a spectrum that is sufficiently broad around the relevant system frequencies is usually approximated as white. We have to emphasize that Eqs. (1.35) are the physicist's way of writing stochastic differential equations. While the trajectories traced out by a Brownian particle are indeed *continuous*, they are *not differentiable*.[12] The derivative of the fluctuating force $\xi(t)$ cannot be defined. Physically, this has to do with the fact that the time interval between two subsequent measurements of the trajectory cannot be made arbitrarily small without reaching the timescale of the molecular motion, at which point the shocks dealt by the fluctuating force stop to be temporally uncorrelated. In mathematics, Eqs. (1.35) are written in differential form as

$$\begin{aligned} \mathrm{d}q(t) &= \frac{1}{m}p(t)\mathrm{d}t, \\ \mathrm{d}p(t) &= -V'(q(t))\mathrm{d}t - \frac{\lambda}{m}p(t)\mathrm{d}t + \sqrt{2\lambda kT}\mathrm{d}W(t), \end{aligned} \tag{1.38}$$

where $\mathrm{d}W(t) \equiv \xi(t)\mathrm{d}t$ is the *Wiener process* [54]. Setting the potential term to zero, $V(q(t)) = 0$, we recover free Brownian motion, which allows for a straightforward solution of Eqs. (1.35). By

[12] That is, the limit $\lim_{\Delta t \to 0} \Delta q / \Delta t$ does not exist.

making the ansatz $\mathrm{d}p(t) = \mathrm{e}^{-\lambda t/m}\mathrm{d}p_I(t)$ we find $\mathrm{d}p_I(t) = \mathrm{e}^{\lambda t/m}\sqrt{2\lambda kT}\mathrm{d}W(t)$ and hence

$$p(t) = \mathrm{e}^{-\lambda t/m}\left(p(0) + \sqrt{2\lambda kT}\int_0^t \mathrm{e}^{\lambda t'/m}\mathrm{d}W(t')\right). \tag{1.39}$$

This is the exact solution for the fluctuating momentum of the microparticle. With this in hand, we can calculate the momentum correlations

$$\begin{aligned}
\langle p(t)p(t')\rangle - \mathrm{e}^{-\lambda(t+t')/m}\langle p^2(0)\rangle &= 2\lambda kT\,\mathrm{e}^{-\lambda(t+t')/m}\int_0^t\int_0^{t'}\mathrm{e}^{\lambda(\bar{t}+\bar{t}')/m}\langle \mathrm{d}W(\bar{t})\mathrm{d}W(\bar{t}')\rangle \\
&= 2\lambda kT\,\mathrm{e}^{-\lambda(t+t')/m}\int_0^t\int_0^{t'}\mathrm{d}\bar{t}\mathrm{d}\bar{t}'\;\mathrm{e}^{\lambda(\bar{t}+\bar{t}')/m}\delta(\bar{t}-\bar{t}') \\
&= 2\lambda kT\,\mathrm{e}^{-\lambda(t+t')/m}\int_0^{\min(t,t')}\mathrm{d}\tau\;\mathrm{e}^{2\lambda\tau/m} \\
&= mkT\left(\mathrm{e}^{-\lambda|t-t'|/m} - \mathrm{e}^{-\lambda(t+t')/m}\right),
\end{aligned} \tag{1.40}$$

where we have used $\langle\xi(t)\rangle = 0$. For long times, we then have correctly that

$$\frac{\langle p^2(t)\rangle}{2m} \xrightarrow[t\to\infty]{} \frac{1}{2}kT, \tag{1.41}$$

which is our second encounter with the *fluctuation-dissipation* theorem (FDT): the average kinetic energy turns out to be $kT/2$ for one-dimensional Brownian motion, in agreement with the equipartition theorem of statistical mechanics. Naturally, Langevin originally constructed Eqs. (1.35) in such a way as to fulfill this relation. Yet the physics behind it is both deep and important. It demonstrates the connection between the concept of temperature and random motion. It also shows that as the energy stored in the directed initial motion of the microparticle is lost through friction, this energy does not vanish: it is converted into heat. After reaching the steady-state, small amounts of this heat are converted back into kinetic energy such that on the average, the energy lost to friction is compensated by that gained through fluctuations. This is how the FDT relates to thermodynamic equilibrium.

1.4.2 From Stochastic Differential Equations to the Classical Path Integral

The derivation given in the following is important since it shows poignantly how the classical path integral is connected to probability theory. The central idea is to discretize time and then to infer the probability distribution of the path from the known distribution of the noise. Instead of the momentum $p(t)$, now consider an arbitrary stochastic variable $x(t)$ described by

$$\mathrm{d}x(t) = \alpha x(t)\mathrm{d}t + \sqrt{D}\;\mathrm{d}W(t). \tag{1.42}$$

To connect to the physical case from above, replace $x(t)$ with the momentum and set $\alpha = -\lambda/m$, $D = 2\lambda kT$. The Wiener process $W(t)$ is distributed according to $(W(t) - W(t')) \sim \mathcal{N}(0, t - t')$. For the construction of the classical path integral, we follow Hänggi [55], but also Kamenev [56] for the regularization. A more recent discussion can be found in [57]. The first question to address is how to discretize Eq. (1.42)? In stochastic calculus, the discretization is crucial (Itô-Stratonovich dilemma [58]). Here, we subdivide the time interval into N pieces of size $\varepsilon = (t_N - t_0)/N$. The equidistant lattice points are $t_n = t_0 + \varepsilon n$, and we use the shorthands $x_n = x(t_n)$, $W_n = W(t_n)$. The discretized version of Eq. (1.42) then becomes

$$x_n - x_{n-1} = \alpha x_{n-1} \cdot \varepsilon + \sqrt{D}\,(W_n - W_{n-1})\,, \tag{1.43}$$

where $\xi_n \equiv \sqrt{D}\,(W_n - W_{n-1}) \sim \mathcal{N}(0, D\varepsilon)$ is the normal-distributed noise. This is a *retarded* regularization (Itô), since x_n depends only on ξ_j with $j \leq n$ (through x_{n-1}).[13] The aim is now to find the probability for a transition from a fixed initial point (x_0, t_0) to a fixed later point $(x, t > t_0)$:

$$p(x|x_0) = \int_{-\infty}^{\infty} \left(\prod_{n=1}^{N-1} \mathrm{d}x_n \right)\; p(x_N = x, x_{N-1}, ..., x_1|x_0), \tag{1.44}$$

where we marginalize over all intermediate points. From probability theory, we know that upon substitution,

$$p(x) = p(\xi) \left| \frac{\partial \xi}{\partial x} \right| = p(\xi) \det \mathcal{J}^{-1}. \tag{1.45}$$

With the retarded discretization, the Jacobian becomes

$$\begin{aligned} \frac{\partial x_n}{\partial \xi_n} &= 1, \\ \frac{\partial x_n}{\partial \xi_j} &= \begin{cases} \mathcal{J}_{nj},\ j \leq n, \\ 0,\ j > n, \end{cases} \end{aligned} \tag{1.46}$$

which means $\mathcal{J}$ is a lower triangular matrix with unit diagonal, and the Jacobian determinant equals unity. For the joint distribution on the right-hand side of Eq. (1.44), we hence have

$$\begin{aligned} p(x_N, ..., x_1|x_0) &= p(\xi_N, ..., \xi_1) \\ &= \int_{-\infty}^{\infty} \left(\prod_{n=1}^{N} \frac{\mathrm{d}z_n}{2\pi} \right)\; \chi(z_1, ..., z_N)\; \exp\left\{ \mathrm{i} \sum_{n=1}^{N} \varepsilon z_n \left[\frac{x_n - x_{n-1}}{\varepsilon} - \alpha x_{n-1} \right] \right\}, \end{aligned}$$

where we have introduced the *curtailed characteristic functional* χ [55], and substituted for ξ_n by means of Eq. (1.43). From stochastic processes, we know that an Ornstein-Uhlenbeck process

[13] For a *symmetric* regularization (Stratonovich), the path integral acquires additional terms from a non-trivial Jacobian.

$\mathrm{d}X_t = \alpha X_t \mathrm{d}t + \sqrt{D}\mathrm{d}W_t$ is distributed according to

$$X_T = e^{\alpha T} X_0 + \sqrt{D} \int_0^T e^{\alpha(T-s)} \mathrm{d}W_s \sim \mathcal{N}\left(X_0 e^{\alpha T},\ \frac{D\left(e^{2\alpha T} - 1\right)}{2\alpha} \right),$$

which means that the characteristic functional is

$$\chi_{\mathrm{OU}}(z) = \exp\left\{ \mathrm{i} X_0 e^{\alpha T} z - \frac{D\left(e^{2\alpha T} - 1\right) z^2}{4\alpha} \right\}.$$

When we expand the exponential in the exponential for small $T \equiv \varepsilon$, we find with $X_0 = 0$ that

$$\chi_{\mathrm{OU}}(z) = \exp\left\{ -\frac{D\varepsilon}{2} z^2 \right\}.$$

For χ, we thus obtain

$$\chi(z_1, ..., z_N) = \prod_{n=1}^{N} \chi(z_n) = \prod_{n=1}^{N} \exp\left\{ -\frac{D\varepsilon}{2} z_n^2 \right\} = \exp\left\{ -\frac{D}{2}\varepsilon \sum_{n=1}^{N} z_n^2 \right\}, \tag{1.47}$$

because, as mentioned above, $\varepsilon\xi_n \sim \mathcal{N}(0,\ D\varepsilon)$. As a final step, we have to perform the continuum limit. The characteristic functional becomes that of a delta-correlated Gaussian process,

$$\chi(z) = \exp\left\{ -\frac{D}{2} \int_{t_0}^{t_N} \mathrm{d}t\ z^2(t) \right\}, \tag{1.48}$$

such that for the transition probability (i.e. the path integral), we arrive at

$$\begin{aligned} p(x|x_0) &= \int_{x(t_0)=x_0}^{x(t_N)=x} \mathcal{D}x(t) \int \mathcal{D}z(t)\ \chi(z) \exp\left\{ \mathrm{i} \int_{t_0}^{t_N} \mathrm{d}t\ z(t)[\dot{x}(t) - \alpha x(t)] \right\} \\ &= \int \mathcal{D}x(t)\mathcal{D}z(t) \exp\left\{ \mathrm{i} \int_{t_0}^{t_N} \mathrm{d}t\ \left[\mathrm{i}Dz^2/2 + z(\dot{x} - \alpha x) \right] \right\}, \end{aligned} \tag{1.49}$$

with the functional integral measures

$$\begin{aligned} \mathcal{D}z(t) &= \lim_{N\to\infty} \prod_{n=1}^{N} \frac{\mathrm{d}z_n}{2\pi}, \\ \mathcal{D}x(t) &= \lim_{N\to\infty} \left(\prod_{n=1}^{N-1} \mathrm{d}x_n \right). \end{aligned} \tag{1.50}$$

It should be stressed here that the simple form of Eq. (1.49) relies on the additivity of the noise in Eq. (1.42). If the constant $\sqrt{D}$ was replaced by an arbitrary function $g(x)$ as in [55], thus making

the noise multiplicative, the result would be more complicated. A word should also be said about the so-called *response field* z: as one can see from the derivation, z comes in through expressing the noise via its characteristic functional. In this capacity, the role of the response field is entirely transparent. This is less true of the "quantum field" ϕ_q frequently encountered in presentations of the Schwinger-Keldysh path integral. As we will see below, however, ϕ_q is exactly equivalent to the response field z, a fact that is important to appreciate in order to properly understand the Schwinger-Keldysh formalism.

Presently, the response field z may also be removed via the Hubbard-Stratonovich transformation, by means of which Eq. (1.49) may be related to the equivalent *Onsager-Machlup* path integral. Performing the Gaussian integration over the response variable $z_n(t)$, one finds

$$\begin{aligned}&\int_{-\infty}^{\infty}\frac{\mathrm{d}z_n}{2\pi}\,\exp\left\{-\frac{D\varepsilon}{2}z_n^2+\mathrm{i}\varepsilon z_n\left[\frac{x_n-x_{n-1}}{\varepsilon}-\alpha x_{n-1}\right]\right\}\\&=\frac{1}{\sqrt{2\pi D\varepsilon}}\exp\left\{-\frac{\varepsilon}{2D}\left[\frac{x_n-x_{n-1}}{\varepsilon}-\alpha x_{n-1}\right]^2\right\},\end{aligned}\tag{1.51}$$

which is quadratic in the path rather than in the response variable.

1.4.3 From the Path Integral to the Fokker-Planck Equation

To derive the Fokker-Planck equation from the path integral, we follow Ref. [56]. For the present Markovian case, it is possible to perform a transfer-matrix derivation. For greater generality, we go over to the case where $\alpha x_{n-1}\equiv A(x_{n-1})$, $D/2\equiv D(x_{n-1})$. Then the transition probabilities from point to point are related by

$$\begin{aligned}p(x_n,t_n|x_{n-1})=\int_{-\infty}^{\infty}\frac{\mathrm{d}z_n}{2\pi}\int_{-\infty}^{\infty}\mathrm{d}x_{n-1}\,\exp\left\{\mathrm{i}z_n\left[x_n-x_{n-1}-\varepsilon A(x_{n-1})\right]-\varepsilon D(x_{n-1})z_n^2\right\}\\\times\,p(x_{n-1},t_{n-1}|x_{n-2}).\end{aligned}\tag{1.52}$$

To simplify the notation, we set $t_n\equiv t$, $x_n\equiv x$, $z\equiv z_n$, and $t_{n-1}=t-\varepsilon$, $x_{n-1}\equiv x-\Delta x$. Expanding the drift and diffusion coefficients, and dropping the conditionals in the probability densities, we then have

$$\begin{aligned}p(x,t)=\int_{-\infty}^{\infty}\frac{\mathrm{d}z}{2\pi}\int_{-\infty}^{\infty}\mathrm{d}\Delta x\,\exp\Bigg\{&\mathrm{i}z\left[\Delta x-\varepsilon A(x)+\varepsilon A'(x)\Delta x\right]\\&-\varepsilon z^2\left[D(x)-D'(x)\Delta x+\frac{D''(x)}{2}\Delta x^2\right]\Bigg\}p(x-\Delta x,t-\varepsilon).\end{aligned}\tag{1.53}$$

Note how we expanded the drift coefficient $A(x)$ to first order in Δx, the diffusion coefficient $D(x)$, however, to second order. The reason for this is that $z\sim\varepsilon^{-1/2}$, $\Delta x\sim\varepsilon^{1/2}$. Hence,

to have a consistent expansion, the diffusion coefficient must be expanded to second order to compensate for the Gaussian square in the response variable, z^2. As a next step, we expand $p(x-\Delta x, t-\varepsilon) = p(x,t) - p'(x,t)\Delta x + \frac{1}{2}p''(x,t)\Delta x^2 - \varepsilon\dot{p}(x,t)$, resulting in

$$\begin{aligned} p(x,t) = \int_{-\infty}^{\infty}\frac{\mathrm{d}z}{2\pi}\int_{-\infty}^{\infty}\mathrm{d}\Delta x\ \exp\left\{\mathrm{i}z\Delta x - \varepsilon D(x)z^2\right\}\Big[1 - \mathrm{i}\varepsilon z A + \mathrm{i}\varepsilon\Delta x A' + \varepsilon z^2\Delta x D' \\ + \tfrac{1}{2}(-\mathrm{i}\varepsilon z A)^2 + \tfrac{1}{2}(\varepsilon z^2\Delta x D')^2 - \tfrac{1}{2}\varepsilon z^2\Delta x^2 D''\Big]\Big[p - \Delta x p' + \tfrac{1}{2}\Delta x^2 p'' - \varepsilon\dot{p}\Big], \end{aligned} \tag{1.54}$$

where we have collected the terms of order $\sim \varepsilon^0$ in the remaining exponential. All other terms were collected in a second exponential which was subsequently expanded to order $\sim \varepsilon^1$. Observe how this means that, e.g. a term like $\varepsilon z^2\Delta x D' \sim \varepsilon^{1/2}$ must be taken to second order in the expansion. Now, we need to calculate all of the moments appearing on the right-hand side, where the two-dimensional Gaussian density is

$$f(z,\Delta x) = \exp\left\{-\varepsilon D\left[z^2 - \frac{\mathrm{i}z\Delta x}{\varepsilon D}\right]\right\} = \exp\left\{-\frac{\Delta x^2}{4\varepsilon D} - \varepsilon D\left(z - \frac{\mathrm{i}\Delta x}{2\varepsilon D}\right)^2\right\}. \tag{1.55}$$

This calculation is performed in App. B.4. As a result, Eq. (1.54) is equivalent to

$$\dot{p} = Dp'' - Ap' - A'p + 2D'p' + D''p + \mathcal{O}(\varepsilon). \tag{1.56}$$

Taking $\varepsilon \to 0$, we finally come out with the well-known *Fokker-Planck equation*

$$\frac{\partial}{\partial t}p(x,t) = -\frac{\partial}{\partial x}A(x)p(x,t) + \frac{\partial^2}{\partial x^2}D(x)p(x,t), \tag{1.57}$$

for arbitrary drift $A(x)$ and diffusion "matrix" $D(x)$. Given the retarded regularization of the path integral above, it is no surprise that we found the Fokker-Planck equation in Itô form. If we write the diffusion matrix as $D(x) = \frac{1}{2}\sigma^2(x)$, the corresponding Fokker-Planck equation in Stratonovich form is

$$\begin{aligned} \frac{\partial}{\partial t}p(x,t) &= -\frac{\partial}{\partial x}A(x)p(x,t) + \frac{1}{2}\frac{\partial}{\partial x}\sigma(x)\frac{\partial}{\partial x}\sigma(x)p(x,t) \\ &= -\frac{\partial}{\partial x}\left\{A(x) + \frac{1}{2}\sigma(x)\sigma'(x)\right\}p(x,t) + \frac{1}{2}\frac{\partial^2}{\partial x^2}\sigma^2(x)p(x,t), \end{aligned} \tag{1.58}$$

where the so-called *spurious drift* appears as $\frac{1}{2}\sigma(x)\sigma'(x)$.

1.4.4 Equivalence of Fokker-Planck and Langevin Equation

To complete the cycle that has led us from the Langevin equation via the path integral to the Fokker-Planck equation, we follow van Kampen [58] to show that the Fokker-Planck equation

belonging to our original stochastic process (1.42),

$$\frac{\partial}{\partial t}p(x,t) = -\alpha\frac{\partial}{\partial x}xp(x,t) + \frac{D}{2}\frac{\partial^2}{\partial x^2}p(x,t), \tag{1.59}$$

is equivalent to the Langevin equation

$$\dot{x}(t) = \alpha x(t) + \xi(t), \tag{1.60}$$

where the noise is assumed to be a Gaussian process of mean zero with $\langle \xi(t)\xi(t')\rangle = D\delta(t-t')$. Analogously to Eq. (1.39), the solution of this stochastic differential equation is

$$x(t) = x_0 e^{\alpha t} + \int_0^t \mathrm{d}t'\; e^{\alpha(t-t')}\xi(t'). \tag{1.61}$$

For the first two moments, we hence find from Eq. (1.60) that

$$\begin{aligned} \langle x(t)\rangle &= x_0 e^{\alpha t}, \\ \langle x^2(t)\rangle &= x_0^2 e^{2\alpha t} - \frac{D}{2\alpha}\left(1 - e^{2\alpha t}\right). \end{aligned} \tag{1.62}$$

In the Fokker-Planck framework, we may derive a differential equation for the first moment, assuming that $p(x,t)$ vanishes at $x = \pm\infty$,

$$\begin{aligned} \frac{\partial}{\partial t}\langle x\rangle &= \int_{-\infty}^{\infty}\mathrm{d}x\; x\,\dot{p}(x,t) \\ &= \int_{-\infty}^{\infty}\mathrm{d}x\; x\left[-\alpha\frac{\partial}{\partial x}x\,p + D\frac{\partial^2}{\partial x^2}p\right] \\ &= \int_{-\infty}^{\infty}\mathrm{d}x\;\left(\frac{\partial}{\partial x}x\right)\left[\alpha\,x\,p - D\frac{\partial}{\partial x}p\right] \\ &= \alpha\,\langle x\rangle\,, \end{aligned} \tag{1.63}$$

the solution to which is $\langle x\rangle = x_0 e^{\alpha t}$. Applying the same integration by parts as above twice to the diffusive part, we find for the second moment

$$\begin{aligned} \frac{\partial}{\partial t}\langle x^2\rangle &= \int_{-\infty}^{\infty}\mathrm{d}x\; x^2\dot{p}(x,t) = \int_{-\infty}^{\infty}\mathrm{d}x\; x^2\left[-\frac{\partial}{\partial x}\alpha x p + D\frac{\partial^2}{\partial x^2}p\right] \\ &= 2\alpha\,\langle x^2\rangle + 2D, \end{aligned} \tag{1.64}$$

the solution to which, as one may verify, is given by the second of Eqs. (1.62). For a Gaussian process, this is all we need to show, and we will not go into further detail here. This completes our tour of classical stochastic methods. In the remaining part of this Chp. we introduce the first of the tools used throughout the rest of this thesis to describe interacting open quantum systems.

1.5 Open Quantum Systems

There are many similarities between classical stochastic systems and open quantum systems (at least in the case of bosons). One reason for this is that even for a quantum system coupled to a bath which is also quantum, the resulting noise that enters the effective system description can still be essentially classical. In the following, we build on this analogy and introduce open quantum systems first via the quantum Langevin equation. Subsequently, the quantum Wiener process will help us to introduce the main tool for Chp. 4, the quantum master equation. Because it is of such importance in treating open quantum systems in general, we also give a second derivation from first principles. A discussion of phase-space methods concludes Chp. 1.

1.5.1 Quantum Langevin Equation

The closest quantum-mechanical analogy to the Langevin equation (1.35) of classical Brownian motion is the quantum harmonic oscillator coupled to a thermal reservoir. Gardiner's textbook [59] on quantum stochastic methods is the standard reference for this kind of problem. An excellent discussion of quantum Langevin equations can also be found in [60]. As for the classical analogy, the equation of motion ($\hbar = 1$)

$$\dot{a}(t) = -\mathrm{i}\omega_0 a(t) - \frac{\lambda}{2}a(t) + \sqrt{\lambda}\,\Gamma(t) \tag{1.65}$$

goes over into the Heisenberg equation of the operator $a(t)$ for $\lambda \to 0$.[14] The most important difference, however, is that now $\Gamma(t)$ is also an operator with the properties

$$\begin{aligned} [\Gamma(t), \Gamma^\dagger(t')] &= \delta(t-t'), \\ \langle \Gamma^\dagger(t')\Gamma(t)\rangle &= \bar{N}(\omega_0)\delta(t-t'), \end{aligned} \tag{1.67}$$

and $\langle \Gamma(t)\rangle = 0$. It is important to notice that $\bar{N}$ is frequency-dependent and related to the Planck spectrum by

$$\bar{N}(\omega) = \frac{1}{\exp\left(\hbar\omega/kT\right) - 1}. \tag{1.68}$$

An example relevant for this thesis is a single-mode cavity with frequency ω_0 such that $\hbar\omega_0 \gg kT$, in which case $\bar{N}(\omega_0) \to 0$ and the quantum noise reduces to zero-point fluctuations. The analogy

[14] Throughout this thesis we will keep the "operator hat" implicit for bosonic operators, i.e. $\hat{a} \equiv a$. For completeness, the quantum Langevin equations for $\hat{q}$ and $\hat{p}$ can be shown to read

$$\begin{aligned} \dot{\hat{q}} &= \frac{1}{m}\hat{p} - \lambda\hat{q} + \sqrt{\lambda\hbar/m\omega_0}(\Gamma + \Gamma^\dagger), \\ \dot{\hat{p}} &= -m\omega_0^2\hat{q} - \lambda\hat{p} - \mathrm{i}\sqrt{\lambda\hbar m\omega_0}(\Gamma - \Gamma^\dagger). \end{aligned} \tag{1.66}$$

to classical stochastics can be formalized by writing Eq. (1.65) in differential form as

$$\mathrm{d}a(t) = -\frac{\mathrm{i}}{\hbar}[a(t), \hat{H}]\mathrm{d}t - \frac{\lambda}{2}a(t)\mathrm{d}t + \sqrt{\lambda}\,[a(t), a^\dagger(t)]\mathrm{d}B(t), \tag{1.69}$$

where now $\mathrm{d}B(t)$ is the *quantum Wiener process* and $\hat{H} = \omega_0 a^\dagger a$. As shown by Gardiner [59], a quantum Itô calculus can be built by carefully defining its properties. The solution to Eq. (1.65) may be found with a similar ansatz as above: $a(t) = \mathrm{e}^{-(\mathrm{i}\omega_0+\lambda/2)t}a_I(t)$, which leads to[15]

$$a(t) = \mathrm{e}^{-(\mathrm{i}\omega_0+\lambda/2)t}\left(a(0) + \sqrt{\lambda}\int_0^t \mathrm{d}\bar{t}\,\mathrm{e}^{(\mathrm{i}\omega_0+\lambda/2)\bar{t}}\Gamma(\bar{t})\right). \tag{1.70}$$

This preserves the commutator if $[a(0), \Gamma^\dagger(t)] = 0$, as one may also glean from the following calculations. For the special case of $\bar{N}(\omega_0) = 0$ we then obtain

$$\begin{aligned}\langle a^\dagger(t')a(t)\rangle &= \mathrm{e}^{-\mathrm{i}\omega_0(t-t')}\mathrm{e}^{-\lambda(t+t')/2}\Bigg(\langle a^\dagger(0)a(0)\rangle \\ &\quad + \lambda\int_0^{t'}\mathrm{d}\bar{t}'\int_0^t \mathrm{d}\bar{t}\,\mathrm{e}^{(\mathrm{i}\omega_0+\lambda/2)\bar{t}}\mathrm{e}^{-(\mathrm{i}\omega_0-\lambda/2)\bar{t}'}\langle\Gamma^\dagger(\bar{t}')\Gamma(\bar{t})\rangle\Bigg) \\ &= \mathrm{e}^{-\mathrm{i}\omega_0\tau}\mathrm{e}^{-\lambda T}\langle a^\dagger(0)a(0)\rangle,\end{aligned} \tag{1.71}$$

where we have introduced the "center-of-mass" time $T = \left(t + t'\right)/2$ (not to be confused with temperature), and the "relative" time $\tau = t - t'$. These are also called *Wigner coordinates* [61]. In the same way, for the reversed operator ordering, we have

$$\begin{aligned}\langle a(t)a^\dagger(t')\rangle &= \mathrm{e}^{-\mathrm{i}\omega_0(t-t')}\mathrm{e}^{-\lambda(t+t')/2}\Bigg(\langle a(0)a^\dagger(0)\rangle \\ &\quad + \lambda\int_0^{t'}\mathrm{d}\bar{t}'\int_0^t \mathrm{d}\bar{t}\,\mathrm{e}^{(\mathrm{i}\omega_0+\lambda/2)\bar{t}}\mathrm{e}^{-(\mathrm{i}\omega_0-\lambda/2)\bar{t}'}\langle\Gamma(\bar{t})\Gamma^\dagger(\bar{t}')\rangle\Bigg) \\ &= \mathrm{e}^{-\mathrm{i}\omega_0\tau}\mathrm{e}^{-\lambda(t+t')/2}\left(\langle a(0)a^\dagger(0)\rangle + \mathrm{e}^{\lambda\min(t,t')} - 1\right) \\ &= \mathrm{e}^{-\mathrm{i}\omega_0\tau}\left(\mathrm{e}^{-\lambda(t+t')/2}\langle a(0)a^\dagger(0)\rangle + \mathrm{e}^{-\lambda|t-t'|/2} - \mathrm{e}^{-\lambda(t+t')/2}\right) \\ &= \mathrm{e}^{-\mathrm{i}\omega_0\tau}\left(\mathrm{e}^{-\lambda T}\langle a(0)a^\dagger(0)\rangle + \mathrm{e}^{-\lambda|\tau|/2} - \mathrm{e}^{-\lambda T}\right).\end{aligned} \tag{1.72}$$

For the commutator we thus find indeed

$$[a(t), a^\dagger(t)] = \mathrm{e}^{-\lambda t}[a(0), a^\dagger(0)] + 1 - \mathrm{e}^{-\lambda t} = 1. \tag{1.73}$$

[15] This procedure is actually a lot simpler than for the stochastic classical harmonic oscillator, where it is not straightforward to find a closed-form solution like (1.70) for $p(t)$.

From these solutions, we can also build a bridge to the analytical properties of the retarded and advanced Green functions. These are defined as

$$\begin{aligned} G^R(t,t') &= -\mathrm{i}\theta(t-t')\langle[a(t),a^\dagger(t')]\rangle = -\mathrm{i}\theta(t-t')\mathrm{e}^{-\mathrm{i}\omega_0(t-t')}\mathrm{e}^{-\lambda(t-t')/2}, \\ G^A(t,t') &= \quad \mathrm{i}\theta(t'-t)\langle[a(t),a^\dagger(t')]\rangle = \quad \mathrm{i}\theta(t'-t)\mathrm{e}^{-\mathrm{i}\omega_0(t-t')}\mathrm{e}^{+\lambda(t-t')/2}, \end{aligned} \tag{1.74}$$

where for closed systems one usually writes an infinitesimal η instead of our finite λ. Their Fourier transforms are

$$G^{R/A}(\omega) = \int_{-\infty}^{\infty} \mathrm{d}\tau\ \mathrm{e}^{\mathrm{i}\omega\tau} G^{R/A}(\tau) = \frac{1}{2}\frac{1}{(\omega-\omega_0)\pm\mathrm{i}\lambda/2}, \tag{1.75}$$

with the plus sign corresponding to the retarded Green function. The spectral function is then [61, 62]

$$A(\omega) = \mathrm{i}\left(G^R(\omega) - G^A(\omega)\right) = -2\,\mathrm{Im}\,G^R(\omega) = \frac{\lambda/2}{(\omega-\omega_0)^2 + (\lambda/2)^2}, \tag{1.76}$$

which recovers the Lorentzian line shape one expects for the open, low-temperature single-mode cavity.

1.5.2 Master Equation from Quantum Wiener Process

The Heisenberg equation for an arbitrary operator is equivalent to the von Neumann equation for the density matrix in closed-system quantum mechanics. In the same vein, it is possible to derive a *master equation* for the density matrix from the open-system extension of the Heisenberg equation (which is the quantum Langevin equation). The general quantum Wiener process is defined by

$$\mathrm{d}a = -\frac{\mathrm{i}}{\hbar}[a,H_S]\mathrm{d}t + \frac{\lambda}{2}\left(2\hat{L}^\dagger a\hat{L} - \{a,\hat{L}^\dagger\hat{L}\}\right)\mathrm{d}t + \sqrt{\lambda}[a,\hat{L}^\dagger]\mathrm{d}B + \sqrt{\lambda}\mathrm{d}B^\dagger[\hat{L},a], \tag{1.77}$$

where we have introduced the anti-commutator $\{\hat{X},\hat{Y}\} := \hat{X}\hat{Y} + \hat{Y}\hat{X}$ and $\hat{L}$ can in principle be any system operator. Now the average of an arbitrary system operator a is

$$\begin{aligned} \langle a(t)\rangle &= \mathrm{Tr}_S\,\mathrm{Tr}_R\,[a(t)\hat{\rho}_R\otimes\hat{\rho}_S(t_0)] \\ &= \mathrm{Tr}_S\,\mathrm{Tr}_R\,[U(t_0,t)a(t_0)U(t,t_0)\hat{\rho}_R\otimes\hat{\rho}_S(t_0)] \\ &= \mathrm{Tr}_S\,\{a(t_0)\,\mathrm{Tr}_R\,[U(t,t_0)\hat{\rho}_R\otimes\hat{\rho}_S(t_0)U(t_0,t)]\} \\ &= \mathrm{Tr}_S\,\{a(t_0)\,\mathrm{Tr}_R\,[\hat{\rho}_R\otimes\hat{\rho}_S(t)]\} = \mathrm{Tr}_S\,\{a(t_0)\hat{\rho}_S(t)\}\,. \end{aligned} \tag{1.78}$$

Here we have assumed that the total density matrix can be written in product form with $\hat{\rho}_R$ being the reservoir and $\hat{\rho}_S$ the system density matrix. Furthermore, we have assumed that the reservoir density matrix is time-independent, to which we will come back in the next subsection. With

$\langle \mathrm{d}B(t)\rangle = 0$, we can write

$$\langle \mathrm{d}a(t)\rangle = -\frac{\mathrm{i}}{\hbar}\langle [a, H_S]\rangle \mathrm{d}t + \frac{\lambda}{2}\langle 2\hat{L}^\dagger a \hat{L} - \{a, \hat{L}^\dagger \hat{L}\}\rangle \mathrm{d}t, \tag{1.79}$$

or equivalently

$$\begin{aligned}\frac{\mathrm{d}}{\mathrm{d}t}\langle a(t)\rangle &= -\frac{\mathrm{i}}{\hbar}\,\mathrm{Tr}_S\left\{\hat{\rho}_S(t)[a(0), H_S]\right\} + \frac{\lambda}{2}\,\mathrm{Tr}_S\left\{\hat{\rho}_S(t)\left(2\hat{L}^\dagger a(0)\hat{L} - \{a(0), \hat{L}^\dagger\hat{L}\}\right)\right\} \\ &= -\frac{\mathrm{i}}{\hbar}\,\mathrm{Tr}_S\left\{a(0)[H_S, \hat{\rho}_S(t)]\right\} + \frac{\lambda}{2}\,\mathrm{Tr}_S\left\{a(0)\left(2\hat{L}\hat{\rho}_S(t)\hat{L}^\dagger - \{\hat{L}^\dagger\hat{L}, \hat{\rho}_S(t)\}\right)\right\},\end{aligned} \tag{1.80}$$

where we have cycled the operators under the trace. Since

$$\frac{\mathrm{d}}{\mathrm{d}t}\langle a(t)\rangle = \frac{\mathrm{d}}{\mathrm{d}t}\,\mathrm{Tr}_S\left\{a(t_0)\hat{\rho}_S(t)\right\} = \mathrm{Tr}_S\left\{a(t_0)\frac{\mathrm{d}}{\mathrm{d}t}\hat{\rho}_S(t)\right\}, \tag{1.81}$$

where a could be replaced by an arbitrary operator $\hat{X}$, there must also hold

$$\frac{\mathrm{d}}{\mathrm{d}t}\hat{\rho}_S(t) = -\frac{\mathrm{i}}{\hbar}[H_S, \hat{\rho}_S(t)] + \frac{\lambda}{2}\left(2\hat{L}\hat{\rho}_S(t)\hat{L}^\dagger - \{\hat{L}^\dagger\hat{L}, \hat{\rho}_S(t)\}\right), \tag{1.82}$$

which completes this derivation of the master equation for the system density matrix. Since we have started from the quantum Langevin equation, behind which many assumptions are hidden that we have not yet discussed in detail, next we will give a derivation of the master equation from first principles.

1.5.3 Derivation of the Master Equation from First Principles

For this detailed derivation of the quantum master equation, we again follow the exposition given by Gardiner [59]. The starting point is a Hamiltonian of the form

$$H = H_R \otimes \mathbb{1}_S + \mathbb{1}_R \otimes H_S + V_{RS}, \tag{1.83}$$

where we have a reservoir (or bath) Hamiltonian H_R, a system Hamiltonian H_S, and a reservoir-system coupling V_{RS} which is a matrix on the full $(d_R \times d_S)$-dimensional Hilbert space $\mathcal{H}_{RS} = \mathcal{H}_R \otimes \mathcal{H}_S$. By the very nature of the separation of a physical entity into reservoir and system, we assume that V_{RS} induces only weak coupling between the two parts. Otherwise, speaking of separation would not be meaningful. The quantum dynamics of reservoir plus system is then described by the von Neumann equation. After going to the interaction picture w.r.t. $H - V_{RS}$, we assume for the interaction-picture density matrix as before that

$$\hat{\rho}_I(t) = \hat{\rho}_R \otimes \hat{\rho}_S(t). \tag{1.84}$$

There are really two assumptions hidden here. The first is that by dropping the time-dependence of $\hat{\rho}_R$, we have taken the reservoir to be so vast as not to be affected by the coupling to the much smaller system. The second concerns the separation into a reservoir and a system density matrix. The full density matrix has to have unit trace and be Hermitian, such that of the $(d_R \times d_S)^2$ complex coefficients of an arbitrary matrix on $\mathcal{H}_{RS}$, we are left with $d_R \times d_S - 1$ real coefficients on the diagonal, and $(d_R \times d_S)^2 - d_R \times d_S$ real coefficients off-diagonally. In total, therefore, the most general density matrix on the full space has $(d_R \times d_S)^2 - 1$ independent real coefficients. Since general density matrices on either subspace possess only $d_X^2 - 1$ independent real coefficients, where $X = R, S$, we see immediately that the most general density matrices on the joint space *cannot* be of the form $\hat{\rho}_R \otimes \hat{\rho}_S$. The reduced density matrix in the interaction picture is now given by the reservoir trace over the full interaction-picture density matrix,

$$\hat{\rho}_S(t) = \mathrm{Tr}_R\, \hat{\rho}_I(t). \tag{1.85}$$

In the interaction picture, we have the von Neumann equation

$$\dot{\hat{\rho}}_I(t) = -\frac{\mathrm{i}}{\hbar}\left[V_I(t), \hat{\rho}_I(t)\right], \tag{1.86}$$

where $V_I = \mathrm{e}^{\mathrm{i}(H - V_{RS})t}\, V_{RS}\, \mathrm{e}^{-\mathrm{i}(H - V_{RS})t}$. It is equivalent to

$$\hat{\rho}_I(t) = \hat{\rho}_I(0) - \frac{\mathrm{i}}{\hbar}\int_0^t \mathrm{d}t' \left[V_I\left(t'\right), \hat{\rho}_I(t')\right]. \tag{1.87}$$

If we iterate this by replacing $\hat{\rho}_I(t')$ with $\hat{\rho}_I(0) - \frac{\mathrm{i}}{\hbar}\int_0^{t'} \mathrm{d}t'' \left[V_I\left(t''\right), \hat{\rho}_I(t'')\right]$, we obtain

$$\hat{\rho}_I(t) = \hat{\rho}_I(0) - \frac{\mathrm{i}}{\hbar}\int_0^t \mathrm{d}t' \left[V_I\left(t'\right), \hat{\rho}_I(0)\right] - \frac{1}{\hbar^2}\int_0^t \mathrm{d}t' \int_0^{t'} \mathrm{d}t'' \left[V_I\left(t'\right), \left[V_I\left(t''\right), \hat{\rho}_I\left(t''\right)\right]\right],$$

which can also be written as

$$\begin{aligned}\frac{\mathrm{d}}{\mathrm{d}t}\hat{\rho}_I(t) &= -\frac{\mathrm{i}}{\hbar}\left[V_I\left(t\right), \hat{\rho}_I(0)\right] - \frac{1}{\hbar^2}\int_0^t \mathrm{d}t'' \left[V_I\left(t\right), \left[V_I\left(t''\right), \hat{\rho}_I\left(t''\right)\right]\right] \\ &= -\frac{\mathrm{i}}{\hbar}\left[V_I\left(t\right), \hat{\rho}_I(0)\right] - \frac{1}{\hbar^2}\int_0^t \mathrm{d}\tau \left[V_I\left(t\right), \left[V_I\left(t-\tau\right), \hat{\rho}_I\left(t-\tau\right)\right]\right],\end{aligned} \tag{1.88}$$

Tracing this over the reservoir, we come out with

$$\frac{\mathrm{d}}{\mathrm{d}t}\hat{\rho}_S(t) = -\frac{1}{\hbar^2}\int_0^t \mathrm{d}\tau\, \mathrm{Tr}_R \left[V_I\left(t\right), \left[V_I\left(t-\tau\right), \hat{\rho}_R \otimes \hat{\rho}_S\left(t-\tau\right)\right]\right], \tag{1.89}$$

where we have set $\mathrm{Tr}_R\left[V_I\left(t\right), \hat{\rho}_I(0)\right] = 0$. This is an integro-differential equation of a kind that we will encounter and solve later in this thesis (cf. Chp. 5). Presently, we ask if there is not a plausible physical assumption to turn it into an ordinary differential equation? Consider the reservoir trace under the integral to be a function $f(\tau)$ defined on the interval $[0, \infty)$. If the

correlation between reservoir and system is very short-lived, this function will only have support on a very narrow subset $[0, \tau_c]$, where $\tau_c \ll t$ is the correlation time. From the perspective of frequency space, this says the reservoir will have an extremely broad (if not white) spectrum. Moreover, if the system changes on a timescale $\tau_s \gg \tau_c$, we can take $\hat{\rho}_S(t-\tau) = \hat{\rho}_S(t)$ for all times $\tau \in [0, \tau_c]$. Now, instead of taking the upper integral boundary in Eq. (1.89) to be τ_c, for mathematical convenience we do essentially the opposite and extend it to infinity. This is equivalent to the assumption that t is already practically infinite compared to τ_c. Note that there is an order to these two points: only after throwing away the τ-dependence of $\hat{\rho}_S$ may we send the integral boundary to infinity. Reversing this order would mean that the system could not have changed in the past. Accordingly, our final result for the master equation is

$$\frac{\mathrm{d}}{\mathrm{d}t}\hat{\rho}_S(t) = -\frac{1}{\hbar^2}\int_0^\infty \mathrm{d}\tau \,\mathrm{Tr}_R\left[V_I(t), \left[V_I(t-\tau), \hat{\rho}_R \otimes \hat{\rho}_S(t)\right]\right]. \tag{1.90}$$

Neglecting the τ-dependence of $\hat{\rho}_S$ is called the (first) *Markov assumption* in the style of probability theory where a conditional probability density $p(t_n|t_{n-1}, ..., t_0)$ over a time series $t_0, ..., t_n$ is said to have the *Markov property* if $p(t_n|t_{n-1}, ..., t_0) = p(t_n|t_{n-1})$. Turning a *retarded* integro-differential equation, where the future depends on the entire history of the system since $t_0 = 0$, into a differential equation achieves basically the same thing.

1.5.4 Phase-Space Methods: Wigner Representation

A further, convenient way to describe open quantum systems is via phase-space methods. They are appealing because of their close analogy to classical physics. There exist several standard methods: P, Q and Wigner representation corresponding to the mapping of operator expectation values in normal, anti-normal and symmetric order to expectation values of quasi-probability distributions. The Wigner distribution comes closest to a distribution over classical phase space. The standard reference is again Gardiner's book [59] on quantum noise.

For certain special cases such as the open single-mode cavity, these distributions can be completely positive functions that obey a proper Fokker-Planck equation. This is in general not true for interacting problems where, for instance, the Wigner representation maps a standard Hubbard-like quartic term to third-order derivatives in a "generalized" Fokker-Planck equation. Such an equation cannot be transformed into a stochastic differential equation by canonical methods. While there exists very interesting work on how such transformations may still be achieved [63–65], to the author's knowledge these methods have not yet found widespread application.

More attention has been given to a strain of work that tries to avoid the appearance of generalized Fokker-Planck equations by increasing the dimension of the phase space to which the density matrix is mapped. This has led to the so-called *positive* and *gauge* P representations [66–68] which allow for proper Fokker-Planck equations and hence for standard transformations to stochastic differential equations even for interacting quantum systems. The drawback is that the interaction terms are in general mapped to multiplicative-noise contributions (cf. B.3.2) which are difficult to handle numerically for large noise (i.e. strong interactions). Thus there appears to be a "conservation of difficulty", as expected. While all of these methods apply only to bosonic systems, work on fermionic Q functions does exist [69, 70].

To map the master equation of our open single-mode cavity (which follows from Eq. (1.82) for $\hat{L} = a$) to a Wigner distribution $\mathcal{W}$, we need the following correspondences

$$\begin{aligned}
a^\dagger a\hat{\rho} \longleftarrow & \left(\alpha^* - \frac{1}{2}\frac{\partial}{\partial\alpha}\right)\left(\alpha + \frac{1}{2}\frac{\partial}{\partial\alpha^*}\right)\mathcal{W}\left(\alpha,\alpha^*\right) \\
&= \left[|\alpha|^2 - \frac{1}{2}\frac{\partial}{\partial\alpha}\alpha + \frac{1}{2}\alpha^*\frac{\partial}{\partial\alpha^*} - \frac{1}{4}\frac{\partial^2}{\partial\alpha\partial\alpha^*}\right]\mathcal{W}\left(\alpha,\alpha^*\right) \\
\hat{\rho}a^\dagger a \longleftarrow & \left(\alpha - \frac{1}{2}\frac{\partial}{\partial\alpha^*}\right)\left(\alpha^* + \frac{1}{2}\frac{\partial}{\partial\alpha}\right)\mathcal{W}\left(\alpha,\alpha^*\right) \\
&= \left[|\alpha|^2 - \frac{1}{2}\frac{\partial}{\partial\alpha^*}\alpha^* + \frac{1}{2}\alpha\frac{\partial}{\partial\alpha} - \frac{1}{4}\frac{\partial^2}{\partial\alpha\partial\alpha^*}\right]\mathcal{W}\left(\alpha,\alpha^*\right) \\
a\hat{\rho}a^\dagger \longleftarrow & \left(\alpha^* + \frac{1}{2}\frac{\partial}{\partial\alpha}\right)\left(\alpha + \frac{1}{2}\frac{\partial}{\partial\alpha^*}\right)\mathcal{W}\left(\alpha,\alpha^*\right) \\
&= \left[|\alpha|^2 + \frac{1}{2}\frac{\partial}{\partial\alpha}\alpha + \frac{1}{2}\alpha^*\frac{\partial}{\partial\alpha^*} + \frac{1}{4}\frac{\partial^2}{\partial\alpha\partial\alpha^*}\right]\mathcal{W}\left(\alpha,\alpha^*\right).
\end{aligned} \tag{1.91}$$

Applying these to the master equation, we find the corresponding proper Fokker-Planck equation (cf. App. B.1) for the Wigner distribution

$$\begin{aligned}
\dot{\mathcal{W}}\left(\alpha,\alpha^*\right) &= \left[-\mathrm{i}\omega_0\left(\alpha^*\frac{\partial}{\partial\alpha^*} + \frac{1}{2} - \alpha\frac{\partial}{\partial\alpha} - \frac{1}{2}\right) - \frac{\lambda}{2}\left(2|\alpha|^2 - 1 - \frac{1}{2}\frac{\partial^2}{\partial\alpha\partial\alpha^*}\right)\right]\mathcal{W}\left(\alpha,\alpha^*\right) \\
&\quad + \lambda\left[|\alpha|^2 + \frac{1}{2}\left(\alpha\frac{\partial}{\partial\alpha} + 1\right) + \frac{1}{2}\alpha^*\frac{\partial}{\partial\alpha^*} + \frac{1}{4}\frac{\partial^2}{\partial\alpha\partial\alpha^*}\right]\mathcal{W}\left(\alpha,\alpha^*\right) \\
&= -\mathrm{i}\omega_0\left[\alpha^*\frac{\partial}{\partial\alpha^*} - \alpha\frac{\partial}{\partial\alpha}\right]\mathcal{W}\left(\alpha,\alpha^*\right) + \frac{\lambda}{2}\left[\frac{\partial}{\partial\alpha}\alpha + \frac{\partial}{\partial\alpha^*}\alpha^* + \frac{\partial^2}{\partial\alpha\partial\alpha^*}\right]\mathcal{W}\left(\alpha,\alpha^*\right) \\
&= \left[\left(\mathrm{i}\omega_0 + \frac{\lambda}{2}\right)\frac{\partial}{\partial\alpha}\alpha - \left(\mathrm{i}\omega_0 - \frac{\lambda}{2}\right)\frac{\partial}{\partial\alpha^*}\alpha^* + \frac{\lambda}{2}\frac{\partial^2}{\partial\alpha\partial\alpha^*}\right]\mathcal{W}\left(\alpha,\alpha^*\right) \\
&= \left[\omega_0\left(\frac{\partial}{\partial p}q - \frac{\partial}{\partial q}p\right) + \frac{\lambda}{2}\left(\frac{\partial}{\partial q}q + \frac{\partial}{\partial p}p\right) + \frac{\lambda}{4}\left(\frac{1}{2}\frac{\partial^2}{\partial q^2} + \frac{1}{2}\frac{\partial^2}{\partial p^2}\right)\right]\mathcal{W}(q,p),
\end{aligned} \tag{1.92}$$

where in the last step, we have used $\alpha = q + \mathrm{i}p$ and $\partial_\alpha = \left(\partial_q - \mathrm{i}\partial_p\right)/2$ to emphasize the connection to a distribution on classical phase space. Observe how there is diffusion in both the spatial and the momentum coordinate. The corresponding stochastic differential equations are

$$\begin{aligned}
\mathrm{d}p &= -\omega_0 q\mathrm{d}t - \lambda p\mathrm{d}t/2 + \sqrt{\lambda/4}\,\mathrm{d}W_p, \\
\mathrm{d}q &= \quad \omega_0 p\mathrm{d}t - \lambda q\mathrm{d}t/2 + \sqrt{\lambda/4}\,\mathrm{d}W_q.
\end{aligned} \tag{1.93}$$

To bridge the gap to Sec. 1.4, we note here that the corresponding *classical* path integral is

$$\begin{aligned} S[p,q,\hat{p},\hat{q}] &= \int_{t_0}^{t} \mathrm{d}\bar{t}\, \left[\hat{p}\left(\dot{p} + w_0 q + \lambda p/2\right) + \hat{q}\left(\dot{q} - \omega_0 p + \lambda q/2\right) + \mathrm{i}\lambda\left(\hat{p}^2 + \hat{q}^2\right)/8\right] \\ &\equiv \int_{t_0}^{t} \mathrm{d}\bar{t}\, \left[\hat{\phi}^*\left(\mathrm{i}\partial_{\bar{t}} - \omega_0 + \mathrm{i}\lambda/2\right)\phi - \hat{\phi}\left(\mathrm{i}\partial_{\bar{t}} + \omega_0 - \mathrm{i}\lambda/2\right)\phi^* + \mathrm{i}\lambda\hat{\phi}^*\hat{\phi}\right], \end{aligned} \tag{1.94}$$

where the hats *do not* indicate operator-valuedness but label the response fields, and we have made the reverse transformation back to a complex representation according to

$$\begin{aligned} \phi &= \sqrt{2}\alpha = \sqrt{2}\left(q + \mathrm{i}p\right), \\ \hat{\phi} &= \frac{\mathrm{i}}{2}\frac{\hat{q} + \mathrm{i}\hat{p}}{\sqrt{2}}. \end{aligned} \tag{1.95}$$

In the terminology of 1.4.2, the path integral (1.94) has two response fields $z_1 = \hat{p}$ and $z_2 = \hat{q}$. Later on, we will see that it is both identical to the Schwinger-Keldysh path integral of the open single-mode cavity and the Martin-Siggia-Rose functional integral belonging to Eqs. (1.42).[16]

[16] This is actually no surprise, but still instructive.

CHAPTER 2

Non-Equilibrium Quantum Field Theory

The upcoming Chp. begins with an introduction to the Schwinger-Keldysh formalism and its relation to classical stochastic processes in Sec. 2.1. This is extended by a detailed illustration of the *two-particle-irreducible effective action* (2PIEA) as an approach to self-consistent perturbation theory in Sec. 2.2. Finally, we discuss the numerical solution of the so-called *Kadanoff-Baym equations* in Sec. 2.3.

2.1 Schwinger-Keldysh Formalism

When dealing with non-equilibrium quantum field theory (QFT), one necessarily encounters the question "What is the Schwinger-Keldysh formalism?", which we shall try to answer in the following. In recent years, with the growing interest in non-equilibrium phenomena, the technique has become more relevant. To properly put it into perspective, one should contrast it with QFT in particle physics, and with QFT in equilibrium.

The two classic authors on the subject are Schwinger [71] and Keldysh [72].[1] Schwinger describes the method rather sharply in terms of operators. Keldysh introduces the rotation to the more physical "RAK" representation which is named after him. There exist a number of review articles that are decent starting points for getting familiar with the technique. The first is the classic by Kubo [74] on the fluctuation-dissipation theorem in equilibrium, which can give a good motivation for the more general non-equilibrium problem. Ref. [11] is a good place to start: it derives the Keldysh path integral from a master equation and introduces the one-particle irreducible (1PI) effective action; it also treats the functional renormalization group. The two reviews by Berges [75, 76] are highly recommendable, although perhaps more advanced, as they are based on the *two-particle* irreducible effective action (2PIEA). They have detailed discussions of initial conditions and non-perturbative approximation techniques. Ref. [77] is an older piece that is possibly good for comparison and further reading, but mostly here for completeness.

Kamenev's book [56] is sort of the standard for the path-integral based approach. It gives another derivation of the path integral from a discrete-time expansion in terms of coherent states.

[1] A precursor to Ref. [71] is [73].

Among the applications are interacting Bose gases. It uses effective-action concepts without ever stating this clearly, which is a drawback, but has a relevant chapter on classical stochastics. The latest version of Altland & Simons's book [78] has a lot of material on field theory methods both for classical and quantum non-equilibrium problems, presented in two separate chapters. Their derivation of the Keldysh path integral is practically identical to Kamenev's, but there is further material that may provide a complementary perspective. Calzetta's book [79] is slightly cryptic when it comes to notation, but it has a very good chapter on Bose gases with a discussion of existing approaches (Φ-derivable, conserving and gapless approximations from 2PIEA). Rammer [61] is a reference work based solely on operators, for those who prefer that. It is very abstract, yet good for looking up identities and reading about general diagrammatics concepts. Stefanucci's book [80] is based on operators as well and derives everything in terms of the so-called *Langereth rules*. It is also strong on advanced diagrammatics.

The following two articles are about applications of the method to cold Bose gases. Ref. [81] is a good resource for an example of how the 2PIEA technique can be brought to bear on an actual problem. It also discusses the famous Hartree-Fock-Bogoliubov equations and their derivation. Ref. [82] is interesting because it compares classical and quantum dynamics from the perspective of the Schwinger-Keldysh path integral, showing how the cubic response-field vertex gives rise to the non-classical dynamics (this will be explained below).

Concerning the relation of master equation and Keldysh functional integral, Ref. [83] can be recommended. It contains a relatively detailed derivation of the "Markovian dissipative action" that is the functional equivalent of the Lindblad master equation in the usual Born-Markov approximation and is well suited for comparison to Schwinger's original treatment. Ref. [84] is an application where the method is used in a way close to the original style given by Schwinger, which puts the emphasis on the fact that at least for interacting systems the method is about the response of the system to a "sudden modulation".

The Schwinger-Keldysh path integral should not be discussed without relating it to classical non-equilibrium systems. Ref. [85] is the classic resource for the Martin-Siggia-Rose (MSR) functional integral, although [85] is based entirely on operators and the functional integral was introduced only later in [86] and [87]. The "response field" also occurring in the Keldysh formalism is introduced for classical systems, which provides an alternative approach to the Onsager-Machlup path integral (s. 1.4.2).

2.1.1 From Scattering Amplitudes to Expectation Values

In particle physics, the primary concern is to calculate transition amplitudes asymptotically [88]

$$S_{f\leftarrow i} = \langle \psi_f | \psi_i \rangle = \lim_{\substack{t\to+\infty \\ t_0\to-\infty}} \langle \psi_f(t) | \hat{S} | \psi_i(t_0) \rangle \,, \tag{2.1}$$

where $|\psi_i(t_0)\rangle$ is the initial state of the system, $|\psi_f(t)\rangle$ the final state, and $\hat{S}$ is the S-matrix

$$\hat{S} = \lim_{\substack{t\to+\infty \\ t_0\to-\infty}} \hat{U}\left(t, t_0\right) = \lim_{\substack{t\to+\infty \\ t_0\to-\infty}} \exp\left(-\mathrm{i}\hat{H}\left(t - t_0\right)\right) \tag{2.2}$$

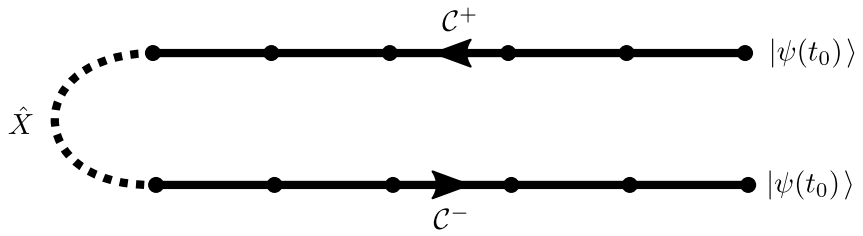

Figure 2.1: Schwinger-Keldysh contour.

In equilibrium, to calculate thermal expectation values, knowledge of the thermal density matrix

$$\hat{\rho} \propto \exp(-\beta \hat{H}) \tag{2.3}$$

is required. By treating the inverse temperature β as an imaginary time $\tau = it$, an operator analogous to (2.2) is obtained, from which point onwards standard QFT techniques carry over [77]. Neither of these approaches, however, pertains to the most general situations that may occur in a dynamical system. To capture the latter, one would like to be able to calculate time-dependent expectation values of an arbitrary operator [71]

$$\langle \hat{X}(t) \rangle = \langle \psi(t) | \hat{X} | \psi(t) \rangle = \langle \psi\,(t_0) | \,\hat{U}\,(t_0, t)\,\hat{X}\,\hat{U}(t, t_0)\,|\psi\,(t_0)\rangle \tag{2.4}$$

where now, notably, the initial and final state are identical.

2.1.2 Including Mixed States

Since we have to work with the full forward and backward evolution at any rate, we may just as well make the technique completely general and allow for mixed states to contribute to the above time-dependent expectation value. This can be achieved by calculating the latter via the density matrix,

$$\langle \hat{X}(t) \rangle = \mathrm{Tr}[\hat{\rho}\hat{X}(t)] = \mathrm{Tr}\left[\hat{\rho}\hat{U}\,(t_0, t)\,\hat{X}\,\hat{U}(t, t_0)\right] = \mathrm{Tr}\left[\hat{U}(t, t_0)\hat{\rho}\hat{U}\,(t_0, t)\,\hat{X}\right] = \mathrm{Tr}[\hat{\rho}(t)\hat{X}].$$

The Schwinger-Keldysh partition function is then

$$Z = \mathrm{Tr}[\hat{\rho}(t)] \stackrel{!}{=} 1. \tag{2.5}$$

By expanding the time-dependent density matrix into coherent states along the contour, a non-equilibrium path integral can be derived [11, 56, 78]. Upon turning Z into a generating functional, the expectation value can then be calculated. As shown in Fig. 2.1, this is how the closed time contour (CTP) arises. Note that the direction of time on the backward branch is indeed reversed: where before only the time-ordering operator $\mathcal{T}$ was required, there is now also an anti-time-ordering operator $\widetilde{\mathcal{T}}$. Furthermore, any point in time on the backward contour must be considered later than any point on the forward contour. On the level of Green functions, this means that,

instead of a single time-ordered Green function, there will now be four different Green functions

$$G(t,t') = -\mathrm{i}\langle \mathcal{T}_{\mathcal{C}}(\hat{a}(t)\hat{a}^\dagger(t'))\rangle = \begin{cases} G^T(t,t'), & t,\, t' \in \mathcal{C}^+ \\ G^{\tilde{T}}(t,t'), & t,\, t' \in \mathcal{C}^- \\ G^<(t,t'), & t \in \mathcal{C}^+,\, t' \in \mathcal{C}^- \\ G^>(t,t'), & t \in \mathcal{C}^-,\, t' \in \mathcal{C}^+, \end{cases}$$

where we have introduced contour time-ordering $\mathcal{T}_{\mathcal{C}}$. Defined in this way, $G(t,t')$ may also be written as

$$G(t,t') = -\mathrm{i}F(t,t') - \frac{1}{2}\,\mathrm{sign}_{\mathcal{C}}(t-t')\rho(t,t'), \tag{2.6}$$

with the statistical and spectral functions

$$\begin{aligned} F(t,t') &= \frac{1}{2}\langle\{a(t), a^\dagger(t')\}\rangle, \\ \rho(t,t') &= \mathrm{i}\langle[a(t), a^\dagger(t')]\rangle, \end{aligned} \tag{2.7}$$

respectively. We have also introduced the contour sign function $\mathrm{sign}_{\mathcal{C}}(t-t') = \theta_{\mathcal{C}}(t-t') - \theta_{\mathcal{C}}(t'-t)$. Another way of writing these functions is

$$\rho(t,t') = G^<(t,t') - G^>(t,t'), \tag{2.8}$$

$$F(t,t') = \frac{\mathrm{i}}{2}\left(G^<(t,t') + G^>(t,t')\right). \tag{2.9}$$

For closed systems, a convenient way of applying the formalism is to work out the Dyson equation for the time-ordered Green function, and then to replace time-ordering by contour time-ordering [76],

$$G_0^{-1}(t)G(t,t') = \delta_{\mathcal{C}}(t-t') + \int_{\mathcal{C}} \mathrm{d}\bar{t}\; \Sigma(t,\bar{t})G(\bar{t},t'). \tag{2.10}$$

Formally writing the contour integral as $\int_{\mathcal{C}} \mathrm{d}\bar{t} = \int_{t_0}^{\infty} \mathrm{d}\bar{t} + \int_{\infty}^{t_0} \mathrm{d}\bar{t}$, evaluating the contour sign functions under the integral, and separating the parts that are symmetric in contour-time difference $(t-t')$ from those that are anti-symmetric (proportional to $\mathrm{sign}_{\mathcal{C}}(t-t')$) then results in explicit equations of motion for $F(t,t')$ and $\rho(t,t')$. For the self-energy Σ, one uses a decomposition analogous to (2.6).

A more direct way of achieving the same thing in terms of the greater and lesser functions goes as follows (cf. Fig. 2.2). Fix the external times t, t' to the forward and backward branch, respectively, or vice versa. Expand the contour into three pieces,

$$\int_{\mathcal{C}} \mathrm{d}\bar{t} = \int_{t_0}^{\min(t,t')} \mathrm{d}\bar{t} + \int_{\min(t,t')}^{\max(t,t')} \mathrm{d}\bar{t} + \int_{\max(t,t')}^{t_0} \mathrm{d}\bar{t}, \tag{2.11}$$

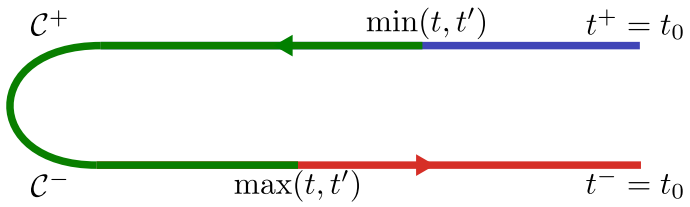

Figure 2.2: Schwinger-Keldysh contour for the greater and lesser Green functions $G^>$, $G^<$.

and apply the corresponding greater and lesser signs to Green function and self-energy [80]. The left-hand side of Eq. (2.10) contributes

$$\begin{aligned} \mathrm{i}\partial_t \left[\theta_\mathcal{C}\left(t-t'\right) G^>\left(t,t'\right) + \theta_\mathcal{C}\left(t'-t\right) G^<\left(t,t'\right)\right] &= \mathrm{i}\delta_\mathcal{C}\left(t-t'\right)\left[G^>(t,t) - G^<(t,t)\right] \\ &\quad + \theta_\mathcal{C}\left(t-t'\right)\mathrm{i}\partial_t G^>\left(t,t'\right) \\ &\quad + \theta_\mathcal{C}\left(t'-t\right)\mathrm{i}\partial_t G^<\left(t,t'\right), \end{aligned} \tag{2.12}$$

with $\mathrm{i}\left[G^>(t,t) - G^<(t,t)\right] = 1$. In total, one finds

$$\begin{aligned} G_0^{-1}(t)G^<(t,t') &= \int_{t_0}^{t} \mathrm{d}\bar{t}\, \Sigma^>(t,\bar{t})G^<(\bar{t},t') + \int_{t}^{t'} \mathrm{d}\bar{t}\, \Sigma^<(t,\bar{t})G^<(\bar{t},t') \\ &\quad + \int_{t'}^{t_0} \mathrm{d}\bar{t}\, \Sigma^<(t,\bar{t})G^>(\bar{t},t'), \\ G_0^{-1}(t)G^>(t,t') &= \int_{t_0}^{t'} \mathrm{d}\bar{t}\, \Sigma^>(t,\bar{t})G^<(\bar{t},t') + \int_{t'}^{t} \mathrm{d}\bar{t}\, \Sigma^>(t,\bar{t})G^>(\bar{t},t') \\ &\quad + \int_{t}^{t_0} \mathrm{d}\bar{t}\, \Sigma^<(t,\bar{t})G^>(\bar{t},t'). \end{aligned} \tag{2.13}$$

To get an idea of how the equations of motion in "center-of-mass" time T look like, consider Eq. (5.52).

2.1.3 Open Systems

The equations we have derived so far do not depend on G^T and $G^{\tilde{T}}$, but only on $G^<$ and $G^>$ or, equivalently, on F and ρ. This already goes beyond equilibrium physics, where only the spectral function is relevant, while the analog of the statistical function is fixed to either the Bose or Fermi distribution. The missing dependence on G^T and $G^{\tilde{T}}$ enters once we make the system open. It is possible to argue that this does not, in fact, correspond to a situation more general than for closed systems, since any so-called "open" system can be made into a closed one by restoring the coupling to the reservoir, the removal of which yielded the open-system dynamics in the first place. Yet in practice, (almost) all systems are at least weakly open, and it is certainly hardly ever possible to study the full system including the reservoir.

Schwinger, in his typical style, asks the reader to "imagine that the positive and negative senses

of time development are governed by different dynamics" [71]. In which physical situations will this be realized? It turns out that the most straightforward cases one can think of are open systems. As an example, take a single cavity mode of frequency ω_0, coupled to an environment at a low temperature, such that $\hbar\omega_0 \gg \beta^{-1}$. Semi-classically, this can be modelled by making the Hamiltonian non-Hermitian [89],

$$\hat{H} = (\omega_0 - \mathrm{i}\lambda/2)\, a^\dagger a. \tag{2.14}$$

The corresponding evolution operator $\hat{U}$ is now no longer unitary, that is, it describes a situation as envisaged by Schwinger. To have a proper microscopic description where probability is conserved, it is necessary to include so-called *quantum jumps* into the description. This can be done by working with the Lindblad master equation

$$\partial_t \hat{\rho} = -\mathrm{i}\left[\hat{H}\hat{\rho} - \hat{\rho}\hat{H}^\dagger\right] + \lambda a \hat{\rho} a^\dagger \tag{2.15}$$

In its most general formulation as given by Schwinger, the formalism easily captures this kind of dynamics. The Schwinger action that appears in the coherent-state expansion of the non-equilibrium partition function Z is [11]

$$S[\phi^*_\pm, \phi_\pm] = \int_{t_0}^{t} \mathrm{d}\bar{t} \left[\phi^*_+ \left(\mathrm{i}\partial_{\bar{t}} - \omega_0 + \mathrm{i}\lambda/2\right)\phi_+ - \phi^*_- \left(\mathrm{i}\partial_{\bar{t}} - \omega_0 - \mathrm{i}\lambda/2\right)\phi_- - \mathrm{i}\lambda\phi_+\phi^*_-\right]. \tag{2.16}$$

Note how this contains a contribution across the two branches of the contour. The respective equations of motion for the greater and lesser Green functions are then

$$\begin{aligned} 0 &= \left(\mathrm{i}\partial_t - \omega_0 + \mathrm{i}\lambda/2\right) G^<(t,t'), \\ 0 &= \left(\mathrm{i}\partial_t - \omega_0 - \mathrm{i}\lambda/2\right) G^>(t,t') + \mathrm{i}\lambda G^T(t,t'), \end{aligned} \tag{2.17}$$

where now the time-ordered Green function appears explicitly. The anti-time-ordered Green function would appear, for instance, when coupling to a bath at finite temperature. In the equal-time limit, these equations become

$$\begin{aligned} \partial_t G^<(t,t) &= -\lambda G^<(t,t), \\ \partial_t G^>(t,t) &= \lambda G^>(t,t) - \lambda\left[G^T(t,t) + G^{\tilde{T}}(t,t)\right] \\ &= \lambda G^>(t,t) - \lambda\left[G^>(t,t) + G^<(t,t)\right], \end{aligned} \tag{2.18}$$

which essentially serves to illustrate how the commutator is preserved over time by the quantum jumps.

2.1.4 Keldysh Rotation

Shortly after Schwinger, Keldysh independently gave an alternative formulation of the technique [72]. It is based on an identity involving all of the four Green functions introduced above,

$$G^T(t,t') + G^{\tilde{T}}(t,t') - \left(G^>(t,t') + G^<(t,t')\right) = 0, \tag{2.19}$$

which we have already employed in Eq. (2.18). This suggests defining a new set of Green functions according to the transformation

$$\begin{pmatrix} 0 & G^A \\ G^R & G^K \end{pmatrix} = \frac{1}{2}\begin{pmatrix} 1 & -1 \\ 1 & 1 \end{pmatrix}\begin{pmatrix} G^T & G^< \\ G^> & G^{\tilde{T}} \end{pmatrix}\begin{pmatrix} 1 & 1 \\ -1 & 1 \end{pmatrix}, \tag{2.20}$$

where in the top left corner, Eq. (2.19) comes to bear. The retarded, advanced, and Keldysh (R, A, and K) Green functions are related to Schwinger's representation by

$$\begin{aligned} G^R(t,t') &= -\theta(t-t')\left(G^<(t,t') - G^>(t,t')\right) = -\theta(t-t')\rho(t,t'), \\ G^A(t,t') &= \quad\theta(t'-t)\left(G^<(t,t') - G^>(t,t')\right) = \quad\theta(t'-t)\rho(t,t'), \\ G^K(t,t') &= G^<(t,t') + G^>(t,t') = -2\mathrm{i}F(t,t'). \end{aligned} \tag{2.21}$$

Within the path integral, the same transformation is effected by letting [56]

$$\phi_\pm = \frac{1}{\sqrt{2}}(\phi \pm \hat{\phi}), \tag{2.22}$$

where ϕ is related to the classical field, and $\hat{\phi}$ is the so-called response field.[2] It has the property $\langle\hat{\phi}\rangle = 0$. The transformed Keldysh action reads

$$S_{\text{Keldsyh}}[\phi^*,\phi,\hat{\phi}^*,\hat{\phi}] = \int_{t_0}^{t} \mathrm{d}\bar{t}\ \left[\hat{\phi}^*\left(\mathrm{i}\partial_{\bar{t}} - \omega_0 + \mathrm{i}\lambda/2\right)\phi + \phi^*\left(\mathrm{i}\partial_{\bar{t}} - \omega_0 + \mathrm{i}\lambda/2\right)\hat{\phi} + \mathrm{i}\lambda\hat{\phi}^*\hat{\phi}\right]. \tag{2.23}$$

Pay attention to the fact that this is identical to the classical path integral of Eq. (1.94) up to an integration by parts.

2.1.5 MSR Path Integral from Wigner Representation

As mentioned above, Martin, Siggia, and Rose (MSR) gave an operator formalism for treating classical stochastic systems [85]. The respective path-integral approach was subsequently published

[2] In most texts, the field ϕ is written as ϕ_c and called the "classical" field. However, when expanding an interacting field theory perturbatively, ϕ may acquire corrections that displace it from the trivial saddle-point Φ. Since the latter corresponds to the classical configuration, it seems more appropriate to call Φ the classical field. The response field is usually denoted by ϕ_q and called "quantum" field. Since it exists fully analogously in the classical case, this is, however, somewhat misleading.

by Janssen and De Dominicis [86, 87]. A great merit of the Keldysh representation is that it relates in a simple way to these classical counterparts. For certain special cases, such as the above example of the open single-mode cavity, there is a complete equivalence, such as for the Wigner representation of the master equation (2.15) which was found to be

$$\dot{\mathcal{W}}\left(\phi,\phi^*\right) = \left[\left(\mathrm{i}\omega_0 + \frac{\lambda}{2}\right)\frac{\partial}{\partial\phi}\phi - \left(\mathrm{i}\omega_0 - \frac{\lambda}{2}\right)\frac{\partial}{\partial\phi^*}\phi^* + \lambda\frac{\partial^2}{\partial\phi\partial\phi^*}\right]\mathcal{W}\left(\phi,\phi^*\right). \tag{2.24}$$

The MSR action of this Fokker-Planck equation reads

$$S_{\mathrm{MSR}}[\phi^*,\phi,\hat{\phi}^*,\hat{\phi}] = \int_{t_0}^{t}\mathrm{d}\bar{t}\,\left[\hat{\phi}^*\left(\mathrm{i}\partial_{\bar{t}} - \omega_0 + \mathrm{i}\lambda/2\right)\phi - \hat{\phi}\left(\mathrm{i}\partial_{\bar{t}} + \omega_0 - \mathrm{i}\lambda/2\right)\phi^* + \mathrm{i}\lambda\hat{\phi}^*\hat{\phi}\right], \tag{2.25}$$

which is indeed the same as Eq. (1.94) and becomes identical to S_{Keldsyh} after an integration by parts (assuming the response field vanishes at the boundaries). Naturally, this analogy does not continue to hold for more complicated systems. Remember that a Hubbard-like interaction $H_{\mathrm{int}} = ga^\dagger a^\dagger aa$ produces an equation for the Wigner distribution that includes derivatives of higher than second order and hence is not of Fokker-Planck type. Accordingly, in the Keldysh action, non-classical vertices of the form $g\phi^*\hat{\phi}^*\hat{\phi}\hat{\phi}$ appear, which carries three response fields and is hence no longer Gaussian in these fields. For a further discussion of these vertices, see Ref. [82].

2.1.6 Vertical Branch of the Contour

This paragraph is a brief discussion of the approximation of a system's past represented by the vertical branch that one finds frequently attached to the closed time contour [32, 80]. In an interacting system (and only there), the dynamics is inherently non-Markovian. One can see this from the memory integrals in the slave-particle dynamics coming in Chp. 5 of this thesis, for instance. The only exception to this is Hartree-Fock, which in this sense is a "Markovian" approximation. When one initializes a non-equilibrium problem with some boundary condition for the Green functions, the memory integrals over the past are still zero - they will build up only after the system has started to evolve. This essentially means that one is pretending that the system was not interacting up to the point where the simulation starts. The inclusion of the vertical branch is an attempt at correcting for this, yet this can only be an approximation to the true situation where one would wait until a steady-state is reached (which in certain problems is very expensive), then disturb the system and study the relaxation.

2.2 Two-Particle-Irreducible Effective Action

The two-particle-irreducible effective action (2PIEA) is a well-defined approach to self-consistent perturbation theory. Originally, the technique goes back to Cornwall, Jackiw and Tomboulis [90]. A standard book on the subject can be found in Ref. [91]. What is self-consistency and why is it desirable? As explained in the classic article by Baym and Kadanoff [92], it is important for

any perturbative approximation to adhere to the conservation laws inherent to the theory under consideration. This can be achieved by deriving the self-energy from a so-called Φ-*functional*, and the 2PIEA provides a systematic way of constructing such functionals [79]. In the resulting Dyson equation, the self-energy then depends on the full Green function instead of the bare one, which gives rise to self-consistency. For time-dependent non-equilibrium problems, Ref. [75] provides another good reason for why a resummed perturbative approximation is superior to bare perturbation theory: infinite resummation of so-called *secular terms* ensures a *uniform* approximation of the exact solution, that is, the order of the error does not grow over time. As for two-particle-irreducibility, it is shown by Rammer [93] how resumming self-energy insertions into dressed self-energies has the effect that the resulting skeleton diagrams are 2PI. This must be so in order to avoid over-counting of diagrams that are already taken into account implicitly via the resummation. In a closely related manner, Berges [76] proves by contradiction that if the dressed self-energy is to be one-particle-irreducible (1PI), as we know it should be, then the effective action must only contain 2PI diagrams. In this Chp., we shall recapitulate how the resummation of bare propagators leads to a self-consistent generating functional and to the cancellation of one-particle-reducible (1PR) diagrams by deriving the two-loop expansion of a ϕ^4 theory.

2.2.1 Two-Loop Expansion

For the detailed derivation of the 2PIEA to two-loop order, we follow Ref. [94] conceptually, although we depart from its template on several occasions. Further interesting discussions of nPI techniques in general can be found in [95–99]. Throughout this Sec., the variable x will denote both time and space: $x \equiv (t, \mathbf{x})$. The starting point of our derivation is the *cumulant-generating functional*, which is defined as

$$W[j,K] := -\mathrm{i}\hbar \ln \int \mathcal{D}\phi \exp\left\{\frac{\mathrm{i}}{\hbar}\left[S[\phi] + \int \mathrm{d}\bar{x}\; j(\bar{x})\phi(\bar{x}) + \frac{1}{2}\int \mathrm{d}\bar{x}\mathrm{d}\bar{x}'\; \phi(\bar{x})K(\bar{x},\bar{x}')\phi(\bar{x}')\right]\right\}, \tag{2.26}$$

where we have introduced the one-point and two-point external sources $j(x)$ and $K(x,y)$. The *classical* field $\Phi(x)$ is obtained as the solution to

$$0 = \frac{\delta S[\Phi]}{\delta \Phi} + j(x) + \int \mathrm{d}\bar{x}\; \Phi(\bar{x})K(\bar{x},x), \tag{2.27}$$

assuming a symmetric kernel $K(x,y) = K(y,x)$. We furthermore introduce the inverse Green function

$$G_0^{-1}(x,y) := -\mathrm{i}\left[\frac{\delta^2 S[\Phi]}{\delta\Phi(x)\delta\Phi(y)} + K(x,y)\right]. \tag{2.28}$$

The field ϕ is now decomposed into classical field and fluctuations as

$$\phi(x) = \Phi(x) + \sqrt{\hbar}\delta\phi(x). \tag{2.29}$$

To have a specific example to work with, we pick the Onsager-Machlup-like action

$$S[\phi] = \int \mathrm{d}\bar{x} \left\{ \frac{1}{D} \left(\frac{\dot{\phi}(\bar{x})}{2} \right)^2 - \frac{m^2}{2}\phi^2(\bar{x}) - \frac{g}{4!}\phi^4(\bar{x}) \right\}, \tag{2.30}$$

where for brevity we have dropped spatial derivatives. The first step of the loop expansion is to develop the cumulant-generating functional into a power series in $\hbar$,

$$W[j,K] = W^{(0)}[j,K] + W^{(1)}[j,K] + W^{(2)}[j,K] + \mathcal{O}(\hbar^3), \tag{2.31}$$

where to lowest order

$$\begin{aligned} W^{(0)}[j,K] &= -\mathrm{i}\hbar \ln \exp\left\{ \frac{\mathrm{i}}{\hbar} \left[S[\Phi] + \int \mathrm{d}\bar{x}\; j(\bar{x})\Phi(\bar{x}) + \frac{1}{2}\int \mathrm{d}\bar{x}\mathrm{d}\bar{x}'\; \Phi(\bar{x})K(\bar{x},\bar{x}')\Phi(\bar{x}') \right] \right\} \\ &= S[\Phi] + \int \mathrm{d}\bar{x}\; j(\bar{x})\Phi(\bar{x}) + \frac{1}{2}\int \mathrm{d}\bar{x}\mathrm{d}\bar{x}'\; \Phi(\bar{x})K(\bar{x},\bar{x}')\Phi(\bar{x}'). \end{aligned}$$

Expanding our action around the classical field for small fluctuations, we find

$$\begin{aligned} S[\Phi+\delta\phi] = \int \mathrm{d}\bar{x} \Bigg\{ & \frac{1}{D}\left[\left(\dot{\Phi}(\bar{x})/2\right)^2 + \hbar\left(\delta\dot{\phi}(\bar{x})/2\right)^2 + \frac{1}{2}\sqrt{\hbar}\dot{\Phi}\delta\dot{\phi} \right] \\ & - \frac{m^2}{2}\left[\Phi^2 + \hbar\delta\phi^2 + 2\sqrt{\hbar}\Phi\delta\phi \right] \\ & - \frac{g}{4!}\left[\Phi^4 + 4\sqrt{\hbar}\Phi^3\delta\phi + 6\hbar\Phi^2\delta\phi^2 + 4\hbar\sqrt{\hbar}\Phi\delta\phi^3 + \hbar^2\delta\phi^4 \right] \Bigg\} \\ = S[\Phi] + S[\hbar^{1/2}\delta\phi] & - \hbar^{1/2}\int \mathrm{d}\bar{x}\; \left\{ \frac{1}{2D}\ddot{\Phi}\delta\phi + m^2\Phi\delta\phi + \frac{g}{3!}\Phi^3\delta\phi \right\} \\ & - \hbar\frac{g}{4}\int \mathrm{d}\bar{x}\; \Phi^2\delta\phi^2 - \hbar^{3/2}\frac{g}{3!}\int \mathrm{d}\bar{x}\; \Phi\delta\phi^3, \end{aligned} \tag{2.32}$$

where we have integrated by parts in the second step. The derivative of our example action is

$$\begin{aligned} \frac{\delta S[\Phi]}{\delta\Phi(x)} &= \int \mathrm{d}\bar{x}\; \left\{ \frac{1}{4D}\frac{\delta}{\delta\Phi(x)}\dot{\Phi}(\bar{x})\dot{\Phi}(\bar{x}) \right\} - m^2\Phi(x) - \frac{g}{3!}\Phi^3(x) \\ &= -\frac{1}{2D}\int \mathrm{d}\bar{x}\; \left\{ \ddot{\Phi}(\bar{x})\delta(x-\bar{x}) \right\} - m^2\Phi(x) - \frac{g}{3!}\Phi^3(x) \\ &= -\frac{1}{2D}\ddot{\Phi}(x) - m^2\Phi(x) - \frac{g}{3!}\Phi^3(x), \end{aligned} \tag{2.33}$$

which we recognize in the curly brackets after the second equality in Eq. (2.32). We can now define

$$\Delta W[j,K] := W[j,K] - W^{(0)}[j,K] = \text{const.} - \mathrm{i}\hbar \ln \int \mathcal{D}\delta\phi \, \exp\left\{\mathrm{i}S_{\text{eff}}/\hbar\right\}, \tag{2.34}$$

with the constant absorbing the Jacobian determinant from the change of variables (2.29). The action in the exponential is given by

$$\begin{aligned} S_{\text{eff}} &= S[\hbar^{1/2}\delta\phi] - \hbar\frac{g}{4}\int \mathrm{d}\bar{x}\ \Phi^2\delta\phi^2 - \hbar^{3/2}\frac{g}{3!}\int \mathrm{d}\bar{x}\ \Phi\delta\phi^3 \\ &\quad + \frac{\hbar}{2}\int \mathrm{d}\bar{x}\ \mathrm{d}\bar{x}'\ \delta\phi(\bar{x})K(\bar{x},\bar{x}')\delta\phi(\bar{x}') \\ &\quad + \hbar^{1/2}\int \mathrm{d}\bar{x}\ \delta\phi(\bar{x})\underbrace{\left(\frac{\delta S[\Phi]}{\delta\Phi(x)} + j(\bar{x}) + \int \mathrm{d}\bar{x}'\ \Phi(\bar{x}')K(\bar{x}',\bar{x})\right)}_{=0} \\ &= S_0[\delta\phi,\Phi,K] - \hbar^{3/2}\frac{g}{3!}\int \mathrm{d}\bar{x}\ \Phi\delta\phi^3 - \hbar^2\frac{g}{4!}\int \mathrm{d}\bar{x}\ \delta\phi^4, \end{aligned} \tag{2.35}$$

where we have used Eq. (2.27) and introduced

$$\begin{aligned} S_0[\delta\phi,\Phi,K]/\hbar = S[\delta\phi] &+ \frac{g}{4!}\int \mathrm{d}\bar{x}\ \delta\phi^4 - \frac{g}{4}\int \mathrm{d}\bar{x}\ \Phi^2\delta\phi^2 \\ &+ \frac{1}{2}\int \mathrm{d}\bar{x}\ \mathrm{d}\bar{x}'\ \delta\phi(\bar{x})K(\bar{x},\bar{x}')\delta\phi(\bar{x}'). \end{aligned} \tag{2.36}$$

To keep track of terms, note that since we pulled out the quartic fluctuations from $S[\hbar^{1/2}\delta\phi]$ in Eq. (2.35), here we have to add them constructively. The classical field Φ and the two-point source K act as additional mass terms for the fluctuations. To two-loop order, that is, to $\mathcal{O}(\hbar^2)$, expanding the exponential, performing the Gaussian integral, and introducing expectation values[3] then yields

$$\begin{aligned} \Delta W[j,K] &\approx -\mathrm{i}\hbar \ln \int \mathcal{D}\delta\phi\ \exp\left\{\frac{\mathrm{i}}{\hbar}S_0[\delta\phi,\Phi,K]\right\}\left[1 - \mathrm{i}\left(\frac{g}{\hbar}\right)\int \mathrm{d}\bar{x}\ \left\{\frac{\hbar^{3/2}}{3!}\Phi\delta\phi^3 + \frac{\hbar^2}{4!}\delta\phi^4\right\}\right. \\ &\qquad \left. - \frac{1}{2}\left(\frac{g}{\hbar}\right)^2\int \mathrm{d}\bar{x}\mathrm{d}\bar{x}'\frac{\hbar^3}{(3!)^2}\Phi(\bar{x})\delta\phi^3(\bar{x})\Phi(\bar{x}')\delta\phi^3(\bar{x}')\right] \\ &= -\mathrm{i}\hbar\ln\left\{\left(\det G_0^{-1}\right)^{-1/2}\left[1 - \hbar\left(\mathrm{i}g\int\frac{\mathrm{d}\bar{x}}{4!}\ \langle\delta\phi^4(\bar{x})\rangle\right.\right.\right. \\ &\quad \left.\left.\left. + \frac{g^2}{2}\int\frac{\mathrm{d}\bar{x}}{3!}\frac{\mathrm{d}\bar{x}'}{3!}\ \Phi(\bar{x})\Phi(\bar{x}')\langle\delta\phi^3(\bar{x})\delta\phi^3(\bar{x}')\rangle\right)\right]\right\} \approx W^{(1)}[j,K] + W^{(2)}[j,K], \end{aligned}$$

[3] To do this, we also have to divide by the normalization $\left(\det G_0^{-1}\right)^{-1/2}$, which consequently appears as an overall factor inside the logarithm.

n	1	2	3	4
$\hbar(\hbar^{-1}g\hbar^{3/2}\Phi\delta\phi^3)^n$		$g^2\hbar^2$		$g^4\hbar^3$
$\hbar(\hbar^{-1}g\hbar^2\delta\phi^4)^n$	$g\hbar^2$	$g^2\hbar^3$	$g^3\hbar^4$	$g^4\hbar^5$

Table 2.1: An overview of the orders of expansion arising from the effective ϕ^3 and the ϕ^4 vertex. The outer factor of $\hbar$ is the overall factor in front of the logarithm in W. The inner factor of $\hbar^{-1}$ is the one multiplying the action in the exponent. The remaining factors of $\hbar^{1/2}$ stem from the fluctuating fields. We have ignored any further conventional factors multiplying the respective vertices (such as $1/4!$). In Chp. 5, we are going to work with a loop expansion of order $\hbar^2$ that is first order in certain couplings yet second order in another.

where a constant (from Gaussian integration) and the "skewness" $\langle\delta\phi^3\rangle$ were dropped, and

$$\begin{aligned} W^{(1)}[j,K] &= -\mathrm{i}\hbar\ln\left(\det G_0^{-1}\right)^{-1/2} = \frac{\mathrm{i}\hbar}{2}\operatorname{Tr}\ln G_0^{-1}, \\ W^{(2)}[j,K] &= \mathrm{i}\hbar^2\Bigg\{\mathrm{i}g\int\frac{\mathrm{d}\bar{x}}{4!}\,3\langle\delta\phi^2(\bar{x})\rangle^2 \\ &+\frac{g^2}{2}\int\frac{\mathrm{d}\bar{x}}{3!}\frac{\mathrm{d}\bar{x}'}{3!}\,\Phi(\bar{x})\Phi(\bar{x}')\Big[9\langle\delta\phi^2(\bar{x})\rangle\langle\delta\phi(\bar{x})\delta\phi(\bar{x}')\rangle\langle\delta\phi^2(\bar{x}')\rangle + 6\langle\delta\phi(\bar{x})\delta\phi(\bar{x}')\rangle^3\Big]\Bigg\}. \end{aligned} \tag{2.37}$$

We expanded the logarithm to first order only since in this particular expansion we do not have to account for the cancellation of disconnected diagrams.[4] Diagrammatically, $W^{(2)}$ is expressed as

$$-\frac{\mathrm{i}}{\hbar^2}W^{(2)} \equiv \frac{\mathrm{i}g}{4!}\times 3\times$$ 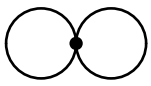 $$+\frac{g^2}{2\cdot(3!)^2}\times\Big[9\times$$ 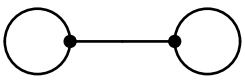 $$+6\times$$ 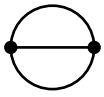 $$\Big],$$

(2.38)

where the lines yet signify the *bare* Green function G_0 and the three- and four-point vertices are *classical*.[5] Tab. 2.1 gives a summary of the different orders of $\hbar$ and g arising in loop and coupling expansions.

[4] This would be necessary, e.g. if we expanded the exponential to second order in g: the integral $\int\mathrm{d}\bar{x}\mathrm{d}\bar{x}'\,\langle\delta\phi^4(\bar{x})\delta\phi^4(\bar{x}')\rangle$ would then have to be accompanied by the corresponding terms from the expansion of the logarithm, $\int\mathrm{d}\bar{x}\mathrm{d}\bar{x}'\,\langle\delta\phi^4(\bar{x})\rangle\langle\delta\phi^4(\bar{x}')\rangle$.

[5] It is easy to commit an error in the prefactor entering the self-energy at the end of the calculation. To avoid this, we summarize the relevant contributions. For a Hartree-Fock self-energy, $W^{(2)}$ comes with a factor of $\mathrm{i}\hbar^2\cdot\mathrm{i}g$ (this ignores any further conventional factors like $1/4!$ as in this Chp. or $1/2$ as for cold Bose gases). When going over to $\Gamma^{(2)}$, this is complemented by a factor of i^2 that comes from converting the expectation values of the fluctuating fields into Green functions. Together with the factor of $2\mathrm{i}$ that enters when turning the derivative of $\Gamma^{(2)}$ with respect to the Green function into the self-energy, this means a Hartree-Fock self-energy ends up with a factor of $2\mathrm{i}\hbar^2 g$. To second order for a theory of type ϕ^3 (which is the relevant case for Chp. 5), the same considerations start with a factor $\mathrm{i}\hbar^2\cdot g^2/2$, which is then complemented by a factor of i^3, such that we finally have $2\mathrm{i}\cdot(-\mathrm{i})\cdot\mathrm{i}\hbar^2\cdot g^2/2 = \mathrm{i}\hbar^2 g^2$.

2.2.2 Effective Action

The average field or *first cumulant* $\langle\phi(x)\rangle \equiv \varphi(x)$ is defined as the derivative of the cumulant-generating functional with respect to the one-point source,

$$\varphi(x) := \frac{\delta W[j,K]}{\delta j(x)} = \exp\left\{-\mathrm{i}W[j,K]/\hbar\right\} \int \mathcal{D}\phi\ \phi(x) \exp\left\{\frac{\mathrm{i}}{\hbar}\left[S[\phi] + j^T\phi + \frac{1}{2}\phi^T K\phi\right]\right\}, \tag{2.39}$$

where we have employed a common shorthand notation in the exponent. This field is to be distinguished from the classical field $\Phi(x)$. Furthermore, we define the *second cumulant*

$$\begin{aligned} G(x,y) := -\frac{\delta^2 W[j,K]}{\delta j(x)\delta j(y)} &= \left[\frac{\mathrm{i}}{\hbar}\frac{\delta W[j,K]}{\delta j(y)} \int \mathcal{D}\phi\ \phi(x) \exp\left\{\frac{\mathrm{i}}{\hbar}\left[S[\phi] + j^T\phi + \frac{1}{2}\phi^T K\phi\right]\right\}\right. \\ &\left. - \frac{\mathrm{i}}{\hbar}\int \mathcal{D}\phi\ \phi(x)\phi(y) \exp\left\{\frac{\mathrm{i}}{\hbar}\left[S[\phi] + j^T\phi + \frac{1}{2}\phi^T K\phi\right]\right\}\right] \exp\left\{-\mathrm{i}W[j,K]/\hbar\right\} \\ &= -\frac{\mathrm{i}}{\hbar}\left[\langle\phi(x)\phi(y)\rangle - \langle\phi(x)\rangle\langle\phi(y)\rangle\right]. \end{aligned} \tag{2.40}$$

The functional derivative with respect to the kernel gives

$$\frac{\delta W[j,K]}{\delta K(x,y)} = \langle\phi(x)\phi(y)\rangle, \tag{2.41}$$

from which we deduce the alternative expression

$$G(x,y) = -\frac{\mathrm{i}}{\hbar}\left[\frac{\delta W[j,K]}{\delta K(x,y)} - \varphi(x)\varphi(y)\right]. \tag{2.42}$$

The *effective action* Γ is now defined as the double *Legendre transform* of the cumulant-generating functional:

$$\begin{aligned} \Gamma[\varphi,G] := W[j[\varphi,G],K[\varphi,G]] &- \int \mathrm{d}\bar{x}\ j(\bar{x})\varphi(\bar{x}) \\ &- \frac{1}{2}\int \mathrm{d}\bar{x}\mathrm{d}\bar{x}'\ K(\bar{x},\bar{x}')\left[\mathrm{i}\hbar G(\bar{x},\bar{x}') + \varphi(\bar{x})\varphi(\bar{x}')\right], \end{aligned} \tag{2.43}$$

where j and K as functions of φ and G are given implicitly via

$$\begin{aligned} \frac{\delta\Gamma[\varphi,G]}{\delta\varphi(x)} &= -j(x) - \int \mathrm{d}\bar{x}\ K(x,\bar{x})\varphi(\bar{x}), \\ \frac{\delta\Gamma[\varphi,G]}{\delta G(x,y)} &= -\frac{\mathrm{i}\hbar}{2}K(x,y). \end{aligned} \tag{2.44}$$

2.2.3 Legendre Transformation

The next step is the crucial one in the procedure: we need to remove the dependence of W on j and K in favor of φ and G. It is, however, not possible to solve (2.44) for j and K directly. Yet one can see that W does not depend on these explicitly, but merely implicitly through Φ and G_0 [94]. Hence, if we could express the latter two in terms of the new variables φ and G, the problem would be solved. Since we are expanding perturbatively in $\hbar$, a series expansion will suffice. As a first step, we expand the new variables in terms of the classical field and bare propagator,

$$\begin{aligned}\varphi[\Phi, G_0] &= \varphi^{(0)}[\Phi, G_0] + \varphi^{(1)}[\Phi, G_0] + \mathcal{O}(\hbar^2),\\ G[\Phi, G_0] &= G^{(0)}[\Phi, G_0] + G^{(1)}[\Phi, G_0] + \mathcal{O}(\hbar^2).\end{aligned} \tag{2.45}$$

Calculating this expansion order by order, we find first that

$$\varphi^{(0)}(x) = \frac{\delta W^{(0)}[j,K]}{\delta j(x)} = \Phi(x). \tag{2.46}$$

From Eq. (2.27), one also has

$$\frac{\delta^2 S[\Phi]}{\delta\Phi(x)\Phi(y)} = -\frac{\delta j(y)}{\delta\Phi(x)} - K(x,y) - \int \mathrm{d}\bar{x}\ \Phi(\bar{x})\frac{\delta K(\bar{x},y)}{\delta\Phi(x)}, \tag{2.47}$$

from which one finds

$$\begin{aligned}G^{(0)}(x,y) &= -\frac{\delta^2 W^{(0)}[j,K]}{\delta j(x)\delta j(y)} = -\frac{\delta\Phi(x)}{\delta j(y)} = -\left(\frac{\delta j(y)}{\delta\Phi(x)}\right)^{-1}\\ &= \left[\frac{\delta^2 S[\Phi]}{\delta\Phi(x)\delta\Phi(y)} + K(x,y)\right]^{-1} = -\mathrm{i}G_0(x,y),\end{aligned} \tag{2.48}$$

where one should prove explicitly that K does not depend on the classical field. This completes the lowest order. To first order, we have

$$\begin{aligned}\varphi^{(1)}(x) &= \frac{\delta W^{(1)}[j,K]}{\delta j(x)} = \frac{\mathrm{i}\hbar}{2}\frac{\delta}{\delta j(x)}\mathrm{Tr}\ln G_0^{-1} = \frac{\mathrm{i}\hbar}{2}\int \mathrm{d}\bar{x}\ \frac{\delta}{\delta j(x)}\ln G_0^{-1}(\bar{x},\bar{x})\\ &= \frac{\mathrm{i}\hbar}{2}\int \mathrm{d}\bar{x}\mathrm{d}\bar{y}\ G_0(\bar{x},\bar{y})\frac{\delta}{\delta j(x)}G_0^{-1}(\bar{y},\bar{x})\\ &= \frac{\mathrm{i}\hbar}{2}\int \mathrm{d}\bar{x}\mathrm{d}\bar{y}\mathrm{d}\bar{z}\ G_0(\bar{x},\bar{y})\frac{\delta G_0^{-1}(\bar{y},\bar{x})}{\delta\Phi(\bar{z})}\frac{\delta\Phi(\bar{z})}{\delta j(x)}\\ &= \frac{\hbar}{2}\int \mathrm{d}\bar{x}\mathrm{d}\bar{y}\mathrm{d}\bar{z}\ G_0(\bar{x},\bar{y})\left[\frac{\delta^3 S[\Phi]}{\delta\Phi(\bar{z})\delta\Phi(\bar{y})\delta\Phi(\bar{x})} + \frac{\delta K(\bar{y},\bar{x})}{\delta\Phi(\bar{z})}\right]\frac{\delta^2 W^{(0)}[j,k]}{\delta j(\bar{z})\delta j(x)}\\ &= \frac{\hbar}{2}\int \mathrm{d}\bar{x}\mathrm{d}\bar{y}\mathrm{d}\bar{z}\ G_0(\bar{x},\bar{y})\frac{\delta^3 S[\Phi]}{\delta\Phi(\bar{z})\delta\Phi(\bar{y})\delta\Phi(\bar{x})}\mathrm{i}G_0(\bar{z},x),\end{aligned} \tag{2.49}$$

where we have used the formula for the derivative of a matrix logarithm from App. A.3, and have replaced $G^{(0)}$ by $-\mathrm{i}G_0$ in the last line. In terms of our exemplary Onsager-Machlup action, one obtains [6]

$$\begin{aligned}\frac{\delta^3 S[\Phi]}{\delta\Phi(x)\delta\Phi(y)\delta\Phi(z)} &= -\frac{g}{3!}\frac{\delta}{\delta\Phi(x)\delta\Phi(y)}\Phi^3(z) = -g\delta(x-z)\delta(y-z)\Phi(z),\\ \varphi^{(1)}(x) &= -\mathrm{i}\frac{g\hbar}{2}\int \mathrm{d}\bar{z}\; G_0(\bar{z},\bar{z})\Phi(\bar{z})G_0(\bar{z},x).\end{aligned} \tag{2.50}$$

The remaining first-order correction to the Green function is

$$\begin{aligned}G^{(1)}(x,y) &= -\frac{\delta^2 W^{(1)}[j,k]}{\delta j(x)\delta j(y)} = -\frac{\mathrm{i}\hbar}{2}\frac{\delta^2}{\delta j(x)\delta j(y)}\operatorname{Tr}\ln G_0^{-1}\\ &= \frac{\hbar}{2}\frac{\delta}{\delta j(y)}\int \mathrm{d}\bar{x}\mathrm{d}\bar{y}\mathrm{d}\bar{z}\; G_0(\bar{x},\bar{y})\frac{\delta^3 S[\Phi]}{\delta\Phi(\bar{z})\delta\Phi(\bar{y})\delta\Phi(\bar{x})}G_0(\bar{z},x)\\ &= \frac{\hbar}{2}\int \mathrm{d}\bar{x}\mathrm{d}\bar{y}\mathrm{d}\bar{z}\mathrm{d}z'\left\{\left[\frac{\delta G_0(\bar{x},\bar{y})}{\delta\Phi\left(z'\right)}G_0(\bar{z},x) + G_0(\bar{x},\bar{y})\frac{\delta G_0(\bar{z},x)}{\delta\Phi\left(z'\right)}\right]\frac{\delta^3 S[\Phi]}{\delta\Phi(\bar{y})\delta\Phi(\bar{x})\delta\Phi(\bar{z})}\right.\\ &\qquad \left. + G_0(\bar{x},\bar{y})\frac{\delta^4 S[\Phi]}{\delta\Phi(\bar{y})\delta\Phi(\bar{x})\delta\Phi(\bar{z})\delta\Phi\left(z'\right)}G_0(\bar{z},x)\right\}\underbrace{\frac{\delta\Phi\left(z'\right)}{\delta j(y)}}_{=\mathrm{i}G_0\left(z',y\right)}.\end{aligned} \tag{2.51}$$

The functional derivative of the bare Green function with respect to the classical field is

$$\begin{aligned}\frac{\delta G_0(x,y)}{\delta\Phi(z')} &= \frac{\delta\left[G_0^{-1}(x,y)\right]^{-1}}{\delta\Phi(z')} = -\int \mathrm{d}x'\mathrm{d}y' G_0\left(x,x'\right)\frac{\delta G_0^{-1}(x',y')}{\delta\Phi\left(z'\right)}G_0(y',y)\\ &= -\mathrm{i}\int \mathrm{d}x'\mathrm{d}y' G_0\left(x,x'\right)\frac{\delta^3 S[\Phi]}{\delta\Phi(x')\delta\Phi(y')\delta\Phi(z')}G_0(y',y)\\ &= \mathrm{i}g\Phi(z')G_0(x,z')G_0(z',y),\end{aligned} \tag{2.52}$$

where we show the concrete result for our example action in the last line. Furthermore, we have used the differentiation rule for an inverse matrix proved in App. A.3. The first-order correction of

[6] In anticipation of Eq. (2.58), note that

$$\varphi^{(1)}(x) = \mathrm{i}\frac{g\hbar}{2}\int \mathrm{d}\bar{z}\; G(\bar{z},\bar{z})\Phi(\bar{z})G(\bar{z},x).$$

the Green function in our example hence becomes

$$\begin{aligned} G^{(1)}(x,y) = -\mathrm{i}\frac{g\hbar}{2}\Bigg\{ \int \mathrm{d}\bar{z}\mathrm{d}z' \left[\frac{\delta G_0(\bar{z},\bar{z})}{\delta\Phi\left(z'\right)} G_0\left(\bar{z},x\right) + G_0(\bar{z},\bar{z})\frac{\delta G_0\left(\bar{z},x\right)}{\delta\Phi\left(z'\right)}\right]\Phi(\bar{z})G_0\left(z',y\right) \\ + \int dz' G_0\left(z',z'\right) G_0\left(z',x\right) G_0\left(z',y\right)\Bigg\} \\ = -\mathrm{i}\frac{g\hbar}{2}\Bigg\{ \mathrm{i}g \int \mathrm{d}\bar{z}\mathrm{d}z'\, \Phi(\bar{z})\Phi(z')\big[G_0\left(\bar{z},z'\right) G_0\left(z',\bar{z}\right) G_0\left(\bar{z},x\right) \\ + G_0(\bar{z},\bar{z}) G_0\left(\bar{z},z'\right) G_0\left(z',x\right)\big] G_0\left(z',y\right) \\ + \int dz' G_0\left(z',z'\right) G_0\left(z',x\right) G_0\left(z',y\right)\Bigg\}. \end{aligned}$$

Inverting Eqs. (2.45), we find for the classical quantities

$$\begin{aligned} \Phi = \varphi - \varphi^{(1)}[\Phi, G_0] + \mathcal{O}(\hbar^2) = \varphi - \varphi^{(1)}[\varphi, G] + \mathcal{O}(\hbar^2), \\ -\mathrm{i}G_0 = G - G^{(1)}[\Phi, G_0] + \mathcal{O}(\hbar^2) = G - G^{(1)}[\varphi, G] + \mathcal{O}(\hbar^2). \end{aligned} \tag{2.53}$$

Here, the second equalities are decisive for our goal of expressing the classical quantities in terms of the Legendre-transformed variables: since the first-order corrections are by definition already $\mathcal{O}(\hbar)$, it is consistent to have them depend on the full φ and G. Upon replacing the classical quantities by the full in $W^{(2)}$, the effective action becomes

$$\Gamma[\varphi, G] = S[\Phi] + W^{(2)}[\varphi, G] \tag{2.54a}$$

$$+ \frac{\mathrm{i}\hbar}{2}\operatorname{Tr}\ln G_0^{-1} - \frac{1}{2}\int \mathrm{d}\bar{x}\mathrm{d}\bar{x}'\; K(\bar{x},\bar{x}')\mathrm{i}\hbar G(\bar{x},\bar{x}') \tag{2.54b}$$

$$+ \int \mathrm{d}\bar{x}\; j(\bar{x})\left[\Phi(\bar{x}) - \varphi(\bar{x})\right] + \int \mathrm{d}\bar{x}\mathrm{d}\bar{x}'\; \frac{K(\bar{x},\bar{x}')}{2}\left[\Phi(\bar{x})\Phi(\bar{x}') - \varphi(\bar{x})\varphi(\bar{x}')\right]. \tag{2.54c}$$

We have grouped the terms according to the order in which we are going to address them in the following. Starting with (2.54a), the action may now be expanded around the corrected field as

$$\begin{aligned} S[\Phi] = S[\varphi + (\Phi - \varphi)] = S[\varphi] - \int \mathrm{d}\bar{x}\; \varphi^{(1)}[\varphi, G](\bar{x})\frac{\delta S[\varphi]}{\delta\varphi(\bar{x})} \\ + \frac{1}{2}\int \mathrm{d}\bar{x}\mathrm{d}\bar{y}\; \varphi^{(1)}[\varphi, G](\bar{x})\frac{\delta^2 S[\varphi]}{\delta\varphi(\bar{x})\delta\varphi(\bar{y})}\varphi^{(1)}[\varphi, G](\bar{y}) + \mathcal{O}(\hbar^3). \end{aligned} \tag{2.55}$$

The form of the second-order term $W^{(2)}[\varphi, G]$ of the cumulant-generating functional was given in Eq. (2.38), the difference now being that the former bare fields and Green-function lines have been

replaced by the full ones. Moving to (2.54b), notice that by the geometric series

$$\begin{aligned} \mathrm{i}G_0^{-1} &= \left(G - G^{(1)}\right)^{-1} = \left(G\left(\mathbb{1} - G^{-1}G^{(1)}\right)\right)^{-1} \\ &= \left(\mathbb{1} - G^{-1}G^{(1)}\right)^{-1} G^{-1} = \left(\mathbb{1} + G^{-1}G^{(1)}\right) G^{-1} + \mathcal{O}(\hbar^2). \end{aligned} \tag{2.56}$$

Employing shorthand notation in some places and dropping terms of order $\mathcal{O}(\hbar^2)$ as well as constant terms, we find accordingly

$$\begin{aligned} &\operatorname{Tr}\ln G_0^{-1} - \int \mathrm{d}\bar{x}\mathrm{d}\bar{x}'\; K(\bar{x},\bar{x}')G(\bar{x},\bar{x}') = \operatorname{Tr}\ln\left(\mathbb{1} + G^{-1}G^{(1)}\right) G^{-1} - \operatorname{Tr} KG \\ &= \operatorname{Tr}\ln G^{-1} + \operatorname{Tr} G^{-1}G^{(1)} + \int \mathrm{d}\bar{x}\mathrm{d}\bar{y}\left[-\mathrm{i}G_0^{-1}(\bar{x},\bar{y}) + \frac{\delta^2 S[\Phi]}{\delta\Phi(\bar{x})\delta\Phi(\bar{y})}\right] G(\bar{y},\bar{x}) \\ &= \operatorname{Tr}\ln G^{-1} + \operatorname{Tr} G^{-1}G^{(1)} + \int \mathrm{d}\bar{x}\mathrm{d}\bar{y}\Bigg[\frac{\delta^2 S[\Phi]}{\delta\Phi(\bar{x})\delta\Phi(\bar{y})}G(\bar{y},\bar{x}) - G^{-1}(\bar{x},\bar{y})G(\bar{y},\bar{x}) \\ &\qquad\qquad - \int \mathrm{d}z'\mathrm{d}z'' G^{-1}(\bar{x},z')G^{(1)}(z',z'')G^{-1}(\bar{x},z')G(z'',\bar{y})\Bigg] \\ &= \operatorname{Tr}\ln G^{-1} + \operatorname{Tr} G^{-1}G^{(1)} + \int \mathrm{d}\bar{x}\mathrm{d}\bar{y}\left[\frac{\delta^2 S[\Phi]}{\delta\Phi(\bar{x})\delta\Phi(\bar{y})}G(\bar{y},\bar{x}) - \delta(0) - G^{-1}(\bar{x},\bar{y})G^{(1)}(\bar{y},\bar{x})\right] \\ &= \operatorname{Tr}\ln G^{-1} + \int \mathrm{d}\bar{x}\mathrm{d}\bar{y}\frac{\delta^2 S[\Phi]}{\delta\Phi(\bar{x})\delta\Phi(\bar{y})}G(\bar{y},\bar{x}), \end{aligned}$$

where we have expanded the logarithm in going from the first to the second line and also dropped $\delta(0)$. The second term of the last line is expanded around the full average field φ according to

$$\frac{\delta^2 S[\Phi]}{\delta\Phi(\bar{x})\delta\Phi(\bar{y})} = \frac{\delta^2 S[\varphi]}{\delta\varphi(\bar{x})\delta\varphi(\bar{y})} - \int \mathrm{d}\bar{z}\; \varphi^{(1)}[\varphi,G](\bar{z})\frac{\delta^3 S[\varphi]}{\delta\varphi(\bar{z})\delta\varphi(\bar{y})\delta\varphi(\bar{x})}, \tag{2.57}$$

which yields the remaining terms for (2.54b):

$$\begin{aligned} &\frac{\mathrm{i}\hbar}{2}\operatorname{Tr}\left[\frac{\delta^2 S[\varphi]}{\delta\varphi^2}G\right] - \frac{\mathrm{i}\hbar}{2}\int \mathrm{d}\bar{x}\mathrm{d}\bar{y}\mathrm{d}\bar{z}\; \varphi^{(1)}(\bar{z})\frac{\delta^3 S[\varphi]}{\delta\varphi(\bar{z})\delta\varphi(\bar{y})\delta\varphi(\bar{x})}G(\bar{y},\bar{x}) \\ &= \frac{\mathrm{i}\hbar}{2}\operatorname{Tr}\left[\frac{\delta^2 S[\varphi]}{\delta\varphi^2}G\right] + \frac{\mathrm{i}g^2\hbar^2}{4}\int \mathrm{d}\bar{z}\mathrm{d}\bar{z}'\; \mathrm{i}G(\bar{z}',\bar{z}')\varphi(\bar{z}')\; G(\bar{z}',\bar{z})\varphi(\bar{z})G(\bar{z},\bar{z}) \\ &= \frac{\mathrm{i}\hbar}{2}\operatorname{Tr}\left[\frac{\delta^2 S[\varphi]}{\delta\varphi^2}G\right] - \left(\frac{g\hbar}{2}\right)^2 \times \end{aligned} \tag{2.58}$$

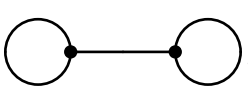

,

where the second term is referred to as the "dumb-bell" graph. Observe also how the new inverse Green function $\delta^2 S[\varphi]/\delta\varphi^2$ is evaluated at the corrected saddle-point $\varphi(x)$. Finally, line (2.54c) is equal to

$$
\begin{aligned}
&-\int \mathrm{d}\bar{x} j(\bar{x})\varphi^{(1)}[\varphi,G](\bar{x}) + \frac{1}{2}\int \mathrm{d}\bar{x}\mathrm{d}\bar{y}\ \varphi^{(1)}[\varphi,G](\bar{x})K(\bar{x},\bar{y})\varphi^{(1)}[\varphi,G](\bar{y}) \\
&-\int \mathrm{d}\bar{x}\mathrm{d}\bar{y}\ \varphi(\bar{x})K(\bar{x},\bar{y})\varphi^{(1)}[\varphi,G](\bar{y}) \\
&= -\int \mathrm{d}\bar{x}\left\{ j(\bar{x}) + \int \mathrm{d}\bar{y} K(\bar{y},\bar{x})\left[\varphi(\bar{y}) - \varphi^{(1)}[\varphi,G](\bar{y})\right]\right\}\varphi^{(1)}[\varphi,G](\bar{x}) \\
&-\frac{1}{2}\int \mathrm{d}\bar{x}\mathrm{d}\bar{y}\ \varphi^{(1)}\left[\varphi,G\right](\bar{x})K(\bar{x},\bar{y})\psi^{(1)}[\varphi,G](\bar{y}) \\
&= \int \mathrm{d}\bar{x}\frac{\delta S[\Phi]}{\delta\Phi(\bar{x})}\varphi^{(1)}[\varphi,G](\bar{x}) - \frac{1}{2}\int \mathrm{d}\bar{x}\mathrm{d}\bar{y}\ \varphi^{(1)}\left[\varphi,G\right](\bar{x})K(\bar{x},\bar{y})\psi^{(1)}[\varphi,G](\bar{y}) \\
&= \int \mathrm{d}\bar{x}\left[\frac{\delta S[\varphi]}{\delta\varphi(\bar{x})} - \int \mathrm{d}\bar{y}\frac{\delta^2 S[\varphi]}{\delta\varphi(\bar{x})\delta\varphi(\bar{y})}\varphi^{(1)}\left[\varphi,G\right](\bar{y})\right]\varphi^{(1)}\left[\varphi,G\right](\bar{x}) \\
&-\frac{1}{2}\int \mathrm{d}\bar{x}\mathrm{d}\bar{y}\ \varphi^{(1)}\left[\varphi,G\right](\bar{x})K(\bar{x},\bar{y})\psi^{(1)}[\varphi,G](\bar{y}).
\end{aligned}
\tag{2.59}
$$

Adding to this Eq. (2.55) produces

$$
\begin{aligned}
&S[\varphi] - \frac{1}{2}\int \mathrm{d}\bar{x}\mathrm{d}\bar{y}\ \varphi^{(1)}\left[\varphi,G\right](\bar{x})\left[\frac{\delta^2 S[\varphi]}{\delta\varphi(\bar{x})\delta\varphi(\bar{y})} + K(\bar{x},\bar{y})\right]\psi^{(1)}[\varphi,G](\bar{y}) \\
&= S[\varphi] - \frac{1}{2}\left(\frac{g\hbar}{2}\right)^2 \mathrm{i}^2 \int \mathrm{d}\bar{x}\mathrm{d}\bar{y}\mathrm{d}\bar{z}\mathrm{d}\bar{z}'\ G(\bar{z}',\bar{z}')\varphi(\bar{z}')G(\bar{z}',\bar{x})G^{-1}(\bar{x},\bar{y})G(\bar{z},\bar{z})\varphi(\bar{z})G(\bar{z},\bar{y}) \\
&= S[\varphi] + \frac{1}{2}\left(\frac{g\hbar}{2}\right)^2 \int \mathrm{d}\bar{z}\mathrm{d}\bar{z}'\ G(\bar{z}',\bar{z}')\varphi(\bar{z}')G(\bar{z},\bar{z})\varphi(\bar{z})G(\bar{z},\bar{z}') \\
&= S[\varphi] + \frac{1}{2}\left(\frac{g\hbar}{2}\right)^2 \times
\end{aligned}
\tag{2.60}
$$

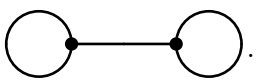

.

When replacing $G_0 \to \mathrm{i}G$ in the dumb-bell part of $W^{(2)}$ shown in Eq. (2.38), we gain a factor of i^3, such that the overall prefactor of the dumb-bell graph in $W^{(2)}$ becomes

$$\mathrm{i}^4 \frac{g^2\hbar^2}{2\cdot(3!)^2} \times 9 = \frac{1}{2}\left(\frac{g\hbar}{2}\right)^2. \tag{2.61}$$

With Eqs. (2.58) and (2.60), this demonstrates in an illustrative fashion how the one-particle-reducible (1PR) graphs cancel in this construction. As no two-particle-reducible diagrams appear in our specific expansion, their cancellation could not be demonstrated accordingly. At any rate, the remaining diagrams contributing to the effective action $\Gamma[\varphi, G]$ via Eqs. (2.54a) and (2.38), the so-called "double-bubble" and the "sunset" diagrams, are both 2PI, as they should be. We will not prove the conserving properties of the self-energy derivable from $\Gamma[\varphi, G]$ at this point but refer to the extensive literature cited above.

2.2.4 Equations of Motion & Self-Energy

In terms of a generalized matrix notation, the physical equations of motion for the symmetry-broken field $\varphi(x) \equiv \varphi_i$ and the dressed Green function $G(x,y) \equiv G_{ij}$ are obtained from Eqs. (2.44) by setting the external sources to zero,

$$\begin{aligned} 0 &= \frac{\delta\Gamma[\boldsymbol{\varphi}, \boldsymbol{G}]}{\delta\varphi_i}, \\ 0 &= \frac{\delta\Gamma[\boldsymbol{\varphi}, \boldsymbol{G}]}{\delta G_{ij}}. \end{aligned} \tag{2.62}$$

The first of these two yields a Gross-Pitaevskii-type of equation with corrections to the classical saddle-point Φ_i coming from the derivatives $\delta W^{(2)}[\boldsymbol{\varphi}, \boldsymbol{G}]/\delta\varphi_i$ of the interacting part of the effective action $\Gamma[\boldsymbol{\varphi}, \boldsymbol{G}]$. The second equation reads

$$0 = \frac{\delta}{\delta G_{ij}}\left[\frac{\mathrm{i}\hbar}{2}\mathrm{Tr}\,\ln \boldsymbol{G}^{-1} + \frac{\mathrm{i}\hbar}{2}\mathrm{Tr}\,\boldsymbol{G}_0^{-1}\boldsymbol{G} + W^{(2)}[\boldsymbol{\varphi}, \boldsymbol{G}]\right], \tag{2.63}$$

with the bare inverse Green function now being defined by $(\boldsymbol{G}_0^{-1})_{ij} = \delta^2 S[\boldsymbol{\varphi}]/\delta\varphi_i\delta\varphi_j$. After switching indices, this becomes the familiar Dyson equation

$$(\boldsymbol{G}^{-1})_{ij} = (\boldsymbol{G}_0^{-1})_{ij} - (\boldsymbol{\Sigma})_{ij}, \tag{2.64}$$

which when contracted with $\boldsymbol{G}$ from the right yields an equation in differential form. The resummed 1PI self-energy is obtained from the 2PI generating diagrams as

$$(\boldsymbol{\Sigma})_{ij}[\boldsymbol{\varphi}, \boldsymbol{G}] := \frac{2\mathrm{i}}{\hbar}\frac{\delta W^{(2)}[\boldsymbol{\varphi}, \boldsymbol{G}]}{\delta G_{ji}}. \tag{2.65}$$

2.3 Two-Time Evolution of Kadanoff-Baym Equations

For non-equilibrium problems, the Dyson equation (2.64) acquires a special structure due to the dependence of the Green function $G(x,y) = G(x,t;x',t')$ on *two times*. In this Sec., we will focus only on this two-time dependence and drop any other dependencies of the Green function, i.e. $G = G(t,t')$. Historically, these equations of motion are known as the *Kadanoff-Baym* equations [100, 101]. Further references discussing their numerical solution are [76, 102]. A comprehensive discussion of their properties can be found in the textbook [80]. Two applications to physical problems are studied in Refs. [103, 104]. Numerically, the main difficulty arising from the two-time structure is the computational cost: in the presence of memory integrals, it scales as n^3, where n is the number of grid points. Ref. [105] discusses how this can be reduced to a linear scaling by certain approximations. In Sec. 5.5, we will learn that for dissipative systems, an almost comparable scaling can be achieved by truncating the memory integrals and computing only a restricted set of points on the two-time grid.

The Kadanoff-Baym equations are usually presented in the context of non-equilibrium QFT. The general problem of two-time expectation values, however, is not restricted to the quantum domain. It appears just as naturally for the classical stochastic processes we have studied above (e.g. Eq. (1.40)). The main difference is that in stochastic processes, the dynamics is seldomly modeled by means of differential equations for expectation values. In order not to limit our horizon prematurely, we will first introduce a set of two-time equations derived from the classical path integral given in Eq. (1.49). These can be interpreted as the Kadanoff-Baym equations of Brownian motion. Their properties are in many ways close to those of their quantum counterparts.

2.3.1 Kadanoff-Baym Equations of Brownian Motion

According to our convention, the inverse Green function of the action

$$S[x,z] = \int_{t_0}^{t} \mathrm{d}t \;\left[\mathrm{i}Dz^2/2 + z(\dot{x} - \alpha x)\right] \tag{2.66}$$

is defined as

$$\boldsymbol{G}_0^{-1}(t,t') = \partial^2 S = \delta(t-t') \begin{pmatrix} 0 & -\partial_t - \alpha \\ \partial_t - \alpha & \mathrm{i}D \end{pmatrix}. \tag{2.67}$$

The corresponding bare Green function reads

$$\boldsymbol{G}_0(t,t') = \begin{pmatrix} G^K(t,t') & G^R(t,t') \\ G^A(t,t') & 0 \end{pmatrix} = \begin{pmatrix} -\mathrm{i}\langle x(t)x(t')\rangle & \langle x(t)z(t')\rangle \\ \langle z(t)x(t')\rangle & 0 \end{pmatrix}. \tag{2.68}$$

The link to the "quantum" case follows from $\hat{\phi} = \mathrm{i}z$, $\phi = x$ and $G^R(t,t') = -\mathrm{i}\langle\phi(t)\hat{\phi}(t')\rangle$, $G^A(t,t') = -\mathrm{i}\langle\hat{\phi}(t)\phi(t')\rangle$. These definitions are, of course, conventional. The missing factors of $-\mathrm{i}$ in the classical $G^{R/A}$ already hint at the fact that the equations we are about to derive are *not*

quantum. The Dyson equation of the problem then becomes

$$\int_{t_0}^{t} \mathrm{d}\bar{t}\, \boldsymbol{G}_0^{-1}(t,\bar{t})\boldsymbol{G}_0(\bar{t},t') = \delta(t-t')\mathbb{1}, \tag{2.69}$$

from which the equation governing the evolution in the "direction" of t' follows as usual by taking the adjoint. For the Keldysh component, one obtains a differential equation

$$\partial_t G^K(t,t') = \alpha G^K(t,t') - \mathrm{i}DG^A(t,t'). \tag{2.70}$$

Transforming to Wigner coordinates, we have

$$\begin{aligned} \partial_T G^K(T,0) &= 2\alpha G^K(T,0) - \mathrm{i}D\left[G^R(T,0) + G^A(T,0)\right] \\ &= 2\alpha G^K(T,0) - \mathrm{i}D, \end{aligned} \tag{2.71a}$$

$$\partial_\tau G^K(T,\tau) = \frac{\mathrm{i}D}{2}\left[G^R(T,\tau) - G^A(T,\tau)\right]. \tag{2.71b}$$

For the retarded and advanced Green functions, the dynamics is governed by

$$(\partial_t \mp \alpha)\, G^{R/A}(t,t') = \pm\delta(t-t'). \tag{2.72}$$

Again going over to Wigner coordinates, we find as expected that

$$\begin{aligned} \partial_T G^{R/A}(T,0) &= 0, \\ (\partial_\tau \mp \alpha)\, G^{R/A}(T,\tau) &= \pm\delta(\tau). \end{aligned} \tag{2.73}$$

These equations are straightforward to solve and yield

$$G^{R/A}(T,\tau) = \Theta(\pm\tau)\mathrm{e}^{\pm\alpha\tau}, \tag{2.74}$$

where we have again used $G^R(T,0) + G^A(T,0) = 1$ to fix the initial conditions. The more interesting question is: How to find G^K for all times (t,t') numerically? Clearly, this problem is different from solving an ordinary differential equation in that time is now suddenly "two-dimensional". The analytical solution that we want to reproduce reads

$$\mathrm{i}G^K(t,t') = \left(\mathrm{i}G^K(0,0) + \frac{D}{2\alpha}\right)\mathrm{e}^{\alpha(t+t')} - \frac{D}{2\alpha}\left(\Theta(t-t')\mathrm{e}^{\alpha(t-t')} + \Theta(t'-t)\mathrm{e}^{\alpha(t'-t)}\right). \tag{2.75}$$

The best strategy is to use a combination of Eqs. (2.70), (2.71a) and the (classical) symmetry property $G^K(t,t') = G^K(t',t)$, a strategy which also works for the equations of non-equilibrium QFT. We will describe the algorithm in general terms in the next subsection, before returning to its application to Brownian motion.

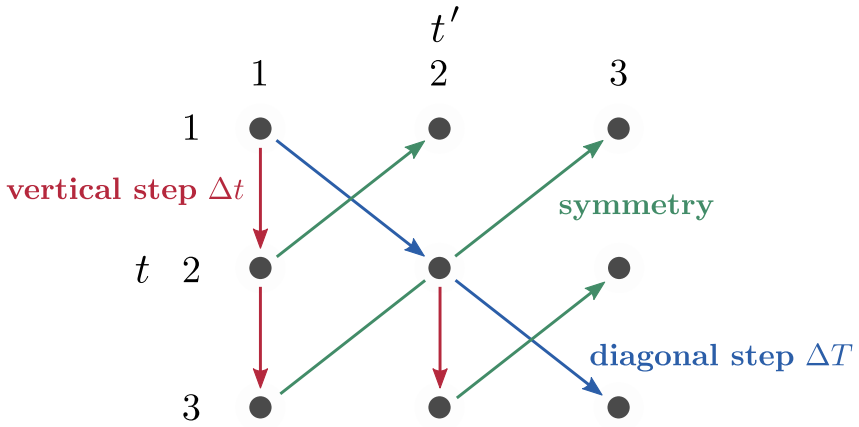

Figure 2.3: Two-time stepping of Kadanoff-Baym equations. The red vertical arrows indicate the evolution governed by Eq. (2.76a), the blue diagonal arrows that governed by Eq. (2.76b). The green arrows show how the symmetry relation may be used to find the points above the diagonal.

2.3.2 Two-Time Structure of the Equations

The Kadanoff-Baym equations of classical and quantum problems alike can be cast into the form

$$\partial_t G(t,t') = -\mathrm{i} f(t,t'), \tag{2.76a}$$
$$\partial_T G(T,0) = -\mathrm{i} f(T,0), \tag{2.76b}$$

where for interacting systems the right-hand sides may depend on the entire history of the system (this will be discussed below). The Green function $G(t,t')$ is usually a matrix in both the degrees of freedom and Schwinger-Keldysh space. Additionally, we can assume a symmetry property relating the values of $G(t,t')$ for $t < t'$ to those for $t > t'$. Combining Eqs. (2.76) with the symmetry relations and an initial condition at $t = t' = t_1$ results in the algorithm illustrated in Fig. 2.3. In both the vertical and the diagonal direction, it reduces the problem to the solution of an ordinary differential equation, which can in principle be tackled by any standard method. However, since for non-trivial interacting problems the right-hand sides of Eqs. (2.76) will require the evaluation of retarded memory integrals, a method is desirable that does not rely on multiple function evaluations, that is, methods like Runge-Kutta are discouraged in favor of multi-step methods such as Adams-Bashforth [106].

Notice that many references [100, 102] solve for $G^{>}(t,t')$ at times $t > t'$ with Eq. (2.76a), yet for $G^{<}(t,t')$ at times $t < t'$ via the adjoint equation in horizontal direction (the diagonal is stepped additionally for $G^{<}(t,t)$, from which $G^{>}(t,t)$ can be obtained). As the lesser and greater Green function are defined on the entire two-time square, the values of $G^{\gtrless}$ at times $t \lessgtr t'$ are then also found from symmetry. In our algorithm, we have instead chosen to solve for both functions on the lower triangle (and on the diagonal).

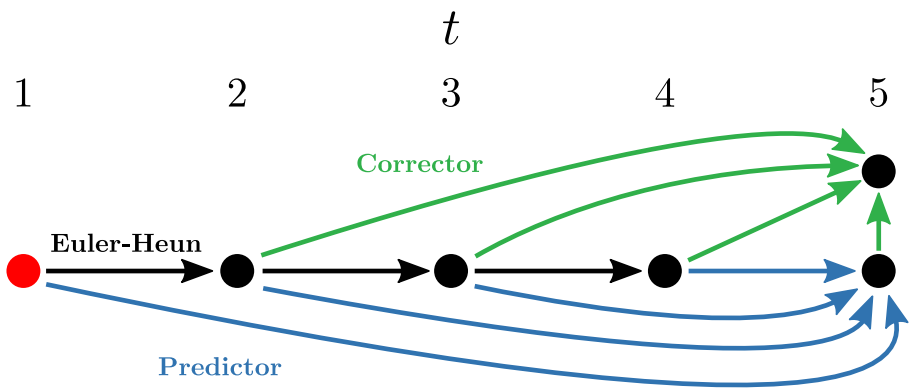

Figure 2.4: Predictor-corrector scheme. The first three points after the initial value (red dot) are computed via the Euler-Heun method (black arrows). The four available points are then fed into the prediction of the future point (blue arrows), which is then used again during the corrector step (green arrows).

2.3.3 Predictor-Corrector Method

The numerical method used for solving two-time Kadanoff-Baym equations used throughout this thesis was applied to a similar problem in Ref. [106]. It is a predictor-corrector scheme that employs a four-step Adams-Bashforth method to predict the future point required to explicitly evaluate a three-step Adams-Moulton method. Since the four-step method indeed requires four points from the past to predict the next point, one needs to compute three more points from the initial value with the one-step Euler-Heun method. The essence of this scheme is shown in Fig. 2.4. On an equidistant grid of points t_k with $k = 1, ..., n+1$ and spacing Δt, the Adams-Bashforth discretization of Eq. (2.76a) becomes

$$G(t_{k+1}, t') = G(t_k, t') - \mathrm{i}\frac{\Delta t}{24}\left(55f(t_k, t') - 59f(t_{k-1}, t') + 37f(t_{k-2}, t') - 9f(t_{k-3}, t')\right). \tag{2.77}$$

The value $G(t_{k+1}, t')$ is required to evaluate the Adams-Moulton corrector step according to

$$G(t_{k+1}, t') = G(t_k, t') - \mathrm{i}\frac{\Delta t}{24}\left(9f(t_{k+1}, t') + 19f(t_k, t') - 5f(t_{k-1}, t') + f(t_{k-2}, t')\right). \tag{2.78}$$

Applied to Eq. (2.76b), the corresponding expressions are

$$\begin{aligned} G(T_{k+1}, 0) &= G(T_k, 0) - \mathrm{i}\frac{\Delta T}{24}\left(55f(T_k, 0) - 59f(T_{k-1}, 0) + 37f(T_{k-2}, 0) - 9f(T_{k-3}, 0)\right), \\ G(T_{k+1}, 0) &= G(T_k, 0) - \mathrm{i}\frac{\Delta T}{24}\left(9f(T_{k+1}, 0) + 19f(T_k, 0) - 5f(T_{k-1}, 0) + f(T_{k-2}, 0)\right), \end{aligned} \tag{2.79}$$

where $\Delta T = \left(\Delta t + \Delta t'\right)/2 = \Delta t$. The right-hand sides only require one function evaluation per step if the previously evaluated function values are kept in memory. It is possible to keep repeating the corrector step until convergence is reached.

2.3.4 Improved Initialization Method

Instead of using the Euler-Heun method at the temporal resolution Δt of the subsequent multi-step method, one can improve the initialization in a straightforward way. This is desirable because the multi-step method works accurately for larger lattice spacing Δt than does the Euler-Heun method (for which it is well-known that Δt needs to be very small). Looking at Fig. 2.4, we see that the time interval on which the Euler-Heun method is employed is given by $I_{\text{ini}} = [0, 3\Delta t]$. We now introduce a parameter n_{ini} as the number of grid points into which we subdivide the interval I_{ini}. Then we apply the predictor-corrector scheme as outlined in paragraph 2.3.3 on the interval I_{ini} with a lattice spacing $3\Delta t/n_{\text{ini}}$. Setting $n_{\text{ini}} = 3/\Delta t_{\text{ini}}$ for convenience, this implies that the Euler-Heun methods now works at an improved temporal resolution $\Delta t \cdot \Delta t_{\text{ini}}$. Because $3\Delta t$ is small, n_{ini} does not have to be very large. In practice, we find that the results do not depend noticeably on the chose of n_{ini}.

2.3.5 Retarded Memory Integrals

For interacting systems, a diagrammatic approximation beyond Hartree-Fock will turn Eqs. (2.76) into *integro*-differential equations. We will restrict the discussion to cases where the self-energy itself is local in time, which leads to one-dimensional integrals appearing in $f(t, t')$. These integrals will generally be of the form

$$I_a^b(t, t') = \int_a^b \mathrm{d}\bar{t}\; \Sigma(t, \bar{t}) G(\bar{t}, t'), \tag{2.80}$$

with either $a = t_1$, $b = t, t'$ or $a = t$, $b = t'$. These integrals need to be performed for every point on the grid. Furthermore, the longer the system evolves, the more points have to be summed up under the integrals. These two facts point to the main weakness of the Kadanoff-Baym equations: the computational effort required to solve them scales as n^3. There exist approximations to reduce this effort to a scaling with n such as the generalized Kadanoff-Baym ansatz [105]. As we will see later, in strongly driven-dissipative systems a comparable reduction in cost can be achieved essentially without loss of accuracy. Numerically, we approximate Eq. (2.80) by the trapezoidal rule [76] according to

$$I_{t_i}^{t_j}(t, t')/\Delta t \approx \sum_{k=i}^{j} \left[\Sigma(t, t_k) G(t_k, t')\right] - \frac{1}{2}\left(\Sigma(t, t_i) G(t_i, t') + \Sigma(t, t_j) G(t_j, t')\right). \tag{2.81}$$

For a benchmark problem, we did not find more accurate solutions when using a higher-order quadrature such as Simpson's rule, in agreement with Ref. [33]. Such quadratures have been applied to the solution of Kadanoff-Baym equations in [104, 106].

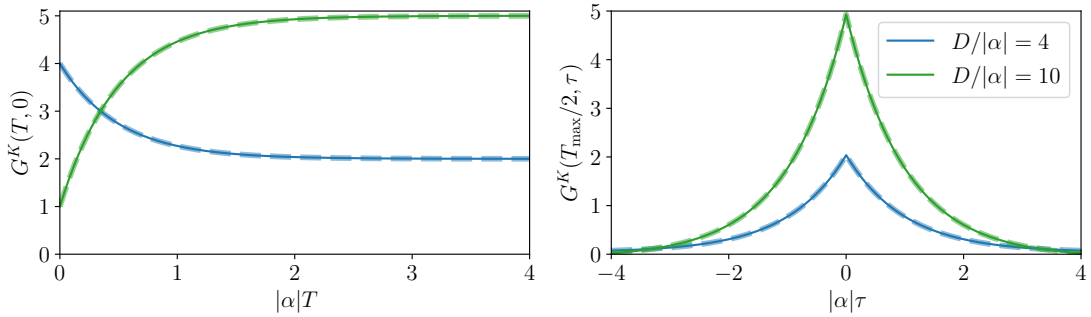

Figure 2.5: Numerical solutions of Eqs. (2.82) for diffusion parameters $D/|\alpha| = 4.0$ (blue) and $D/|\alpha| = 10.0$ (green). The initial conditions are $G^K(0,0) = -\mathrm{i}$ and $G^K(0,0) = -4\mathrm{i}$, respectively. The thicker dashed lines indicate the corresponding analytical solutions of Eq. (2.75). The left panel shows the "forward" evolution in the center-of-mass time T. The right panel shows the relative-time evolution as evaluated in the "middle" of the two-time grid. The numerical solutions were evolved up to a maximal time $|\alpha|\,T_{\max} = 4.0$; the number of steps was $n = 2^{12}$.

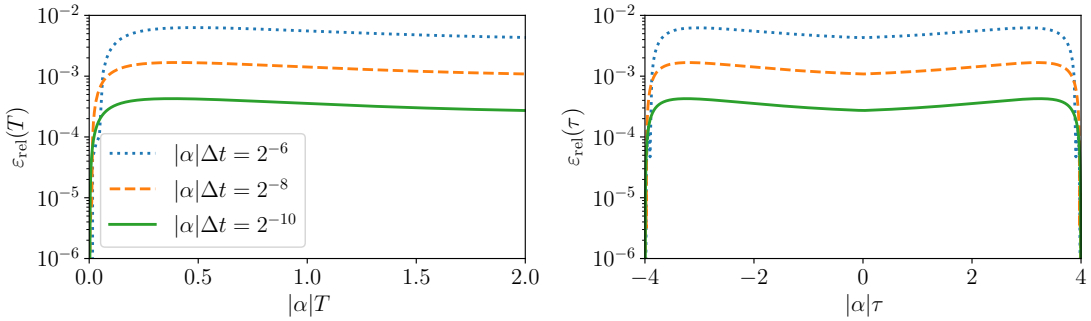

Figure 2.6: Relative errors according to Eq. (2.83) for $D/|\alpha| = 10.0$ with initial condition $G^K(0,0) = -\mathrm{i}$. The numerical solutions were evolved up to time $|\alpha|\,T_{\max} = 4.0$. In the right panel, $T = T_{\max}/2$ as before.

2.3.6 Algorithm Benchmark

To verify the correctness and accuracy of our numerical implementation of the algorithm just outlined, we apply it to the Kadanoff-Baym equations of Brownian motion, the analytical solution to which is given by Eq. (2.75). Since $t > t'$ implies $G^A(t,t') = 0$ and we apply Eq. (2.70) only below the equal-time diagonal (cf. Fig. 2.3), the pair of equations required to fully solve our dynamical problem become

$$\begin{aligned} \partial_t G^K(t,t') &= \alpha G^K(t,t'), \\ \partial_T G^K(T,0) &= 2\alpha G^K(T,0) - \mathrm{i}D. \end{aligned} \tag{2.82}$$

Two solutions for different values of D are shown Fig. 2.5. The corresponding analytical solutions from Eq. (2.75) above are reproduced accurately. Depending on the initial condition and the ratio of parameters, the system either decays or climbs to its steady-state. The Fourier transform of the

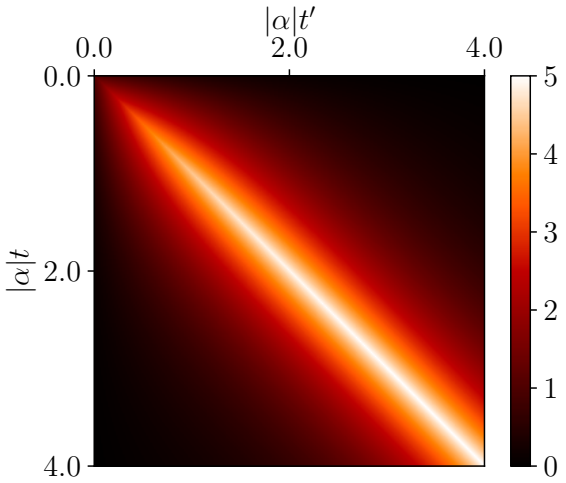

Figure 2.7: $G^K(t,t')$ for parameters $D/|\alpha| = 10.0$ with initial condition $G^K(0,0) = -\mathrm{i}$. The numerical solutions were evolved up to a maximal time $|\alpha|\, T_{\max} = 4.0$; the number of steps was $n = 2^{12}$.

spectrum indicates the Lorentzian line shape. The scaling of the error with increased number of steps is studied in Fig. 2.6. The relative error is calculated according to

$$\varepsilon_{\mathrm{rel}}(T) = \left| G^K(T,0) - G^K_{\mathrm{exact}}(T,0) \right| \cdot \left| G^K_{\mathrm{exact}}(T,0) \right|^{-1}. \tag{2.83}$$

For the error in relative-time direction $\varepsilon_{\mathrm{rel}}(\tau)$, the Keldysh Green function is evaluated at times $G^K(T_{\max}/2, \tau)$. As one may see, the error reduces in proportion to the decreasing step size Δt. We also present the two-time behavior of $G^K(t,t')$ in Fig. 2.7 with the same diffusion constant as for the green curves in Fig. 2.5. This shows both the steady-state value $D\,|\alpha|^{-1}/2$ on the equal-time diagonal and the exponential decay away from it in the orthogonal direction.

CHAPTER 3

Atomic Bose-Einstein Condensates

Before addressing photon condensates in Chps. 4 and 5, the present Chp. is concerned with *atomic* Bose-Einstein condensates. Historically, Bose-Einstein condensation was first observed as late as 1995 in a vapor of rubidium atoms [39], and shortly after in a gas of sodium [107]. As briefly touched upon in 1.1.3, experimentally the major difference between these two types of condensate is how the condensed phase is achieved. Instead of increasing the particle number as in the photonic case, in experiments with clouds of cold atoms one lowers the temperature until condensation sets in. As this is usually done by *removing* the hottest atoms, the particle number is also not truly conserved. Theoretical descriptions of cold-atom BEC still assume particle-number conservation in the sense that one considers the condensate to be already formed and any further loss of atoms to be (at least temporarily) negligible. This is not to be confused with the presence of a thermal cloud with which the condensate can exchange particles.

As will become evident in Chps. 4 and 5, the photon BEC can be modelled by several methods without introducing symmetry breaking explicitly. While satisfactory for simulating the evolution of particle *densities*, information on the condensate *phase* is not easily accessible by such methods. In the present Chp., on the contrary, we first show in 3.1 how to apply manifestly symmetry-broken field theory as developed above to the crucial problem of condensate growth and depletion. Subsequently, we present in 3.2 a theoretical analysis of two cold-atom experiments that provides quantitative insight into how dissipation can arise in closed systems, a question that is of fundamental interest [108].

3.1 Dephasing and Enphasing

In the context of Bose-Einstein condensation, one has to differentiate between a mere particle-number distribution that follows Eq. (1.6) and the presence of a truly *phase-coherent*, symmetry-broken order parameter. For the photon BEC, a discussion of how phase coherence can build up spontaneously as the ground mode is populated macroscopically can be found in Ref. [109]. A related work on cold atomic gases is [110]. The essence of these studies is that for *low-density* Bose gases in the Maxwell-Boltzmann limit, the interaction either with a phonon bath or with other atoms leads to *dephasing* and hence to a destruction of the coherent order parameter. This is the regime

where the quantum Boltzmann equation is applicable. On the contrary, for *high-density* Bose gases, the interaction results in a so-called "enphasing" [109] that enhances the order parameter.

Here, inspired by Ref. [111], we will consider an idealized model of a single bosonic mode the order parameter of which is coupled to its non-condensate occupation via a Lindbladian that can induce de- or enphasing depending on the sign of a constant. Therefore, this simple model brings together all of the ingredients that are necessary to form an albeit basic understanding of phase coherence in Bose-Einstein condensates.[1] Since especially in the "Keldysh" representation, working with the Schwinger-Keldysh formalism is something of an "art" in itself that we shall not have the opportunity to use elsewhere in this thesis, the present Sec. is well-suited to applying this craft. We set $\hbar = 1$.

3.1.1 Master Equation

The Lindblad master equation describing the above physics, complemented by drive and loss processes, reads

$$\begin{aligned}\dot{\hat{\rho}} = &-\mathrm{i}\omega_0[a^\dagger a, \hat{\rho}] + \frac{\lambda}{2}\left\{2a\hat{\rho}a^\dagger - \left(a^\dagger a\hat{\rho} + \hat{\rho}a^\dagger a\right)\right\} + \frac{\gamma}{2}\left\{2a^\dagger\hat{\rho}a - \left(aa^\dagger\hat{\rho} + \hat{\rho}aa^\dagger\right)\right\} \\ &+ D\left\{2a^\dagger a\hat{\rho}a^\dagger a - \left(a^\dagger aa^\dagger a\hat{\rho} + \hat{\rho}a^\dagger aa^\dagger a\right)\right\},\end{aligned} \tag{3.1}$$

where $\lambda > 0$ is the loss parameter, $\gamma > 0$ represents the corresponding gain,[2] and $D \gtrless 0$ is the constant that introduces de- or enphasing to our system. The first thing to learn about the Lindbladian $\mathcal{L}[\hat{n}]\hat{\rho}$ proportional to D is that it does not affect the total particle number, i.e.

$$\partial_t \langle\hat{n}\rangle|_{\lambda=\gamma=0} = \mathrm{Tr}\left\{\dot{\hat{\rho}}a^\dagger a\right\}\Big|_{\lambda=\gamma=0} = 0, \tag{3.2}$$

as one can see immediately from Eq. (3.1). At the same time, the expectation value of the destruction operator obeys

$$\partial_t\langle a\rangle = -\mathrm{i}\omega_0\langle a\rangle + \tfrac{1}{2}(\gamma - \lambda)\langle a\rangle - D\langle a\rangle. \tag{3.3}$$

The general master equation (1.82) is equivalent to a Schwinger action

$$\begin{aligned}S[\phi_\pm^*, \phi_\pm] &= \int \mathrm{d}t\left\{\phi_+^*\mathrm{i}\partial_t\phi_+ - \phi_-^*\mathrm{i}\partial_t\phi_- - \mathrm{i}\mathcal{L}[\phi_\pm^*, \phi_\pm]\right\}, \\ \mathcal{L}[\phi_\pm^*, \phi_\pm] &= -\mathrm{i}(H_+ - H_-) + \tfrac{\lambda}{2}\left[2L_+L_-^* - \left(L_+^*L_+ + L_-^*L_-\right)\right],\end{aligned} \tag{3.4}$$

where the Hamiltonian terms are $H_\pm = H(\phi_\pm^*, \phi_\pm)$. This is our starting point for setting up the effective action.

[1] For a comprehensive overview of theory methods and subtle issues such as phase fluctuations, s. Ref. [112].
[2] A thermal bath would result in $\lambda = \kappa\left(\bar{N} + 1\right)$ and $\gamma = \kappa\bar{N}$.

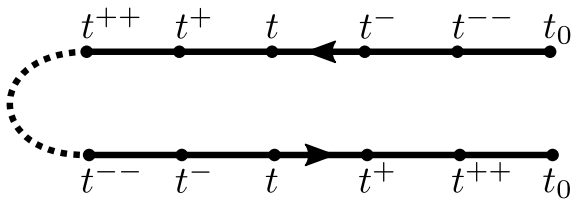

Figure 3.1: Time-ordering along the Schwinger-Keldysh contour. The ordering in real time reverses on the backward branch.

3.1.2 Effective Action & Self-Energy

For simplicity, we will treat the "interaction" vertex proportional to D to lowest order only, that is, in Hartree-Fock approximation. Keeping properly track of time-ordering (s. Fig. 3.1), we find

$$\begin{aligned}\mathcal{L}_D[\phi_\pm^*,\phi_\pm] = -D\,[\,&\phi_+^*(t^{++})\phi_+(t^+)\phi_+^*(t)\phi_+(t^-) + \phi_-^*(t^-)\phi_-(t)\phi_-^*(t^+)\phi_-(t^{++}) \\ &- 2\phi_+^*(t^{++})\phi_+(t^+)\phi_-^*(t^{--})\phi_-(t^-)\,]\,,\end{aligned} \tag{3.5}$$

where $t^\pm = t \pm 0^\pm$, $t^{\pm\pm} = t \pm 2\cdot 0^\pm$. Note that these superscripts have no direct connection with the Schwinger-Keldysh contour: they serve merely as aides for time-ordering. Of course, the contour does still play a role in that the fields on the forward and backward branches are time-ordered oppositely. As we wanted to work in Keldysh representation, we now set

$$\phi_\pm = \frac{1}{\sqrt{2}}(\phi \pm \hat{\phi}), \tag{3.6}$$

and decompose the physical field and the response field into condensate and non-condensate parts according to $\phi = \Phi + \delta\phi$, $\hat{\phi} = \hat{\Phi} + \delta\hat{\phi}$. Then we perform the equivalent of the expansion detailed in Sec. 2.2 to derive the effective action, in the course of which the classical field Φ is replaced by the corrected field φ (and analogously for the response field). Time-ordering is then irrelevant for the mean-fields φ, $\hat{\varphi}$. Furthermore, in Keldysh representation, one needs to keep track of time-ordering only among the adjoint fields $\delta\phi$, $\delta\hat{\phi}^*$, and $\delta\phi^*$, $\delta\hat{\phi}$, respectively. Hence, the time superscripts may be dropped in every other case. To compactify notation, we introduce the field spinor

$$\boldsymbol{\varphi} = (\varphi, \varphi^*, \hat{\varphi}, \hat{\varphi}^*)^T = (\varphi_1, \varphi_2, \varphi_3, \varphi_4)^T. \tag{3.7}$$

The Keldysh action of the corrected fields now reads

$$S_\mathrm{K}[\boldsymbol{\varphi}] = \int \mathrm{d}t\,\left\{\varphi^*\,(\mathrm{i}\partial_t - \omega_0)\,\hat{\varphi} + \hat{\varphi}^*\,(\mathrm{i}\partial_t - \omega_0)\,\varphi - \mathrm{i}\mathcal{L}[\boldsymbol{\varphi}]\right\}, \tag{3.8}$$

with $\mathcal{L}[\boldsymbol{\varphi}] = \mathcal{L}_\lambda[\boldsymbol{\varphi}] + \mathcal{L}_\gamma[\boldsymbol{\varphi}] + \mathcal{L}_D[\boldsymbol{\varphi}]$, where

$$\begin{aligned}
\mathcal{L}_\lambda[\boldsymbol{\varphi}] &= \frac{\lambda}{2}\left[\hat{\varphi}\,\varphi^* - \hat{\varphi}^*\varphi - 2\hat{\varphi}^*\hat{\varphi}\right], \\
\mathcal{L}_\gamma[\boldsymbol{\varphi}] &= \frac{\gamma}{2}\left[\hat{\varphi}^*\varphi - \hat{\varphi}\,\varphi^* - 2\hat{\varphi}^*\hat{\varphi}\right], \\
\mathcal{L}_D[\boldsymbol{\varphi}] &= -D\left[\hat{\varphi}^*\hat{\varphi}^*\varphi\,\varphi + \hat{\varphi}^*\hat{\varphi}\,\varphi^*\varphi + \text{c.c.}\right].
\end{aligned} \tag{3.9}$$

Note the special form of the Lindblad operator in terms of φ and $\hat{\varphi}$, and the sign changes in $\mathcal{L}_\gamma$ compared to $\mathcal{L}_\lambda$. The 'quartic' structure of $\mathcal{L}_D$ is reminiscent of the standard anharmonic oscillator. To wit, the 'true' $|\varphi|^4$ term would, however, look like

$$S_{\text{int}} = g(\hat{\varphi}^*\varphi^*\varphi^2 + \hat{\varphi}^*\hat{\varphi}^2\varphi^* + \text{c.c.}), \tag{3.10}$$

which has either three fields or three response fields, instead of two each as in $\mathcal{L}_D$. The "quantum vs. classical" nature of these vertices is discussed in Ref. [82]. The total effective action becomes

$$\Gamma[\boldsymbol{\varphi}, \boldsymbol{G}] = S_{\text{K}}[\boldsymbol{\varphi}] + \frac{\mathrm{i}}{2}\text{Tr}\,\ln \boldsymbol{G}^{-1} + \frac{\mathrm{i}}{2}\text{Tr}\,\boldsymbol{G}_0^{-1}\boldsymbol{G} + W^{(2)}[\boldsymbol{G}]. \tag{3.11}$$

The part quadratic in the fluctuations, giving rise to the trace logarithms in (3.11), is given by

$$\begin{aligned}
S_{\text{K}}[\boldsymbol{\varphi}, \boldsymbol{\delta\phi}] = \int \mathrm{d}t \Big\{ & \delta\phi^*\left(\mathrm{i}\partial_t - \omega_0\right)\delta\hat{\phi} + \delta\hat{\phi}^*\left(\mathrm{i}\partial_t - \omega_0\right)\delta\phi \\
& -\mathrm{i}\frac{\lambda}{2}\left[\delta\hat{\phi}\delta\phi^* - \delta\hat{\phi}^*\delta\phi - 2\delta\hat{\phi}^*\delta\hat{\phi}\right] - \mathrm{i}\frac{\gamma}{2}\left[\delta\hat{\phi}^*\delta\phi - \delta\hat{\phi}\delta\phi^* - 2\delta\hat{\phi}^*\delta\hat{\phi}\right] \\
& +\mathrm{i}D\Big[\varphi\varphi\delta\hat{\phi}^*\delta\hat{\phi}^* + \varphi^*\varphi^*\delta\hat{\phi}\delta\hat{\phi} + 2\varphi^*\varphi\delta\hat{\phi}^*\delta\hat{\phi} + 2\hat{\varphi}^*\varphi^*\delta\hat{\phi}\delta\phi \\
& + \hat{\varphi}^*\varphi\delta\hat{\phi}(t^+)\delta\phi^*(t) + \hat{\varphi}^*\varphi\delta\hat{\phi}(t^-)\delta\phi^*(t) \\
& + 2\left(\hat{\varphi}^*\varphi\delta\hat{\phi}^*(t^+)\delta\phi(t) + \hat{\varphi}^*\varphi\delta\hat{\phi}^*(t^-)\delta\phi(t)\right) + \ldots\Big]\Big\},
\end{aligned} \tag{3.12}$$

where we did not bother to write terms proportional to $\hat{\varphi}$ because we only need those proportional to $\hat{\varphi}^*$ to calculate the condensate, and we used $\hat{\varphi} = \hat{\varphi}^* = 0$ several times on terms where such average responses field appear quadratically.[3] This leads to an inverse bare Green function

$$\boldsymbol{G}_0^{-1} = \delta(t-t')\begin{pmatrix} 0 & 0 & 0 & -\mathrm{i}\partial_t - \Omega_0 \\ 0 & 0 & \mathrm{i}\partial_t - \Omega_0^* & 0 \\ 0 & -\mathrm{i}\partial_t - \Omega_0^* & 2\mathrm{i}D\varphi^*\varphi^* & \mathrm{i}\left(\lambda+\gamma\right) + 2\mathrm{i}D\varphi^*\varphi \\ \mathrm{i}\partial_t - \Omega_0 & 0 & \mathrm{i}\left(\lambda+\gamma\right) + 2\mathrm{i}D\varphi^*\varphi & 2\mathrm{i}D\varphi\varphi \end{pmatrix},$$

where we introduced the complex parameter $\Omega_0 = \omega_0 - \mathrm{i}\left(\lambda-\gamma\right)/2$, and $\hat{\varphi} = 0$ can be applied also to the remaining terms linear in these fields when multiplying Greens functions with $\boldsymbol{G}_0^{-1}$ (these terms are still needed for the calculation of the condensate, though).

[3] These terms may be discarded immediately since even after functional differentiation with respect to the average response fields, they remain proportional to $\hat{\varphi} = \hat{\varphi}^* = 0$.

Next, we have to look at the quartic terms contributing to $W^{(2)}$, which to lowest non-trivial order, that is, Hartree-Fock, amounts to keeping the so-called "double-bubble" diagram. It is here where finally we have to keep track of time-ordering. It is neither feasible nor instructive to show $W^{(2)}$ in full, as the full expansion will produce a plethora of terms differing only through their time-ordering. Therefore, we simply illustrate how to deal with these. A typical term appearing in the expansion will be

$$\delta\hat{\phi}^*(t^{++})\delta\hat{\phi}(t^+)\delta\phi(t^-)\delta\phi^*(t^{--}) = \delta\hat{\phi}^*(t^+)\delta\hat{\phi}(t^+)\left|\delta\phi(t)\right|^2, \tag{3.13}$$

where we have simplified the time arguments according to the rules stated above (the superscripts may be shifted arbitrarily as long as the relative time-order of the adjoint fields is preserved). In terms of Green functions, we then find

$$\begin{aligned}
W^{(2)}[\boldsymbol{G}] = -\mathrm{i}D\int\mathrm{d}\,t\Bigg\{&\frac{1}{2}\Bigg[\sum_{\mu,\nu=\pm}G_{41}(t^\mu,t)G_{32}(t^\nu,t)+4\Big(G_{42}(t,t)\;G_{31}(t,t)+G_{43}(t,t)G_{21}(t,t)\Big)\Bigg]\\
&+\frac{1}{4}\Bigg[\sum_{\mu,\nu=\pm}G_{32}(t^\mu,t)G_{32}(t^\nu,t)+4\Big(G_{32}(t^+,t)G_{32}(t^-,t)+G_{22}(t,t)G_{33}(t,t)\Big)\Bigg]\\
&+\frac{1}{4}\Bigg[\sum_{\mu,\nu=\pm}G_{41}(t^\mu,t)G_{41}(t^\nu,t)+4\Big(G_{41}(t^+,t)G_{41}(t^-,t)+G_{11}(t,t)G_{44}(t,t)\Big)\Bigg]\\
&+\frac{1}{2}\sum_{\mu=\pm}\mu\cdot\Big(G_{32}(t^\mu,t)+G_{41}(t^\mu,t)\Big)\Big(G_{43}(t,t)-G_{21}(t,t)\Big)\\
&-\frac{1}{4}\sum_{\mu=\pm}\mu\cdot\Big(G_{42}(t^\mu,t)G_{11}(t,t)+G_{31}(t^\mu,t)G_{22}(t,t)\Big)\Bigg\}.
\end{aligned}$$

This leads to a self-energy

$$\boldsymbol{\Sigma}(t,t') = 2\mathrm{i}\frac{\delta W^{(2)}[\boldsymbol{G}]}{\delta\boldsymbol{G}} = -2\mathrm{i}\cdot\frac{\mathrm{i}D}{2}\delta(t-t')\begin{pmatrix}\boldsymbol{\sigma}_{\boldsymbol{\phi},\boldsymbol{\phi}}(t,t) & \boldsymbol{\sigma}_{\boldsymbol{\phi},\hat{\boldsymbol{\phi}}}(t,t)\\ \boldsymbol{\sigma}_{\hat{\boldsymbol{\phi}},\boldsymbol{\phi}}(t,t) & \boldsymbol{\sigma}_{\hat{\boldsymbol{\phi}},\hat{\boldsymbol{\phi}}}(t,t)\end{pmatrix}, \tag{3.14}$$

where we ignore the influence of time-ordering (on $\delta(t-t')$), and

$$\begin{aligned}
\boldsymbol{\sigma}_{\boldsymbol{\phi},\boldsymbol{\phi}} &= \begin{pmatrix}0 & \sigma_{\phi,\phi^*}\\ \sigma_{\phi^*,\phi} & 0\end{pmatrix},\ \boldsymbol{\sigma}_{\boldsymbol{\phi},\hat{\boldsymbol{\phi}}} = \begin{pmatrix}0 & \sigma_{\phi,\hat{\phi}^*}\\ \sigma_{\phi^*,\hat{\phi}} & 0\end{pmatrix},\\
\boldsymbol{\sigma}_{\hat{\boldsymbol{\phi}},\boldsymbol{\phi}} &= \begin{pmatrix}0 & \sigma_{\hat{\phi},\phi^*}\\ \sigma_{\hat{\phi}^*,\phi} & 0\end{pmatrix},\ \boldsymbol{\sigma}_{\hat{\boldsymbol{\phi}},\hat{\boldsymbol{\phi}}} = \begin{pmatrix}G_{22}(t,t) & 2G_{21}(t,t)-\sigma_{\phi,\phi^*}\\ 2G_{21}(t,t)-\sigma_{\phi^*,\phi} & G_{11}(t,t)\end{pmatrix},
\end{aligned} \tag{3.15}$$

with components

$$\begin{aligned}
\sigma_{\phi,\phi^*} = \sigma_{\phi^*,\phi} &= \tfrac{1}{2}\Big(G_{41}(t^-,t)-G_{41}(t^+,t)+G_{32}(t^-,t)-G_{32}(t^+,t)\Big)\\
&= \tfrac{1}{2}\big(\underbrace{G^R(t,t^-)}_{=-\mathrm{i}}-\underbrace{G^R(t,t^+)}_{=0}+\underbrace{G^A(t^-,t)}_{=\mathrm{i}}-\underbrace{G^A(t^+,t)}_{=0}\big)=0,
\end{aligned} \tag{3.16}$$

and

$$\begin{aligned}\sigma_{\phi,\hat{\phi}^*} = \sigma_{\hat{\phi}^*,\phi} &= 2\left(G_{41}(t^+,t) + G_{41}(t^-,t)\right) + G_{32}(t^+,t) + G_{32}(t^-,t) = -\mathrm{i},\\ \sigma_{\phi^*,\hat{\phi}} = \sigma_{\hat{\phi},\phi^*} &= 2\left(G_{32}(t^+,t) + G_{32}(t^-,t)\right) + G_{41}(t^+,t) + G_{41}(t^-,t) = \mathrm{i},\end{aligned} \tag{3.17}$$

which nicely illustrates how time-ordering translates into an explicit evaluation of equal-time advanced and retarded Green functions. Note that to arrive at these results, we used the definitions

$$\begin{aligned}G_{32}(t,t') &= -\mathrm{i}\langle\delta\phi_3(t)\delta\phi_2(t')\rangle = -\mathrm{i}\langle\delta\hat{\phi}(t)\delta\phi^*(t')\rangle = G^A(t,t'),\\ G_{41}(t,t') &= -\mathrm{i}\langle\delta\phi_4(t)\delta\phi_1(t')\rangle = -\mathrm{i}\langle\delta\hat{\phi}^*(t)\delta\phi(t')\rangle = G^R(t',t),\end{aligned} \tag{3.18}$$

and further properties of the Green functions at equal times, e.g. $\mathrm{i}G_{31}(t,t) = \langle\hat{\varphi}(t)\varphi(t)\rangle = 0$, which is true because it relates to the equal-time commutator of two identical operators.

3.1.3 Equations of Motion

Moving forward to the results of the calculation, we find that we need to calculate[4]

$$\frac{\delta \boldsymbol{G}_0^{-1}}{\delta\hat{\varphi}^*}(t,t') = 2\mathrm{i}D\begin{pmatrix} 0 & 0 & \delta(t-t')\varphi^*(t') & \delta^{\pm}(t-t')\varphi(t') \\ 0 & 0 & \delta^{\pm}(t-t')\varphi(t')/2 & 0 \\ \delta(t-t')\varphi^*(t') & \delta^{\pm}(t-t')\varphi(t')/2 & 0 & 0 \\ \delta^{\pm}(t-t')\varphi(t') & 0 & 0 & 0 \end{pmatrix},$$

where we have introduced the shorthand $\delta^{\pm}(t-t') = \delta(t^+-t') + \delta(t^--t')$. This allows us to calculate the equation of motion of the condensate amplitude $\varphi(t)$ by taking the derivative with respect to the adjoint field $\hat{\varphi}^*$, evaluating $G^{R/A}(t,t)$ as before:

$$\begin{aligned}0 &= -2\mathrm{i}\frac{\delta\Gamma[\boldsymbol{\varphi},\boldsymbol{G}]}{\delta\hat{\varphi}^*} = -2\mathrm{i}\frac{\delta S_{\mathrm{K}}[\boldsymbol{\varphi}]}{\delta\hat{\varphi}^*} + \mathrm{Tr}\frac{\delta\boldsymbol{G}_0^{-1}}{\delta\hat{\varphi}^*}\boldsymbol{G}\\ &= -2\mathrm{i}\frac{\delta S_{\mathrm{K}}[\boldsymbol{\varphi}]}{\delta\hat{\varphi}^*} + \int \mathrm{d}\bar{t}\,\mathrm{Tr}\frac{\delta\boldsymbol{G}_0^{-1}}{\delta\hat{\varphi}^*}(t,\bar{t})\boldsymbol{G}(\bar{t},t')\\ &= -2\mathrm{i}\left(\mathrm{i}\partial_t - \omega_0 + \tfrac{\mathrm{i}}{2}(\lambda-\gamma)\right)\varphi + 2\mathrm{i}D\varphi^*\left(G_{13}(t,t) + G_{31}(t,t)\right)\\ &+ \ \mathrm{i}D\varphi\left[G^A(t^+,t) + G^A(t^-,t) + G^A(t,t^+) + G^A(t,t^-)\right]\\ &+ 2\mathrm{i}D\varphi\left[G^R(t^+,t) + G^R(t^-,t) + G^R(t,t^+) + G^R(t,t^-)\right]\\ &= -2\mathrm{i}\left(\mathrm{i}\partial_t - \omega_0 + \tfrac{\mathrm{i}}{2}(\lambda-\gamma)\right)\varphi + 2D\varphi.\end{aligned} \tag{3.19}$$

[4] Here, keep in mind Eq. (A.21).

To find the Keldysh Green function $G^K(t,t')$, we calculate

$$\begin{aligned} 0 &= \int \mathrm{d}\bar{t} \sum_k [\boldsymbol{G}_0^{-1}(t,\bar{t}) - \boldsymbol{\Sigma}(t,\bar{t})]_{4k} [\boldsymbol{G}(\bar{t},t')]_{k2} \\ &= \left(\mathrm{i}\partial_t - \omega_0 + \tfrac{\mathrm{i}}{2}(\lambda-\gamma)\right) G^K(t,t') \\ &+ \mathrm{i}\left(\lambda+\gamma+2D\varphi^*\varphi\right) G^A(t,t') + 2\mathrm{i}D\varphi^2 G_{42}(t,t') \\ &- D\left[-\mathrm{i}G^K(t,t') + 2G^K(t,t)G^A(t,t') + G_{11}(t,t)G_{42}(t,t')\right]. \end{aligned} \tag{3.20}$$

In the "horizontal" direction, by taking the adjoint and switching the time arguments, we find

$$\begin{aligned} 0 &= \left(-\mathrm{i}\partial_{t'} - \omega_0 - \tfrac{\mathrm{i}}{2}(\lambda-\gamma)\right)\left(-G^K(t,t')\right) \\ &- \mathrm{i}\left(\lambda+\gamma+2D\varphi^*\varphi\right) G^R(t,t') - 2\mathrm{i}D\left(\varphi^*\right)^2 \left[G_{42}(t',t)\right]^\dagger \\ &- D\left[-\mathrm{i}G^K(t,t') - 2G^K(t',t')G^R(t,t') + \left[G_{11}(t',t')G_{42}(t',t)\right]^\dagger\right], \end{aligned} \tag{3.21}$$

where we have used the Green-function identity $G^R(t,t') = [G^A(t',t)]^\dagger$. Adding Eqs. (3.20) and (3.21) and taking $t' \to t^+$, we obtain the equation of motion along the time diagonal as

$$\begin{aligned} 0 &= \left(\mathrm{i}\partial_t + \mathrm{i}(\lambda-\gamma)\right) G^K(t,t) + \mathrm{i}\left(\lambda+\gamma+2D\varphi^*\varphi\right)\left(G^A(t,t^+) - G^R(t,t^+)\right) \\ &\quad + 2\mathrm{i}DG^K(t,t) - 2DG^K(t,t)\left(G^A(t,t^+) - G^R(t,t^+)\right) \\ &= \left(\mathrm{i}\partial_T + \mathrm{i}(\lambda-\gamma)\right) G^K(T,0) - \left(\lambda+\gamma+2D\varphi^*\varphi\right), \end{aligned} \tag{3.22}$$

where we have used $G^A(t,t^+) - G^R(t,t^+) = \mathrm{i}$. Eqs. (3.19) and (3.22) can now be rewritten as

$$\begin{aligned} \dot{\varphi} &= -\mathrm{i}\omega_0\varphi - \frac{1}{2}(\lambda-\gamma+2D)\,\varphi, \\ \dot{G}^K &= -(\lambda-\gamma)\,G^K - \mathrm{i}\left(\lambda+\gamma+2D|\varphi|^2\right). \end{aligned} \tag{3.23}$$

To make these expressions more physically transparent, we set $\varphi(t) = \sqrt{2N(t)}\mathrm{e}^{\mathrm{i}\theta(t)}$ and $G^K(t,t) = -\mathrm{i}(2\delta N(t)+1)$, where N and δN are the condensate and non-condensate occupation, respectively.[5] For these quantities, we finally obtain the simple equations

$$\begin{aligned} \dot{N} &= (\gamma-\lambda-2D)\,N, \\ \delta\dot{N} &= \gamma(\delta N+1) - \lambda\delta N + 2DN, \end{aligned} \tag{3.24}$$

[5] This implies $\sqrt{2N}\mathrm{e}^{-\mathrm{i}\theta}\dot{\varphi} = \dot{N} + 2\mathrm{i}N\dot{\theta}$, from which one can see that $\dot{\theta} = -\omega_0$. The factor of two under the square root is necessary to ensure number conservation in exchange with G^K, which corresponds to symmetric or Wigner operator ordering, yet *without* a factor of $1/2$.

which we may interpret as follows. Notice that for $\lambda = \gamma = 0$, which is the case of interest, we have $\dot{N} + \delta\dot{N} = 0$. This tells us that the particles removed from (added to) the condensate go to (come from) the non-condensate. On the one hand, for $D > 0$, which corresponds to *phase diffusion*, the condensate is depleted and goes to an empty steady state. On the other hand, for $D < 0$, the same is true of the *non-condensate*. The latter case mimics the enphasing scenario described in [109, 110]. Thus we can conclude that while the total particle number is indeed unaffected, the phase coherence of the condensate is either destroyed or enhanced.

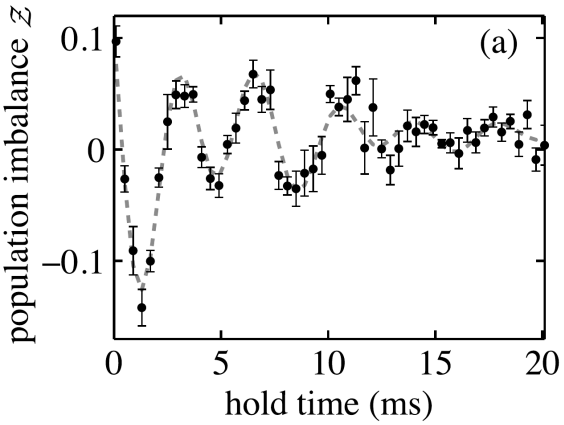

Figure 3.2: Strongly damped Bose-Josephson oscillations as observed in experiment B [116]. For more details, see also [117].

3.2 Fluctuation Damping of Isolated, Oscillating Bose-Einstein Condensates

As experimental systems almost ideally separated from the environment, ultracold atomic gases may serve as a prototype of *closed* quantum systems out of equilibrium. Discussing such systems is only superficially not in line with studying *open* quantum systems. The question we want to pose in this Sec. is rather how an isolated quantum system may still show signs of dissipation? However, we will not touch upon the fundamentals of this question, but merely refer to a known route to dissipative effects in condensate dynamics, which is to include fluctuations and interaction effects beyond the Hartree-Fock-Bogoliubov (HFB) approximation. The excitation of non-condensate quasiparticles can then lead to a damping of oscillatory condensate dynamics [108, 113, 114].

Furthermore, the analysis of Ref. [35], on which this Sec. is based, was restricted to demonstrating in some quantitative detail that many quasiparticles are created in a specific experimental setting, without actually taking interactions into account beyond the HFB approximation, which is ultimately *Markovian* and thus cannot account for effects of dissipation [113].

The experiments by Albiez *et al.* [115] clearly displayed undamped dynamics for extended periods of time (Fig. 3.3). In contrast to this, the experiment in question here is the experimental setting by LeBlanc *et al.* [116], where strong damping of the so-called *Bose-Josephson oscillations* was observed (Fig. 3.2). In the following, we will refer to these two as experiments A and B, respectively. As detailed in Ref. [117], the reason for the observed damping remained unexplained at the time. Ref. [35] addressed this open problem and, thereby, contributed to understanding the role played by the trap geometry in creating fluctuations. A brief introduction to Bose-Josephson junctions will be given next. Notice that parts of the work presented in this Chp. are taken from Ref. [35], of which the author of this thesis is the first author.

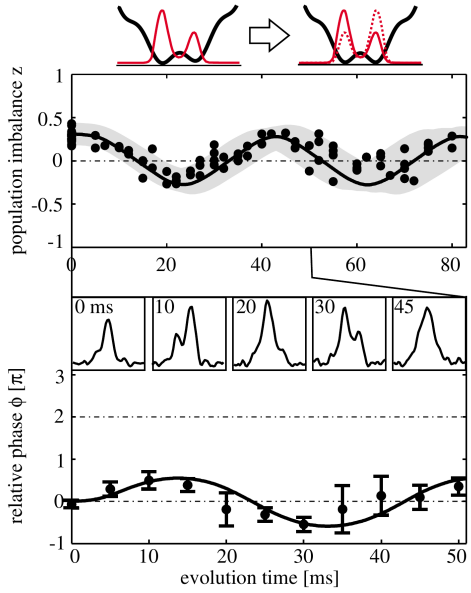

Figure 3.3: Undamped Bose-Josephson oscillations as observed in experiment A [115]. A sketch of the double-well potential and the localized left and right wavefunctions can be seen at the top.

3.2.1 Bose-Josephson Junctions

Classically, no current will flow between two conducting pieces of material when they are separated by an insulator. Cooled down into the superconducting regime, however, the coherence length of the quantum mechanical wavefunction may become large enough to "leak" through the insulator into the other piece of superconductor, thus creating an overlap that leads to a finite tunneling probability of the Cooper pairs. This is known as the *Josephson effect* [118]. A similar effect can occur when two ultracold atomic Bose-Einstein condensates are separated by a potential barrier [119]. If the barrier is low, the two coherent matter waves localized in either well also possess an overlap that induces a tunneling matrix element. The resulting Bose-Josephson oscillations have been observed in a number of experiments [115, 116, 120].

The paradigmatic model for this system is the *two-mode approximation*, which was proposed in Ref. [121] and has been widely investigated [122–136]. Despite its seeming simplicity, due to non-linearity it gives rise to a variety of interesting physical effects beyond Bose-Josephson oscillations, the most prominent of which is *macroscopic quantum self-trapping* (MQST) [122]. As recapitulated in App. C, its phase-space structure also enables the appearance of so-called π-oscillations [124]. An interesting description in terms of phase-space methods has been given in Ref. [134]. In the context of the two-mode approximation, it has been noted how a dynamical instability can give rise to significant contributions beyond mean-field even when the condensate occupation is large [130, 131]. As shown in detail in App. C, this is due to a critical slowing down brought about by the repulsive interaction between the atoms. A soft mode, however, is not observed in either of the two experiments in question. This mechanism can, therefore,

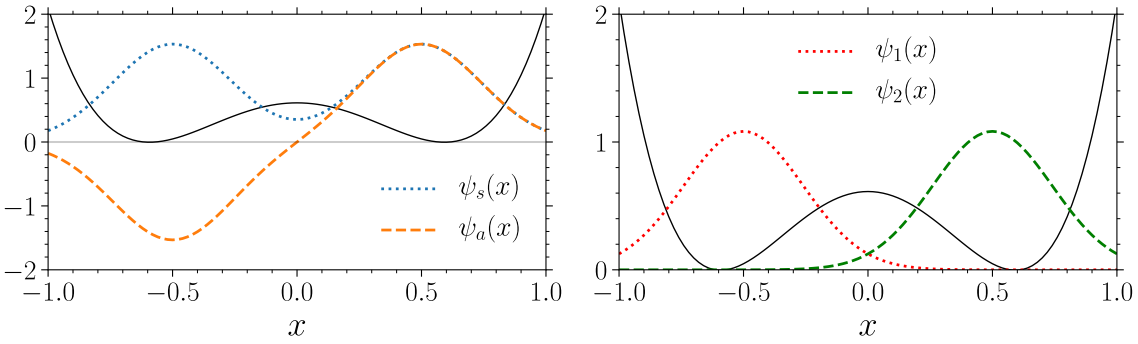

Figure 3.4: Sketch of the x-components of the eigenfunctions $\psi(\mathbf{r}) = \psi(x)\psi(y)\psi(z)$ of a symmetric, separable double-well potential $V_{\text{ext}}(\mathbf{r}) = V(x) + V(y) + V(z)$. The potential along the x-direction, $V(x)$, is indicated as a solid (black) line.

not be responsible for the presumed excitation of quasiparticles in experiment B. One possible way of going beyond the standard two-mode approximation is described in [135]: instead of computing the eigenmodes of the external trap, a renormalization by an effective interaction is taken into account, which leads to an "improved two-mode model". While we do take similar non-local coupling terms into consideration, another way to model the experiments without solving a fully space-dependent problem is to increase the number of trap eigenmodes beyond two. This possibility is also discussed in [135]. In contrast to their approach, however, we will work with the unrenormalized trap eigenstates. Hence, a first step beyond the two-mode model is to investigate a *three-mode* approximation more closely. The stability analysis of an according system is also given in App. C. Another model related yet different from ours was studied in Ref. [137]. In the end, a realistic description of the early dynamics of the experiments requires to take even more modes into account. The three-mode approximation still provides an idea of how the creation of quasiparticles may occur without critical slowing down in the observed Bose-Josephson oscillations.

3.2.2 Quantum Field Theory of a Trapped Bose Gas

There are two standard approaches to the description of the non-equilibrium dynamics of ultracold bosonic atoms. The first is operator-based and starts from the Heisenberg equation for the field operator [138]. The second is via quantum field theory and the corresponding coherent-state path integral [81], which is the approach we are going to present here. For the exemplary case of the two-mode approximation, in App. C we fall back on the operator-based approach to verify the results we derived from quantum field theory. Accordingly, we begin with the action S for a trapped, atomic Bose gas with a contact interaction, which reads

$$S\left[\psi,\psi^*\right] = \int \mathrm{d}^3r\mathrm{d}t\left[\psi^*(\mathbf{r},t)G_0^{-1}(\mathbf{r},t)\psi(\mathbf{r},t) - \frac{\tilde{g}}{2}\psi^*(\mathbf{r},t)\psi^*(\mathbf{r},t)\psi(\mathbf{r},t)\psi(\mathbf{r},t)\right]. \quad (3.25)$$

We have introduced the complex bosonic field $\psi(\mathbf{r},t)$, the coupling parameter $\tilde{g} = 4\pi\hbar^2 a_s/m$ proportional to the s-wave scattering length a_s [139, 140], and the inverse bare Green function

$$G_0^{-1}(\mathbf{r},t) = \mathrm{i}\partial_t - \left(-\hbar^2\nabla^2/2m + V_{\text{ext}}(\mathbf{r})\right), \tag{3.26}$$

where $V_{\text{ext}}(\mathbf{r})$ is the external trapping potential to which the atoms are confined. The spatial dependence of the field $\psi(\mathbf{r},t)$ may now be resolved into the complete, orthonormal basis of single-particle eigenfunctions of the trap [114], which we write as $\{\psi_s(\mathbf{r}), \psi_a(\mathbf{r}), \psi_3(\mathbf{r}), \psi_4(\mathbf{r}), \dots\}$. The bosonic field hence becomes

$$\psi(\mathbf{r},t) = \psi_s(\mathbf{r})\phi_s(t) + \psi_a(\mathbf{r})\phi_a(t) + \sum_{m=3}^{M} \psi_m(\mathbf{r})\phi_m(t), \tag{3.27}$$

with time-dependent complex amplitudes $\phi_{s,\,a}(t)$ and $\phi_m(t)$. The parameter M designates the number of modes to be taken into account. The wavefunctions $\psi_i(\mathbf{r})$ are the solutions of the stationary Schrödinger equation with the potential $V_{\text{ext}}(\mathbf{r})$. Their eigenfrequencies are $\{\varepsilon_s, \varepsilon_a, \varepsilon_3, \varepsilon_4, \dots\}$. The wavefunctions $\psi_s(\mathbf{r})$ and $\psi_a(\mathbf{r})$ are the two lowest eigenfunctions of $V_{\text{ext}}(\mathbf{r})$. As sketched in Fig. 3.4, they extend over both wells and have even (s) and odd (a) parity, respectively. In view of the anticipated dynamics with different occupation numbers in the two wells, it is useful to define the superpositions $\psi_{1,2}(\mathbf{r}) = [\psi_s(\mathbf{r}) \mp \psi_a(\mathbf{r})]/\sqrt{2}$, since these are localized in the left or right well, respectively (s. Fig. 3.4). With the expansion (3.27), the action takes the form $S = S_0 + S_{\text{int}}$. The quadratic and interacting parts are

$$S_0 = \int \mathrm{d}t \left\{ \sum_{i=1}^{M} \left[\phi_i^*(t)\left(\mathrm{i}\partial_t - \varepsilon_i\right)\phi_i(t)\right] - J\left[\phi_1^*(t)\phi_2(t) + \phi_2^*(t)\phi_1(t)\right] \right\}, \tag{3.28}$$

$$S_{\text{int}} = -\frac{1}{2}\sum_{i,j,k,l=1}^{M} U_{ijkl} \int \mathrm{d}t\, \phi_i^*(t)\phi_j^*(t)\phi_k(t)\phi_l(t), \tag{3.29}$$

respectively, where $\phi_{1,\,2}(t)$ are the antisymmetric and symmetric superpositions of the time-dependent field amplitudes $\phi_{s,a}(t)$, respectively. In this mode representation, the spatial dependence of the Bose field $\psi(\mathbf{r},t)$ is absorbed into overlap integrals according to

$$\varepsilon_i = \int \mathrm{d}^3 r\, \psi_i(\mathbf{r}) \left(-\frac{\hbar^2\nabla^2}{2m} + V_{\text{ext}}(\mathbf{r})\right) \psi_i(\mathbf{r}), \tag{3.30a}$$

$$J = \int \mathrm{d}^3 r\, \psi_1(\mathbf{r}) \left(-\frac{\hbar^2\nabla^2}{2m} + V_{\text{ext}}(\mathbf{r})\right) \psi_2(\mathbf{r}), \tag{3.30b}$$

$$U_{ijkl} = \tilde{g} \int \mathrm{d}^3 r\, \psi_i(\mathbf{r})\psi_j(\mathbf{r})\psi_k(\mathbf{r})\psi_l(\mathbf{r}), \tag{3.30c}$$

where without loss of generality the eigenfunctions $\psi_i(\mathbf{r})$ are chosen real. Note that $\varepsilon_1 = \varepsilon_2 = (\varepsilon_s + \varepsilon_a)/2$ and $J = (\varepsilon_s - \varepsilon_a)/2$, and that the hybridizing bare Josephson coupling $J < 0$ exists

only between the two localized lowest modes $\psi_1(\mathbf{r})$ and $\psi_2(\mathbf{r})$, while the modes with $i \geq 3$ are mutually orthogonal eigenmodes of the trap. For the symmetric double-well, the zero of energy may be defined as $\varepsilon_1 = \varepsilon_2 = 0$. For $M \to \infty$, the representation in terms of the single-particle trap eigenmodes defined by Eqs. (3.28), (3.29) and (3.30) is exact. Numerically, the decomposition in Eq. (3.27) is akin to a Galerkin method: replacing the space-dependence by summations over eigenfunctions leads to a significant simplification of the numerical initial-value problem when truncating the decomposition at a finite value of M.

For experiment A [115], four modes were found to be sufficient to produce good agreement with the experimental data. Furthermore, the Josephson oscillations remained stable over the period of experimental observation. For experiment B [116], on the contrary, we found that at least six modes are relevant for the dynamics, and that the resulting Josephson oscillations are indeed unstable.

3.2.3 Experimental Trapping Potentials & Computation of Parameters

The trapping potential employed in experiment A is given by

$$V_A(\mathbf{r}) = \frac{m}{2}\left[\omega_x^2 x^2 + \omega_y^2 y^2 + \omega_z^2 z^2\right] + \frac{V_0}{2}\left[1 + \cos\left(\frac{2\pi x}{d}\right)\right], \tag{3.31}$$

where the frequencies can be found in Ref. [115]. Since a Hamiltonian with this potential is separable, the eigenfunctions are products of the eigenfunctions in each spatial dimension. Hence, the diagonalization of the non-interacting trap system reduces to three separate diagonalizations, which can be performed by applying standard library methods (e.g. Ref. [141]), yielding all eigenvalues and eigenfunctions of the trap. The confining potential of experiment B [116] is more involved and reads

$$V_B(\mathbf{r}) = m'_F \hbar \sqrt{\delta(\mathbf{r})^2 + \left(\frac{\mu_\mathrm{B} g_F B_{\mathrm{RF},\perp}(\mathbf{r})}{2\hbar}\right)^2} + \frac{m}{2}\omega_y^2 y^2. \tag{3.32}$$

where definitions and parameters are given in [116]. Since Eq. (3.32) is not separable along the spatial axes, the Hamiltonian dimension is too large for direct numerical diagonalization. In order to be as close to the actual experiment as possible, one should not approximate $V_B(\mathbf{r})$ by an expression that would be easily accessible numerically. Therefore, one has to resort to an algorithm that can handle very large matrices, such as the *Jacobi-Davidson* algorithm [142]. Furthermore, it is crucial to have a precise starting guess for the initial vector spanning the search subspace. A working practice is to use a library method [141] to obtain a coarse-grained guess from direct diagonalization and to interpolate this guess to twice the precision, which can then be used as a starting vector for the Jacobi-Davidson algorithm to retrieve the actual vector at the doubled resolution. In combination with a sparse-matrix class, this procedure achieves the desired performance, that is, one can obtain about ten states for resolutions of up to $\mathcal{N} = 100$ grid points in three dimensions. The separable potential $V_A(\mathbf{r})$ can moreover be used to confirm the accuracy of the algorithm.

Experiment	N	z	N_1	N_2	N_3	N_4	N_5	N_6
A	1150	0.290	742	408	0	0	–	–
B	4500	0.116	2436	1914	75	75	0	0

Table 3.1: Occupation numbers at time $t = 0$ used for the numerical calculations.

3.2.4 HFB Equations in Multi-Mode Approximation

Instead of repeating the derivation of the equations of motion for the present problem, we point to the previous Sec. 3.1 and remark that the derivation follows along the very same lines when the dissipative D-vertices are replaced by the U_{ijkl}. Furthermore, this derivation is performed with all details in paragraph C.1.6 of App. C for the two-mode approximation. To facilitate a compact notation, it is useful to introduce the following matrix in "Bogoliubov" space,

$$\begin{aligned} \boldsymbol{G}^K_{ij}(t,t') &= \begin{pmatrix} G_{ij}(t,t') & g_{ij}(t,t') \\ -g^*_{ij}(t,t') & -G^*_{ij}(t,t') \end{pmatrix} \\ &= -\mathrm{i} \begin{pmatrix} \langle \delta\phi_i(t)\delta\phi^*_j(t')\rangle & \langle \delta\phi_i(t)\delta\phi^*_j(t')\rangle \\ \langle \delta\phi^*_i(t)\delta\phi^*_j(t')\rangle & \langle \delta\phi^*_i(t)\delta\phi_j(t')\rangle \end{pmatrix}, \end{aligned} \tag{3.33}$$

where we have dropped the "Keldysh" superscript in the matrix components. In terms of the latter, the multi-mode Gross-Pitaevskii equation in trap eigenbasis, modified by the coupling to the non-condensate part, becomes

$$\begin{aligned} 0 = \left(i\delta_{ij}\partial_t - h_{ij}\right)\varphi_j - \frac{U_{ijkl}}{2}\left[\varphi^*_j\varphi_k\varphi_l + i\varphi^*_j g_{kl}(t,t)\right. \\ \left. + i\varphi_k G_{jl}(t,t) + i\varphi_l G_{jk}(t,t)\right] \end{aligned} \tag{3.34}$$

where the summation over repeated indices is implied. Since we are working in Hartree-Fock approximation, both the inverse propagator and the self-energy are local in time. Dropping the Keldysh self-energy component from the infinitesimal damping formally required to regularize the dynamics, we can write the Dyson equations for the Keldysh Green functions as

$$0 = \int \mathrm{d}\bar{t}\; \delta(t-\bar{t}) \left\{ \left[\mathbf{G}^R_0\right]^{-1}_{ij}(t) - \boldsymbol{\Sigma}^R_{ij}(t) \right\} \mathbf{G}^K_{jk}\left(\bar{t},t'\right). \tag{3.35}$$

The bare inverse retarded Green function and the retarded self-energy read

$$\begin{aligned} \left[\mathbf{G}^R_0\right]^{-1}_{ij}(t) &= \begin{pmatrix} i\delta_{ij}\partial_t - h_{ij} & 0 \\ 0 & -i\delta_{ij}\partial_t - h_{ij} \end{pmatrix}, \\ \boldsymbol{\Sigma}^R_{ij}(t) &= \begin{pmatrix} \Sigma_{ij}(t) & \sigma_{ij}(t) \\ \sigma^*_{ij}(t) & \Sigma_{ij}(t) \end{pmatrix}, \end{aligned} \tag{3.36}$$

where the components are

$$\Sigma_{ij}(t) = U_{ijkl}\left[\varphi_k^*(t)\varphi_l(t) + \mathrm{i}G_{kl}(t,t)\right], \tag{3.37a}$$

$$\sigma_{ij}(t) = \frac{U_{ijkl}}{2}\left[\varphi_k(t)\varphi_l(t) + \mathrm{i}g_{kl}(t,t)\right]. \tag{3.37b}$$

Note that we included the "mass terms" proportional to the condensate fields in the self-energy instead of the inverse propagator. Finally, the equations of motion for the Keldysh components become

$$0 = \left(i\delta_{ij}\partial_t - h_{ij} - \Sigma_{ij}(t)\right)G_{jk}(t,t') + \sigma_{ij}(t)g_{jk}^*(t,t') \tag{3.38a}$$

$$0 = \left(i\delta_{ij}\partial_t - h_{ij} - \Sigma_{ij}(t)\right)g_{jk}(t,t') + \sigma_{ij}(t)G_{jk}^*(t,t'). \tag{3.38b}$$

Looking to Eq. (3.34), we see that it is sufficient to solve for G_{ij} and the anomalous g_{ij} in the equal-time limit, which as before can be obtained by combining Eqs. (3.38) with their adjoint counterparts. The initial conditions for the dynamical problem specified by Eqs. (3.34) and (3.38) are now chosen such that all non-condensate contributions vanish, while the condensate occupations and phases as well as the interaction parameters are determined by the respective experiment. Before going over to the results, it is useful to define the *population imbalance*

$$z(t) = \frac{|\varphi_1|^2 - |\varphi_2|^2}{|\varphi_1|^2 + |\varphi_2|^2} \tag{3.39}$$

for the two condensates localized in the left and right potential well. This is the main quantity measured in the experiments (cf. Figs. 3.2 and 3.3). As in our previous discussion of de- and enphasing, we also have a non-condensate part

$$\delta N(t) = \sum_{i=1}^{M}\frac{1}{2}\left(\mathrm{i}G_{ii}(t,t) - 1\right), \tag{3.40}$$

which can be used as a proxy for the stability of the condensate part. In contrast to the scenario described in 3.1, in a closed system there is no externally induced dephasing. We understand from the investigation of the two-mode approximation in C.1, however, that a dynamical instability can essentially have the same effect and also lead to "decoherence" [131]. In a system with more than two modes, moreover, there is the possibility of having one frequency going soft while others remain finite. In the three-mode system of Sec. C.2, the instability of the system is due to the renormalized single-particle energy $\tilde{\varepsilon}_3$ coming close to the effective Josephson frequency $\tilde{\omega}_J$, an effect that can be understood as an instance of *parametric resonance*. The renormalized Josephson oscillations turn out to be rapid enough to excite the quasiparticles of the third mode even when these also receive an energy shift due to their interaction with the two localized condensates. This puts us in a position to appreciate how damping due to quasiparticles could occur in the experiments of Ref. [116] without any observed slowing down of the Josephson frequency. The non-linearity in conjunction with any specific trap can result in an (undesired) instability of the

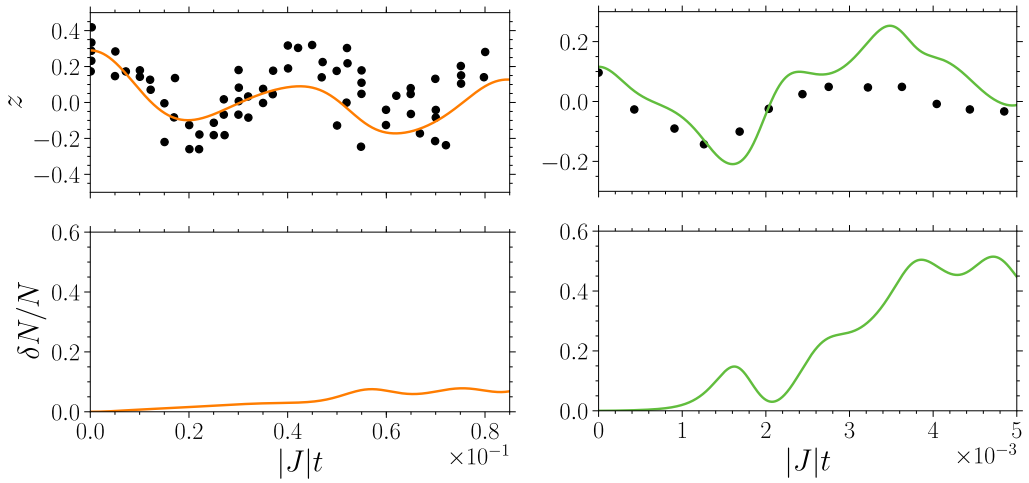

Figure 3.5: Population imbalance $z(t)$ and relative fraction of fluctuations $\delta N(t)/N$ for experiment A *(left)* and B *(right)*. The experimental data points (black circles) are taken from Refs. [115] and [116], respectively. The initial conditions and parameters for the calculations are listed in Tab. 3.1 and Ref. [35].

ground state of interest, which in double-well experiments is always embodied by the two left- and right-localized modes. Since, in the trap-eigenmode picture, these two states always couple to higher excited states, the two-mode approximation can become inadequate.

3.2.5 Comparison with Experiments

To examine how experiments A and B fit into the resonance scenario described above, in Fig. 3.5 we present the results of our computations for experiment A with $M = 4$ modes included, while for experiment B we took $M = 6$ modes into account. For the former, the agreement with the experiment is very good regarding both the frequency and the amplitude of the Josephson oscillations. The fraction of fluctuations remains below 10%, indicating that this experimental setup is away from the resonance discussed above. Note that there is no fitting of parameters involved. For experiment B, we assume a small initial condensate occupation of the modes $m = 3, 4$, as listed in Tab. 3.1, because of the small excitation energy of these modes with regard to the larger interaction parameters. Here, the agreement with experiment is quantitatively acceptable only for short times. At the point where the agreement starts to decrease, our results show a fast and efficient excitation of fluctuations, which indicates that this experimental setup is in the resonant regime. Importantly, we find that the efficient creation of fluctuations for the parameters of experiment B is robust, independent of the small condensate occupation of the modes with $m = 3, 4$ as well as the precise value of N. The reason for the reduced quantitative agreement with experiment can indeed be understood from the behavior of the fluctuation fraction. In the lower right panel of Fig. 3.5, the departure of the theoretical results from the experimental data is significant for times when the non-condensate fraction $\delta N(t)/N$ is large, which indicates that the HFB approximation employed in this Sec. is not sufficient and higher-order corrections should be included to account for the inelastic collisions of quasiparticles. Beyond-HFB diagrammatics will be of importance in Chp. 5.

CHAPTER 4

Second-Order Correlation Functions of Photon Bose-Einstein Condensates

Physical systems in thermal equilibrium are well understood. Natural systems, and in particular organic matter, however, are seldomly found in conditions of thermal equilibrium. Rather, there is energy going *into* the system via certain processes and energy going *out of* the system via others. This energy flow drives the system away from equilibrium. Earth is the most prominent example of such a non-equilibrium system: energy enters it in the form of visible light from the sun and is later on radiated away in the infrared. As a matter of fact, photon condensates are closely analogous: light of a shorter wavelength excites the organic dye molecules and is converted into photons of longer wavelength before it leaves the cavity.

For systems in thermal equilibrium, the machinery of equilibrium statistical mechanics allows one to calculate straightforwardly, for instance, the spectral intensity distribution of a photon gas. As we have seen in paragraph 1.1.1, this results in a Bose-Einstein distribution. In non-equilibrium scenarios where Boltzmann's considerations no longer apply (cf. the introduction to Sec. 1.1), however, an equally general formalism does not exist. As we remarked in paragraph 2.1.3, one consequence of this is that in non-equilibrium quantum field theory, the statistical function is no longer fixed to the Bose distribution function but becomes a degree of freedom on the same footing as the spectral function. To bridge the gap between well-understood equilibrium and still largely unexplored non-equilibrium phenomena, it seems reasonable to start by investigating a system as it is gradually driven away from equilibrium. In this respect, the photon BEC holds an ideal position because it can be operated both very close and further away from equilibrium. Though it is in fact never in a perfect thermal equilibrium state, it reliably undergoes Bose-Einstein condensation, which remains true even as the system is driven more strongly. As we will see in the following, the earliest signs of the non-equilibrium character of the driven-dissipative photon gas do not manifest in the spectral intensity distribution but in the time dependence of the intensity fluctuations. The energy flow through the system makes it non-Hermitian and induces a novel driven-dissipative transition in the second-order coherence of the photon condensate characterized by the appearance of an exceptional point. If only the static intensity spectrum was considered, this transition would go unnoticed, as would the fact that the system is not truly in equilibrium.

Chp. 4 is organized as follows. After introducing the non-equilibrium model of the photon condensate in Sec. 4.1 by deriving it from a microscopic Hamiltonian via a polaron transformation and the Born-Markov approximation, we describe the methods required to study second-order correlation functions in Sec. 4.2 and also present some illustrative solutions. Finally, in Sec. 4.3 we apply the developed methods to understand the experimental data. Notice that parts of the work presented in this Chp. are taken from Ref. [36], of which the author of this thesis is a co-author.

4.1 Non-Equilibrium Model of the Photon BEC

As mentioned above, the photon BEC is *not* a closed system: the cavity mirrors are not perfect, for which reason the photons do not stay inside the cavity indefinitely, which in turn necessitates the introduction of an external optical pumping to supply excitations to the system. Furthermore, the quantum efficiency of the dye molecules only amounts to about 95%, which means that a fraction of the absorbed photons will not be re-emitted. For all of these reasons, the photon BEC should be modeled as an *open system*. The cavity loss, the optical pumping, and the electronic loss due to imperfect quantum efficiency can be described within the previously encountered framework of the *master equation*, as was done in Ref. [16] for the first time. A more detailed discussion of the same model may be found in [17].

The Franck-Condon principle was discussed in the introduction (cf. 1.3.1) as the physical foundation of the interaction between the photons and dye molecules. We understood in broad terms how the molecular vibrations alter the electronic transition frequency: insufficient or excess energy of an incoming photon may be compensated by destruction or creation of a corresponding amount of phonons. A two-level system with a similarly "fluctuating" transition frequency is described in Ref. [15] by means of the modified Jaynes-Cummings Hamiltonian

$$H_X = \omega_0 a^\dagger a + g\left(a^\dagger \sigma^- + a\sigma^+\right) + \frac{\Delta}{2}\sigma^z + \frac{1}{2}X(t)\sigma^z, \tag{4.1}$$

where $X(t)$ is a fluctuating quantity. The model in Ref. [16] is now a physically motivated alteration of the Hamiltonian (4.1). Since the fluctuations of the dye-molecule transition are generated by the phonon coupling, a promising idea is to replace $X(t)$ by some function of the phonon operators. The question then is of course: which function? The physics of the Franck-Condon principle provides the answer. As we learned above, the equilibrium positions of the constituent atoms in the dye molecules depend on the electronic state. When an electronic transition takes place, the atoms are suddenly in a non-equilibrium state and begin to vibrate. If one idealizes these molecular vibrations with the help of a single phonon mode per molecule with operators b_m and $b_m^\dagger$, this means that the rest position of the phononic oscillator should be coupled to the electronic transition, which suggests the following Hamiltonian [16, 143] for a collection of M molecules and multiple cavity modes:

$$H = \sum_k \omega_k a_k^\dagger a_k + \sum_{m=1}^{M}\left[\frac{\Delta}{2}\sigma_m^z + \Omega\, b_m^\dagger b_m + \Omega\sqrt{S}\,\sigma_m^z\left(b_m + b_m^\dagger\right) + g\sum_k\left(a_k\sigma_m^+ + a_k^\dagger\sigma_m^-\right)\right]. \tag{4.2}$$

The cavity-photon modes with transverse dispersion ω_k are represented by the bosonic operators a_k and $a_k^\dagger$. The vibrational states of dye molecule m have an oscillator frequency Ω. The electronic two-level system of molecule m is described by the Pauli matrix σ_m^z and raising/lowering operators $\sigma_m^\pm$, the electronic transition frequency being Δ. The Franck-Condon coupling is parametrized by the so-called *Huang-Rhys parameter* S, where the phonon position operators are $\hat{x}_m \sim (b_m + b_m^\dagger)$. Since $\sigma_m^z = \sigma_m^+\sigma_m^- - \sigma_m^-\sigma_m^+$, the effect of this term will be a displacement of the phononic oscillator with the sign depending on whether the molecule is in the electronic ground or excited state. The effect of having several vibrational modes is discussed in [17].

For the rest of this Sec., we will follow [15–17, 19] in developing the Hamiltonian (4.2) into a description of the open-system dynamics of the photon BEC. The first step is to make a *polaron transformation* to deal with the potentially strong Franck-Condon coupling parameterized by S. After that, the second step is to derive a master equation by treating the phonons as a bath to which the system is weakly coupled via the optical transition parameter g.

4.1.1 Polaron Transformation

In this paragraph, we will perform an exemplary polaron transformation on the Hamiltonian

$$\tilde{H} = \omega_0 a^\dagger a + \Omega b^\dagger b + \frac{\Delta}{2}\sigma^z + g\left(a\sigma^+ + a^\dagger\sigma^-\right) + \Omega\sqrt{S}\sigma^z(b + b^\dagger) \tag{4.3}$$

from which the analogous transformation of the Hamiltonian (4.2) may be obtained straightforwardly. The polaron transformation is defined via the unitary operator

$$\hat{U} = \exp\left\{-\sqrt{S}\sigma^z\left(b^\dagger - b\right)\right\}. \tag{4.4}$$

As this expression suggests, it is designed to undo the shift proportional to the phonon position operator. To apply it to the present case, we need to calculate the action of $\hat{U}$ on the separate terms in the Hamiltonian by means of a commutator expansion,[1] i.e.

$$\begin{aligned}
\hat{U}^\dagger\sigma^z\hat{U} &= \sigma^z + \sqrt{S}\left(b^\dagger - b\right)[\sigma^z, \sigma^z] + \ldots = \sigma^z, \\
\hat{U}^\dagger\sigma^\pm\hat{U} &= \sigma^\pm + \sqrt{S}\left(b^\dagger - b\right)[\sigma^z, \sigma^\pm] + \ldots \\
&= \sigma^\pm \pm 2\sqrt{S}\left(b^\dagger - b\right)\sigma^\pm + \frac{1}{2!}\left(2\sqrt{S}\left(b^\dagger - b\right)\right)^2\sigma^\pm \pm \ldots \\
&= \sigma^\pm \exp\left\{\pm 2\sqrt{S}\left(b^\dagger - b\right)\right\}, \\
\hat{U}^\dagger b\hat{U} &= b + \sqrt{S}\sigma^z[b^\dagger - b, b] + \ldots = b - \sqrt{S}\sigma^z.
\end{aligned} \tag{4.5}$$

From the last line, we can also see that $\hat{U}^\dagger b^\dagger\hat{U} = b^\dagger - \sqrt{S}\sigma^z$. This implies $\hat{U}^\dagger b^\dagger b\hat{U} = \hat{U}^\dagger b^\dagger\hat{U}\hat{U}^\dagger b\hat{U} = b^\dagger b - \sqrt{S}\sigma^z\left(b + b^\dagger\right) + S\cdot\mathbb{1}$. By construction, the second term will exactly cancel the Franck-Condon coupling proportional to $\Omega\sqrt{S}$. For the total Hamiltonian, dropping the

[1] $\mathrm{e}^{\hat{S}}\,\hat{X}\,\mathrm{e}^{-\hat{S}} = \hat{X} + [\hat{S}, \hat{X}] + \frac{1}{2!}[\hat{S}, [\hat{S}, \hat{X}]] + \ldots$

constant, we come out with

$$\hat{U}^\dagger \tilde{H} \hat{U} = \omega_0 a^\dagger a + \Omega b^\dagger b + \frac{\Delta}{2}\sigma^z + g\left(a\sigma^+ \hat{D}(2\sqrt{S}) + a^\dagger \sigma^- \hat{D}(-2\sqrt{S})\right), \tag{4.6}$$

where $\hat{D}(\alpha) = \exp\{\alpha b^\dagger - \alpha^* b\}$ is the displacement operator of the phonon mode. Going back to the general Hamiltonian (4.2), by sequentially applying $\hat{U}_m = \exp\{-\sqrt{S}\sigma^z(b_m^\dagger - b_m)\}$ to each molecule, we find $\hat{U}_m^\dagger H \hat{U}_m = H_S + H_R + V_{RS}$, where the system part reads

$$H_S = \sum_k \omega_k a_k^\dagger a_k + \sum_{m=1}^{M} \frac{\Delta}{2}\sigma_m^z, \tag{4.7}$$

the reservoir part is $H_R = \sum_{m=1}^{M} \Omega\, b_m^\dagger b_m$, and the system-reservoir coupling becomes

$$V_{RS} = g\sum_k \sum_{m=1}^{M}\left(a_k \sigma_m^+ \hat{D}_m(2\sqrt{S}) + a_k^\dagger \sigma_m^- \hat{D}_m(-2\sqrt{S})\right), \tag{4.8}$$

with the displacement operators $\hat{D}_m$ being defined analogously to before. The presence of these operators changes the former Jaynes-Cummings coupling into an interaction where the emission and absorption of photons is accompanied by potentially multiple creation and destruction events of vibrational quanta. Since V_{RS} is proportional to g, in its new form the Hamiltonian lends itself to a perturbative expansion along the lines of paragraph 1.5.3.

4.1.2 Removal of First-Order Contribution

Assuming a thermal reservoir density matrix at inverse temperature β, one may use the identity [19]

$$\langle \hat{D}(\alpha)\rangle_R = \exp\left\{-\frac{|\alpha|^2}{2}\coth\frac{\beta\omega}{2}\right\}, \tag{4.9}$$

which holds for the harmonic oscillator with frequency ω, to calculate

$$\langle \hat{D}_m(\pm 2\sqrt{S})\rangle_R = \exp\left\{-2S\coth\frac{\beta\Omega}{2}\right\}. \tag{4.10}$$

where $\langle X\rangle_R = \mathrm{Tr}_R\, X\rho_R$. In analogy to a proper cumulant expansion, this first-order average ought to be factored out of the perturbative expansion [19]. Note that this step was not discussed in Ref. [16]. Hence, we introduce a constructive zero and write

$$\hat{D}_m(2\sqrt{S}) = \hat{D}_m = (\hat{D}_m - \langle \hat{D}_m\rangle_R) + \langle \hat{D}_m\rangle_R,$$

and define the coherent term

$$H_{\text{coh}} = g_\beta \sum_k \sum_{m=1}^{M} \left(a_k \sigma_m^+ + a_k^\dagger \sigma_m^- \right), \tag{4.11}$$

with the thermally averaged coupling constant $g_\beta = g \exp\{-2S \coth \beta\Omega/2\}$. This term would have to be added to the system part of the total Hamiltonian. However, since the experiments relevant to this Chp. operate in the regime $g_\beta/g \ll 1$ [19], and the detunings are very large compared to the coherent coupling, $|\omega_k - \Delta| \gg g$, the cavity mode effectively couples to the molecules only incoherently via the Lindblad operators to be derived below. Therefore, the contribution of H_{coh} can be neglected, which then agrees with the approach of [16].

4.1.3 Cavity Loss, Optical Pumping and Imperfect Quantum Efficiency

Assuming that the photons and the molecules are coupled to external baths that do not influence each other, we can include the discussed processes of cavity loss κ, external optical pumping $\Gamma_\uparrow$, and imperfect quantum efficiency $\Gamma_\downarrow$, by writing down the master equation [16, 19]

$$\dot{\rho}(t) = -\mathrm{i}[H_S + H_R + V_{RS}, \rho(t)] + \sum_k \frac{\kappa}{2} \mathcal{L}[a_k]\rho(t) + \sum_{m=1}^{M} \left[\frac{\Gamma_\uparrow}{2} \mathcal{L}[\sigma_m^+] + \frac{\Gamma_\downarrow}{2} \mathcal{L}[\sigma_m^-] \right] \rho(t), \tag{4.12}$$

where the Lindbladians are defined as $\mathcal{L}[L]\rho(t) = 2L\rho(t)L^\dagger - \{L^\dagger L, \rho(t)\}$. This assumes the cut-off frequency of the cavity to be so large that the surrounding electromagnetic environment may be considered to be at zero temperature.

4.1.4 Born-Markov Approximation

Continuing with our discussion of the Hamiltonian part

$$H = H_S + H_R + g \sum_k \sum_{m=1}^{M} \left[a_k \sigma_m^+ \left(\hat{D}_m(2\sqrt{S}) - \langle \hat{D}_m \rangle_R \right) + a_k^\dagger \sigma_m^- \left(\hat{D}_m(-2\sqrt{S}) - \langle \hat{D}_m \rangle_R \right) \right],$$

we are now ready for the perturbative treatment in the weak optical coupling g. As underlined once more by the form in which we have written the Hamiltonian, the phonons play the role of the reservoir. The first step is to transform V_{RS} to the interaction picture with respect to $H_S + H_R$. For

the sake of completeness, note that the interaction picture of the phonon annihilation operator is

$$\begin{aligned}\frac{1}{2\sqrt{S}}\,\mathrm{e}^{\mathrm{i}\Omega b_m^\dagger b_m}\,b_m\,\mathrm{e}^{-\mathrm{i}\Omega b_m^\dagger b_m} &= b_m + \mathrm{i}\Omega t[b_m^\dagger b_m, b_m] + \frac{(\mathrm{i}\Omega t)^2}{2!}[b_m^\dagger b_m,[b_m^\dagger b_m, b_m]] + ... \\ &= b_m - \mathrm{i}\Omega t b_m + \frac{(\mathrm{i}\Omega t)^2}{2!}b_m - ... \\ &= b_m \sum_{k=0}^{\infty}\frac{(-\mathrm{i}\Omega t)^k}{k!} = b_m\,\mathrm{e}^{-\mathrm{i}\Omega t}.\end{aligned} \tag{4.13}$$

To find the interaction picture of the displacement operator, one may perform

$$\mathrm{e}^{\mathrm{i}\Omega b_m^\dagger b_m}\left(b_m^\dagger - b_m\right)^k \mathrm{e}^{-\mathrm{i}\Omega b_m^\dagger b_m} = \left(\mathrm{e}^{\mathrm{i}\Omega b_m^\dagger b_m}\left(b_m^\dagger - b_m\right)\mathrm{e}^{-\mathrm{i}\Omega b_m^\dagger b_m}\right)^k = \left(b_m^\dagger\,\mathrm{e}^{\mathrm{i}\Omega t} - b_m\,\mathrm{e}^{-\mathrm{i}\Omega t}\right)^k,$$

from which one obtains

$$\mathrm{e}^{\mathrm{i}\Omega b_m^\dagger b_m}\,\hat{D}_m(\pm 2\sqrt{S})\,\mathrm{e}^{-\mathrm{i}\Omega b_m^\dagger b_m} = \hat{D}_m(\pm 2\sqrt{S}\,\mathrm{e}^{\mathrm{i}\Omega t}).$$

For the Pauli matrices, one generally has

$$\mathrm{e}^{\mathrm{i}\Delta t\sigma^z/2}\,\sigma^\pm\,\mathrm{e}^{-\mathrm{i}\Delta t\sigma^z/2} = \mathrm{diag}(\mathrm{e}^{\mathrm{i}\Delta t/2},\,\mathrm{e}^{-\mathrm{i}\Delta t/2})\sigma^\pm\,\mathrm{diag}(\mathrm{e}^{-\mathrm{i}\Delta t/2},\,\mathrm{e}^{+\mathrm{i}\Delta t/2}) = \mathrm{e}^{\pm\mathrm{i}\Delta t}\,\sigma^\pm.$$

In total, these considerations yield the interaction picture of the system-reservoir coupling as

$$\begin{aligned}V_I(t) = g\sum_k\sum_{m=1}^{M}\Big[&\mathrm{e}^{-\mathrm{i}\delta_k t}\,a_k\sigma_m^+\left(\hat{D}_m(2\sqrt{S}\,\mathrm{e}^{\mathrm{i}\Omega t}) - \langle\hat{D}_m\rangle_R\right) \\ &+ \mathrm{e}^{\mathrm{i}\delta_k t}\,a_k^\dagger\sigma_m^-\left(\hat{D}_m(-2\sqrt{S}\,\mathrm{e}^{\mathrm{i}\Omega t}) - \langle\hat{D}_m\rangle_R\right)\Big],\end{aligned} \tag{4.14}$$

where we have introduced the detuning between cavity mode k and dye molecules as $\delta_k = \omega_k - \Delta$. Performing the perturbative expansion to second order in g, the master equation for the system density matrix then requires the evaluation of

$$\begin{aligned}\mathrm{Tr}_R\left[V_I(t)\rho_I(0)\right] &= \mathrm{Tr}_R\left[V_I(t)\rho_R\otimes\rho_S(0)\right] \\ &= g\sum_k\sum_{m=1}^{M}\Big(\mathrm{e}^{-\mathrm{i}\delta_k t}\langle\hat{D}_m(t) - \langle\hat{D}_m\rangle_R\rangle_R\left[a_k\sigma_m^+,\rho_S(0)\right] \\ &+ \mathrm{e}^{\mathrm{i}\delta_k t}\langle\hat{D}_m^\dagger(t) - \langle\hat{D}_m\rangle_R\rangle_R\left[a_k^\dagger\sigma_m^-,\rho_S(0)\right]\Big) = 0,\end{aligned} \tag{4.15}$$

which is zero per construction and where one should keep in mind that generally, the partial trace of a commutator need not be zero. We also need to evaluate

$$\begin{aligned}
&\int_0^\infty \mathrm{d}\tau \ \mathrm{Tr}_R \left[V_I(t), \left[V_I(t-\tau), \rho_I(t)\right]\right] \\
&= \int_0^\infty \mathrm{d}\tau \ \mathrm{Tr}_R \Big\{ V_I(t)V_I(t-\tau)\rho_I(t) - V_I(t)\rho_I(t)V_I(t-\tau) \\
&\qquad\qquad - V_I(t-\tau)\rho_I(t)V_I(t) + \rho_I(t)V_I(t-\tau)V_I(t) \Big\} \\
&= g^2 \sum_{k,\,l} \sum_{m,\,n=1}^{M} \int_0^\infty \mathrm{d}\tau \ V_{klmn}(t, t-\tau),
\end{aligned} \tag{4.16}$$

with

$$\begin{aligned}
V_{klmn}(t,t-\tau) = {} & \mathrm{e}^{-\mathrm{i}\delta_k t}\,\mathrm{e}^{\mathrm{i}\delta_l(t-\tau)} \left(\langle \hat{D}_m(t)\hat{D}_n^\dagger(t-\tau)\rangle_R - \langle \hat{D}_m\rangle_R^2 \right) \ a_k\sigma_m^+ a_l^\dagger \sigma_n^- \rho_S(t) \\
& - \mathrm{e}^{-\mathrm{i}\delta_k t}\,\mathrm{e}^{\mathrm{i}\delta_l(t-\tau)} \left(\langle \hat{D}_n^\dagger(t-\tau)\hat{D}_m(t)\rangle_R - \langle \hat{D}_m\rangle_R^2 \right) \ a_k\sigma_m^+ \rho_S(t) a_l^\dagger \sigma_n^- \\
& + \mathrm{e}^{\mathrm{i}\delta_k t}\,\mathrm{e}^{-\mathrm{i}\delta_l(t-\tau)} \left(\langle \hat{D}_m^\dagger(t)\hat{D}_n(t-\tau)\rangle_R - \langle \hat{D}_m\rangle_R^2 \right) \ a_k^\dagger\sigma_m^- a_l \sigma_n^+ \rho_S(t) \\
& - \mathrm{e}^{\mathrm{i}\delta_k t}\,\mathrm{e}^{-\mathrm{i}\delta_l(t-\tau)} \left(\langle \hat{D}_n(t-\tau)\hat{D}_m^\dagger(t)\rangle_R - \langle \hat{D}_m\rangle_R^2 \right) \ a_k^\dagger\sigma_m^- \rho_S(t) a_l \sigma_n^+ \\
& + \mathrm{e}^{-\mathrm{i}\delta_k(t-\tau)}\,\mathrm{e}^{\mathrm{i}\delta_l t} \left(\langle \hat{D}_m(t-\tau)\hat{D}_n^\dagger(t)\rangle_R - \langle \hat{D}_m\rangle_R^2 \right) \ \rho_S(t) a_k\sigma_m^+ a_l^\dagger \sigma_n^- \\
& - \mathrm{e}^{-\mathrm{i}\delta_k(t-\tau)}\,\mathrm{e}^{\mathrm{i}\delta_l t} \left(\langle \hat{D}_n^\dagger(t)\hat{D}_m(t-\tau)\rangle_R - \langle \hat{D}_m\rangle_R^2 \right) \ a_k\sigma_m^+ \rho_S(t) a_l^\dagger \sigma_n^- \\
& + \mathrm{e}^{\mathrm{i}\delta_k(t-\tau)}\,\mathrm{e}^{-\mathrm{i}\delta_l t} \left(\langle \hat{D}_m^\dagger(t-\tau)\hat{D}_n(t)\rangle_R - \langle \hat{D}_m\rangle_R^2 \right) \ \rho_S(t) a_k^\dagger\sigma_m^- a_l \sigma_n^+ \\
& - \mathrm{e}^{\mathrm{i}\delta_k(t-\tau)}\,\mathrm{e}^{-\mathrm{i}\delta_l t} \left(\langle \hat{D}_n(t)\hat{D}_m^\dagger(t-\tau)\rangle_R - \langle \hat{D}_m\rangle_R^2 \right) \ a_k^\dagger\sigma_m^- \rho_S(t) a_l \sigma_n^+ \ ,
\end{aligned} \tag{4.17}$$

where we have dropped anomalous contributions.[2] Since the dye molecules are solved in water at room temperature, we assume there are no correlations between the vibrations of different molecules, such that only those contributions to Eq. (4.16) survive which have $n = m$. Furthermore, it is helpful to employ the *secular approximation* [18], which in the present case means to discard all terms with $k \neq l$ since they oscillate with $\exp\{\pm\mathrm{i}\,(\omega_k - \omega_l)\,t\}$ in the interaction picture. To evaluate the reservoir expectation values in Eq. (4.16), we need the commutator

$$[\mathrm{e}^{\mathrm{i}\Omega t}\, b_m^\dagger - \mathrm{e}^{-\mathrm{i}\Omega t}\, b_m, \mathrm{e}^{-\mathrm{i}\Omega(t-\tau)}\, b_m - \mathrm{e}^{\mathrm{i}\Omega(t-\tau)}\, b_m^\dagger] = -\mathrm{e}^{\mathrm{i}\Omega\tau} + \mathrm{e}^{-\mathrm{i}\Omega\tau} = -2\mathrm{i}\sin\Omega\tau. \tag{4.18}$$

[2] Pay attention to how every second line, with the occurrence of the jump terms, the two displacement operators switch positions compared to the previous line. This comes from the cyclic property of the trace over the reservoir.

Then

$$\begin{aligned}\hat{D}_m(t)\hat{D}_m^\dagger(t-\tau) &= \exp\left\{2\sqrt{S}\left(\mathrm{e}^{\mathrm{i}\Omega t}\,b_m^\dagger - \mathrm{e}^{-\mathrm{i}\Omega t}\,b_m\right)\right\} \\ &\quad\times\ \exp\left\{-2\sqrt{S}\left(\mathrm{e}^{\mathrm{i}\Omega(t-\tau)}\,b_m^\dagger - \mathrm{e}^{-\mathrm{i}\Omega(t-\tau)}\,b_m\right)\right\} \\ &= \exp\left\{2\sqrt{S}\left[\left(\mathrm{e}^{\mathrm{i}\Omega t} - \mathrm{e}^{\mathrm{i}\Omega(t-\tau)}\right)b_m^\dagger - \text{c.c.}\right] - 4\mathrm{i}S\sin\Omega\tau\right\} \\ &= \hat{D}_m\left(2\sqrt{S}\,\mathrm{e}^{\mathrm{i}\Omega t}\left(1-\mathrm{e}^{-\mathrm{i}\Omega\tau}\right)\right)\exp\left\{-4\mathrm{i}S\sin\Omega\tau\right\},\end{aligned}$$

and from Eq. (4.9)

$$\begin{aligned}\langle\hat{D}_m(t)\hat{D}_m^\dagger(t-\tau)\rangle_R &= \exp\left\{-4S\left[(1-\cos\Omega\tau)\coth\frac{\beta\Omega}{2} + \mathrm{i}\sin\Omega\tau\right]\right\} \\ &= \langle\hat{D}_m^\dagger(t)\hat{D}_m(t-\tau)\rangle_R.\end{aligned} \tag{4.19}$$

The right-hand side of the master equation then involves the integral

$$\begin{aligned}K(\delta) = g^2\int_0^\infty \mathrm{d}\tau\ \mathrm{e}^{\mathrm{i}\delta\tau}\Bigg(&\exp\left\{-4S\left[(1-\cos\Omega\tau)\coth\frac{\beta\Omega}{2} + \mathrm{i}\sin\Omega\tau\right]\right\} \\ &- \exp\left\{-4S\coth\frac{\beta\Omega}{2}\right\}\Bigg)\end{aligned} \tag{4.20}$$

where, contrary to Refs. [15, 16], the molecular driven-dissipative contributions to the master equation (4.12) are not incorporated as a convergence factor $\exp\left\{-\left(\Gamma_\uparrow+\Gamma_\downarrow\right)\tau/2\right\}$.[3] The reason is that for the weak external pumping employed in the experiments discussed below, the influence of the rapid relaxation of the reservoir on the broadening of the molecular spectrum described by $K(\delta)$ is much larger than any additional broadening due to $\Gamma_{\uparrow,\downarrow}$. It is, therefore, valid to assume

[3] Regarding the derivation of this factor, Ref. [15] quotes the one given in [144]. Apart from the natural emergence of this factor in the framework of Chp. 5, another way to derive it could be via quantum Langevin equations. From paragraph 1.5.2 we know the quantum Wiener processes

$$\mathrm{d}\sigma_m^\pm = -\mathrm{i}[\sigma_m^\pm, H_S]\mathrm{d}t - \frac{\Gamma_\uparrow+\Gamma_\downarrow}{2}\sigma_m^\pm\mathrm{d}t + \sqrt{\Gamma_{\uparrow,\downarrow}}[\sigma_m^\pm,\sigma_m^\mp]\mathrm{d}W_m + \sqrt{\Gamma_{\downarrow,\uparrow}}\mathrm{d}W_m^\dagger[\sigma_m^\mp,\sigma_m^\pm], \tag{4.21}$$

where we have used the symbol $W_m(t)$ instead of $B(t)$, or the corresponding quantum Langevin equations

$$\dot{\sigma}_m^\pm(t) = \pm\mathrm{i}\Delta\sigma_m^\pm(t) - \frac{\Gamma_\uparrow+\Gamma_\downarrow}{2}\sigma_m^\pm(t) \pm \sqrt{\Gamma_{\uparrow,\downarrow}}\sigma_m^z(t)\Lambda_m(t) \mp \sqrt{\Gamma_{\downarrow,\uparrow}}\Lambda_m^\dagger(t)\sigma_m^z(t), \tag{4.22}$$

where we have written $\Lambda_m(t)$ instead of $\Gamma(t)$. These are solved by

$$\sigma_m^\pm(t) = \mathrm{e}^{\pm\mathrm{i}\Delta t-(\Gamma_\uparrow+\Gamma_\downarrow)t/2}\left(\sigma_m^\pm + \int_0^t \mathrm{d}\bar{t}\ \mathrm{e}^{\mp\mathrm{i}\Delta\bar{t}+(\Gamma_\uparrow+\Gamma_\downarrow)\bar{t}/2}\left[\pm\sqrt{\Gamma_{\uparrow,\downarrow}}\sigma_m^z(t)\Lambda_m(t) \mp \sqrt{\Gamma_{\downarrow,\uparrow}}\Lambda_m^\dagger(t)\sigma_m^z(t)\right]\right),$$

which are not, however, closed-form solutions since $\sigma_m^z(t)$ in turn depends on $\sigma_m^\pm(t)$. However, dropping the noise terms, one could envisage going to the "interaction picture" also with respect to the exponential damping in order to produce the convergence factor.

that the molecular spectrum remains constant over the experimentally explored range of external pumping strengths. The more general formalism to be developed in Chp. 5 includes not only the above convergence factor, but also correctly models the additional broadening due to the *photon* dissipation κ, a process that is not considered in Refs. [15, 16]. In the form given in Eq. (4.20), the spectrum then fulfills the Kennard-Stepanov relation

$$\frac{K(+\delta)}{K(-\delta)} = \mathrm{e}^{\beta\delta}, \tag{4.23}$$

which is essentially an instance of the Kubo-Martin-Schwinger relation [73, 145].

Moving back to the evaluation of the double commutator in our perturbative expansion, we have

$$\begin{aligned}
\int_0^\infty \mathrm{d}\tau\, V_{kkmm}(t, t-\tau) = K(-\delta_k)\Big(& a_k(t)\sigma_m^+(t)a_k^\dagger(t)\sigma_m^-(t)\rho_S(t) \\
& - a_k^\dagger(t)\sigma_m^-(t)\rho_S(t)a_k(t)\sigma_m^+(t)\Big) \\
+K(+\delta_k)\Big(& a_k^\dagger(t)\sigma_m^-(t)a_k(t)\sigma_m^+(t)\rho_S(t) \\
& - a_k(t)\sigma_m^+(t)\rho_S(t)a_k^\dagger(t)\sigma_m^-(t)\Big) \\
+K^*(-\delta_k)\Big(& \rho_S(t)a_k(t)\sigma_m^+(t)a_k^\dagger(t)\sigma_m^-(t) \\
& - a_k^\dagger(t)\sigma_m^-(t)\rho_S(t)a_k(t)\sigma_m^+(t)\Big) \\
+K^*(+\delta_k)\Big(& \rho_S(t)a_k^\dagger(t)\sigma_m^-(t)a_k(t)\sigma_m^+(t) \\
& - a_k(t)\sigma_m^+(t)\rho_S(t)a_k^\dagger(t)\sigma_m^-(t)\Big),
\end{aligned} \tag{4.24}$$

which evaluates to

$$\begin{aligned}
\int_0^\infty \mathrm{d}\tau\, V_{kkmm}(t, t-\tau) = \mathrm{Re}\left[K(-\delta_k)\right]\Big(& \Big\{a_k(t)a_k^\dagger(t)\sigma_m^+(t)\sigma_m^-(t), \rho_S(t)\Big\} \\
& - 2a_k^\dagger(t)\sigma_m^-(t)\rho_S(t)a_k(t)\sigma_m^+(t)\Big) \\
+ \mathrm{Re}\left[K(+\delta_k)\right]\Big(& \Big\{a_k^\dagger(t)a_k(t)\sigma_m^-(t)\sigma_m^+(t), \rho_S(t)\Big\} \\
& - 2a_k(t)\sigma_m^+(t)\rho_S(t)a_k^\dagger(t)\sigma_m^-(t)\Big) \\
+ \mathrm{i}\,\mathrm{Im}\left[K(-\delta_k)\right]& \left[a_k(t)a_k^\dagger(t)\sigma_m^+(t)\sigma_m^-(t), \rho_S(t)\right] \\
+ \mathrm{i}\,\mathrm{Im}\left[K(\delta_k)\right]& \left[a_k^\dagger(t)a_k(t)\sigma_m^-(t)\sigma_m^+(t), \rho_S(t)\right].
\end{aligned} \tag{4.25}$$

For similar reasons as when we discarded H_{coh}, the Lamb shifts given by the imaginary parts of the function $K(\delta)$ may be ignored in the investigation of the incoherent dynamics of the system [17]. Undoing the interaction picture, and introducing the notation $\Gamma_k^\pm = 2\,\mathrm{Re}\left[K(\pm\delta_k)\right]$, we can

finally write down the master equation of the photon BEC as

$$\begin{aligned}\dot{\rho}(t) = &-\mathrm{i}[H_0, \rho(t)] + \sum_k \frac{\kappa}{2}\mathcal{L}[a_k]\rho(t) + \sum_{m=1}^{M}\left[\frac{\Gamma_\uparrow}{2}\mathcal{L}[\sigma_m^+] + \frac{\Gamma_\downarrow}{2}\mathcal{L}[\sigma_m^-]\right]\rho(t) \\ &+ \sum_k \sum_{m=1}^{M}\left[\frac{\Gamma_k^-}{2}\mathcal{L}[a_k^\dagger\sigma_m^-] + \frac{\Gamma_k^+}{2}\mathcal{L}[a_k\sigma_m^+]\right]\rho(t),\end{aligned} \tag{4.26}$$

where ρ is now the system density matrix in the Schrödinger picture and $H_0 = \sum_k \delta_k a_k^\dagger a_k$. Notice that as long as one considers only the evolution of occupation numbers, i.e. expectation values that do not depend on the relative phase between photons and dye molecules, the Hamiltonian contribution to this master equation may just as well be dropped.

4.1.5 Rate Equations and Steady State

To lowest order in the expectation-value hierarchy, the equations of motion following from Eq. (4.26) are given by

$$\partial_t\langle a_k^\dagger a_k\rangle = -\kappa\langle a_k^\dagger a_k\rangle - \frac{1}{2}\sum_{m=1}^{M}\left[\Gamma_k^+\langle a_k^\dagger a_k\,(1-\sigma_m^z)\rangle - \Gamma_k^-\langle a_k a_k^\dagger\,(1+\sigma_m^z)\rangle\right], \tag{4.27a}$$

$$\begin{aligned}\partial_t\langle\sigma_m^z\rangle = &\,\Gamma_\uparrow(1-\langle\sigma_m^z\rangle) - \Gamma_\downarrow(1+\langle\sigma_m^z\rangle) \\ &+ \sum_k\left[\Gamma_k^+\langle a_k^\dagger a_k\,(1-\sigma_m^z)\rangle - \Gamma_k^-\langle a_k a_k^\dagger\,(1+\sigma_m^z)\rangle\right],\end{aligned} \tag{4.27b}$$

where the system average is $\langle X\rangle(t) = \mathrm{Tr}\,X\rho(t)$. Assuming that the molecules are all behave identically, one may ignore the molecular index m and replace the sum over the M molecules in Eq. (4.27a) by a factor of M, e.g. $\sum_m\langle\sigma_m^z\rangle \equiv M\langle\sigma^z\rangle$. Similarly, by summing over m in Eq. (4.27b), and using

$$\begin{aligned}M\partial_t\langle\sigma^z\rangle &= 2\partial_t\langle M_\uparrow\rangle, \\ M\langle 1+\sigma^z\rangle &= 2\langle M_\uparrow\rangle, \\ M\langle 1-\sigma^z\rangle &= 2\langle M-M_\uparrow\rangle,\end{aligned} \tag{4.28}$$

with analogous replacements for the higher-order expectation values, we arrive at the *rate equations*

$$\partial_t\langle n_k\rangle = -\kappa\langle n_k\rangle - \Gamma_k^+\langle n_k\left(M-M_\uparrow\right)\rangle + \Gamma_k^-\langle(n_k+1)\,M_\uparrow\rangle, \tag{4.29a}$$

$$\begin{aligned}\partial_t\langle M_\uparrow\rangle = &\,\Gamma_\uparrow\left(M-\langle M_\uparrow\rangle\right) - \Gamma_\downarrow\langle M_\uparrow\rangle \\ &+ \sum_k\left[\Gamma_k^+\langle n_k\left(M-M_\uparrow\right)\rangle - \Gamma_k^-\langle(n_k+1)\,M_\uparrow\rangle\right].\end{aligned} \tag{4.29b}$$

The second equation now describes the collective dynamics of the number of excited molecules. A further simplification can be made by assuming the factorization $\langle n_k M_\uparrow \rangle \approx \langle n_k \rangle \langle M_\uparrow \rangle$. As discussed in [17], in the equilibrium limit where $\kappa, \Gamma_{\uparrow,\downarrow} \to 0$, the rate equations then predict a steady-state Bose-Einstein distribution

$$\frac{\langle n_k + 1 \rangle}{\langle n_k \rangle} = \frac{\Gamma_k^+ \langle M - M_\uparrow \rangle}{\Gamma_k^- \langle M_\uparrow \rangle} = \mathrm{e}^{\beta \delta_k} \frac{\sum_l \Gamma_l^- \langle n_l + 1 \rangle}{\sum_l \Gamma_l^+ \langle n_l \rangle}, \tag{4.30}$$

where we have used Eq. (4.29a) for the first, and Eq. (4.29b) and the Kennard-Stepanov relation $\Gamma_k^+ / \Gamma_k^- = \mathrm{e}^{\beta \delta_k}$ for the second equality. This completes our derivation of the non-equilibrium model of the photon BEC.

4.2 Second-Order Coherence

In this Sec., we examine the temporal dynamics of the photon BEC in a regime where a driven-dissipative steady state is induced by a balance of cavity losses and continuous dye pumping. This leads to the appearance of *exceptional points* in the frequency and decay rate of the photon second-order correlation $g^{(2)}(\tau)$, even though their spectrally resolved number distribution remains, within experimental uncertainties, indistinguishable from an equilibrium Bose-Einstein distribution. This constitutes a novel form of non-equilibrium transition.

The coupling of cavity modes to the dye molecules entails that the latter act as both a heat bath and a particle "reservoir": dye excitations may be converted into cavity photons and vice versa. On one hand, for a dye reservoir which is large relative to the photon population, this results in strong number fluctuations and a zero-delay second-order coherence $g^{(2)}(0) = 2$, i.e. as for a thermal light source. Fluctuations as large as the average occupation do indeed occur within the condensed phase. On the other hand, at smaller relative sizes of photon population and dye reservoir, the condensate can also be operated in the canonical-statistics regime where number fluctuations are weak and consequently $g^{(2)}(0) = 1$. A previous discussion of the static second-order coherence $g^{(2)}(0)$ as well as the time-dependent first-order coherence $g^{(1)}(\tau)$ of the photon BEC was given in Ref. [17].

Apart from records of the thermal number spectrum of the stationary photon gases, in the experiments the transverse cavity ground mode (condensate mode) is always singled out. Since at any time the number of available (non-excited) molecules in the reservoir is overwhelmingly large compared to the total number of excited-state photons $\sum_{k \neq 0} \langle a_k^\dagger a_k \rangle$, such that what the ground mode sees of the excitation "reservoir" is essentially unaffected by the presence of the thermal tail, the analysis may be restricted to the photon correlations in the condensate, i.e. we will consider only the ground mode $k = 0$, where $\omega_c \equiv \omega_0$ is the cavity cut-off. The latter is chosen such that the ground-mode detuning is $\delta \equiv \delta_0 = \omega_c - \Delta < 0$. For clarity, we will express the incoherent

couplings $\Gamma_0^{\pm}$ of the molecules to the ground mode as

$$\begin{aligned} B_{\text{em}} &\equiv \Gamma_0^-, \\ B_{\text{abs}} &\equiv \Gamma_0^+. \end{aligned} \tag{4.31}$$

Finally, from here on, we will drop the cavity-mode subscript on the photon operators and write $a \equiv a_0$. For completeness, the master equation to be studied henceforth is

$$\dot{\rho} = \frac{\kappa}{2}\mathcal{L}[a]\rho + \frac{1}{2}\sum_{m=1}^{M}\left\{\Gamma_\uparrow\mathcal{L}[\sigma_m^+] + \Gamma_\downarrow\mathcal{L}[\sigma_m^-] + B_{\text{em}}\mathcal{L}[a^\dagger\sigma_m^-] + B_{\text{abs}}\mathcal{L}[a\sigma_m^+]\right\}\rho, \tag{4.32}$$

where we have dropped H_0 since, as explained before, it does not contribute to the dynamics of the quantities of interest.

4.2.1 Density-Matrix Ansatz

The fact that Eq. (4.32) does not depend on the phase difference between the photon and molecule sector of the system enables an ansatz for the density matrix to be made in the diagonal form

$$\rho(t) = \sum_{n=0}^{\infty}\sum_{m=0}^{M} P_{nm}(t)\,|n\rangle\langle n| \otimes \rho_m, \tag{4.33}$$

where ρ_m is the incoherent mixture of M molecules m of which are excited, and P_{nm} is the classical joint probability distribution for the number of ground-mode photons n and the number of molecular excitations m. Using this ansatz in the master equation gives rise to an equation for $\dot{P}_{nm}$ (cf. Ref. [17]). Note that the Lindbladians of Eq. (4.32) indeed only couple the P_{nm} among themselves and hence do not necessitate the consideration of any (coherent) off-diagonal matrix elements. To briefly illustrate the ansatz, set $M = 4$. Then

$$\rho_3 = \frac{1}{4}\left(|1110\rangle\langle 1110| + |1101\rangle\langle 1101| + |1011\rangle\langle 1011| + |0111\rangle\langle 0111|\right), \tag{4.34}$$

which gives, e.g.

$$\begin{aligned} \sum_{j=1}^{4}\sigma_j^-\rho_3\sigma_j^+ = \frac{1}{4}\Big(&|0110\rangle\langle 0110| + |0101\rangle\langle 0101| + |0011\rangle\langle 0011| \\ &+ |1010\rangle\langle 1010| + |1001\rangle\langle 1001| + |0011\rangle\langle 0011| \\ &+ |1100\rangle\langle 1100| + |1001\rangle\langle 1001| + |0101\rangle\langle 0101| \\ &+ |1100\rangle\langle 1100| + |1010\rangle\langle 1010| + |0110\rangle\langle 0110|\Big) = 3\rho_2, \end{aligned} \tag{4.35}$$

since

$$\begin{aligned}\rho_2 = \frac{1}{6}\Big(&|1100\rangle\langle 1100| + |1010\rangle\langle 1010| + |1001\rangle\langle 1001| \\ &+ |0101\rangle\langle 0101| + |0011\rangle\langle 0011| + |0110\rangle\langle 0110| \Big).\end{aligned} \tag{4.36}$$

The joint distribution P_{nm} provides an alternative approach to finding the rate equations of the photon BEC. It furthermore offers are well-defined truncation scheme via the assumption that P_{nm} is Gaussian. Below, this will prove to be a valuable tool especially for the higher-order expectation values required for the study of the second-order coherence function. It is of relevance for Chp. 5 that this procedure precludes the study of phenomena for which the coherence between photons and molecules cannot be neglected.

4.2.2 Calculation of Expectation Values from Classical Distribution

From the classical probability distribution P_{nm}, expectation values may now be calculated as follows. The photon occupation number is defined as

$$\langle n\rangle = \sum_{n=0}^{\infty} nP_n = \sum_{m=0}^{M}\sum_{n=0}^{\infty} nP_{nm},$$

where we obtain the marginal distribution P_n by summing over the molecular excitation number m. Now the cavity-loss process, for example, contributes to the equation of motion of the photon number a term

$$\begin{aligned}\partial_t\langle n\rangle = \sum_{m=0}^{M}\sum_{n=0}^{\infty} n\dot{P}_{nm} &\simeq \kappa \sum_{m=0}^{M}\sum_{n=0}^{\infty}\Big[n(n+1)P_{n+1,m} - n^2P_{nm}\Big] \\ &= \kappa \sum_{m=0}^{M}\sum_{n=1}^{\infty}\Big[n(n+1)P_{n+1,m} - n^2P_{nm}\Big] \\ &= \kappa \sum_{m=0}^{M}\left[\sum_{n=2}^{\infty}(n-1)nP_{nm} - \sum_{n=1}^{\infty} n^2P_{nm}\right] \\ &= \kappa \sum_{m=0}^{M}\sum_{n=1}^{\infty}\Big[(n-1)n - n^2\Big]P_{nm} \\ &= -\kappa\sum_{m=0}^{M}\sum_{n=0}^{\infty} nP_{nm} = -\kappa\langle n\rangle,\end{aligned} \tag{4.37}$$

where we have shifted photon summation index several times. To calculate the time derivative $\dot{P}_{nm}$, we have used, e.g.

$$\begin{aligned}\sum_{n=0}^{\infty} P_{nm} a \left|n\right\rangle\!\left\langle n\right| a^{\dagger} &= \sum_{n=1}^{\infty} P_{nm} a \left|n\right\rangle\!\left\langle n\right| a^{\dagger} \\ &= \sum_{n=1}^{\infty} n P_{nm} \left|n-1\right\rangle\!\left\langle n-1\right| \\ &= \sum_{n=0}^{\infty} (n+1)\, P_{n+1,m} \left|n\right\rangle\!\left\langle n\right| .\end{aligned} \tag{4.38}$$

For one of the remaining two terms (the emission term), one finds similarly

$$\begin{aligned}& B_{\text{em}} \sum_{m=0}^{M} \sum_{n=0}^{\infty} \left[n^2 (m+1) P_{n-1,m+1} - n(n+1) m P_{nm} \right] \\ &= B_{\text{em}} \sum_{m=1}^{M} \sum_{n=1}^{\infty} \left[n^2 m P_{n-1,m} - n(n+1) m P_{nm} \right] \\ &= B_{\text{em}} \sum_{m=1}^{M} \sum_{n=0}^{\infty} \left[(n+1)^2 m - n(n+1) m \right] P_{nm} \\ &= B_{\text{em}} \sum_{m=0}^{M} \sum_{n=0}^{\infty} (n+1) m \left[n+1-n \right] P_{nm} \\ &= B_{\text{em}} \langle (n+1) M_{\uparrow} \rangle,\end{aligned} \tag{4.39}$$

such that this term contributes

$$\partial_t \langle n \rangle \simeq B_{\text{em}} \left(\langle M_{\uparrow} \rangle (\langle n \rangle + 1) + \sigma^2_{n,\, M_{\uparrow}} \right), \tag{4.40}$$

where we introduced the covariance $\sigma^2_{n,\, M_{\uparrow}} = \langle n M_{\uparrow} \rangle - \langle n \rangle \langle M_{\uparrow} \rangle$. The two variances in turn are $\sigma^2_X = \langle X^2 \rangle - \langle X \rangle^2$ with $X = n,\, M_{\uparrow}$. Repeating what we did for the cavity-loss contribution to the equation of motion of the first moment of P_n, we find for its second moment that

$$\begin{aligned}\partial_t \langle n^2 \rangle = \sum_{m=0}^{M} \sum_{n=0}^{\infty} n^2 \dot{P}_{nm} &\simeq \kappa \sum_{m=0}^{M} \sum_{n=0}^{\infty} \left[n^2 (n+1) P_{n+1,m} - n^3 P_{nm} \right] \\ &= \kappa \sum_{m=0}^{M} \sum_{n=1}^{\infty} \left[(n-1)^2 n - n^3 \right] P_{nm} = \kappa (\langle n \rangle - 2 \langle n^2 \rangle).\end{aligned} \tag{4.41}$$

With $\partial_t \langle n\rangle^2 = 2\langle n\rangle \partial_t \langle n\rangle = -2\kappa \langle n\rangle^2$, it follows that

$$\partial_t \sigma_n^2 \simeq \kappa(\langle n\rangle - 2\langle n^2\rangle + 2\langle n\rangle^2) = \kappa(\langle n\rangle - 2\sigma_n^2). \tag{4.42}$$

Again for the emission term, we calculate

$$\begin{aligned}
&B_{\text{em}} \sum_{m=0}^{M}\sum_{n=0}^{\infty} \left[n^3(m+1)P_{n-1,m+1} - n^2(n+1)mP_{nm}\right] \\
&= B_{\text{em}} \sum_{m=0}^{M}\sum_{n=0}^{\infty} \left[(n+1)^3 - n^2(n+1)\right] mP_{nm} \\
&= B_{\text{em}} \sum_{m=0}^{M}\sum_{n=0}^{\infty} (n+1)(2n+1)mP_{nm} \\
&= B_{\text{em}} \langle \left(2n^2+3n+1\right) M_\uparrow\rangle = B_{\text{em}} \left(3\langle nM_\uparrow\rangle + \langle M_\uparrow\rangle + 2\langle n^2 M_\uparrow\rangle\right) \\
&= B_{\text{em}} \left[3(\sigma^2_{n,M_\uparrow} + \langle n\rangle\langle M_\uparrow\rangle) + \langle M_\uparrow\rangle + 2(\langle n^2\rangle\langle M_\uparrow\rangle + 2\langle n\rangle\langle nM_\uparrow\rangle - 2\langle n\rangle^2\langle M_\uparrow\rangle)\right],
\end{aligned} \tag{4.43}$$

where we have used the Gaussian identity $\langle X^2Y\rangle = \langle X^2\rangle\langle Y\rangle + 2\langle X\rangle\langle XY\rangle - 2\langle X\rangle^2\langle Y\rangle$, implying the assumption that P_{nm} is Gaussian.[4] This gives the contribution of the emission term

$$\begin{aligned}
\partial_t \sigma_n^2 &\simeq B_{\text{em}} \langle \left(2n^2+3n+1\right) M_\uparrow\rangle - 2B_{\text{em}}\langle n\rangle \left[\langle M_\uparrow\rangle + \langle nM_\uparrow\rangle\right] \\
&= B_{\text{em}} \left[3\sigma^2_{n,M_\uparrow} + \langle n\rangle\langle M_\uparrow\rangle + \langle M_\uparrow\rangle + 2\langle n\rangle\langle nM_\uparrow\rangle + 2\langle n^2\rangle\langle M_\uparrow\rangle - 4\langle n\rangle^2\langle M_\uparrow\rangle\right] \\
&= B_{\text{em}} \Big[3\sigma^2_{n,M_\uparrow} + \langle n\rangle\langle M_\uparrow\rangle + \langle M_\uparrow\rangle \\
&\qquad +2(\langle n\rangle\sigma^2_{n,M_\uparrow} + \langle M_\uparrow\rangle\sigma_n^2 + 2\langle n\rangle^2\langle M_\uparrow\rangle) - 4\langle n\rangle^2\langle M_\uparrow\rangle\Big] \\
&= B_{\text{em}} \left[(2\langle n\rangle + 3)\sigma^2_{n,M_\uparrow} + \langle n\rangle\langle M_\uparrow\rangle + \langle M_\uparrow\rangle + 2\langle M_\uparrow\rangle\sigma_n^2\right],
\end{aligned} \tag{4.46}$$

which agrees with the result from Ref. [17]. The remaining contributions to this equation and the other equations for the first and second cumulants can be calculated in the manner just detailed (cf. Eq. (4.50)).

[4] For a bivariate normal distribution with mean vector $\boldsymbol{\mu} = (\langle X\rangle, \langle Y\rangle)^T$ and covariance matrix

$$\boldsymbol{\Sigma} = \begin{pmatrix} \langle X^2\rangle - \langle X\rangle^2 & \langle XY\rangle - \langle X\rangle\langle Y\rangle \\ \langle XY\rangle - \langle X\rangle\langle Y\rangle & \langle Y^2\rangle - \langle Y\rangle^2 \end{pmatrix}, \tag{4.44}$$

one has

$$\begin{aligned}
\langle X^2Y\rangle &= \langle X\rangle^2\langle Y\rangle + \langle Y\rangle\left[\langle X^2\rangle - \langle X\rangle^2\right] + 2\langle X\rangle\left[\langle XY\rangle - \langle X\rangle\langle Y\rangle\right] \\
&= \langle X^2\rangle\langle Y\rangle + 2\langle X\rangle\langle XY\rangle - 2\langle X\rangle^2\langle Y\rangle.
\end{aligned} \tag{4.45}$$

4.2.3 Calculation of Expectation Values from Master Equation

The direct way of calculating the dynamical equations for the expectations values from the master equation may, of course, be employed alternatively. Again replacing the sum over all molecules by a factor of M, this yields the single-mode special case of Eqs. (4.27a), reading

$$\partial_t\langle a^\dagger a\rangle = -\kappa\langle a^\dagger a\rangle - \frac{M}{2}B_{\text{abs}}\langle a^\dagger a\,(1-\sigma^z)\rangle + \frac{M}{2}B_{\text{em}}\langle aa^\dagger\,(1+\sigma^z)\rangle, \tag{4.47a}$$

$$\partial_t\langle\sigma^z\rangle = \Gamma_\uparrow\,(1-\langle\sigma^z\rangle) - \Gamma_\downarrow\,(1+\langle\sigma^z\rangle) + B_{\text{abs}}\langle a^\dagger a\,(1-\sigma^z)\rangle - B_{\text{em}}\langle aa^\dagger\,(1+\sigma^z)\rangle. \tag{4.47b}$$

Comparing these to the equations one finds from P_{nm},

$$\partial_t\langle n\rangle = -\kappa\langle n\rangle - B_{\text{abs}}\langle n\left(M-M_\uparrow\right)\rangle + B_{\text{em}}\langle(n+1)\,M_\uparrow\rangle, \tag{4.48a}$$

$$\partial_t\langle M_\uparrow\rangle = \Gamma_\uparrow\left(M-\langle M_\uparrow\rangle\right) - \Gamma_\downarrow\langle M_\uparrow\rangle + B_{\text{abs}}\langle n\left(M-M_\uparrow\right)\rangle - B_{\text{em}}\langle(n+1)\,M_\uparrow\rangle, \tag{4.48b}$$

we see that the heuristic rationale which lead to Eqs. (4.29a) and (4.29b) is equivalent to making the incoherent density-matrix ansatz (4.33). The next-order expectation values such as $\langle a^\dagger a\sigma^z\rangle$ may be found from the higher-order equations

$$\begin{aligned}\partial_t\langle a^\dagger a^\dagger aa\rangle &= -2\kappa\langle a^\dagger a^\dagger aa\rangle - 2MB_{\text{abs}}\langle a^\dagger a^\dagger aa\sigma^-\sigma^+\rangle \\ &\quad + 2MB_{\text{em}}\left(\langle a^\dagger a^\dagger aa\sigma^+\sigma^-\rangle + 2\langle a^\dagger a\sigma^+\sigma^-\rangle\right),\end{aligned} \tag{4.49a}$$

$$\begin{aligned}\partial_t\langle a^\dagger a\sigma^+\sigma^-\rangle &= -\kappa\langle a^\dagger a\sigma^+\sigma^-\rangle + \Gamma_\uparrow\langle a^\dagger a\sigma^-\sigma^+\rangle - \Gamma_\downarrow\langle a^\dagger a\sigma^+\sigma^-\rangle \\ &\quad + B_{\text{abs}}\langle a^\dagger a^\dagger aa\sigma^-\sigma^+\rangle - B_{\text{em}}\left(\langle a^\dagger a^\dagger aa\sigma^+\sigma^-\rangle + 2\langle a^\dagger a\sigma^+\sigma^-\rangle\right) \\ &\quad - (M-1)B_{\text{abs}}\langle a^\dagger a\sigma^+\sigma^-\tilde\sigma^-\tilde\sigma^+\rangle + (M-1)B_{\text{em}}\langle aa^\dagger\sigma^+\sigma^-\tilde\sigma^+\tilde\sigma^-\rangle,\end{aligned} \tag{4.49b}$$

$$\begin{aligned}\partial_t\langle\sigma^+\sigma^-\tilde\sigma^+\tilde\sigma^-\rangle &= \Gamma_\uparrow\left(\langle\sigma^-\sigma^+\tilde\sigma^+\tilde\sigma^-\rangle + \langle\sigma^+\sigma^-\tilde\sigma^-\tilde\sigma^+\rangle\right) - 2\Gamma_\downarrow\langle\sigma^+\sigma^-\tilde\sigma^+\tilde\sigma^-\rangle \\ &\quad + B_{\text{abs}}\left(\langle a^\dagger a\sigma^-\sigma^+\tilde\sigma^+\tilde\sigma^-\rangle + \langle a^\dagger a\sigma^+\sigma^-\tilde\sigma^-\tilde\sigma^+\rangle\right) - 2B_{\text{em}}\langle aa^\dagger\sigma^+\sigma^-\tilde\sigma^+\tilde\sigma^-\rangle.\end{aligned} \tag{4.49c}$$

The Pauli matrices $\tilde\sigma^\pm$ describe any molecule that is not identical to $\sigma^\pm$. In this operator form, the expectation values that are quartic in the Pauli matrices, in particular, are difficult to truncate.

4.2.4 Truncation of the Expectation-Value Hierarchy

Under the assumption that P_{nm} is Gaussian, however, Eqs. (4.49) can be truncated rigorously. Starting with Eq. (4.49a), we find unambigously that

$$\begin{aligned}
\partial_t\langle n^2\rangle &= \partial_t\langle a^\dagger a a^\dagger a\rangle = \partial_t\langle a^\dagger a^\dagger a a\rangle + \partial_t\langle a^\dagger a\rangle \\
&= \kappa(\langle n\rangle - 2\langle n^2\rangle) + B_{\text{em}}\left[2\langle(n^2+n)M_\uparrow\rangle + \langle(n+1)M_\uparrow\rangle\right] \\
&- B_{\text{abs}}\left[2\langle(n^2-n)(M-M_\uparrow)\rangle + \langle n(M-M_\uparrow)\rangle\right] \\
&= \kappa(\langle n\rangle - 2\langle n^2\rangle) + B_{\text{em}}\left[2\langle n^2 M_\uparrow\rangle + \langle(3n+1)M_\uparrow\rangle\right] \\
&- B_{\text{abs}}\left[2\langle n^2(M-M_\uparrow)\rangle - \langle n(M-M_\uparrow)\rangle\right] \\
&= \kappa(\langle n\rangle - 2\langle n^2\rangle) + B_{\text{em}}\left[4\langle n\rangle\langle nM_\uparrow\rangle + 2\langle M_\uparrow\rangle\langle n^2\rangle - 4\langle M_\uparrow\rangle\langle n\rangle^2 + \langle(3n+1)M_\uparrow\rangle\right] \\
&- B_{\text{abs}}\left[2\langle n^2\rangle(M-\langle M_\uparrow\rangle) + 4\langle M_\uparrow\rangle\langle n\rangle^2 - 4\langle n\rangle\langle nM_\uparrow\rangle - \langle n(M-M_\uparrow)\rangle\right].
\end{aligned} \tag{4.50}$$

In decomposing the expectation values of four Pauli matrices, one has to be more careful. It turns out that this has to be done as follows:

$$\begin{aligned}
M(M-1)\langle\sigma^+\sigma^-\tilde\sigma^+\tilde\sigma^-\rangle &= \langle M_\uparrow^2\rangle - \langle M_\uparrow\rangle, \\
M(M-1)\langle\sigma^+\sigma^-\tilde\sigma^-\tilde\sigma^+\rangle &= M\langle M_\uparrow\rangle - \langle M_\uparrow^2\rangle.
\end{aligned} \tag{4.51}$$

To understand why, consider the special case $M = 3$. Then the total set of molecular states is

$$\left\{\{|000\rangle\},\{|100\rangle,|010\rangle,|001\rangle\},\{|110\rangle,|101\rangle,|011\rangle\},\{|111\rangle\}\right\}. \tag{4.52}$$

If we only consider the molecular system and assume that the four incoherent mixtures of the states in each subset are equally probable, [5] then the overall normalization of the incoherent density matrix is $1/4$, and $\langle M_\uparrow\rangle = 6/4$ and $\langle M_\uparrow^2\rangle = 14/4$. Furthermore, for the action of the operators we find

$$\begin{aligned}
\mathrm{Tr}\sum_{j\neq 1}\sigma_1^+\sigma_1^-\tilde\sigma_j^+\tilde\sigma_j^-\rho_2 &= 2/3, \\
\mathrm{Tr}\sum_{j\neq 1}\sigma_1^+\sigma_1^-\tilde\sigma_j^+\tilde\sigma_j^-\rho_3 &= 2.
\end{aligned} \tag{4.53}$$

The contributions from $\rho_{m=0,1}$ obviously vanish. For the second ordering,

$$\mathrm{Tr}\sum_{j\neq 1}\sigma_1^+\sigma_1^-\tilde\sigma_j^-\tilde\sigma_j^+\rho_{m=1,2} = 2/3, \tag{4.54}$$

[5] Later on, this normalization will be fixed by P_{nm}.

with contributions from $\rho_{m=0,3}$ vanishing. Consequently,

$$\begin{aligned} M(M-1)\langle\sigma^+\sigma^-\tilde{\sigma}^+\tilde{\sigma}^-\rangle &= \mathrm{Tr}\sum_{k,\,j\neq k}\sigma_k^+\sigma_k^-\tilde{\sigma}_j^+\tilde{\sigma}_j^-\frac{\rho_2+\rho_3}{4} = \frac{2+6}{4} = \frac{14-6}{4} \\ &= \langle M_\uparrow^2\rangle - \langle M_\uparrow\rangle, \\ M(M-1)\langle\sigma^+\sigma^-\tilde{\sigma}^-\tilde{\sigma}^+\rangle &= \mathrm{Tr}\sum_{k,\,j\neq k}\sigma_k^+\sigma_k^-\tilde{\sigma}_j^-\tilde{\sigma}_j^+\frac{\rho_1+\rho_2}{4} = \frac{2+2}{4} = \frac{18-14}{4} \\ &= M\langle M_\uparrow\rangle - \langle M_\uparrow^2\rangle. \end{aligned} \tag{4.55}$$

Note that the sum over k simply contributes a factor of three. Applying it to Eq. (4.49b), we find

$$\begin{aligned} \partial_t\langle nM_\uparrow\rangle &= M\partial_t\langle a^\dagger a\sigma^+\sigma^-\rangle \\ &= -\kappa\langle nM_\uparrow\rangle + \Gamma_\uparrow\langle n(M-M_\uparrow)\rangle - \Gamma_\downarrow\langle nM_\uparrow\rangle \\ &+ B_{\text{abs}}\left(\langle n^2(M-M_\uparrow)\rangle - \langle n(M-M_\uparrow)\rangle\right) - B_{\text{em}}\left(\langle n^2M_\uparrow\rangle + \langle nM_\uparrow\rangle\right) \\ &- B_{\text{abs}}\langle n(M-M_\uparrow)M_\uparrow\rangle + B_{\text{em}}\langle(n+1)(M_\uparrow^2-M_\uparrow)\rangle \\ &= -\kappa\langle nM_\uparrow\rangle + \Gamma_\uparrow\langle n(M-M_\uparrow)\rangle - \Gamma_\downarrow\langle nM_\uparrow\rangle \\ &+ B_{\text{abs}}\Big[2\langle M_\uparrow\rangle\langle n\rangle^2 - 2\langle n\rangle\langle M_\uparrow\rangle^2 - M(\langle n\rangle + \langle nM_\uparrow\rangle) + \langle n\rangle\langle M_\uparrow^2\rangle \\ &+ 2(\langle M_\uparrow\rangle - \langle n\rangle + 1/2)\langle nM_\uparrow\rangle + (M-\langle M_\uparrow\rangle)\langle n^2\rangle\Big] \\ &+ B_{\text{em}}\Big[2\langle M_\uparrow\rangle\langle n\rangle^2 - 2\langle n\rangle\langle M_\uparrow\rangle^2 - \langle M_\uparrow\rangle + (\langle n\rangle+1)\langle M_\uparrow^2\rangle \\ &+ 2(\langle M_\uparrow\rangle - \langle n\rangle - 1)\langle nM_\uparrow\rangle - \langle M_\uparrow\rangle\langle n^2\rangle\Big]. \end{aligned} \tag{4.56}$$

Finally, for Eq. (4.49c), we obtain

$$\begin{aligned} \partial_t\langle M_\uparrow^2\rangle &= M(M-1)\partial_t\langle\sigma^+\sigma^-\tilde{\sigma}^+\tilde{\sigma}^-\rangle + \partial_t\langle M_\uparrow\rangle \\ &= 2\Gamma_\uparrow\left(M\langle M_\uparrow\rangle - \langle M_\uparrow^2\rangle\right) - 2\Gamma_\downarrow\left(\langle M_\uparrow^2\rangle - \langle M_\uparrow\rangle\right) \\ &+ 2B_{\text{abs}}\langle n(MM_\uparrow - M_\uparrow^2)\rangle - 2B_{\text{em}}\langle(n+1)(M_\uparrow^2-M_\uparrow)\rangle \\ &+ \Gamma_\uparrow\left(M-\langle M_\uparrow\rangle\right) - \Gamma_\downarrow\langle M_\uparrow\rangle + B_{\text{abs}}\langle\left(M-M_\uparrow\right)n\rangle - B_{\text{em}}\langle(n+1)\,M_\uparrow\rangle \\ &= \Gamma_\uparrow\left(2M\langle M_\uparrow\rangle + M - \langle M_\uparrow\rangle - 2\langle M_\uparrow^2\rangle\right) + \Gamma_\downarrow\left(\langle M_\uparrow\rangle - 2\langle M_\uparrow^2\rangle\right) \\ &+ B_{\text{abs}}\left((2M-1)\langle nM_\uparrow\rangle + M\langle n\rangle - 4\langle M_\uparrow\rangle\langle nM_\uparrow\rangle - 2\langle n\rangle\langle M_\uparrow^2\rangle + 4\langle n\rangle\langle M_\uparrow\rangle^2\right) \\ &- B_{\text{em}}\left(4\langle M_\uparrow\rangle\langle nM_\uparrow\rangle + 2\langle n\rangle\langle M_\uparrow^2\rangle - 4\langle n\rangle\langle M_\uparrow\rangle^2 + 2\langle M_\uparrow^2\rangle - (\langle n\rangle+1)\langle M_\uparrow\rangle\right). \end{aligned} \tag{4.57}$$

The truncation rules (4.51) thus lead to equations that are identical to those one obtains from calculating with P_{nm}. Eqs. (4.50), (4.56) and (4.57) are needed to find the steady-state expectation

values in conjunction with Eqs. (4.48).

4.2.5 Dynamics of Second-order Correlation Function

The time-dependent photon density-density or second-order correlation function measured in the experiment is defined as

$$g^{(2)}(\tau) = \left.\frac{\langle n(t+\tau)n(t)\rangle}{\langle n(t)\rangle^2}\right|_{t\to\infty} = \frac{\mathrm{Tr}\left[a^\dagger a\ \mathrm{e}^{\hat{\mathcal{L}}\tau}\tilde{\rho}_\infty\right]}{\mathrm{Tr}\left[a^\dagger a\rho_\infty\right]^2}, \tag{4.58}$$

where $\hat{\mathcal{L}}$ is the total Lindblad superoperator belonging to the master equation (4.32), $\rho_\infty = \lim_{t\to\infty}\rho(t)$ denotes the steady-state density matrix, and we introduce an *effective* density matrix[6]

$$\tilde{\rho}_\infty := a^\dagger a\rho_\infty.$$

Defining also the corresponding effective average $\overline{X}(\tau) := \mathrm{Tr}X\mathrm{e}^{\hat{\mathcal{L}}\tau}\tilde{\rho}_\infty$, the second-order coherence becomes simply

$$g^{(2)}(\tau) = \frac{\overline{n}(\tau)}{\langle n\rangle_\infty^2}. \tag{4.59}$$

The effective averages $\overline{n}$ and $\overline{M}_\uparrow$ obey almost the same equations as $\langle n\rangle$ and $\langle M_\uparrow\rangle$, the only difference arising from the fact that the trace of the effective density matrix is not normalized, $\mathrm{Tr}\,\tilde{\rho}_\infty = \langle n\rangle_\infty$, which entails

$$\Gamma_\uparrow M\,\mathrm{Tr}\left[\sigma^-\sigma^+\tilde{\rho}_\infty\right] = \Gamma_\uparrow\left(\langle n\rangle_\infty M - \overline{M_\uparrow}\right).$$

Thus, one finds equations of motion analogous to Eqs. (4.48),

$$\partial_\tau\overline{n} = -\kappa\overline{n} - B_{\text{abs}}\overline{n(M-M_\uparrow)} + B_{\text{em}}\overline{(n+1)M_\uparrow}, \tag{4.60a}$$

$$\partial_\tau\overline{M_\uparrow} = \Gamma_\uparrow\left(\langle n\rangle_\infty M - \overline{M_\uparrow}\right) - \Gamma_\downarrow\overline{M_\uparrow} + B_{\text{abs}}\overline{n(M-M_\uparrow)} - B_{\text{em}}\overline{(n+1)M_\uparrow}. \tag{4.60b}$$

It is important to note that the form of these equations is independent of the operator ordering in the definition of $g^{(2)}(\tau)$ in Eq. (4.58). Their structure is determined by $\hat{\mathcal{L}}$ rather than the per se arbitrary effective density matrix. What does change are the initial conditions. This, however, is negligible for the relatively large photon numbers relevant experimentally, the difference being on the order of $1/\langle n\rangle_\infty$.

The relation between Eqs. (4.48) and (4.60) may also be understood from the density-matrix ansatz. If ρ_∞ is represented as a diagonal matrix with elements P^∞_{nm}, then $\tilde{\rho}_\infty$ will also be diagonal with elements $\tilde{P}^\infty_{nm}(\tau=0) = nP^\infty_{nm}$.[7] These provide the initial conditions for a system of

[6] Note in passing that, for the normal-ordered second-order correlation function, one would need to set $\tilde{\rho}_\infty = a\rho_\infty a^\dagger$.

[7] The obvious representation that comes to mind is $\rho_\infty = \mathrm{diag}\,(P^\infty_{00},...,P^\infty_{0M},P^\infty_{10},...,)$ and $\tilde{\rho}_\infty(\tau=0) =$

equations formally identical to that given by the equation for $\dot{P}_{nm}$ in Ref. [17].

As before, the higher-order moments $\overline{nM_\uparrow}$ need to be truncated in practice, which can be achieved using the Gaussian identity from above applied to the steady-state expectation values, i.e.

$$\langle n^2 M_\uparrow \rangle_\infty = 2\langle n \rangle_\infty \langle nM_\uparrow \rangle_\infty + \langle M_\uparrow \rangle_\infty \langle n^2 \rangle_\infty - 2\langle n \rangle_\infty^2 \langle M_\uparrow \rangle_\infty, \tag{4.61}$$

where the average is

$$\langle X \rangle_\infty = \sum_{n=0}^{\infty} \sum_{m=0}^{M} X P_{nm}^\infty. \tag{4.62}$$

But since

$$\langle nX \rangle_\infty = \sum_{n=0}^{\infty} \sum_{m=0}^{M} nX P_{nm}^\infty = \sum_{n=1}^{\infty} \sum_{m=0}^{M} X \tilde{P}_{nm}^\infty = \overline{X}, \tag{4.63}$$

Eq. (4.61) also implies

$$\overline{nM_\uparrow} = \langle n \rangle_\infty \overline{M_\uparrow} + \langle n \rangle_\infty \langle nM_\uparrow \rangle_\infty + \langle M_\uparrow \rangle_\infty \overline{n} - 2\langle n \rangle_\infty^2 \langle M_\uparrow \rangle_\infty. \tag{4.64}$$

By computing the steady-state density matrix directly, one can also check that this relation is fulfilled quite well already for intermediate system sizes with molecule numbers of order $M \sim 10^2$. If we furthermore introduce the vector

$$\boldsymbol{g}(\tau) = \begin{pmatrix} \Delta g_n^{(2)} \\ \Delta g_{n,\,M_\uparrow}^{(2)} \end{pmatrix} = \begin{pmatrix} \overline{n} - \langle n \rangle_\infty^2 \\ \overline{M_\uparrow} - \langle n \rangle_\infty \langle M_\uparrow \rangle_\infty \end{pmatrix}, \tag{4.65}$$

Eqs. (4.60) become

$$\begin{aligned} \partial_\tau \Delta g_n^{(2)} &= \langle n \rangle_\infty \left\{ -\kappa \langle n \rangle_\infty - B_{\text{abs}} \langle n(M - M_\uparrow) \rangle_\infty + B_{\text{em}} \langle (n+1) M_\uparrow \rangle_\infty \right\} \\ &\quad - \kappa \Delta g_n^{(2)} - B_{\text{abs}} \left[(M - \langle M_\uparrow \rangle_\infty) \Delta g_n^{(2)} - \langle n \rangle_\infty \Delta g_{n,\,M_\uparrow}^{(2)} \right] \\ &\quad + B_{\text{em}} \left[(\langle n \rangle_\infty + 1) \Delta g_{n,\,M_\uparrow}^{(2)} + \langle M_\uparrow \rangle_\infty \Delta g_n^{(2)} \right], \end{aligned} \tag{4.66a}$$

$$\begin{aligned} \partial_\tau \Delta g_{n,\,M_\uparrow}^{(2)} &= \langle n \rangle_\infty \left\{ \Gamma_\uparrow (M - \langle M_\uparrow \rangle_\infty) - \Gamma_\downarrow \langle M_\uparrow \rangle_\infty \right. \\ &\quad \left. + B_{\text{abs}} \langle n \left(M - M_\uparrow \right) \rangle_\infty - B_{\text{em}} \langle (n+1)\, M_\uparrow \rangle_\infty \right\} \\ &\quad - (\Gamma_\uparrow + \Gamma_\downarrow) \Delta g_{n,\,M_\uparrow}^{(2)} + B_{\text{abs}} \left[(M - \langle M_\uparrow \rangle_\infty) \Delta g_n^{(2)} - \langle n \rangle_\infty \Delta g_{n,\,M_\uparrow}^{(2)} \right] \\ &\quad - B_{\text{em}} \left[(\langle n \rangle_\infty + 1) \Delta g_{n,\,M_\uparrow}^{(2)} + \langle M_\uparrow \rangle_\infty \Delta g_n^{(2)} \right]. \end{aligned} \tag{4.66b}$$

Using the steady-state solutions of Eqs. (4.48) to eliminate the curly brackets, we end up with the

diag $(P_{10}^\infty, ..., P_{1M}^\infty, 2P_{20}^\infty, ...)$.

linear system

$$\partial_\tau \boldsymbol{g}(\tau) = \begin{pmatrix} -\kappa - \tilde{\Gamma}_M & \tilde{\Gamma}_n \\ \tilde{\Gamma}_M & -\left(\Gamma_\uparrow + \Gamma_\downarrow\right) - \tilde{\Gamma}_n \end{pmatrix} \boldsymbol{g}(\tau), \tag{4.67}$$

where

$$\begin{aligned} \tilde{\Gamma}_M &= B_{\text{abs}}(M - \langle M_\uparrow \rangle_\infty) - B_{\text{em}} \langle M_\uparrow \rangle_\infty, \\ \tilde{\Gamma}_n &= B_{\text{abs}} \langle n \rangle_\infty + B_{\text{em}}(\langle n \rangle_\infty + 1). \end{aligned} \tag{4.68}$$

The constant $\tilde{\Gamma}_M$ is composed of an absorption term proportional to the number of ground-state molecules in the steady state $(M - \langle M_\uparrow \rangle_\infty)$, and a corresponding emission term with the number of excited molecules. The constant $\tilde{\Gamma}_n$ is given by an absorption term, and the terms corresponding to stimulated and spontaneous emission. Eq. (4.67) is formally equivalent to the system of equations obeyed by the linear fluctuations around the steady state, as it should be. The derivation we have given is hence an explicit proof of the so-called *quantum regression theorem* [146] as applied to our particular system. Note that the essence of this theorem is already contained in the semigroup structure of Eq. (4.58).

4.2.6 Eigenvalues of Second-Order Coherence Dynamics

The matrix in Eq. (4.67) is non-Hermitian because of time-reversal symmetry breaking in the driven-dissipative system. As a result, its eigenvalues are found to be complex, $\lambda_{1,2} = \lambda' \pm \mathrm{i}\,\lambda''$, where $\lambda', \lambda'' \in \mathbb{R}$. In terms of the quantities defined in Eqs. (4.68), the eigenvalues are given by

$$\lambda_{1,2} = -\gamma \pm \sqrt{\gamma^2 - \omega_0^2}, \tag{4.69}$$

where

$$2\gamma = \kappa + \Gamma_\uparrow + \Gamma_\downarrow + \tilde{\Gamma}_M + \tilde{\Gamma}_n, \tag{4.70a}$$

$$\omega_0^2 = \kappa\tilde{\Gamma}_n + (\kappa + \tilde{\Gamma}_M)(\Gamma_\uparrow + \Gamma_\downarrow). \tag{4.70b}$$

The second-order correlation function will be *oscillating* whenever $\gamma^2 - \omega_0^2 < 0$, and *bi-exponentially* damped otherwise. Without drive and dissipation ($\kappa = \Gamma_\uparrow = \Gamma_\downarrow = 0$), we have a two-component system which shows a single relaxation time, i.e. the system possesses one zero eigenvalue and a purely real eigenvalue $\lambda = -(\tilde{\Gamma}_M + \tilde{\Gamma}_n)$. Accordingly, the open-system character is necessary to achieve an imaginary part for the eigenvalues and hence an oscillating solution. For the second-order correlation function, one finds general solutions of the form

$$g^{(2)}(\tau) = 1 + \mathrm{e}^{-\gamma\tau}\left(c_1 \mathrm{e}^{\sqrt{\gamma^2-\omega_0^2}} + c_2 \mathrm{e}^{-\sqrt{\gamma^2-\omega_0^2}}\right), \tag{4.71}$$

with $\gamma > 0$ ensuring stability in the oscillating regime. In principle, the system could become unstable in the bi-exponential regime, yet we will see below that this does not occur for physically

relevant parameters. The initial conditions for the dynamics of the second-order correlation functions are found from the steady-state solutions for the second cumulants,

$$\begin{aligned} \Delta g_n^{(2)}(0) &= \langle n^2 \rangle_\infty - \langle n \rangle_\infty^2, \\ \Delta g_{n,\,M_\uparrow}^{(2)}(0) &= \langle n M_\uparrow \rangle_\infty - \langle n \rangle_\infty \langle M_\uparrow \rangle_\infty, \end{aligned} \tag{4.72}$$

which, as mentioned, can be obtained from Eqs. (4.50), (4.56) and (4.57) together with Eqs. (4.48).

4.2.7 Approximation Near Equilibrium

For small drive and dissipation, i.e. when the system is close to equilibrium, Eq. (4.30) can be assumed to be approximately valid, leading to the relation

$$B_{\text{abs}}(M - \langle M_\uparrow \rangle_\infty) \approx B_{\text{em}} \langle M_\uparrow \rangle_\infty + B_{\text{em}} \frac{\langle M_\uparrow \rangle_\infty}{\langle n \rangle_\infty}, \tag{4.73}$$

which in turn entails

$$\tilde{\Gamma}_M \approx B_{\text{em}} \frac{\langle M_\uparrow \rangle_\infty}{\langle n \rangle_\infty}. \tag{4.74}$$

Experimentally, one can make the further approximations[8]

$$\begin{aligned} \kappa &\gg \Gamma_\uparrow \gg \Gamma_\downarrow, \\ \langle M_\uparrow \rangle_\infty &\gg \langle n \rangle_\infty \gg 1, \\ B_{\text{em}} &\gg B_{\text{abs}}, \end{aligned} \tag{4.75}$$

where the latter depends via the Kennard-Stepanov relation on both the temperature and the detuning at which the experiment is conducted. Using these to simplify the eigenvalues $\lambda_{1,\,2}$, we find[9]

$$\begin{aligned} 2\gamma &\approx B_{\text{em}} \left(\langle M_\uparrow \rangle_\infty / \langle n \rangle_\infty + \langle n \rangle_\infty \right), \\ \omega_0^2 &\approx \kappa B_{\text{em}} \langle n \rangle_\infty. \end{aligned} \tag{4.76}$$

4.2.8 Expansion in Inverse Molecule Number

While Eqs. (4.76) are appealing for their simplicity, they are not valid if the system is driven more strongly. Also, they still depend on secondary quantities (the steady-state occupations) instead of system parameters. Since $\langle n \rangle_\infty$ can be measured and $\langle M_\uparrow \rangle$ approximated, practically this is not a problem. Theoretically, however, it is still appealing to have explicit expressions at least in some limit. Fortunately, because of the large number of molecules $M \gg 1$ in the system,[10] it is possible

[8] Actual numbers are provided below.

[9] This makes use of the expression $\langle n \rangle_\infty \approx M\Gamma_\uparrow/\kappa$ derived in 4.2.8 to justify $\tilde{\Gamma}_M \Gamma_\uparrow \approx B_{\text{em}}\kappa \ll \kappa\tilde{\Gamma}_n$.

[10] For the steady-state experiments in the large traps, M is usually on the order of 10^9.

to derive more general analytical results from an expansion in the inverse molecule number $1/M$ [17], which can be done as follows. We expand the steady-state photon number into a series

$$\langle n\rangle_\infty = Mn^0 + n^1 + \mathcal{O}(1/M), \tag{4.77}$$

and similarly for $\langle M_\uparrow\rangle_\infty$, σ_n^2, $\sigma_{M_\uparrow}^2$, $\sigma_{n,\,M_\uparrow}^2$.[11] Inserting these series' into the respective equations and separating powers, one obtains

$$\langle n\rangle_\infty = \frac{M\left(B_{\text{em}}\Gamma_\uparrow - B_{\text{abs}}\Gamma_\downarrow\right)}{\kappa\left(B_{\text{em}}+B_{\text{abs}}\right)} + \mathcal{O}(1), \tag{4.78}$$

$$\langle M_\uparrow\rangle_\infty = \frac{MB_{\text{abs}}+\kappa}{B_{\text{abs}}+B_{\text{em}}} + \mathcal{O}(1/M), \tag{4.79}$$

for the steady-state occupations[12] and for the second cumulants

$$\begin{aligned}
\sigma_n^2 &= \frac{MB_{\text{em}}\left(B_{\text{em}}\Gamma_\uparrow + B_{\text{abs}}\Gamma_\uparrow + B_{\text{abs}}\kappa\right)}{\kappa\left(B_{\text{em}}+B_{\text{abs}}\right)^2} + \mathcal{O}(1),\\
\sigma_{M_\uparrow}^2 &= \frac{MB_{\text{em}}B_{\text{abs}}}{\left(B_{\text{em}}+B_{\text{abs}}\right)^2} + \mathcal{O}(1),\\
\sigma_{n,\,M_\uparrow}^2 &= -\frac{MB_{\text{em}}B_{\text{abs}}}{\left(B_{\text{em}}+B_{\text{abs}}\right)^2} + \mathcal{O}(1).
\end{aligned} \tag{4.80}$$

With $\Gamma_\downarrow = \epsilon\Gamma_\uparrow$ and $B_{\text{abs}} = \mathrm{e}^{\beta\delta}B_{\text{em}}$, we now find for the steady state that

$$\langle n\rangle_\infty \approx \frac{M\Gamma_\uparrow\left(1-\mathrm{e}^{\beta\delta+\ln\epsilon}\right)}{(1+\mathrm{e}^{\beta\delta})\kappa}, \tag{4.81a}$$

$$\langle M_\uparrow\rangle_\infty \approx \frac{M\mathrm{e}^{\beta\delta}B_{\text{em}}+\kappa}{(1+\mathrm{e}^{\beta\delta})B_{\text{em}}}, \tag{4.81b}$$

which provides a useful heuristic connecting the experimentally accessible $\langle n\rangle_\infty$ to the unknown pumping rate $\Gamma_\uparrow$ in the form

$$\langle n\rangle_\infty \approx M\Gamma_\uparrow/\kappa. \tag{4.82}$$

[11] Note that we do not introduce further notation to highlight the steady-state values of σ_n^2, $\sigma_{M_\uparrow}^2$ and $\sigma_{n,\,M_\uparrow}^2$.

[12] The first-order term for the photon number is already quite lengthy and does not contribute significantly for $M \gg 1$: $n^1 = \frac{B_{\text{em}}B_{\text{abs}}^2 - B_{\text{em}}^2B_{\text{abs}} - B_{\text{em}}\Gamma_\downarrow\Gamma_\uparrow - B_{\text{em}}\Gamma_\uparrow^2 + B_{\text{abs}}\Gamma_\downarrow^2 + B_{\text{abs}}\Gamma_\downarrow\Gamma_\uparrow}{B_{\text{em}}^2\Gamma_\uparrow - B_{\text{em}}B_{\text{abs}}\Gamma_\downarrow + B_{\text{em}}B_{\text{abs}}\Gamma_\uparrow - B_{\text{abs}}^2\Gamma_\downarrow}$.

4.2.9 Approximation for Large Molecule Numbers

Applying the $1/M$ expansion to the eigenvalues $\lambda_{1,2}$, we may write

$$\begin{aligned}\tilde{\Gamma}_M &= -\kappa,\\ \tilde{\Gamma}_n &= M\Gamma_\uparrow B_{\text{em}}\left(1-\mathrm{e}^{\beta\delta+\ln\epsilon}\right)/\kappa,\end{aligned} \tag{4.83}$$

from which we find

$$\gamma = \frac{\Gamma_\uparrow}{2}\left(1+\epsilon+\frac{MB_{\text{em}}}{\kappa}\left(1-\mathrm{e}^{\beta\delta+\ln\epsilon}\right)\right) \approx \left(1-\mathrm{e}^{\beta\delta+\ln\epsilon}\right)\frac{M\Gamma_\uparrow B_{\text{em}}}{2\kappa}, \tag{4.84a}$$

$$\omega_0^2 = \left(1-\mathrm{e}^{\beta\delta+\ln\epsilon}\right)M\Gamma_\uparrow B_{\text{em}}. \tag{4.84b}$$

This means that the eigenvalues become

$$\lambda_{1,2} = -\left(1-\mathrm{e}^{\beta\delta+\ln\epsilon}\right)\left\{\frac{M\Gamma_\uparrow B_{\text{em}}}{2\kappa} \pm \sqrt{\left(\frac{M\Gamma_\uparrow B_{\text{em}}}{2\kappa}\right)^2 - \frac{M\Gamma_\uparrow B_{\text{em}}}{\left(1-\mathrm{e}^{\beta\delta+\ln\epsilon}\right)}}\right\}, \tag{4.85}$$

an expression that turns out to be a good approximation in an intermediate regime as the system moves away from equilibrium. For $M\Gamma_\uparrow B_{\text{em}} > 4\kappa^2/\left(1-\mathrm{e}^{\beta\delta+\ln\epsilon}\right)$, the eigenvalues become purely real. It is important to note, however, that Eq. (4.85) is not valid for $\Gamma_\uparrow \to 0$, in which case it predicts $\lambda_{1,2} = 0$. Expanding the square root for large $\Gamma_\uparrow$ and taking $\epsilon \to 0$, one finds asymptotically that

$$\lambda_{1,2} = -\frac{M\Gamma_\uparrow B_{\text{em}}}{2\kappa} \pm \frac{M\Gamma_\uparrow B_{\text{em}}}{2\kappa} \mp \kappa = \begin{cases} \kappa - M\Gamma_\uparrow B_{\text{em}}/\kappa,\\ -\kappa. \end{cases} \tag{4.86}$$

Note that the approximation leading to Eq. (4.85) is not employed in the analysis of the experimental data. It rather serves to illustrate how the openness of the system influences the eigenvalues through the steady-state occupations by making the dependence on $\Gamma_\uparrow$ and κ explicit.

4.2.10 Solution of Truncated First-Moment Equations

For large M, the influence of $\sigma^2_{n,M_\uparrow}$ in Eqs. (4.48) is negligible, meaning one can use $\langle nM_\uparrow\rangle \approx \langle n\rangle\langle M_\uparrow\rangle$ and solve them as a closed system of equations.[13] This results in

$$\begin{aligned}\langle n\rangle_\infty &= \frac{B_{\text{em}}\langle M_\uparrow\rangle_\infty}{\kappa + B_{\text{abs}}(M-\langle M_\uparrow\rangle_\infty) - B_{\text{em}}\langle M_\uparrow\rangle_\infty},\\ \langle M_\uparrow\rangle_\infty &= \frac{1}{2a}\left(b \pm \sqrt{b^2 - 4aM\Gamma_\uparrow\left(MB_{\text{abs}}+\kappa\right)}\right).\end{aligned} \tag{4.87}$$

[13] The second-moment equations are needed still to find the initial values of the second-order correlations.

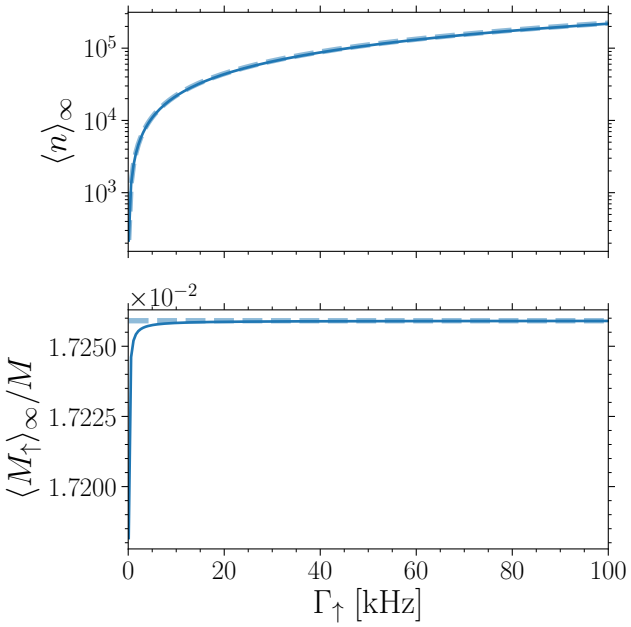

Figure 4.1: Eqs. (4.87) plotted against the external pumping $\Gamma_\uparrow$ for parameters $M = 5.17 \cdot 10^9$, $\kappa = 2.33$ GHz, $B_{\text{em}} = 2.50 \cdot 10^{-5}$ GHz, $\Gamma_\downarrow = 0$ and $B_{\text{em}}/B_{\text{abs}} = 57$ (Kennard-Stepanov relation corresponding to a cut-off wavelength of $\lambda_c \approx 571.3$ nm). The dashed lines are Eqs. (4.82) and (4.81b). Visibly, they agree well with the results from the truncated first-moment equations, the deviation of $\langle M_\uparrow \rangle_\infty$ for small $\Gamma_\uparrow$ being on the order of merely 10^5 molecules.

with $a = (B_{\text{em}} + B_{\text{abs}})\left(\Gamma_\downarrow + \Gamma_\uparrow\right)$ and $b = M\Gamma_\uparrow (B_{\text{em}} + B_{\text{abs}}) + B_{\text{em}}\kappa + \left(\Gamma_\downarrow + \Gamma_\uparrow\right)(MB_{\text{abs}} + \kappa)$. It is instructive to compare these solutions to the approximate expressions from the $1/M$ expansion, which is done in Fig. 4.1 for typical experimental parameters. Illustratively, employing a non-linear solver to find steady-state solutions to the set of five equations provided by (4.48), (4.50), (4.56) and (4.57), a value of $\Gamma_\uparrow = 1.15 \cdot 10^{-5}$ GHz leads to steady-state occupations $\langle n \rangle_\infty = 2.51 \cdot 10^4$, $\langle M_\uparrow \rangle_\infty = 8.92 \cdot 10^7$ and steady-state (co-) variances $\sigma_n^2 = 8.77 \cdot 10^7$, $\sigma_{M_\uparrow}^2 = 4.08 \cdot 10^8$ and $\sigma_{n,\,M_\uparrow}^2 = -8.77 \cdot 10^7$. For the much lower value of $\Gamma_\uparrow = 9.17 \cdot 10^{-7}$ GHz, we find steady-state occupations $\langle n \rangle_\infty = 2.00 \cdot 10^3$, $\langle M_\uparrow \rangle_\infty = 8.92 \cdot 10^7$ and steady-state (co-) variances $\sigma_n^2 = 4.00 \cdot 10^6$, $\sigma_{M_\uparrow}^2 = 1.87 \cdot 10^8$ and $\sigma_{n,\,M_\uparrow}^2 = -4.00 \cdot 10^6$. The fact that $\sigma_n^2 \approx -\sigma_{n,\,M_\uparrow}^2$ is supported by Eqs. (4.80).[14] Both results clearly support the assumption $\langle nM_\uparrow \rangle \approx \langle n \rangle \langle M_\uparrow \rangle$ at least when looking for steady states since $\langle n \rangle_\infty \langle M_\uparrow \rangle_\infty \gg |\sigma_{n,\,M_\uparrow}^2|$.

[14] In the numerator of σ_n^2, the term proportional to κ is the dominant one for the current parameters.

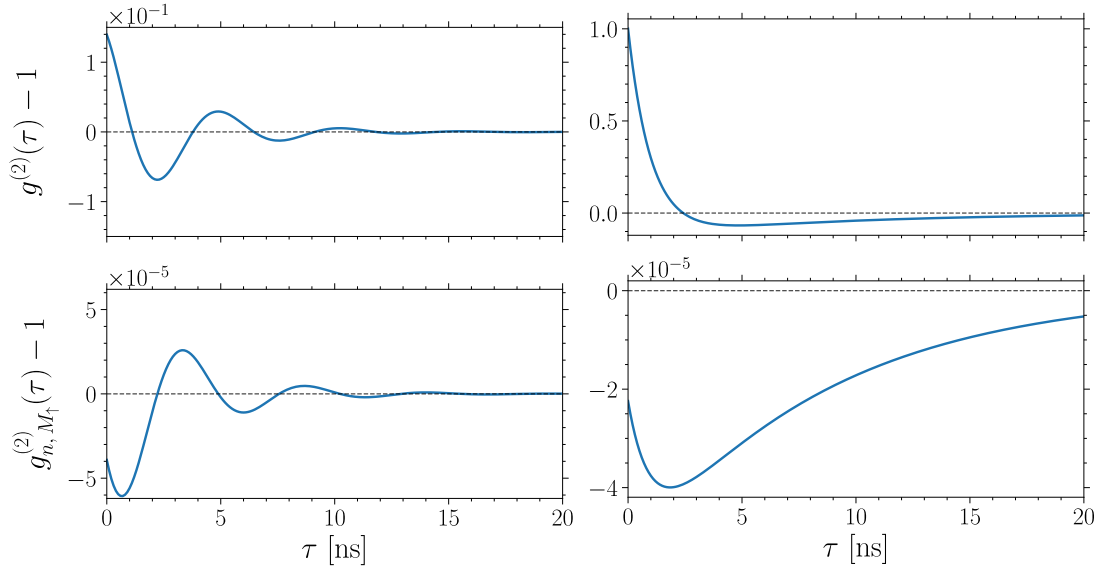

Figure 4.2: Time-dependent second-order correlations function for the parameters of Fig. 4.1 with *(left)* $\Gamma_\uparrow = 1.15 \cdot 10^{-5}$ GHz and *(right)* $\Gamma_\uparrow = 9.17 \cdot 10^{-7}$ GHz. The zero-delay values are $g^{(2)}(0) = 1.14$, $g^{(2)}_{n,M_\uparrow}(0) = 1.00 - 3.92 \cdot 10^{-5}$, and $g^{(2)}(0) = 2.00$, $g^{(2)}_{n,M_\uparrow}(0) = 1.00 - 2.24 \cdot 10^{-5}$, respectively.

4.2.11 Exemplary Solutions

The oscillating solutions for the second-order correlation functions at $\Gamma_\uparrow = 1.15 \cdot 10^{-5}$ GHz are plotted in Fig. 4.2. Their functional form can be expressed as

$$\begin{aligned} g^{(2)}(\tau) &= 1 + \frac{\Delta g^{(2)}_n(\tau)}{\langle n \rangle^2_\infty} \\ &= 1 + \frac{\mathrm{e}^{-\gamma\tau}}{\langle n \rangle^2_\infty} \left[\sigma^2_n \cos\omega\tau + \frac{\gamma}{\omega} \left(\sigma^2_n + 2\sigma^2_{n,M_\uparrow} \right) \sin\omega\tau \right], \\ g^{(2)}_{n,M_\uparrow}(\tau) &= 1 + \frac{\Delta g^{(2)}_{n,M_\uparrow}(\tau)}{\langle n \rangle_\infty \langle M_\uparrow \rangle_\infty} \\ &= 1 + \frac{\mathrm{e}^{-\gamma\tau}}{\langle n \rangle_\infty \langle M_\uparrow \rangle_\infty} \left[\sigma^2_{n,M_\uparrow} \cos\omega\tau - \left(\frac{\omega^2 + \gamma^2}{2\gamma\omega} \sigma^2_n + \frac{\gamma}{\omega} \sigma^2_{n,M_\uparrow} \right) \sin\omega\tau \right], \end{aligned} \tag{4.88}$$

where $g^{(2)}_{n,M_\uparrow}(\tau)$ is the second-order "cross-correlation". The numerical values for decay rate and frequency are $\gamma = 0.319$ GHz and $\omega = 1.177$ GHz, respectively. Complementary to this, the bi-exponentially damped solutions for the second-order correlation functions at $\Gamma_\uparrow = 9.17 \cdot 10^{-7}$ GHz are plotted in Fig. 4.2. In turn, their functional form can be expressed as $c_1 \mathrm{e}^{-\gamma_1\tau} + c_2 \mathrm{e}^{-\gamma_2\tau}$, where the constants $c_{1,2}$ can be found from the eigenvectors and the zero-delay values. The two

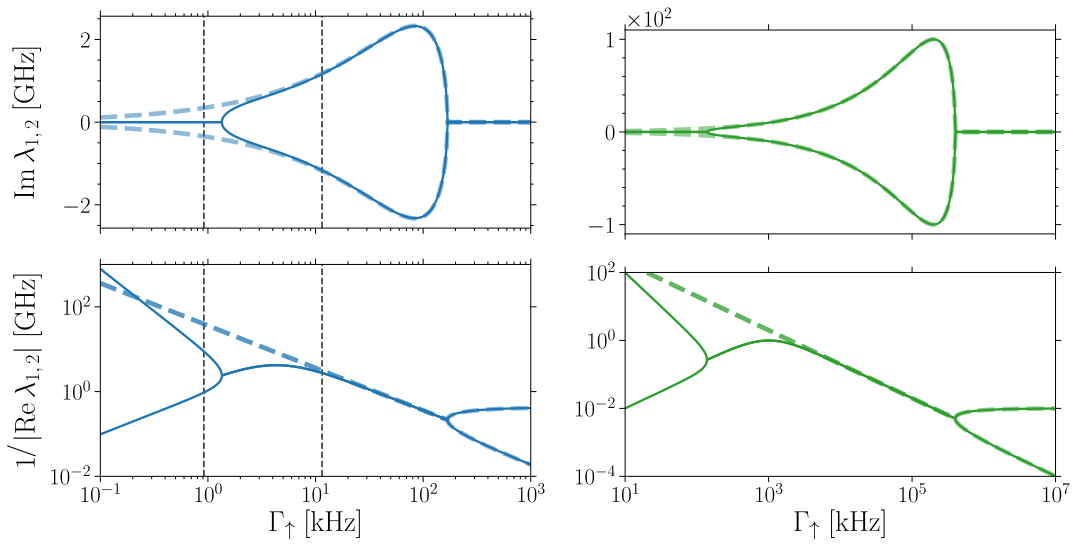

Figure 4.3: The eigenvalues of Eq. (4.69) as a function of $\Gamma_\uparrow$ for parameters *(left)* as in Fig. 4.1, and *(right)* $M = 1.00 \cdot 10^9$, $\kappa = 100$ GHz, $B_{\mathrm{em}} = 1.00 \cdot 10^{-4}$ GHz, $\Gamma_\downarrow = 0$ and $B_{\mathrm{em}}/B_{\mathrm{abs}} = 10$. Two exceptional points appear in the spectrum as the system moves away from equilibrium. The vertical lines *(left)* mark $\Gamma_\uparrow = \{1.15 \cdot 10^{-5},\ 9.17 \cdot 10^{-7}\}$ GHz, the values corresponding to Fig. 4.2. The dashed curves show Eq. (4.85). A brief discussion of exceptional points is given in the text.

decay rates have values $\gamma_1 = 0.119$ GHz and $\gamma_2 = 0.996$ GHz.

The behavior of the eigenvalues as a function of pump power is shown in Fig. 4.3 for two different sets of parameters and compared to analytical results from the expansion in the inverse molecule number. In both cases, as $\Gamma_\uparrow$ increases, the system passes through two exceptional points. At these points, the square root in Eq. (4.69) switches from real to imaginary (imaginary to real). Correspondingly, the decay changes from a single rate to two different rates (two different rates to a single rate). Looking at the eigenvectors as the exceptional points are approached, one observes how two distinct eigenvectors gradually approach each other until they become identical,[15] which distinguishes this so-called *coalescence* [147] from the usual degeneracy where two *distinct* eigenvectors possess the same eigenvalue.

Instead of keeping the cavity loss κ fixed and looking at the eigenvalues, it is also instructive to study the occurrence of the exceptional points as a function of both κ and $\Gamma_\uparrow$, which is done in Fig. 4.4. Visibly, this gives rise to a kind of phase diagram where the bi-exponentially decaying solutions outside of the curve are separated from the oscillating ones on the inside. It is even possible to entirely avoid the oscillating regime for very small κ by circumnavigating the lower tip of the curve as one drives the system further away from equilibrium. In looking at this diagram, one should keep in mind that the emission and absorption coefficients B_{em} and B_{abs} do depend on $\Gamma_\uparrow$ via Eq. (4.20). As mentioned above, this is not relevant experimentally at the moment.

[15] The left and right eigenvectors of a non-Hermitian matrix are generally not the same.

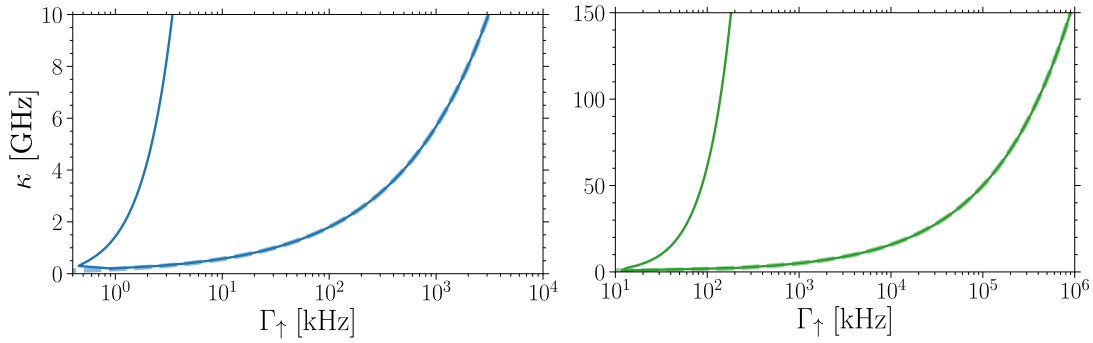

Figure 4.4: The zeros of the square root in Eq. (4.69) for the two cases of Figs. 4.2 and 4.3. The dashed curves show $\Gamma_\uparrow = 4\kappa^2 M^{-1} B_{\text{em}}^{-1}$, the corresponding result from Eq. (4.85) when B_{abs} and $\Gamma_\downarrow$ are neglected.

Addressing the question of the shape of the phase diagram far away from equilibrium, however, will require taking this effect into account. As a matter of fact, it will indeed be necessary to extend the existing model [16] which altogether ignores the influence of the cavity loss κ. This will be one of the subjects of Chp. 5.

4.3 Application to Experiment

The final part of the present Chp. is devoted to the comparison of the developed theory with actual experiments. Note that this Sec. is derived from Ref. [36], which does not contain the experimental observation of the exceptional point at the transition from the bi-exponential to the oscillating regime. For the presentation and discussion of the experimental verification of this transition, consider instead Ref. [37].

To measure the mode intensities and the temporal intensity-intensity correlations, i.e. the mode occupation numbers and the second-order coherence, the microcavity emission is directed through a mode filter to separate the condensate mode $k = 0$ from the higher-order photons with $k > 0$. The light passing through the mode filter is then imaged onto a photomultiplier, the output signal of which is simultaneously recorded by two oscilloscopes, with the cross-correlation used for the further analysis of the intensity fluctuations. The higher-order modes contribute weakly to the intensity near the optical axis in the far-field, such that some photons from these modes erroneously pass the mode filter. This systematic error in the filtering reduces the experimentally measured values of $g^{(2)}(0)$. As a result, the experimental intensity-intensity correlations can be expected to be lower than the theoretically calculated values. One does not, however, expect any influence on the temporal shape of the correlation signal.

The dephasing time τ_φ of the dye transition[16] is much shorter than the photon cavity lifetime,

[16] This is fixed by the collision time of solvent and dye molecules on the order of 10^{-14} s.

$\tau_\varphi \ll \tau_\mathrm{p}$.[17] As the experiment operates in the weak-coupling regime, where the trapped particles are photons instead of polaritons, coherence between dye excitations and photons cannot be established. The photon lifetime is, furthermore, much shorter than the non-radiative decay time of the dye molecules, $\tau_\mathrm{p} \ll \tau_\text{non-rad}$.[18] The sum of cavity photons (including the thermal tail) and dye excitations can hence be taken as conserved on the scale of the photon lifetime τ_p, while the stationary photon number is conserved only on average. Approximately, also the sum of condensate photons and dye excitations is conserved, as the exchange between thermal-tail photons and condensate photons happens via the bath and, as mentioned, the dye excitations outnumber the (thermal) photons by orders of magnitude [3]. In the regime where several absorptions and emissions take place before any single photon leaves the cavity, the cavity reaches a thermal spectral distribution at the rovibrational temperature of the dye, which is around room temperature (300 K). Fig. 4.5 presents data of the optical spectrum for varying steady-state condensate occupations $\langle n \rangle_\infty$ (i.e. at different external-pumping rates). The match between measurements and equilibrium theory supports the idea that a thermal spectrum is achieved to good approximation in the experiments, even though pumping and losses drive the system permanently away from equilibrium. Finally, above the critical total photon number, the thermal photon gas produces a BEC, indicated by the ground-mode peak in the spectrum around the low-frequency cavity cut-off.

By changing the steady-state photon number $\langle n \rangle_\infty$ relative to the number of dye molecules within the mode volume, the system can be tuned from the small-reservoir regime with Poissonian number statistics and $g^{(2)}(0) \approx 1$ to a strongly fluctuating regime of large reservoirs with Bose-Einstein statistics and $g^{(2)}(0) \approx 2$. The initial values for the dynamics of the second-order correlation functions are found from the steady-state solutions for the second moments, $\langle n^2 \rangle_\infty$ and $\langle n M_\uparrow \rangle_\infty$. Typical measurements for the time dependence of the second-order correlation function are given in Fig. 4.6 for condensate numbers $\langle n \rangle_\infty \approx 4620$ and $\langle n \rangle_\infty \approx 17100$, respectively, showing damped, oscillatory behavior, which can be understood from the theoretical discussion above. Within the experimentally investigated parameters, the oscillations persist as the system is tuned from the grand-canonical to the canonical regime. As can be seen in Fig. 4.6, the photon number fluctuations (relative to the average condensate number) decrease at higher average condensate numbers, which indeed correspond to a relatively smaller dye reservoir. This was studied in more detail in earlier experimental work [4]. For the present system, the theoretical values for $g^{(2)}(0)$ of the condensate mode at $\langle n \rangle_\infty \approx 4620$ and $\langle n \rangle_\infty \approx 17100$ are ≈ 2.0 and ≈ 1.3 respectively. The smaller values of $g^{(2)}(0)$ observed in the experiments are, as discussed, attributed to the systematic error in the mode filtering, which moves the correlation signal towards $g^{(2)}(\tau) = 1$ for all times τ. The solid lines in Fig. 4.6 are fits of Eq. (4.71) to the experimental data. The systematic error hence results in a decrease of the coefficients c_1, c_2 compared to the theory values. The experimental estimates of the second-order relaxation time $\tau_c = 1/|\gamma|$ and the oscillation frequency $\omega = \mathrm{Im}\sqrt{\gamma^2 - \omega_0^2}$ of $g^{(2)}$ are found by fitting the theoretical model to the data as depicted in Fig. 4.6. The variation of the oscillation frequency ω as a function the condensate number $\langle n \rangle_\infty$ is shown in Fig. 4.7. An increase of the oscillation frequency of the second-order coherence function with the condensate occupation

[17] $\tau_\mathrm{p} \approx 0.5$ ns, as determined by cavity losses.
[18] $\tau_\text{non-rad}$ lies around 50 ns [148].

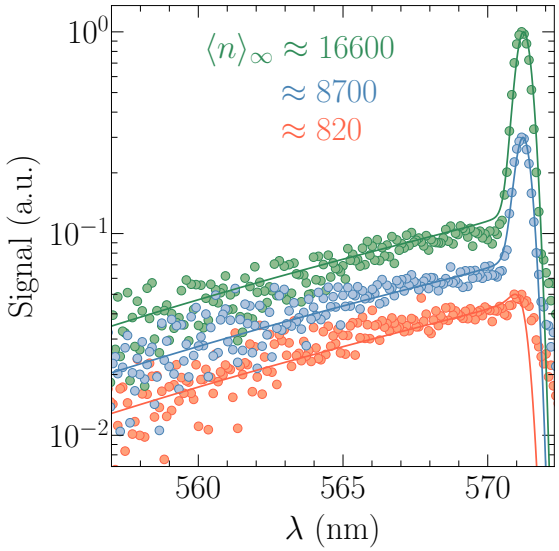

Figure 4.5: Optical spectra (arbitrary units) as a function of wavelength λ, obtained from the cavity leakage through the mirrors. The experiment was conducted at a cut-off wavelength of $\lambda_c = 571.3$ nm. Solid lines indicate fits of the Bose-Einstein distribution at 300 K to the data (broadened by the experimental resolution), the steady-state condensate number $\langle n \rangle_\infty$ being the only free parameter. The fit results for $\langle n \rangle_\infty$ are given in the legend. The spectra at different $\langle n \rangle_\infty$ are vertically shifted vertically to improve visibility.

is observed. The solid line in Fig. 4.7 is obtained using a fit of the theoretical eigenvalues of Eq. (4.67) to the experimental data, where the model parameters $\kappa, \Gamma_\uparrow$, and B_{em} are used as fit parameters while the nonradiative decay rate $\Gamma_\downarrow$ is set to zero.

The experimental data are fitted well for different values of $\langle n \rangle_\infty$ by three parameters which come out consistent with experimentally estimated values. This can be interpreted (supported by the fits shown in Fig. 4.6) as evidence that the $g^{(2)}$ oscillations can be traced back to the physics described by the rate equations, that is, the breaking of time-reversal symmetry due to drive and dissipation, which move the system off equilibrium, as well as the coupling between the two subsystems made up of dye molecules and cavity photons, respectively.

Interestingly, in spite of the non-equilibrium features visible in $g^{(2)}(\tau)$, the number spectrum follows an *equilibrium* Bose-Einstein distribution within experimental accuracy (see Fig. 4.5). The physical origin of this intriguing behavior is the (stationary) transport of photons from the dye reservoir into the resonator and out into the environment, while the average condensate occupation is constant and the photon gas reaches an equilibrium spectral distribution via the contact with the thermal dye molecules. The calculations show, furthermore, that the zero-delay second-order coherence $g^{(2)}(0) > 1$ is not affected by drive and dissipation, while the time dependence of the second-order coherence $g^{(2)}(\tau)$ does change with the latter. The induced photon transport brings about non-trivial structure in the intensity-intensity correlations, as observed in the presented experiments. Related effects are known from nanoelectronics, e.g. current-carrying,

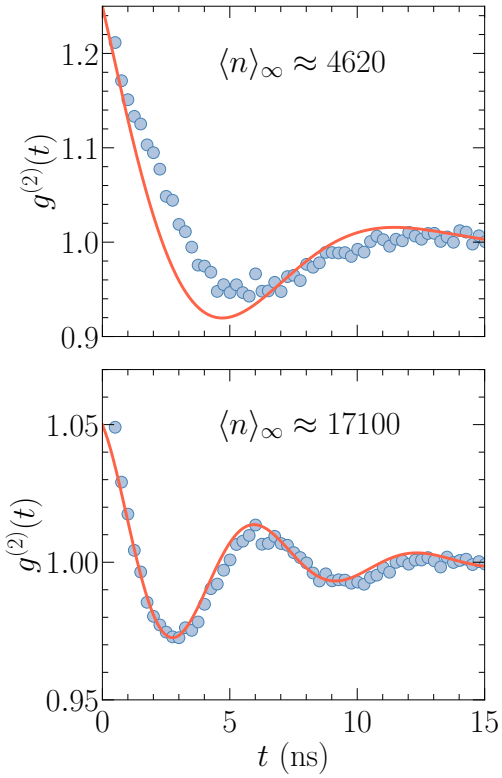

Figure 4.6: Typical results for the time dependence of the second-order correlation function for two different condensate numbers. The solid lines are fits to Eq. (4.71). The envelope of the observed correlation signal $g^{(2)}(\tau)$ decays with a relaxation time of about 4 ns.

metallic nanowires, where the electron energy distribution is thermalized via rapid electron-electron interactions in the wire [149].

To summarize, we theoretically derived an oscillatory second-order coherence function of an open photon Bose-Einstein condensate that was also observed experimentally by investigating the emission of a dye microcavity. Its origin goes back to the driven-dissipative character of the light condensate. The presented results show that even when the spectral photon distribution is compatible with thermal equilibrium within experimental accuracy, the fluctuation dynamics depend sensitively on the openness of the system. As mentioned, one can observe similar behavior in the hot-electron regime of electronic quantum wires at large bias voltage, where non-thermal noise, even though non-oscillatory, is generated by the current. Because of the frequent electron-electron collisions in the wire, this co-exists with an equilibrium (Fermi-Dirac) distribution of the electron energy. In Ref. [36], this phenomenon was described for a photon system for the first time.

The damped oscillations of $g^{(2)}(\tau)$ observed in photon condensates are reminiscent of laser relaxation oscillations. However, there are certain important differences: for one thing, a laser

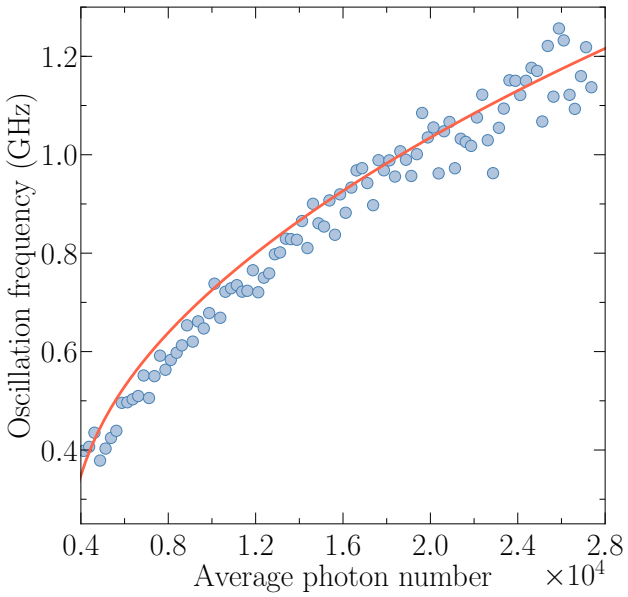

Figure 4.7: Oscillation frequency of the second-order coherence $g^{(2)}(\tau)$ as a function of the condensate occupation $\langle n \rangle_\infty$, as measured in the experiment (dots) and predicted by the rate equations (solid line). The parameters are $M = 5.17 \cdot 10^9$, $\kappa = 2.33$ GHz, $B_{\mathrm{em}} = 2.50 \cdot 10^{-5}$ GHz, $B_{\mathrm{em}}/B_{\mathrm{abs}} \approx 57$ (Kennard-Stepanov relation corresponding to a cut-off wavelength $\lambda_c = 571.3$ nm), $\Gamma_\downarrow = 0$.

is in a state far from equilibrium with a non-thermal spectral distribution. Contrary to this, photon condensates are operated off, yet close to equilibrium, and follow an equilibrium Bose-Einstein distribution, while they still show clear non-equilibrium dynamics in the intensity-intensity correlations. Furthermore, for steady-state lasers $g^{(2)}(\tau) = 1$ for all τ. This means that a non-trivial $g^{(2)}(\tau)$ cannot occur unless the system is perturbed externally, as happens with laser relaxation oscillations when a laser is switched on. For photon condensates which are not deep in the canonical regime where the reservoir very small, the steady state is characterized by $g^{(2)}(0) > 1$, and thus sustaining fluctuations that are responsible for the spontaneous excitation of the oscillations.

CHAPTER 5

Non-Equilibrium Pseudo-Particle Approach to Open Quantum Systems

The microscopic model of the photon BEC introduced in Ref. [16] explicitly includes all essential degrees of freedom that are present in the experiment. As discussed in the previous chapter, the Hamiltonian reads

$$\begin{aligned} H = \sum_k \omega_k a_k^\dagger a_k + \sum_{m=1}^{M} \Bigg[& \frac{\Delta}{2}\sigma_m^z + \Omega\, b_m^\dagger b_m \\ & + \Omega\sqrt{S}\,\sigma_m^z \left(b_m + b_m^\dagger\right) + g\sum_k \left(a_k \sigma_m^+ + a_k^\dagger \sigma_m^-\right) \Bigg]. \end{aligned} \tag{5.1}$$

The subsequently employed phenomenological or macroscopic description, however, is based on the physically well-motivated idea that the phonons b_m, $b_m^\dagger$ can be treated as a reservoir and hence be integrated out. This assumes a coupling of the phonons to a bath of harmonic oscillators (representing the water in which the molecules are dissolved) with a relaxation rate λ that is by far the fastest timescale in the system. In terms of a master equation for the full system, this can be described by

$$\dot{\rho} = -\mathrm{i}[H,\rho] + \sum_{m=1}^{M} \frac{\lambda}{2}\left(\bar{N}(\Omega)+1\right)\mathcal{L}[b_m]\rho + \frac{\lambda}{2}\bar{N}(\Omega)\mathcal{L}[b_m^\dagger]\rho, \tag{5.2}$$

where $\bar{N}(\Omega)$ represents the temperature-dependent occupation of the water bath surrounding the molecules. Physically, the Lindbladians in Eq. (5.2) describe the approach of the oscillators b_m, $b_m^\dagger$ to a steady state with average occupation $\bar{N}$ over a timescale $1/\lambda$ which is typically a few ps or shorter. When this timescale is assumed to be so short that this steady state is reached immediately relative to the change of all other quantities in the system, then the phonons may be assumed to be thermal from the outset and treated as a reservoir accordingly. In addition, an assumption about the frequency spectrum of the phonons must be made. The presence of only a single frequency Ω is likely an oversimplification.

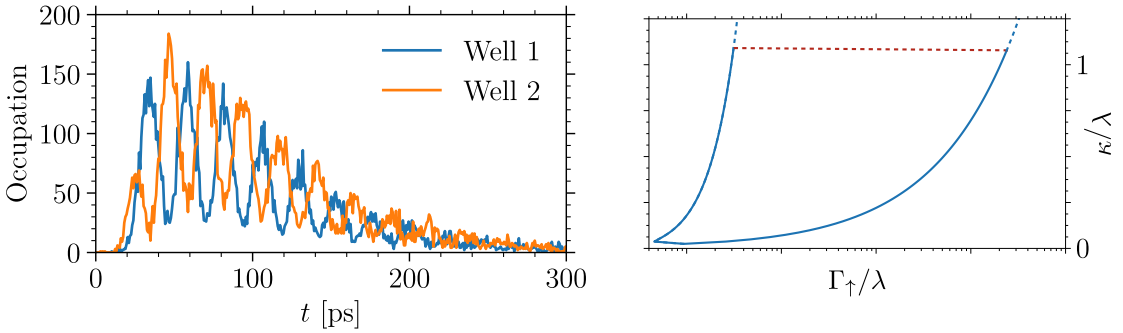

Figure 5.1: Motivations for generalizing the existing model of the photon condensate. *(Left)* Experimentally measured oscillations of two cavity modes confined to a double-well potential at a cutoff of 594 nm (data courtesy of Christian Kurtscheid). The period of the coherent tunneling is on the order of 10 ps, which is potentially not much faster than the vibrational relaxation time $1/\lambda$. *(Right)* Sketch of the $g^{(2)}$ phase diagram from Chp. 4. To answer the question of whether the oscillating regime is bounded from above, the system parameter κ needs to be increased until it begins to compete with λ.

The separation of timescales is certainly valid for the steady-state experiments where the mode populations fluctuate on a nanosecond range [53]. Importantly though, the introduction of micro-potentials [150] to photon-BEC experiments has enabled the creation of potential structures that allow for a coherent coupling between different photon modes. An excellent example is a double-well potential realized in Ref. [12], where the coherent overlap between the wave functions in the two wells creates a tunneling matrix element. From the left panel of Fig. 5.1 one may see that this induces very fast oscillations of periods that are on the order of 10 ps, suggesting these experiments are entering into a regime where a system timescale becomes competitive with the phonon relaxation rate. This may serve as a first motivation to look for a *non-Markovian* extension of the macroscopic rate equations that have been employed so far in the description of the photon BEC. A second and more immediate motivation arises from the interesting question whether the oscillating regime of the $g^{(2)}$ phase diagram studied in Chp. 4 is bounded from above (right panel of Fig. 5.1). To answer this question, it should be theoretically admissible to increase the cavity loss κ without bound, which necessarily entails that it is going to enter into competition with the reservoir relaxation rate λ. We can already anticipate that in this way κ will acquire influence on the emission and absorption spectra.

To achieve such a non-Markovian model where the parameter λ enters explicitly, it is necessary to keep the phonons b_m, $b_m^\dagger$ in the description. This means that the coherent Jaynes-Cummings terms $g(a_k\sigma_m^+ + a_k^\dagger\sigma_m^-)$ will also be present. As we have seen in the previous chapter for a single photon mode, the approach of Refs. [16–18] is, however, essentially based on a semi-classical product ansatz for the system density matrix

$$\rho(t) = \sum_{n=0}^{\infty}\sum_{m=0}^{M} P_{nm}(t)|n\rangle\langle n| \otimes \rho_m, \tag{5.3}$$

which precludes the inclusion of coherent terms such as the Jaynes-Cummings couplings. While

one can envision modifying this ansatz to include coherence between the *photon* modes [18], coherence between the two parts of the system, photons and molecules, is a more difficult matter. In the single-mode picture of the previous chapter, the reason is that the rate equations resulting from the calculation with the product ansatz can only be truncated systematically when the essentially classical particle-number distribution P_{nm} is assumed to be Gaussian. Unfortunately, this does not give a rule for the truncation of expectation values depending on phase differences between the two parts of the system, that is, those induced by the coherent couplings. Therefore, heuristic truncation techniques found in the literature [19] cannot be systematically controlled. The potentially severe consequences of this will be illustrated below.

5.1 Pseudo-Particles

The technique of using canonical operators to represent impurity spins goes back to Abrikosov [21]. The main idea is to expand operators that do not have canonical commutation relations in terms of operators that do, and hence to allow for treatment by standard field-theory techniques (most importantly perturbation theory). In a two-level system or spin $1/2$, for example, either the ground or excited state must always be "occupied". If each is represented by a new fermion operator, respectively, the trouble arises that unphysical states are introduced: the doubly occupied and unoccupied states. This must be compensated for by an *operator constraint* that excludes the unphysical states. The question then arises: How to enforce this constraint in the perturbation series? Essentially, the Green functions will be projected onto the physical subspace by means of an auxiliary chemical potential. This will be described in the following for both equilibrium and non-equilibrium problems.

In the context of the infinite-U Anderson model [22], a combination of fermions and so-called *auxiliary bosons* has been introduced [23–27] which together must satisfy a single operator constraint. These techniques are valid in equilibrium field theory. The extension to non-equilibrium has been given in [28, 29, 31]. A more recent exposition in non-equilibrium may also be found in [32]. The microscopic model of the photon BEC invites a representation in terms of auxiliary bosons only: each vibrational state of the dye molecule will be described by a pair of bosonic creation and destruction operators. The constraint will enforce single occupation across these states. We give a particular formulation of the technique in terms of greater and lesser Green functions only. Previous works also include advanced and retarded [28, 29] or Matsubara Green functions [32] into the description, which is entirely equivalent, of course, yet sometimes less transparent.

A model superficially similar to ours was given in Ref. [151]. However, it is rather an ad-hoc description and not a faithful representation of the proper microscopic Hamiltonian. A previous attempt to represent the two-level systems by fermions did not enforce the operator constraint and was hence unsuccessful [152]. Furthermore, to the author's knowledge we are the first to extend the technique to *open systems* by introducing dissipative processes that respect the operator constraint and conserve the pseudo-particle number. This requires a full synthesis of the projection method and Schwinger-Keldysh field theory. The methods that follow here have been developed with the microscopic model of the photon BEC in mind, yet may be applied to *any* system where there is a large set of incoherent spins coupled coherently to a collection of cavity modes.

5.1.1 Auxiliary-Boson Representation

A single dye molecule ($M = 1$) in the microscopic model has a quantum state $|\sigma,\, n\rangle$, where $\sigma = g,\, e$ refers to ground and excited state, respectively, and n denotes the vibrational state of the molecule. For each of these states, we introduce creation and destruction operators $d_{\sigma,\,n}$, $d^{\dagger}_{\sigma,\,n}$ with $[d_{\sigma,\,n}, d^{\dagger}_{\upsilon,\,m}] = \delta_{\sigma\upsilon}\delta_{nm}$ and $d^{\dagger}_{\sigma,\,n}\,|\mathrm{vac}\rangle = |\sigma,\, n\rangle$. Then the physical operators in Eq. (5.1) may be expressed via the auxiliary bosons as

$$b = \sum_{n=0}^{\infty}\sum_{\sigma}\sqrt{n+1}\; d^{\dagger}_{\sigma,\,n}d_{\sigma,\,n+1}, \tag{5.4}$$

and

$$\begin{aligned}\sigma^{+} &= \sum_{n=0}^{\infty} d^{\dagger}_{e,\,n}d_{g,\,n},\\ \sigma^{z} &= \sum_{n=0}^{\infty}\left[d^{\dagger}_{e,\,n}d_{e,\,n} - d^{\dagger}_{g,\,n}d_{g,\,n}\right],\end{aligned} \tag{5.5}$$

where we have dropped the subscript m on the molecular operators. If this representation is to be faithful, we have to enforce the operator constraint

$$\hat{Q} = \sum_{n=0}^{\infty}\sum_{\sigma} d^{\dagger}_{\sigma,\,n}d_{\sigma,\,n} = 1. \tag{5.6}$$

One may then check easily that the auxiliary-boson representation just given does indeed reproduce the correct commutation relations for the phonon operators b, $b^{\dagger}$ and the Pauli matrices. For instance,

$$\begin{aligned}[b, b^{\dagger}] &= \sum_{n,\,m}\sum_{\sigma\upsilon}\sqrt{n+1}\sqrt{m+1}\;[d^{\dagger}_{\sigma,\,n}d_{\sigma,\,n+1}, d^{\dagger}_{\upsilon,\,m+1}d_{\upsilon,\,m}]\\ &= \sum_{n,\,m}\sum_{\sigma\upsilon}\sqrt{(n+1)\,(m+1)}\Big\{d^{\dagger}_{\sigma,\,n}\left(\delta_{\sigma\upsilon}\delta_{nm} + d^{\dagger}_{\upsilon,\,m+1}d_{\sigma,\,n+1}\right)d_{\upsilon,\,m}\\ &\quad - d^{\dagger}_{\upsilon,\,m+1}\left(\delta_{\sigma\upsilon}\delta_{nm} + d^{\dagger}_{\sigma,\,n}d_{\upsilon,\,m}\right)d_{\sigma,\,n+1}\Big\}\\ &= \sum_{\sigma}\left\{\sum_{n=0}^{\infty}(n+1)\,d^{\dagger}_{\sigma,\,n}d_{\sigma,\,n} - \sum_{n=1}^{\infty} n\; d^{\dagger}_{\sigma,\,n}d_{\sigma,\,n}\right\}\\ &= \sum_{n=0}^{\infty}\sum_{\sigma} d^{\dagger}_{\sigma,\,n}d_{\sigma,\,n} = \hat{Q}.\end{aligned} \tag{5.7}$$

The quartic contributions may only be dropped under the assumption that the operators never act on anything other than states in the physical subspace. This will be ensured by the projection via the auxiliary chemical potential to be introduced in the next section.

In pseudo-particle representation and still for $M = 1$, the Hamiltonian (5.1) becomes

$$H = \sum_k \omega_k a_k^\dagger a_k + \sum_{n=0}^{\infty} \Big[(\Omega n + \Delta/2) d_{e,\,n}^\dagger d_{e,\,n} + (\Omega n - \Delta/2) d_{g,\,n}^\dagger d_{g,\,n} + \Omega \sqrt{S\,(n+1)} \left(d_{e,\,n+1}^\dagger d_{e,\,n} - d_{g,\,n+1}^\dagger d_{g,\,n} + \text{h.c.} \right) + g \sum_k (a_k^\dagger d_{g,\,n}^\dagger d_{e,\,n} + a_k d_{e,\,n}^\dagger d_{g,\,n}) \Big]. \tag{5.8}$$

5.1.2 Green-Function Representation

It is useful at this point to briefly introduce the Green functions in terms of which we will express our problem from now on. For the cavity modes a_k, $a_k^\dagger$, the molecular ground-state operators $d_{g,\,m}$, $d_{g,\,m}^\dagger$, and the molecular excited-state operators $d_{e,\,m}$, $d_{e,\,m}^\dagger$, the corresponding Green functions are defined by

$$D_{kl}^<(t,t') = -\mathrm{i}\langle a_l^\dagger(t') a_k(t)\rangle, \tag{5.9a}$$
$$D_{kl}^>(t,t') = -\mathrm{i}\langle a_k(t) a_l^\dagger(t')\rangle, \tag{5.9b}$$
$$G_{mn}^<(t,t') = -\mathrm{i}\langle d_{g,\,n}^\dagger(t') d_{g,\,m}(t)\rangle, \tag{5.9c}$$
$$G_{mn}^>(t,t') = -\mathrm{i}\langle d_{g,\,m}(t) d_{g,\,n}^\dagger(t')\rangle, \tag{5.9d}$$
$$E_{mn}^<(t,t') = -\mathrm{i}\langle d_{e,\,n}^\dagger(t') d_{e,\,m}(t)\rangle, \tag{5.9e}$$
$$E_{mn}^>(t,t') = -\mathrm{i}\langle d_{e,\,m}(t) d_{e,\,n}^\dagger(t')\rangle. \tag{5.9f}$$

Frequently, we will use a compact matrix notation where $[\boldsymbol{G}^{\lessgtr}(t,t')]_{mn} = G_{mn}^{\lessgtr}(t,t')$. As we have seen in the previous subsection, the pseudo-particle greater and lesser functions ($G^{\lessgtr}$ and $E^{\lessgtr}$) scale differently with the auxiliary fugacity ζ. Since this fact is crucial for enforcing the operator constraint in non-equilibrium, we will not use other representations such as statistical and spectral functions [76].

5.1.3 Conserving Approximation

Diagrammatically, we again follow the 2PIEA construction detailed in Sec. 2.1. The vertex in Eq. (5.8) does not contribute to first order in g since we do not assume symmetry breaking for the

photon field. To second order in g, the effective action acquires vertex diagrams

$$W^{(2)} \sim g^2$$  , (5.10)

where the wiggly line denotes the photon, the dashed line the excited-state, and the solid line the ground-state propagator, respectively. Note that the 2PIEA construction is equivalent to a Φ-derivable approach [79]. This means that our diagrammatic approximation is *conserving*, which is a necessary requirement for enforcing the operator constraint faithfully.

The self-energies are obtained from the vertex diagrams in Eq. 5.1.3 by differentiation with respect to the propagators. In terms of the contour-time-ordered Green functions, the self-energies then become

$$\Sigma_D(t,t') = \mathrm{i}g^2 \,\mathrm{Tr}\left[\boldsymbol{E}(t,t')\boldsymbol{G}(t',t)\right], \tag{5.11a}$$
$$\boldsymbol{\Sigma}_G(t,t') = \mathrm{i}g^2 \boldsymbol{E}(t,t') \,\mathrm{Tr}\left[\boldsymbol{D}(t',t)\right], \tag{5.11b}$$
$$\boldsymbol{\Sigma}_E(t,t') = \mathrm{i}g^2 \boldsymbol{G}(t,t') \,\mathrm{Tr}\left[\boldsymbol{D}(t,t')\right], \tag{5.11c}$$

such that in Schwinger-Keldysh representation, they read

$$\Sigma_D^<(t,t') = \mathrm{i}g^2 \,\mathrm{Tr}\left[\boldsymbol{E}^<(t,t')\boldsymbol{G}^>(t',t)\right], \tag{5.12a}$$
$$\Sigma_D^>(t,t') = \mathrm{i}g^2 \,\mathrm{Tr}\left[\boldsymbol{E}^>(t,t')\boldsymbol{G}^<(t',t)\right], \tag{5.12b}$$
$$\boldsymbol{\Sigma}_G^<(t,t') = \mathrm{i}g^2 \boldsymbol{E}^<(t,t') \,\mathrm{Tr}\left[\boldsymbol{D}^>(t',t)\right], \tag{5.12c}$$
$$\boldsymbol{\Sigma}_G^>(t,t') = \mathrm{i}g^2 \boldsymbol{E}^>(t,t') \,\mathrm{Tr}\left[\boldsymbol{D}^<(t',t)\right], \tag{5.12d}$$
$$\boldsymbol{\Sigma}_E^<(t,t') = \mathrm{i}g^2 \boldsymbol{G}^<(t,t') \,\mathrm{Tr}\left[\boldsymbol{D}^<(t,t')\right], \tag{5.12e}$$
$$\boldsymbol{\Sigma}_E^>(t,t') = \mathrm{i}g^2 \boldsymbol{G}^>(t,t') \,\mathrm{Tr}\left[\boldsymbol{D}^>(t,t')\right]. \tag{5.12f}$$

5.1.4 Equilibrium Projection

Within the equilibrium formalism of quantum field theory, a nice presentation of the projection technique has been given by Coleman [26]. Let us denote the auxiliary chemical potential by μ and introduce the corresponding fugacity $\zeta = \mathrm{e}^{-\beta\mu}$. The canonical partition function on a Hilbert space $\mathcal{H}_Q$ with an arbitrary but fixed value of the operator constraint will be written as $\mathrm{Tr}_{\mathcal{H}_Q}[\hat{\rho}_0] = Z_{\mathcal{C}}(Q)$. Then a grand-canonical partition function can be defined by

$$Z_{\mathcal{G}}(\zeta) = \mathrm{Tr}\left[\zeta^{\hat{Q}}\,\hat{\rho}_0\right] = \sum_{Q=0}^{\infty} \zeta^Q \,\mathrm{Tr}_{\mathcal{H}_Q}[\hat{\rho}_0] = Z_{\mathcal{C}}(0) + \zeta Z_{\mathcal{C}}(1) + \mathcal{O}(\zeta^2). \tag{5.13}$$

The decisive factor $\zeta^{\hat{Q}}$ weighs each canonical partition function contributing to $Z_{\mathcal{G}}(\zeta)$ according to its operator-constraint value. Apart from the contribution of the unphysical ground state $\hat{Q} = 0$, the

physically correct $Z_{\mathcal{C}}(1)$ could be obtained from Eq. (5.13) by multiplication with $1/\zeta$, followed by taking either of the equivalent limits $\mu \to \infty$ or $\zeta \to 0$. The operator average associated with $Z_{\mathcal{G}}(\zeta)$ is

$$\langle \hat{X} \rangle_\zeta = Z_{\mathcal{G}}^{-1}(\zeta) \operatorname{Tr}\left[\hat{X}\, \zeta^{\hat{Q}}\, \hat{\rho}_0\right] = Z_{\mathcal{G}}^{-1}(\zeta) \sum_{Q=0}^{\infty} \zeta^Q \operatorname{Tr}_{\mathcal{H}_Q}\left[\hat{X}\, \hat{\rho}_0\right]. \tag{5.14}$$

When $\hat{X}$ annihilates the ground state $\hat{Q} = 0$, its unphysical contribution is removed, and we find the correct average in the physical subspace $\mathcal{H}_1$ as

$$\begin{aligned} \langle \hat{X} \rangle_{\mathcal{H}_1} &= \frac{\operatorname{Tr}_{\mathcal{H}_1}\left[\hat{X}\, \hat{\rho}_0\right]}{Z_{\mathcal{C}}(1)} = \lim_{\zeta \to 0} \frac{\langle \hat{X} \rangle_\zeta}{\langle \hat{Q} \rangle_\zeta} \\ &= \lim_{\zeta \to 0} \frac{Z_{\mathcal{G}}^{-1}(\zeta) \left(\zeta \operatorname{Tr}_{\mathcal{H}_1}\left[\hat{X}\, \hat{\rho}_0\right] + \mathcal{O}(\zeta^2)\right)}{Z_{\mathcal{G}}^{-1}(\zeta) \left(\zeta \operatorname{Tr}_{\mathcal{H}_1}\left[\hat{Q}\, \hat{\rho}_0\right] + \mathcal{O}(\zeta^2)\right)}. \end{aligned} \tag{5.15}$$

For later purposes, it is instructive to look at two special operator averages. First, consider

$$\begin{aligned} \langle d_{g,n} d_{g,n}^\dagger \rangle_\zeta &= Z_{\mathcal{G}}^{-1}(\zeta) \left(\operatorname{Tr}_{\mathcal{H}_0}\left[d_{g,n} d_{g,n}^\dagger\, \hat{\rho}_0\right] + \zeta \operatorname{Tr}_{\mathcal{H}_1}\left[d_{g,n} d_{g,n}^\dagger\, \hat{\rho}_0\right] + \mathcal{O}(\zeta^2)\right) \\ &= Z_{\mathcal{G}}^{-1}(\zeta) \left(\operatorname{Tr}_{\mathcal{H}_0}\left[\hat{\rho}_0\right] + \zeta \operatorname{Tr}_{\mathcal{H}_1}\left[d_{g,n} d_{g,n}^\dagger\, \hat{\rho}_0\right] + \mathcal{O}(\zeta^2)\right) \underset{\zeta \to 0}{=} \mathcal{O}(1), \end{aligned} \tag{5.16}$$

which does not annihilate the ground state. Accordingly, the result is not of order ζ but rather $\mathcal{O}(1)$. Reversing the order of the two operators, we find

$$\begin{aligned} \langle d_{g,n}^\dagger d_{g,n} \rangle_\zeta &= Z_{\mathcal{G}}^{-1}(\zeta) \left(\operatorname{Tr}_{\mathcal{H}_0}\left[d_{g,n}^\dagger d_{g,n}\, \hat{\rho}_0\right] + \zeta \operatorname{Tr}_{\mathcal{H}_1}\left[d_{g,n}^\dagger d_{g,n}\, \hat{\rho}_0\right] + \mathcal{O}(\zeta^2)\right) \\ &= Z_{\mathcal{G}}^{-1}(\zeta) \left(\zeta \operatorname{Tr}_{\mathcal{H}_1}\left[d_{g,n}^\dagger d_{g,n}\, \hat{\rho}_0\right] + \mathcal{O}(\zeta^2)\right) \underset{\zeta \to 0}{=} \mathcal{O}(\zeta) \end{aligned} \tag{5.17}$$

as expected. The same holds for the excited-state operators. These results will be of great importance for the projection technique in *non-equilibrium*, which is the subject of the next section.

5.2 Non-Equilibrium Projection

The following exposition of the pseudo-particle projection in non-equilibrium field theory relies on a derivation of the Schwinger-Keldysh path integral that has been adapted from [11, 56, 78]. These references all have variants of essentially the same standard approach to the problem, which is to expand the density matrix along a discretized closed-time path by means of inserting coherent states at every point. By using this approach on the projection, we give a novel derivation that does not rely on the explicit inclusion of a vertical branch on the Schwinger-Keldysh contour [32], but instead works for an arbitrary Gaussian initial density matrix.

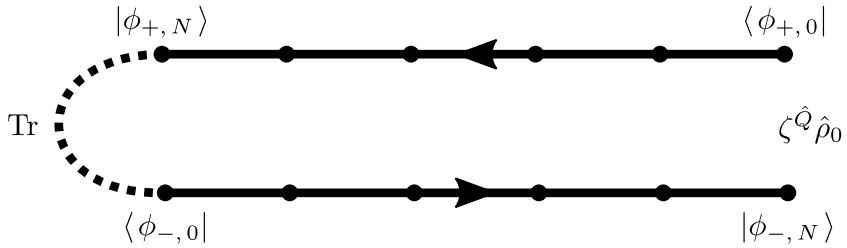

Figure 5.2: Schwinger-Keldysh contour for the expansion of the density matrix.

A sketch of the discretized contour can be seen in Fig. 5.2. The only difference to Sec. 2.1 is that we have replaced the initial density matrix according to

$$\hat{\rho}_0 \leftarrow \zeta^{\hat{Q}}\,\hat{\rho}_0. \tag{5.18}$$

The idea is to project the initial state of the non-equilibrium problem in a way analogous to the equilibrium one. The dynamics of the density matrix is governed by the von Neumann equation

$$\partial_t \hat{\rho} = \mathcal{L}\hat{\rho} = -\mathrm{i}[H, \hat{\rho}]. \tag{5.19}$$

Since we are going to work perturbatively later on, it is sufficient to derive only the free path integral and hence to assume that H is quadratic. Furthermore, without loss of generality, we will give the derivation for a single two-level system without vibrational substructure ($n = 0$), and we will focus on the ground state only. For the reason that ground and excited state are only coupled indirectly via the constraint, the resulting inverse Green function appearing in the derivation of the free path integral will be block diagonal, such that ground and excited state can be considered separately. As will become obvious, the excited state may be included in the derivation without any difficulty.

5.2.1 Scaling of Bare Green Functions

Our aim in this section is to derive the proper ζ scaling of the greater and lesser Green functions that we have anticipated in equilibrium. The initial density matrix can be assumed to be of the form

$$\hat{\rho}_0 = \kappa^{d^\dagger d} \tag{5.20}$$

for some real parameter $\kappa < 1$ [56]. We have dropped the subscripts of the ground-state operators $d_{g,0}$, $d^\dagger_{g,0}$. Since we also keep the presence of the corresponding excited state implicit, during the following derivation $\zeta^{\hat{Q}}$ will be replaced by $\zeta^{d^\dagger d}$. As mentioned, we then "trotterize" the time

evolution induced by the von Neumann equation and insert coherent-state identities

$$\hat{\rho}_n = \int \frac{\mathrm{d}\phi^*_{+,n}\mathrm{d}\phi_{+,n}}{\pi}\frac{\mathrm{d}\phi^*_{-,n}\mathrm{d}\phi_{-,n}}{\pi} e^{-\phi^*_{+,n}\phi_{+,n}} e^{-\phi^*_{-,n}\phi_{-,n}} \left|\phi_{+,n}\right\rangle\!\left\langle\phi_{+,n}\right| \hat{\rho}_n \left|\phi_{-,N-n}\right\rangle\!\left\langle\phi_{-,N-n}\right| \tag{5.21}$$

at every point along the contour. Doing so will result in the Schwinger-Keldysh partition function

$$Z = \int \left(\prod_{k=0}^{N} \frac{\mathrm{d}\phi^*_{+,k}\mathrm{d}\phi_{+,k}}{\pi}\frac{\mathrm{d}\phi^*_{-,k}\mathrm{d}\phi_{-,k}}{\pi}\right) \exp\left\{\mathrm{i}\boldsymbol{\phi}^\dagger \boldsymbol{G}_0^{-1}\boldsymbol{\phi}\right\}, \tag{5.22}$$

with a bare inverse Green function given by

$$\boldsymbol{G}_0^{-1} = -\mathrm{i}\begin{pmatrix} -1 & 0 & \cdots & & & \cdots & 0 & \zeta\cdot\kappa \\ h_+ & -1 & & & & & & 0 \\ & \ddots & \ddots & & & & & \vdots \\ & & h_+ & -1 & & & & \\ & & & 1 & -1 & & & \\ & & & & h_- & \ddots & & \vdots \\ & & & & & \ddots & -1 & 0 \\ & & & & & & h_- & -1 \end{pmatrix}, \tag{5.23}$$

where $h_\pm = 1 \mp \mathrm{i}\delta t\omega_0$ for a single ground state with $\omega_0 = -\Delta/2$. We have also used the operator identity

$$\zeta^{d^\dagger d}\kappa^{d^\dagger d} = \exp\left(d^\dagger d \ln\zeta\right)\exp\left(d^\dagger d\ln\kappa\right) = \exp\left(d^\dagger d\ln\zeta\kappa\right) = (\zeta\kappa)^{d^\dagger d}. \tag{5.24}$$

The determinant of the inverse Green function is

$$\det\left(-\mathrm{i}\boldsymbol{G}_0^{-1}\right) = 1 - \zeta\kappa(h_+h_-)^N \underset{N\to\infty}{\longrightarrow} 1-\zeta\kappa. \tag{5.25}$$

In the continuum limit, $\delta t \to 0,\ N\to\infty$ such that $\delta t N = t$, this yields bare Green functions of the form

$$G_0^T(t,t') = -\mathrm{i}\mathrm{e}^{-\mathrm{i}\omega_0(t-t')}\left(\theta(t-t') + \frac{\zeta\kappa}{1-\zeta\kappa}\right), \tag{5.26a}$$

$$G_0^{\tilde{T}}(t,t') = -\mathrm{i}\mathrm{e}^{-\mathrm{i}\omega_0(t-t')}\left(\theta(t'-t) + \frac{\zeta\kappa}{1-\zeta\kappa}\right), \tag{5.26b}$$

$$G_0^<(t,t') = -\mathrm{i}\mathrm{e}^{-\mathrm{i}\omega_0(t-t')}\frac{\zeta\kappa}{1-\zeta\kappa}, \tag{5.26c}$$

$$G_0^>(t,t') = -\mathrm{i}\mathrm{e}^{-\mathrm{i}\omega_0(t-t')}\left(\frac{\zeta\kappa}{1-\zeta\kappa}+1\right). \tag{5.26d}$$

For $t = t' = 0$, the lesser function should be $\mathrm{i}G_0^<(0,0) = \zeta n_{g,0}$, where the initial occupation $n_{g,0}$ must be such that the constraint is fulfilled, which would be $\hat{Q} \equiv n_{g,0} + n_{e,0} = 1$ for a single set of ground and excited states. Hence, we have $n_{g,0} = \kappa / (1 - \zeta\kappa)$, which means

$$\kappa = \frac{n_{g,0}}{1 + \zeta n_{g,0}} \underset{\zeta \to 0}{\longrightarrow} n_{g,0}. \tag{5.27}$$

Therefore, we find

$$G_0^T(t,t') \underset{\zeta \to 0}{\longrightarrow} -\mathrm{i}\mathrm{e}^{\mathrm{i}\omega_0(t-t')}\theta(t-t'), \tag{5.28a}$$

$$G_0^{\tilde{T}}(t,t') \underset{\zeta \to 0}{\longrightarrow} -\mathrm{i}\mathrm{e}^{\mathrm{i}\omega_0(t-t')}\theta(t'-t), \tag{5.28b}$$

$$\zeta^{-1} G_0^<(t,t') \underset{\zeta \to 0}{\longrightarrow} -\mathrm{i}\mathrm{e}^{\mathrm{i}\omega_0(t-t')} n_{g,0}, \tag{5.28c}$$

$$G_0^>(t,t') \underset{\zeta \to 0}{\longrightarrow} -\mathrm{i}\mathrm{e}^{\mathrm{i}\omega_0(t-t')}. \tag{5.28d}$$

Note how both the time-ordered and the anti-time-ordered Green function merely involve the greater Green function. This is a direct result of the limit $\zeta \to 0$. A similar thing happens for the spectral function. Usually, it is given by

$$\rho_0(t,t') = G_0^<(t,t') - G_0^>(t,t'), \tag{5.29}$$

which is not to be confused with the initial density matrix $\hat{\rho}_0$. But since the lesser Green function scales with ζ, we have

$$\rho_0(t,t') \underset{\zeta \to 0}{\longrightarrow} -G_0^>(t,t'). \tag{5.30}$$

While this might seem odd at first, it actually is a crucial feature of the projection technique. Exactly analogous expressions hold for the bare excited-state Green functions $E_0^{\lessgtr}$.

5.2.2 Scaling of Resummed Green Functions and Self-Energies

So far, we have investigated the bare Green functions occurring for non-interacting problems. As we have seen above, though, a self-consistent perturbative expansion in the small parameter g involves second-order self-energies coupling the pseudo-particles with each other and with the cavity modes. Hence, we have to ask whether the ζ scaling of the bare pseudo-particle Green functions will be modified by the self-consistent resummation of the diagrams? If we assume for a moment that the full Green functions possess the same scaling as the bare ones, the Dyson

equations resulting from the 2PIEA construction will read

$$\begin{aligned}(\mathrm{i}\partial_t - \boldsymbol{h}_G)\,\zeta\boldsymbol{G}^<(t,t') &= \int_{t_0}^{t}\mathrm{d}\bar{t}\;\left[\boldsymbol{\Sigma}_G^>(t,\bar{t}) - \zeta\boldsymbol{\Sigma}_G^<(t,\bar{t})\right]\zeta\boldsymbol{G}^<(\bar{t},t') \\ &\quad - \int_{t_0}^{t'}\mathrm{d}\bar{t}\,\zeta\boldsymbol{\Sigma}_G^<(t,\bar{t})\left[\boldsymbol{G}^>(\bar{t},t') - \zeta\boldsymbol{G}^<(\bar{t},t')\right],\end{aligned} \tag{5.31a}$$

$$\begin{aligned}(\mathrm{i}\partial_t - \boldsymbol{h}_G)\,\boldsymbol{G}^>(t,t') &= \int_{t_0}^{t}\mathrm{d}\bar{t}\;\left[\boldsymbol{\Sigma}_G^>(t,\bar{t}) - \zeta\boldsymbol{\Sigma}_G^<(t,\bar{t})\right]\boldsymbol{G}^>(\bar{t},t') \\ &\quad - \int_{t_0}^{t'}\mathrm{d}\bar{t}\,\boldsymbol{\Sigma}_G^>(t,\bar{t})\left[\boldsymbol{G}^>(\bar{t},t') - \zeta\boldsymbol{G}^<(\bar{t},t')\right],\end{aligned} \tag{5.31b}$$

$$\begin{aligned}(\mathrm{i}\partial_t - \boldsymbol{h}_E)\,\zeta\boldsymbol{E}^<(t,t') &= \int_{t_0}^{t}\mathrm{d}\bar{t}\;\left[\boldsymbol{\Sigma}_E^>(t,\bar{t}) - \zeta\boldsymbol{\Sigma}_E^<(t,\bar{t})\right]\zeta\boldsymbol{E}^<(\bar{t},t') \\ &\quad - \int_{t_0}^{t'}\mathrm{d}\bar{t}\,\zeta\boldsymbol{\Sigma}_E^<(t,\bar{t})\left[\boldsymbol{E}^>(\bar{t},t') - \zeta\boldsymbol{E}^<(\bar{t},t')\right],\end{aligned} \tag{5.31c}$$

$$\begin{aligned}(\mathrm{i}\partial_t - \boldsymbol{h}_E)\,\boldsymbol{E}^>(t,t') &= \int_{t_0}^{t}\mathrm{d}\bar{t}\;\left[\boldsymbol{\Sigma}_E^>(t,\bar{t}) - \zeta\boldsymbol{\Sigma}_E^<(t,\bar{t})\right]\boldsymbol{E}^>(\bar{t},t') \\ &\quad - \int_{t_0}^{t'}\mathrm{d}\bar{t}\,\boldsymbol{\Sigma}_E^>(t,\bar{t})\left[\boldsymbol{E}^>(\bar{t},t') - \zeta\boldsymbol{E}^<(\bar{t},t')\right],\end{aligned} \tag{5.31d}$$

where we have made the ζ scaling explicit and abbreviated the quadratic parts of the dynamics through the matrices $\boldsymbol{h}_{G,\,E}$, respectively. These Dyson equations are integro-differential equations with a *causal* structure: the evolution of the functions depends only on points in the past. This means they can be solved by *explicit* time-stepping, starting with known initial values at time t_0. Looking at the factors of ζ on the right-hand side of the equations, this tells us immediately that any initial scaling in ζ will be conserved by the equations. If in the limit $\zeta \to 0$ there holds $\boldsymbol{G}^<(0,0) = \mathcal{O}(\zeta)$, then $\boldsymbol{G}^<(t,t') = \mathcal{O}(\zeta)$ must hold for all times t, t' because there are no terms $\mathcal{O}(1)$ present on the right-hand side of the respective equation. By close inspection, one may tell that the same is true for the remaining equations. As we have ensured the initial scalings via the projection, we may conclude that even for a self-consistent solution of Eqs. (5.31), the ζ scaling of the bare Green functions will be reproduced in the full Green functions, provided we start with a properly scaled initial condition and employ a conserving approximation. Summarizing, this gives the scalings

$$\boldsymbol{G}^<(t,t') \underset{\zeta\to 0}{=} \mathcal{O}(\zeta), \tag{5.32a}$$

$$\boldsymbol{G}^>(t,t') \underset{\zeta\to 0}{=} \mathcal{O}(1), \tag{5.32b}$$

$$\boldsymbol{E}^<(t,t') \underset{\zeta\to 0}{=} \mathcal{O}(\zeta), \tag{5.32c}$$

$$\boldsymbol{E}^>(t,t') \underset{\zeta\to 0}{=} \mathcal{O}(1). \tag{5.32d}$$

for the full Green functions, and

$$\Sigma_D^<(t,t') \underset{\zeta\to 0}{=} \mathcal{O}(\zeta), \tag{5.33a}$$

$$\Sigma_D^>(t,t') \underset{\zeta\to 0}{=} \mathcal{O}(\zeta), \tag{5.33b}$$

$$\boldsymbol{\Sigma}_G^<(t,t') \underset{\zeta\to 0}{=} \mathcal{O}(\zeta), \tag{5.33c}$$

$$\boldsymbol{\Sigma}_G^>(t,t') \underset{\zeta\to 0}{=} \mathcal{O}(1), \tag{5.33d}$$

$$\boldsymbol{\Sigma}_E^<(t,t') \underset{\zeta\to 0}{=} \mathcal{O}(\zeta), \tag{5.33e}$$

$$\boldsymbol{\Sigma}_E^>(t,t') \underset{\zeta\to 0}{=} \mathcal{O}(1). \tag{5.33f}$$

for the resummed self-energies. Observe how both photon self-energies are $\mathcal{O}(\zeta)$. This will have important consequences in the following.

5.2.3 Projected Dyson Equations

With the scalings of the full Green functions and self-energies established, we may actually perform the projection of Eqs. (5.31) onto the physical subspace. For the lesser Green functions, this means to multiply by $1/\zeta$ and then to take the limit $\zeta \to 0$. For the greater Green functions, the former step is not necessary. This leads us to

$$(\mathrm{i}\partial_t - \boldsymbol{h}_G)\,\boldsymbol{G}^<(t,t') = \int_{t_0}^{t} \mathrm{d}\bar{t}\; \boldsymbol{\Sigma}_G^>(t,\bar{t})\boldsymbol{G}^<(\bar{t},t') - \int_{t_0}^{t'} \mathrm{d}\bar{t}\; \boldsymbol{\Sigma}_G^<(t,\bar{t})\boldsymbol{G}^>(\bar{t},t'), \tag{5.34a}$$

$$(\mathrm{i}\partial_t - \boldsymbol{h}_G)\,\boldsymbol{G}^>(t,t') = \int_{t'}^{t} \mathrm{d}\bar{t}\; \boldsymbol{\Sigma}_G^>(t,\bar{t})\boldsymbol{G}^>(\bar{t},t'), \tag{5.34b}$$

$$(\mathrm{i}\partial_t - \boldsymbol{h}_E)\,\boldsymbol{E}^<(t,t') = \int_{t_0}^{t} \mathrm{d}\bar{t}\; \boldsymbol{\Sigma}_E^>(t,\bar{t})\boldsymbol{E}^<(\bar{t},t') - \int_{t_0}^{t'} \mathrm{d}\bar{t}\; \boldsymbol{\Sigma}_E^<(t,\bar{t})\boldsymbol{E}^>(\bar{t},t'), \tag{5.34c}$$

$$(\mathrm{i}\partial_t - \boldsymbol{h}_E)\,\boldsymbol{E}^>(t,t') = \int_{t'}^{t} \mathrm{d}\bar{t}\; \boldsymbol{\Sigma}_E^>(t,\bar{t})\boldsymbol{E}^>(\bar{t},t'). \tag{5.34d}$$

There are several things to notice about these equations. The type of the self-energies ($>$ or $<$) is always determined by the constituent pseudo-particle Green function. Hence, in the equations for the lesser functions, the right-hand sides always involve a product of greater and lesser pseudo-particle Green functions, whereas for the greater functions only the product of two greater pseudo-particle Green functions survives. This indeed gives a general rule of thumb for doing the projection: drop all terms that do not involve the correct number of greater and lesser signs from the equations. It should be emphasized here that this procedure is *independent* of the specific diagrammatics: instead of the two-loop[1] expansion employed here, we could pick any other set of diagrams and still perform the projection according to the rule just outlined.

[1] Two-loop from the perspective of the 2PI effective action or Φ-functional.

We have not discussed the photon Dyson equation yet. The photons are not pseudo-particles, yet their greater and lesser self-energies still scale with the fugacity. Making the scaling explicit, the Dyson equations would read

$$\begin{aligned}(\mathrm{i}\partial_t - \boldsymbol{h}_D)\,\boldsymbol{D}^{\lessgtr}(t,t') = &\int_{t_0}^{t} \mathrm{d}\bar{t}\ \left[\zeta\Sigma_D^{>}(t,\bar{t}) - \zeta\Sigma_D^{<}(t,\bar{t})\right]\boldsymbol{D}^{\lessgtr}(\bar{t},t') \\ &- \int_{t_0}^{t'} \mathrm{d}\bar{t}\,\zeta\Sigma_D^{\lessgtr}(t,\bar{t})\left[\boldsymbol{D}^{>}(\bar{t},t') - \boldsymbol{D}^{<}(\bar{t},t')\right].\end{aligned} \tag{5.35}$$

How is this apparent conflict to be reconciled? It should be clear that the fugacity scaling of the pseudo-particle Green functions can only work out if the photon Green functions appearing in the self-energies $\boldsymbol{\Sigma}_{G,\,E}^{\lessgtr}$ are $\mathcal{O}(1)$. From this we learn that within these self-energies, the full photon Green functions $\boldsymbol{D}^{\lessgtr}$ have to be replaced by the bare ones:

$$\boldsymbol{D}^{\lessgtr}(t,t') \longleftarrow \boldsymbol{D}_0^{\lessgtr}(t,t'). \tag{5.36}$$

Any alteration of the photons due to the pseudo-particles necessarily would be $\mathcal{O}(\zeta)$, such that its influence in turn certainly drops out of the pseudo-particle self-energies. Therefore, these become

$$\begin{aligned}\boldsymbol{\Sigma}_G^{<}(t,t') &= \mathrm{i}g^2\boldsymbol{E}^{<}(t,t')\,\mathrm{Tr}\left[\boldsymbol{D}_0^{>}(t',t)\right], \\ \boldsymbol{\Sigma}_G^{>}(t,t') &= \mathrm{i}g^2\boldsymbol{E}^{>}(t,t')\,\mathrm{Tr}\left[\boldsymbol{D}_0^{<}(t',t)\right], \\ \boldsymbol{\Sigma}_E^{<}(t,t') &= \mathrm{i}g^2\boldsymbol{G}^{<}(t,t')\,\mathrm{Tr}\left[\boldsymbol{D}_0^{<}(t,t')\right], \\ \boldsymbol{\Sigma}_E^{>}(t,t') &= \mathrm{i}g^2\boldsymbol{G}^{>}(t,t')\,\mathrm{Tr}\left[\boldsymbol{D}_0^{>}(t,t')\right].\end{aligned}$$

How to calculate the effect of the pseudo-particles on the photons will be the next subject.

5.2.4 Full Photon Green Function

To obtain physical results, any quantity involving pseudo-particles must be projected to the physical subspace. As it turns out, this rule can be most easily adhered to when the photon Green functions are not resummed via the Dyson equations involving the self-energies, but rather by means of the T-matrix. Diagrammatically, the general Dyson equation

$$\boldsymbol{D}(t,t') = \boldsymbol{D}_0(t,t') + \int_{\mathcal{C}}\mathrm{d}\bar{t}\ \int_{\mathcal{C}}\mathrm{d}\bar{s}\ \boldsymbol{D}_0(t,\bar{t})\Sigma_D(\bar{t},\bar{s})\boldsymbol{D}(\bar{s},t') \tag{5.37}$$

can be depicted as

(5.38)

where the bare (full) photon Green function is given by the single (double) line and the self-energy by the hatched circle. In terms of the T-matrix, full photon Green function becomes

$$\boldsymbol{D}(t,t') = \boldsymbol{D}_0(t,t') + \int_{\mathcal{C}} \mathrm{d}\bar{t} \int_{\mathcal{C}} \mathrm{d}\bar{s}\, \boldsymbol{D}_0(t,\bar{t}) T_D(\bar{t},\bar{s}) \boldsymbol{D}_0(\bar{s},t') \tag{5.39}$$

which diagrammatically looks like

(5.40)

where the cross-hatched circle is the T-matrix. Notice how the Green function attached to it from the right is now the bare instead of the full one. In contrast to the self-energy given in subsection 5.1.3, the T-matrix is composed of a sum over strings of pseudo-particle bubbles resulting in

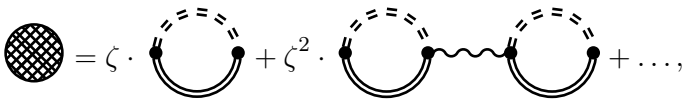

(5.41)

where the double dashed (solid) lines denote the full excited-state (ground-state) propagator. Each term in the T-matrix has a factor of ζ to the power of the number of bubbles. As before, to project it we have to multiply by $1/\zeta$ and then take ζ to zero. This means that in the *projected* T-matrix only the single bubble will survive. Expanding the contour $\mathcal{C}$ as before,

$$\int_{\mathcal{C}} \mathrm{d}\bar{s} = \int_{t_0}^{\min(\bar{t},t')} \mathrm{d}\bar{s} + \int_{\min(\bar{t},t')}^{\max(\bar{t},t')} \mathrm{d}\bar{s} + \int_{\max(\bar{t},t')}^{t_0} \mathrm{d}\bar{s}\,, \tag{5.42}$$

one thus obtains explicit expressions in terms of known quantities. For the resummed lesser function, we have

$$\begin{aligned}
\boldsymbol{D}^< - \boldsymbol{D}_0^< = &\int_{t_0}^{t} \mathrm{d}\bar{t} \left\{ \int_{t_0}^{\bar{t}} \mathrm{d}\bar{s}\, \boldsymbol{D}_0^> T_D^> \boldsymbol{D}_0^< + \int_{\bar{t}}^{t'} \mathrm{d}\bar{s}\, \boldsymbol{D}_0^> T_D^< \boldsymbol{D}_0^< + \int_{t'}^{t_0} \mathrm{d}\bar{s}\, \boldsymbol{D}_0^> T_D^< \boldsymbol{D}_0^> \right\} \\
&+ \int_{t}^{t'} \mathrm{d}\bar{t} \left\{ \int_{t_0}^{\bar{t}} \mathrm{d}\bar{s}\, \boldsymbol{D}_0^< T_D^> \boldsymbol{D}_0^< + \int_{\bar{t}}^{t'} \mathrm{d}\bar{s}\, \boldsymbol{D}_0^< T_D^< \boldsymbol{D}_0^< + \int_{t'}^{t_0} \mathrm{d}\bar{s}\, \boldsymbol{D}_0^< T_D^< \boldsymbol{D}_0^> \right\} \\
&+ \int_{t'}^{t_0} \mathrm{d}\bar{t} \left\{ \int_{t_0}^{t'} \mathrm{d}\bar{s}\, \boldsymbol{D}_0^< T_D^> \boldsymbol{D}_0^< + \int_{t'}^{\bar{t}} \mathrm{d}\bar{s}\, \boldsymbol{D}_0^< T_D^> \boldsymbol{D}_0^> + \int_{\bar{t}}^{t_0} \mathrm{d}\bar{s}\, \boldsymbol{D}_0^< T_D^< \boldsymbol{D}_0^> \right\},
\end{aligned} \tag{5.43}$$

whereas for the resummed greater function we find

$$\begin{aligned}\boldsymbol{D}^{>}-\boldsymbol{D}_0^{>}=&\int_{t_0}^{t'}\mathrm{d}\bar{t}\left\{\int_{t_0}^{\bar{t}}\mathrm{d}\bar{s}\;\boldsymbol{D}_0^{>}T_D^{>}\boldsymbol{D}_0^{<}+\int_{\bar{t}}^{t'}\mathrm{d}\bar{s}\;\boldsymbol{D}_0^{>}T_D^{<}\boldsymbol{D}_0^{<}+\int_{t'}^{t_0}\mathrm{d}\bar{s}\;\boldsymbol{D}_0^{>}T_D^{<}\boldsymbol{D}_0^{>}\right\}\\&+\int_{t'}^{t}\mathrm{d}\bar{t}\left\{\int_{t_0}^{t'}\mathrm{d}\bar{s}\;\boldsymbol{D}_0^{>}T_D^{>}\boldsymbol{D}_0^{<}+\int_{t'}^{\bar{t}}\mathrm{d}\bar{s}\;\boldsymbol{D}_0^{>}T_D^{>}\boldsymbol{D}_0^{>}+\int_{\bar{t}}^{t_0}\mathrm{d}\bar{s}\;\boldsymbol{D}_0^{>}T_D^{<}\boldsymbol{D}_0^{>}\right\}\\&+\int_{t}^{t_0}\mathrm{d}\bar{t}\left\{\int_{t_0}^{t'}\mathrm{d}\bar{s}\;\boldsymbol{D}_0^{<}T_D^{>}\boldsymbol{D}_0^{<}+\int_{t'}^{\bar{t}}\mathrm{d}\bar{s}\;\boldsymbol{D}_0^{<}T_D^{>}\boldsymbol{D}_0^{>}+\int_{\bar{t}}^{t_0}\mathrm{d}\bar{s}\;\boldsymbol{D}_0^{<}T_D^{<}\boldsymbol{D}_0^{>}\right\}.\end{aligned}\tag{5.44}$$

Alternatively, it is possible to calculate the resummed functions in differential form. Eq. (5.39) can by multiplying with the inverse bare Green function be cast to

$$\int_{\mathcal{C}}\mathrm{d}\bar{t}\;\boldsymbol{D}_0^{-1}(t,\bar{t})\boldsymbol{D}(\bar{t},t')=\delta_{\mathcal{C}}(t-t')+\int_{\mathcal{C}}\mathrm{d}\bar{t}\;\int_{\mathcal{C}}\mathrm{d}\bar{s}\;\delta_{\mathcal{C}}(t-\bar{t})T_D(\bar{t},\bar{s})\boldsymbol{D}_0(\bar{s},t'),\tag{5.45}$$

which with $\boldsymbol{D}_0^{-1}(t,t')=\delta_{\mathcal{C}}(t-t')\boldsymbol{D}_0^{-1}(t)$ is equivalent to

$$\boldsymbol{D}_0^{-1}(t)\boldsymbol{D}(t,t')=\delta_{\mathcal{C}}(t-t')+\int_{\mathcal{C}}\mathrm{d}\bar{t}\;T_D(t,\bar{t})\boldsymbol{D}_0(\bar{t},t').\tag{5.46}$$

From here, one may find equations for the greater and lesser functions that formally look similar to standard Dyson equations, yet with the difference that on the right-hand sides, the T-matrices appear instead of the self-energies and $\boldsymbol{D}$ is replaced by $\boldsymbol{D}_0$.

5.2.5 Many Incoherent Molecules

Our considerations so far were limited to the case of a single molecule, $M=1$. In the real experiments, a very large number of molecules is dissolved inside the cavity, with M being on the order of 10^6–10^9. For simplicity, let us for a second think about whether the case $M=2$ could be solved exactly with the present technique. What would the operator constraint look like in this case? There is only one way to ensure that both molecules have single occupation at all times: one has to enforce

$$\hat{Q}_1\hat{Q}_2=1,\tag{5.47}$$

where the subscript $m=1,2$ now indicates the molecule and each $\hat{Q}_m$ has the same form as above. To enforce the expectation value of this *quartic* operator constraint at initial time [33], one has to work *four-particle-irreducibly*, that is, employ the 4PI effective action [95, 99].[2] Clearly,

[2] While even more involved than the present construction, it would be technically very interesting to see whether this problem can still be solved exactly, which would result in a kind of "two-impurity unit cell" that could be used to improve DMFT simulations. As a matter of fact, using the 4PIEA to solve *any* fully time-dependent non-equilibrium system seems not to have been done so far.

for an exact projection of an arbitrary number of molecules M, one would have to work with the 2^MPI effective action, which is impossible. Because of the high temperature ($T \sim 300$ K) of the surrounding water, the molecules may, however, be assumed to be entirely uncorrelated. For this reason, it is justified to replace the product operator constraint $\prod_m \hat{Q}_m = 1$ by the set of constraints $\hat{Q}_m = 1$ for all $m = 1, ..., M$, in other words, to project each molecule separately. This essentially assumes $\langle \prod_m \hat{Q}_m \rangle = \prod_m \langle \hat{Q}_m \rangle$. Furthermore, we can assume $\hat{Q}_1 = ... = \hat{Q}_M$ and hence treat all molecules as though they were completely identical. For experimentally relevant purposes, these assumptions are well-justified. Introducing a set of fugacities ζ_m accordingly, for the T-matrix we then find the familiar-looking expression

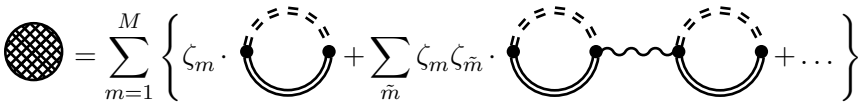

(5.48)

where the two bubbles in the second diagram now belong to *different* molecules (although we treat them identically). Each term appearing in this T-matrix has to be projected separately. Only those survive which have no ζ_m appearing to higher powers than linear. Attaching external legs and treating all bubbles as identical, this is equivalent to

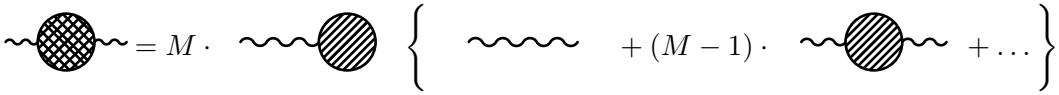

where we have drawn the hatched circles instead of the bubbles. As a series, this can also be written

$$T_M := \sum_{k=1}^{M} \frac{M!}{(M-k)!} \boldsymbol{D}_0 T_D \left(\boldsymbol{D}_0 T_D\right)^{k-1} \boldsymbol{D}_0. \tag{5.49}$$

When this sum converges fast (such that one may take the upper boundary of the sum to infinity and use $M!/\left(M-k\right)! \approx M^k$), it should be a very good approximation to resum the terms in the curly brackets to yield the full photon Green function, yet coupled to the molecules with an enhanced effective vertex strength $\sqrt{M}g$.

The criteria for fast convergence of the series have to be discussed at this point. It will generally not be true that a combination of very large molecule number M, small coupling g and large photon occupations will give rapidly declining contributions from longer chains of bubbles. The driven-dissipative processes that also enter into the dynamics do, however, have such an effect because they narrow the support of the Green functions in two-time space. For instance, the cavity loss alone should suffice to suppress very long bubble chains. Note that this is not in contradiction to the requirement of having many absorption-emission cycles before a photon leaves the cavity. The molecule number is so large that both criteria can be met.

Dropping $\boldsymbol{h}_D$ for brevity, the resulting Dyson-like equations are then

$$\begin{aligned} \mathrm{i}\partial_t \boldsymbol{D}^{\lessgtr}(t,t') = M \int_{t_0}^{t} \mathrm{d}\bar{t}\ \left[T_D^{>}(t,\bar{t}) - T_D^{<}(t,\bar{t})\right] \boldsymbol{D}^{\lessgtr}(\bar{t},t') \\ - M \int_{t_0}^{t'} \mathrm{d}\bar{t}\, T_D^{\lessgtr}(t,\bar{t}) \left[\boldsymbol{D}^{>}(\bar{t},t') - \boldsymbol{D}^{<}(\bar{t},t')\right]. \end{aligned} \tag{5.50}$$

In the "horizontal" time direction,[3]

$$\begin{aligned} \mathrm{i}\partial_{t'} \boldsymbol{D}^{\lessgtr}(t,t') = M \int_{t_0}^{t'} \mathrm{d}\bar{t}\ \left[T_D^{>}(\bar{t},t') - T_D^{<}(\bar{t},t')\right] \boldsymbol{D}^{\lessgtr}(t,\bar{t}) \\ - M \int_{t_0}^{t} \mathrm{d}\bar{t}\, T_D^{\lessgtr}(\bar{t},t') \left[\boldsymbol{D}^{>}(t,\bar{t}) - \boldsymbol{D}^{<}(t,\bar{t})\right], \end{aligned} \tag{5.51}$$

and in the equal-time limit, we find

$$\begin{aligned} \mathrm{i}\partial_T \boldsymbol{D}^{<}(t,t) &= M \int_{t_0}^{t} \mathrm{d}\bar{t}\ \left[T_D^{>}(t,\bar{t})\boldsymbol{D}^{<}(\bar{t},t) - T_D^{<}(t,\bar{t})\boldsymbol{D}^{>}(\bar{t},t)\right. \\ &\quad \left. + \boldsymbol{D}^{<}(t,\bar{t})T_D^{>}(\bar{t},t) - \boldsymbol{D}^{>}(t,\bar{t})T_D^{<}(\bar{t},t)\right] \\ &= \mathrm{i}\partial_T \boldsymbol{D}^{>}(t,t). \end{aligned} \tag{5.52}$$

This completes the technical discussion of the problem. The equations have to be solved together with the projected Dyson equations of the pseudo-particles. Before going over to experimentally realistic cases, in the following we will first discuss a couple of toy cases. This will serve the purpose of verifying the methods we have established on simple examples where either analytical solutions are known or numerical solutions can be obtained by other means than field theory.

[3] The T-matrix picks up a minus when taking the adjoint because of the factor of i in front of the bubble diagram.

$m,\, n$	0	1	2
0	I	II	III
1	II	I	II
2	III	II	I

Table 5.1: Vertex types I, II and III appearing in Eq. (5.53). Only the diagonal (type I) is included into the final description.

5.3 Auxiliary Bosons Applied to Open Systems

The phonon Lindblad operators of the master equation (5.2) have yet to be written in terms of pseudo-particles. It is worth emphasizing that, to the author's knowledge, this has not been discussed in the literature before. For *closed* systems, the Dyson equation can always be written down in terms of the contour-time-ordered Green function, which after evaluating the contour leads to equations involving only the greater and lesser Green functions. As we have seen in 2.1.3, this is no longer true for *open* systems: the structure of the Lindblad operators over the whole contour is such that in the Green-function equations of motion, the (anti-) time-ordered Green functions appear also. This requires a little extra care when applying the projection technique to open systems. For clarity, we go back to the single-molecule case $M = 1$. With the representation (5.4), the operator $\mathcal{L}[b]\rho$ becomes

$$\mathcal{L}[b]\rho = \sum_{m,n=0}^{\infty} \sum_{\sigma,\,\upsilon} \sqrt{m+1}\sqrt{n+1} \Big[2d^{\dagger}_{\sigma,\,m} d_{\sigma,\,m+1} \rho d^{\dagger}_{\upsilon,\,n+1} d_{\upsilon,\,n} - \Big\{ \rho, d^{\dagger}_{\upsilon,\,n+1} d_{\upsilon,\,n} d^{\dagger}_{\sigma,\,m} d_{\sigma,\,m+1} \Big\} \Big]. \tag{5.53}$$

As long as we do not explicitly introduce symmetry breaking for the photon modes, any coherence between ground and excited states can be discarded from the description, which is also a physically reasonable assumption. Hence, only terms with $\sigma = \upsilon$ survive in Eq. (5.53). Since these terms are quartic, we have to apply perturbation theory, which we do to the same order in $\hbar$ as for the Jaynes-Cummings coupling above. The resulting Hartree-Fock diagrammatics has a slightly complicated structure depending on the vibrational states involved in the vertices. There happen to be three different types (s. Tab. 5.1). The most straightforward one is defined by $m = n$ (the diagonal of Tab. 5.1) and reads

$$\mathcal{L}[d^{\dagger}_{\sigma,\,n} d_{\sigma,\,n+1}]\rho = 2d^{\dagger}_{n} d_{n+1} \rho d^{\dagger}_{n+1} d_{n} - \Big\{ \rho, d^{\dagger}_{n+1} d_{n} d^{\dagger}_{n} d_{n+1} \Big\}, \tag{5.54}$$

where we have dropped the index σ for brevity. The second vertex (type II) is given by $m = n + 1$. It only influences the coherence between different vibrational states and not their densities. This can be understood as follows. In the physical subspace, quartic terms involving three different vibrational states such as $\{\rho, d^{\dagger}_{n+1} d_{n} d^{\dagger}_{n+1} d_{n+2}\}$ always vanish identically. In an obvious bra-ket

notation, the only contribution comes from the jump term according to

$$\mathrm{Tr}\left\{|n\rangle\langle n+1| \cdot 2\,|n+1\rangle\langle n+2|\,\rho(t)\,|n+1\rangle\langle n|\right\} = 2\,\mathrm{Tr}\left\{|n+1\rangle\langle n+2|\,\rho(t)\right\}. \tag{5.55}$$

Thus we see that the coherence $|n\rangle\langle n+1|$ between states $|n\rangle$ and $|n+1\rangle$ is influenced by the coherence $|n+1\rangle\langle n+2|$. Since such coherences have little influence on the photon dynamics for large vibrational relaxation rates λ, we are going to ignore this type of vertex. The third and final vertex (type III) connects coherences between states which are two or more quanta apart, e.g. $|n\rangle\langle n+2|$ and $|n+1\rangle\langle n+3|$; these we are also going to ignore.

For the external pumping and electronic loss $\mathcal{L}[\sigma^{\pm}]\rho$, we make a similar simplification in that we only allow for transitions between vibrational states with the same number of quanta. These vertices are then also of type I. For the electronic loss in particular this may constitute an oversimplification; yet since this process is always weak in comparison to the external pumping, we will put $\Gamma_{\downarrow} = 0$ for most applications. A more physical implementation would be to have the vibrational state $n = 0$ of the excited-state manifold only decay to the uppermost vibrational state of the ground-state manifold, a process which would not, however, be related to $\mathcal{L}[\sigma^{-}]\rho$ in a straightforward way. As another remark, for the external pumping one may want to consider introducing a blue detuning by converting ground-state quanta n into excited-state quanta $n + \Delta n$. We will not pursue any such generalization in the following. With these considerations in mind, the final master equation for our system becomes

$$\begin{aligned}\partial_t \rho = -\mathrm{i}[H,\rho] + \frac{1}{2}\Bigg\{ \sum_k \kappa \mathcal{L}[a_k] + \sum_{n=0}^{\infty} \Big[\Gamma_{\uparrow} \mathcal{L}[d^{\dagger}_{e,\,n} d_{g,\,n}] + \Gamma_{\downarrow} \mathcal{L}[d^{\dagger}_{g,\,n} d_{e,\,n}] \\ + \sum_{\sigma} (n+1) \Big(\lambda \left(\bar{N}(\Omega) + 1 \right) \mathcal{L}[d^{\dagger}_{\sigma,\,n} d_{\sigma,\,n+1}] + \lambda \bar{N}(\Omega) \mathcal{L}[d^{\dagger}_{\sigma,\,n+1} d_{\sigma,\,n}] \Big) \Big] \Bigg\} \rho\end{aligned} \tag{5.56}$$

where H is defined in Eq. (5.8). As one may see, the auxiliary-boson Lindbladians all belong to vertex type I in the sense that they involve two *different* auxiliary-boson operators.

5.3.1 Lindblad Operators in Hartree-Fock Approximation

To have a consistent diagrammatic expansion for the four couplings g, $\Gamma_{\uparrow,\downarrow}$ and λ of our theory, we expand the corresponding vertices to second order in $\hbar$. For the incoherent couplings, such a two-loop expansion amounts to keeping the "double-bubble" diagram in the generating functional, or in other words, to working in Hartree-Fock approximation. Since all of the incoherent vertices are of type I, we will treat them collectively by first considering the expansion of the Lindbladian

$$\frac{\Gamma}{2}\mathcal{L}[d_0^{\dagger} d_1]\rho = \Gamma d_0^{\dagger} d_1 \rho d_1^{\dagger} d_0 - \frac{\Gamma}{2}\left\{\rho, d_1^{\dagger} d_0 d_0^{\dagger} d_1\right\}, \tag{5.57}$$

where for the moment the subscripts are placeholders for any of the states contributing to the Lindblad terms in Eq. (5.56) and Γ represents the corresponding incoherent coupling. The first step is to write down the Hartree-Fock equations for this Lindbladian without performing the

pseudo-particle projection. Once the unprojected equations are established, it will be possible to do the projection by taking the established fugacity limit $\zeta \to 0$.

Paying attention to the time-ordering of the operators in the anti-commutator, one may derive the equations of motion analogously to Sec. 3.1. The result is

$$\begin{aligned}
(\mathrm{i}\partial_t - \boldsymbol{h}_G)\,\boldsymbol{G}^<(t,t') = &\ \frac{\Gamma}{2}\begin{pmatrix} G^<_{11}(t,t) & -G^{\lessgtr}_{01}(t,t) \\ G^{\lessgtr}_{10}(t,t) & G^>_{00}(t,t) \end{pmatrix}\boldsymbol{G}^<(t,t') \\
&- \Gamma G^<_{11}(t,t)\begin{pmatrix} G^{\tilde{T}}_{00}(t,t') & G^{\tilde{T}}_{01}(t,t') \\ 0 & 0 \end{pmatrix}, \\
(\mathrm{i}\partial_t - \boldsymbol{h}_G)\,\boldsymbol{G}^>(t,t') = &-\frac{\Gamma}{2}\begin{pmatrix} G^<_{11}(t,t) & G^{\lessgtr}_{01}(t,t) \\ -G^{\lessgtr}_{10}(t,t) & G^>_{00}(t,t) \end{pmatrix}\boldsymbol{G}^>(t,t') \\
&+ \Gamma G^>_{00}(t,t)\begin{pmatrix} 0 & 0 \\ G^T_{10}(t,t') & G^T_{11}(t,t') \end{pmatrix}.
\end{aligned} \tag{5.58}$$

These equations can be evaluated numerically for $t > t'$. For the complete numerical solution, we also need to specify the equations in the equal-time limit. This gives

$$\begin{aligned}
\mathrm{i}\dot{\boldsymbol{G}}^<(T,0) = &\left[\boldsymbol{h}_G, \boldsymbol{G}^<(T,0)\right] + \frac{\Gamma}{2}\begin{pmatrix} G^<_{11}(T,0) & -G^{\lessgtr}_{01}(T,0) \\ G^{\lessgtr}_{10}(T,0) & G^>_{00}(T,0) \end{pmatrix}\boldsymbol{G}^<(T,0) \\
&+ \frac{\Gamma}{2}\boldsymbol{G}^<(T,0)\begin{pmatrix} G^<_{11}(T,0) & G^{\lessgtr}_{01}(T,0) \\ -G^{\lessgtr}_{10}(T,0) & G^>_{00}(T,0) \end{pmatrix} \\
&- \Gamma G^<_{11}(T,0)\begin{pmatrix} G^{\tilde{T}}_{00}(T,0) + G^T_{00}(T,0) & G^{\tilde{T}}_{01}(T,0) \\ G^T_{10}(T,0) & 0 \end{pmatrix}, \\
\mathrm{i}\dot{\boldsymbol{G}}^>(T,0) = &\left[\boldsymbol{h}_G, \boldsymbol{G}^>(T,0)\right] - \frac{\Gamma}{2}\begin{pmatrix} G^<_{11}(T,0) & G^{\lessgtr}_{01}(T,0) \\ -G^{\lessgtr}_{10}(T,0) & G^>_{00}(T,0) \end{pmatrix}\boldsymbol{G}^>(T,0) \\
&- \frac{\Gamma}{2}\boldsymbol{G}^>(T,0)\begin{pmatrix} G^<_{11}(T,0) & -G^{\lessgtr}_{01}(T,0) \\ G^{\lessgtr}_{10}(T,0) & G^>_{00}(T,0) \end{pmatrix} \\
&+ \Gamma G^>_{00}(T,0)\begin{pmatrix} 0 & G^{\tilde{T}}_{01}(T,0) \\ G^T_{10}(T,0) & G^T_{11}(T,0) + G^{\tilde{T}}_{11}(T,0) \end{pmatrix}.
\end{aligned} \tag{5.59}$$

Note that for the off-diagonal Green functions at equal time, greater and lesser signs are indeed interchangeable because of the vanishing commutator. A comparison of a numerically exact solution of these equations with the result of our algorithm from Sec. 2.3 for a Hamiltonian

$$\boldsymbol{h}_G = \begin{pmatrix} 0 & \pi/2 \\ \pi/2 & 2\pi \end{pmatrix} \tag{5.60}$$

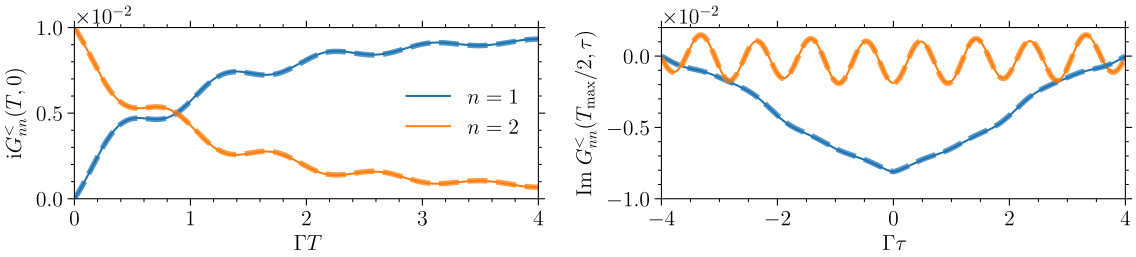

Figure 5.3: Numerical solution of Eqs. (5.58) and (5.59) for $\boldsymbol{h}_G$ as defined in Eq. (5.60) and initial conditions $G^<_{00}(0,0) = 0$, $G^<_{11}(0,0) = -\mathrm{i}\cdot 10^{-2}$ (off-diagonals initially zero). Thick dashed lines indicate the numerically exact solutions. The results were calculated with a step size of $\Gamma\cdot 2^{-7}$ for a number of 2^9 steps ($n_{\text{ini}} = 3\cdot 2^7$).

is shown in Fig. 5.3. As expected, the effect of $\mathcal{L}[d_0^\dagger d_1]\rho$ is to transfer excitations from state 1 into state 0. The oscillations superposed with this incoherent transfer are due to the coherent coupling in $\boldsymbol{h}_G$. As before, the algorithm of Sec. 2.3 reproduces the exact results accurately. One reason for this is that we are well within the perturbative regime due to the small initial occupation $G^<_{11}(0,0)$. For larger initial occupation, the loop expansion starts to deviate slightly from the exact result, as expected.

5.3.2 Projected Lindblad Operators in Hartree-Fock Approximation

The next step is to perform the pseudo-particle projection on Eqs. (5.58) and (5.59). Since ultimately we want to describe the vibrational relaxation, we take one step in that direction and give the equations of motion following from the total operator

$$\frac{\Gamma}{2}\left[(\bar{N}+1)\,\mathcal{L}[d_0^\dagger d_1] + \bar{N}\mathcal{L}[d_1^\dagger d_0]\right]\rho. \tag{5.61}$$

The result for the previous case $\mathcal{L}[d_0^\dagger d_1]$ then follows for $\bar{N} = 0$. Basically, the projection is now performed by removing all terms with too many lesser functions in Eqs. (5.58). But there seemingly arises an ambiguity from the identity of unprojected off-diagonal lesser and greater functions. One has to keep in mind, however, that for pseudo-particles there should hold

$$\boldsymbol{G}^>(T,0) = \begin{pmatrix} G^>_{00}(T,0) & G^>_{01}(T,0) \\ G^>_{10}(T,0) & G^>_{11}(T,0) \end{pmatrix} = \begin{pmatrix} -\mathrm{i} & 0 \\ 0 & -\mathrm{i} \end{pmatrix} \tag{5.62}$$

for all times T. This means that it would be possible to remove all equal-time off-diagonal greater Green functions from the equations (and hence to remove the ambiguity). At the same time, one can observe that the ambiguous terms would also have to be dropped because of their scaling in ζ if they were interpreted as lesser functions. Thus, the requirement of Eq. (5.62) ensures that the projection can be performed consistently. One may verify that Eq. (5.62) is indeed fulfilled by all of the respective equations of motion, in particular by the accordingly projected version of Eq. (5.59).

Adding also the terms required for $\mathcal{L}[d_1^\dagger d_0]\rho$ by switching the appropriate indices, we arrive at

$$\begin{aligned}
\mathrm{i}\partial_t \boldsymbol{G}^<(t,t') &= \boldsymbol{h}_G \boldsymbol{G}^<(t,t') + \frac{\Gamma\bar{N}}{2}\begin{pmatrix} G_{11}^>(t,t) & 0 \\ 0 & G_{00}^>(t,t)\end{pmatrix}\boldsymbol{G}^<(t,t') \\
&\quad + \frac{\Gamma}{2}\begin{pmatrix} 0 & 0 \\ 0 & G_{00}^>(t,t)\end{pmatrix}\boldsymbol{G}^<(t,t'),
\end{aligned} \tag{5.63a}$$

$$\begin{aligned}
\mathrm{i}\partial_t \boldsymbol{G}^>(t,t') &= \boldsymbol{h}_G \boldsymbol{G}^>(t,t') - \frac{\Gamma\bar{N}}{2}\begin{pmatrix} G_{11}^>(t,t) & 0 \\ 0 & G_{00}^>(t,t)\end{pmatrix}\boldsymbol{G}^>(t,t') \\
&\quad + \Gamma\bar{N}\begin{pmatrix} G_{11}^>(t,t) & 0 \\ 0 & G_{00}^>(t,t)\end{pmatrix}\boldsymbol{G}^>(t,t') + \frac{\Gamma}{2}\begin{pmatrix} 0 & 0 \\ 0 & G_{00}^>(t,t)\end{pmatrix}\boldsymbol{G}^>(t,t') \\
&= \boldsymbol{h}_G \boldsymbol{G}^>(t,t') + \frac{\Gamma\bar{N}}{2}\begin{pmatrix} G_{11}^>(t,t) & 0 \\ 0 & G_{00}^>(t,t)\end{pmatrix}\boldsymbol{G}^>(t,t') \\
&\quad + \frac{\Gamma}{2}\begin{pmatrix} 0 & 0 \\ 0 & G_{00}^>(t,t)\end{pmatrix}\boldsymbol{G}^>(t,t').
\end{aligned} \tag{5.63b}$$

These equations evidently possess the correct fugacity scalings. For the equal-time equation of $\boldsymbol{G}^<$, we start from Eqs. (5.59) and again remove all terms with the wrong scaling. This yields

$$\begin{aligned}
\mathrm{i}\dot{\boldsymbol{G}}^<(T,0) &= \left[\boldsymbol{h}_G, \boldsymbol{G}^<(T,0)\right] + \frac{\Gamma\bar{N}}{2}\left\{\begin{pmatrix} G_{11}^>(T,0) & 0 \\ 0 & G_{00}^>(T,0)\end{pmatrix}, \boldsymbol{G}^<(T,0)\right\} \\
&\quad - \Gamma\bar{N}\begin{pmatrix} G_{11}^<(T,0) & 0 \\ 0 & G_{00}^<(T,0)\end{pmatrix}\boldsymbol{G}^>(T,0) \\
&\quad + \frac{\Gamma}{2}\left\{\begin{pmatrix} 0 & 0 \\ 0 & G_{00}^>(T,0)\end{pmatrix}, \boldsymbol{G}^<(T,0)\right\} - \Gamma\begin{pmatrix} G_{11}^<(T,0) & 0 \\ 0 & 0\end{pmatrix}\boldsymbol{G}^>(T,0) \\
&= \left[\boldsymbol{h}_G, \boldsymbol{G}^<(T,0)\right] + \frac{\Gamma}{2}\left\{\begin{pmatrix} \bar{N}G_{11}^>(T,0) & 0 \\ 0 & \left(\bar{N}+1\right)G_{00}^>(T,0)\end{pmatrix}, \boldsymbol{G}^<(T,0)\right\} \\
&\quad - \Gamma\begin{pmatrix} \left(\bar{N}+1\right)G_{11}^<(T,0) & 0 \\ 0 & \bar{N}G_{00}^<(T,0)\end{pmatrix}\boldsymbol{G}^>(T,0),
\end{aligned}$$

where we have introduced an anti-commutator. Again, this equation has the correct fugacity scaling. As discussed above, we do not need an equation for the equal-time evolution of $\boldsymbol{G}^>$. Within both the ground- and excited-state manifolds, the Lindblad operators of Eq. (5.56) couple neighboring vibrational states according to a structure which for the self-energy matrices of Eqs. (5.63) and $n+1$ states in total would look like

$$\left(\bar{N}+1\right)\mathrm{diag}\left(0, G_{00}^>, 2G_{11}^>, ..., nG_{n-1,n-1}^>\right) + \bar{N}\,\mathrm{diag}\left(G_{11}^>, 2G_{22}^>, .., nG_{nn}^>, 0\right). \tag{5.64}$$

We still have to consider the external pumping proportional to $\Gamma_\uparrow$. The relevant matrices for this are $\mathrm{diag}\left(\boldsymbol{E}^{\lessgtr}(t,t'), \boldsymbol{G}^{\lessgtr}(t,t')\right)$, since without symmetry breaking there is no coherence between ground and excited states. In terms of these matrices, the contribution to the equations of motion

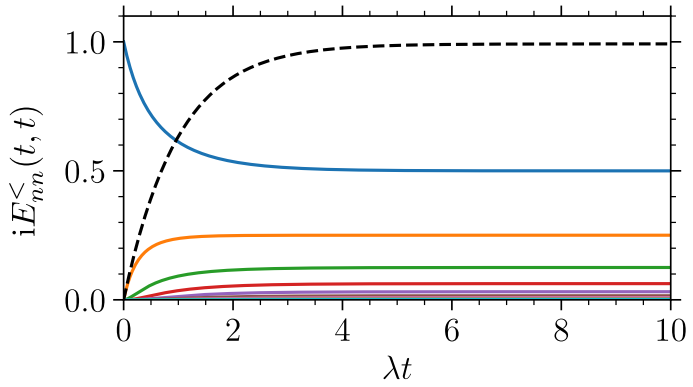

Figure 5.4: Relaxation of the vibrational degrees of freedom in the electronic excited state. The dashed line shows $\mathrm{i}\sum_{n=0}^{p_{\max}} nE^{<}_{nn}(t,t) \to \bar{N}$. The parameters are $g = 0$, i.e. we have decoupled the excited states from the rest of the system, $\Delta/\lambda = 2.0$, $\Omega/\lambda = 0.1$, $S = 0.5$, $\bar{N} = 1.0$, $\Gamma_\uparrow = \Gamma_\downarrow = 0$. The number of vibrational states considered is 10, which is equivalent to a maximal number of phonons $p_{\max} = 9$. The results were calculated with a step size of $10\lambda \cdot 2^{-9}$ for a number of 2^9 steps ($n_{\mathrm{ini}} = 3 \cdot 2^5$).

can be written rather compactly as

$$\mathrm{i}\partial_t \begin{pmatrix} \boldsymbol{E}^{\lessgtr}(t,t') & \mathbf{0} \\ \mathbf{0} & \boldsymbol{G}^{\lessgtr}(t,t') \end{pmatrix} = \frac{\Gamma_\uparrow}{2} \begin{pmatrix} \mathbf{0} & \mathbf{0} \\ \mathbf{0} & \mathrm{diag}(\boldsymbol{E}^{>}(t,t)) \end{pmatrix} \begin{pmatrix} \boldsymbol{E}^{\lessgtr}(t,t') & \mathbf{0} \\ \mathbf{0} & \boldsymbol{G}^{\lessgtr}(t,t') \end{pmatrix}. \tag{5.65}$$

For the forward dynamics, we find

$$\begin{aligned} \mathrm{i} \begin{pmatrix} \dot{\boldsymbol{E}}^{<}(T,0) & \mathbf{0} \\ \mathbf{0} & \dot{\boldsymbol{G}}^{<}(T,0) \end{pmatrix} = \frac{\Gamma_\uparrow}{2} \left\{ \begin{pmatrix} \mathbf{0} & \mathbf{0} \\ \mathbf{0} & \mathrm{diag}(\boldsymbol{E}^{>}(T,0)) \end{pmatrix}, \begin{pmatrix} \boldsymbol{E}^{<}(T,0) & \mathbf{0} \\ \mathbf{0} & \boldsymbol{G}^{<}(T,0) \end{pmatrix} \right\} \\ - \Gamma_\uparrow \begin{pmatrix} \mathrm{diag}(\boldsymbol{G}^{<}(T,0)) & \mathbf{0} \\ \mathbf{0} & \mathbf{0} \end{pmatrix} \begin{pmatrix} \boldsymbol{E}^{>}(T,0) & \mathbf{0} \\ \mathbf{0} & \boldsymbol{G}^{>}(T,0) \end{pmatrix}. \end{aligned} \tag{5.66}$$

The equations for the electronic loss $\Gamma_\downarrow$ follow analogously. Before concluding this section, consider Fig. 5.4 which shows the relaxation of the vibrational degrees of freedom in the electronic excited state induced by the vibrational relaxation in Eq. (5.56). The dashed line indicates the statistical average $\sum_n nE^{<}_{nn}(t,t)$ which correctly approaches $\bar{N}$. We therefore conclude that the master equation (5.56) is capable of describing the phonon thermalization adequately. As a further comment, consider that $k_B/\hbar \approx 0.13$ THz/K. This means typical room temperatures around $T \sim 293$ K are equivalent to frequencies of about 40 THz. For vibrational frequencies Ω in the THz range, $\bar{N}(\Omega)$ will never comprise more than a handful of quanta, as one may see from Fig. 5.5.

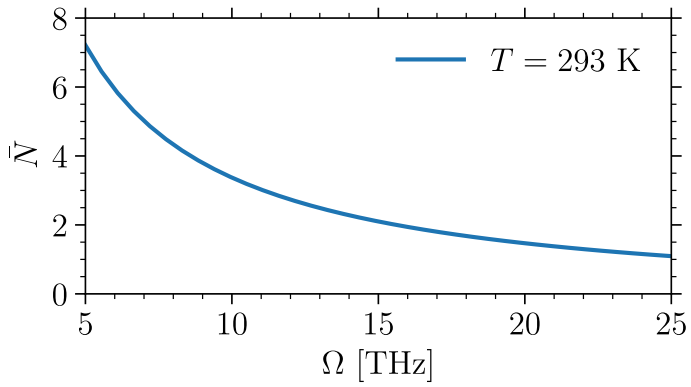

Figure 5.5: According to the thermodynamics of the harmonic oscillator, in the canonical ensemble there holds $2\bar{N}(\Omega) + 1 = 1/\tanh(\beta\hbar\Omega/2)$.

5.4 Benchmark System Dynamics

Before moving to the application of our non-Markovian model to photon condensation, it is instructive to give an illustration of the auxiliary-boson method for the case of a single molecule ($M = 1$), where apart from perturbative limitations, the method is in principle exact. We begin with an investigation of the Jaynes-Cummings model in 5.4.1, where analytical solutions are readily available. In 5.4.2, this is followed by an "open" Jaynes-Cummings model (which includes the cavity loss). Afterwards, we discuss the fulfillment of the *operator* constraint in 5.4.3, before moving on to a four-level system as our final benchmark in 5.4.4. Note that unless stated otherwise, $n_{\text{ini}} = 3 \cdot 2^5$ in all of the simulations still following in Chp. 5.

5.4.1 Some Exact Solutions

The obvious starting point for testing our methods is the simplest special case of the Hamiltonian (5.1), the Jaynes-Cummings model defined by

$$\begin{aligned} H_{\text{JC}} &= \omega_0 a^\dagger a + \frac{\Delta}{2}\sigma^z + g\left(a^\dagger\sigma^- + a\sigma^+\right) \\ &\equiv \delta a^\dagger a + g\left(a^\dagger\sigma^- + a\sigma^+\right), \end{aligned} \tag{5.67}$$

where $\delta = \omega_0 - \Delta$. As is well known, it can be solved analytically [153], the reason for this being essentially that the photon Hilbert space becomes block-diagonal because the change of the photon number is determined entirely by the two-state dynamics of the molecule. What is slightly surprising, however, is that also the integro-differential equations (5.34) admit an analytical solution, at least for the special case defined by an initially excited molecule coupled to an empty cavity. These conditions we express as $D_0^<(t,t') = 0, D_0^>(t,t') = -\mathrm{i}\exp\left(-\mathrm{i}\delta(t-t')\right)$ as well as $G^>(0,0) = -\mathrm{i}$ and $E^\lessgtr(0,0) = -\mathrm{i}$. It is useful to have an analytical solution to benchmark our numerical implementation of the auxiliary-boson Dyson equations and the photon T-matrix integrals. Yet one should certainly not expect this analytical solution to agree perfectly with the

exact solution of the Jaynes-Cummings model. Plugging the bare photon functions into Eqs. (5.34), we find

$$\partial_t G^<(t,t') = \quad \mathrm{i}g^2 \int_0^{t'} \mathrm{d}\bar{t}\, \mathrm{e}^{-\mathrm{i}\delta(\bar{t}-t)} E^<(t,\bar{t}) G^>(\bar{t},t'), \tag{5.68a}$$

$$\partial_t G^>(t,t') = 0, \tag{5.68b}$$

$$\partial_t E^<(t,t') = -\mathrm{i}g^2 \int_0^{t} \mathrm{d}\bar{t}\, \mathrm{e}^{-\mathrm{i}\delta(t-\bar{t})} G^>(t,\bar{t}) E^<(\bar{t},t'), \tag{5.68c}$$

$$\partial_t E^>(t,t') = -\mathrm{i}g^2 \int_{t'}^{t} \mathrm{d}\bar{t}\, \mathrm{e}^{-\mathrm{i}\delta(t-\bar{t})} G^>(t,\bar{t}) E^>(\bar{t},t'). \tag{5.68d}$$

Eq. (5.68b) allows us to simplify these equations even further to

$$\partial_t G^<(t,t') = \quad g^2 \mathrm{e}^{\mathrm{i}\delta t} \int_0^{t'} \mathrm{d}\bar{t}\, \mathrm{e}^{-\mathrm{i}\delta\bar{t}} E^<(t,\bar{t}), \tag{5.69a}$$

$$\partial_t E^<(t,t') = -g^2 \mathrm{e}^{-\mathrm{i}\delta t} \int_0^{t} \mathrm{d}\bar{t}\, \mathrm{e}^{\mathrm{i}\delta\bar{t}} E^<(\bar{t},t'), \tag{5.69b}$$

$$\partial_t E^>(t,t') = -g^2 \mathrm{e}^{-\mathrm{i}\delta t} \int_{t'}^{t} \mathrm{d}\bar{t}\, \mathrm{e}^{\mathrm{i}\delta\bar{t}} E^>(\bar{t},t'). \tag{5.69c}$$

At this point, finding an analytical solution becomes straightforward [154]. The adjoint equations are also required and read for the excited-state functions

$$\partial_{t'} E^<(t,t') = -g^2 \mathrm{e}^{\mathrm{i}\delta t'} \int_0^{t'} \mathrm{d}\bar{t}\, \mathrm{e}^{-\mathrm{i}\delta\bar{t}} E^<(t,\bar{t}), \tag{5.70a}$$

$$\partial_{t'} E^>(t,t') = \quad g^2 \mathrm{e}^{\mathrm{i}\delta t'} \int_{t'}^{t} \mathrm{d}\bar{t}\, \mathrm{e}^{-\mathrm{i}\delta\bar{t}} E^>(t,\bar{t}). \tag{5.70b}$$

To find an elementary solution to Eq. (5.69b), consider

$$\begin{aligned} \partial_t^2 E^<(t,t') &= \mathrm{i}\delta g^2 \mathrm{e}^{-\mathrm{i}\delta t} \int_0^{t} \mathrm{d}\bar{t}\, \mathrm{e}^{\mathrm{i}\delta\bar{t}} E^<(\bar{t},t') - g^2 E^<(t,t') \\ &= -\mathrm{i}\delta \partial_t E^<(t,t') - g^2 E^<(t,t'). \end{aligned} \tag{5.71}$$

Here we have exploited that one may convert linear integral equations of Volterra type such as Eq. (5.69b) into initial-value problems which admit solutions by standard methods.[4] Eq. (5.71) is

[4] The Volterra equations of the second kind [154] corresponding to the integro-differential equation (5.71) read

$$\begin{aligned} E^<(t,t') &= \int_0^{t} \mathrm{d}\bar{t}\, z(\bar{t}) + E^<(0,t'), \\ z(t) &= -g^2 \mathrm{e}^{-\mathrm{i}\delta t} \int_0^{t} \mathrm{d}\bar{t}\, \mathrm{e}^{\mathrm{i}\delta\bar{t}} E^<(\bar{t},t'). \end{aligned} \tag{5.72}$$

equivalent to a *Sturm-Liouville* equation [155]

$$\frac{\mathrm{d}}{\mathrm{d}t}\left(\mathrm{e}^{\mathrm{i}\delta t}\dot{x}(t)\right)+g^2\mathrm{e}^{\mathrm{i}\delta t}x(t)=0, \tag{5.73}$$

which is solved by

$$x(t)=\mathrm{e}^{-\mathrm{i}\delta t/2}\left(A\mathrm{e}^{\mathrm{i}\Omega t}+B\mathrm{e}^{-\mathrm{i}\Omega t}\right), \tag{5.74}$$

where we have introduced $\Omega^2=g^2+\delta^2/4$ and we allow $A,\,B\in\mathbb{C}$. From $x(0)=-\mathrm{i}$ and $\dot{x}(0)=0$, we find $\mathrm{Re}\,A=\mathrm{Re}\,B$ and $\mathrm{Im}\,[A-B]=\delta/2\Omega$. Since we also have to satisfy the adjoint equation, this suggests the solution

$$E^<(t,t')=-\mathrm{i}\mathrm{e}^{-\mathrm{i}\delta(t-t')/2}\left(\cos\Omega t+\frac{\mathrm{i}\delta}{2\Omega}\sin\Omega t\right)\left(\cos\Omega t'-\frac{\mathrm{i}\delta}{2\Omega}\sin\Omega t'\right). \tag{5.75}$$

In the equal-time limit, we thus have

$$E^<(t,t)=-\frac{\mathrm{i}}{2}\left[1+\cos 2\Omega t+(\delta/2\Omega)^2\left(1-\cos 2\Omega t\right)\right]. \tag{5.76}$$

To solve Eq. (5.69c), we proceed along the same lines and find

$$E^>(t,t')=-\mathrm{i}\mathrm{e}^{-\mathrm{i}\delta(t-t')/2}\left(\cos\left(\Omega(t-t')\right)+\frac{\mathrm{i}\delta}{2\Omega}\sin\left(\Omega(t-t')\right)\right). \tag{5.77}$$

To calculate $G^<(t,t')$, Eq. (5.69a) can be integrated from $t_0=0$ to t to give

$$\begin{aligned}G^<(t,t')&=g^2\int_0^t\mathrm{d}\bar{t}\,\mathrm{e}^{\mathrm{i}\delta\bar{t}}\int_0^{t'}\mathrm{d}\bar{t'}\,\mathrm{e}^{-\mathrm{i}\delta\bar{t'}}E^<(\bar{t},\bar{t'})\\&=-\mathrm{i}\,(g/\Omega)^2\,\mathrm{e}^{\mathrm{i}\delta(t-t')/2}\sin\Omega t\sin\Omega t'\\&=-\frac{\mathrm{i}}{2}\,(g/\Omega)^2\,\mathrm{e}^{\mathrm{i}\delta\tau/2}\left[\cos\Omega\tau-\cos 2\Omega T\right],\end{aligned} \tag{5.78}$$

which in the equal-time limit reduces to $G^<(t,t)=-\frac{\mathrm{i}}{2}(g/\Omega)^2\left(1-\cos 2\Omega t\right)$. This in turn ensures $\mathrm{i}E^<(t,t)+\mathrm{i}G^<(t,t)=1$. From Eq. (5.43), the solution for the photon lesser Green function is

$$\begin{aligned}D^<(t,t')&=\mathrm{i}g^2\int_0^t\mathrm{d}\bar{t}\int_{t'}^0\mathrm{d}\bar{t'}\;D_0^>T_D^<D_0^>\\&=\mathrm{e}^{-\mathrm{i}\delta(t-t')}g^2\int_0^t\mathrm{d}\bar{t}\,\mathrm{e}^{\mathrm{i}\delta\bar{t}}\int_0^{t'}\mathrm{d}\bar{t'}\,\mathrm{e}^{-\mathrm{i}\delta\bar{t'}}E^<(\bar{t},\bar{t'})\\&=\mathrm{e}^{-\mathrm{i}\delta(t-t')}G^<(t,t'),\end{aligned} \tag{5.79}$$

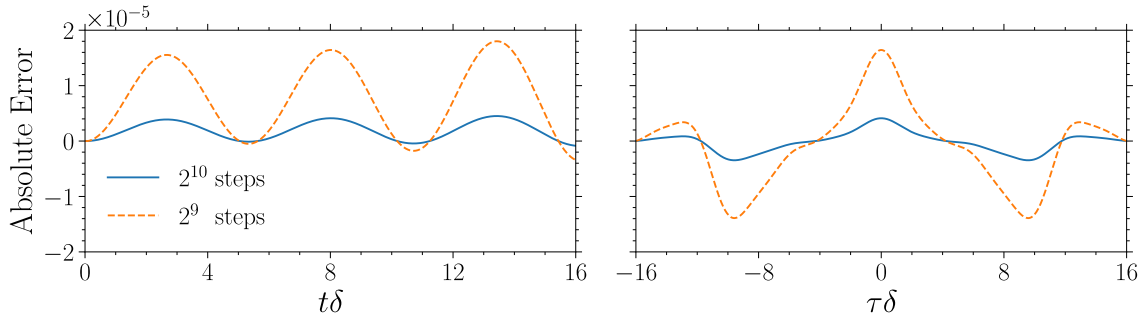

Figure 5.6: Absolute deviation of the numerical predictor-corrector solution of Eqs. (5.34) from the analytical solution $\mathrm{Re}\left[G^<(t,t')E^>(t,t')^*\right]$ given in Eq. (5.85) for (left) $t = t' = T$ and (right) $t = \frac{1}{2}(T_{\max} + \tau)$, $t' = \frac{1}{2}(T_{\max} - \tau)$, where $g/\delta = 2^{-2}$ and $T_{\max}\delta = 16.0$ ($n_{\mathrm{ini}} = 3 \cdot 2^6$).

where only the last integral of the first line of Eq. (5.43) contributes. This confirms our physical intuition about the photon evolution for this special case of the model.

To learn more about these solutions of Eqs. (5.34), we should compare them to the analytical solution of the Jaynes-Cummings model. To follow the established approach, we transform to the frame rotating with the photons [153]. Then, in terms of the coefficients of a wave-function ansatz

$$|\psi(t)\rangle = C_0(t)\,|0\rangle\,|e\rangle + D_0(t)\,|1\rangle\,|g\rangle\,, \tag{5.80}$$

the dynamics is governed by

$$\begin{pmatrix} C_n(t) \\ D_n(t) \end{pmatrix} = \boldsymbol{U}_n(t) \begin{pmatrix} C_n(0) \\ D_n(0) \end{pmatrix} \tag{5.81}$$

with a time-evolution operator

$$\boldsymbol{U}_n(t) = \begin{pmatrix} \cos\beta_n t + \frac{\mathrm{i}\delta}{2\beta_n}\sin\beta_n t & -\frac{\mathrm{i}g\sqrt{n+1}}{\beta_n}\sin\beta_n t \\ -\frac{\mathrm{i}g\sqrt{n+1}}{\beta_n}\sin\beta_n t & \cos\beta_n t - \frac{\mathrm{i}\delta}{2\beta_n}\sin\beta_n t \end{pmatrix}, \tag{5.82}$$

where in general $\beta_n^2 = \delta^2/4 + (n+1)g^2$. For the initial condition $|\psi(0)\rangle = |0\rangle\,|e\rangle$, we have $C_0(0) = 1$ and $D_0(0) = 0$. The solution for the wave function is found to be

$$|\psi(t)\rangle = \left(\cos\Omega t + \frac{\mathrm{i}\delta}{2\Omega}\sin\Omega t\right)|0\rangle\,|e\rangle - \mathrm{i}\frac{g}{\Omega}\sin\Omega t\,|1\rangle\,|g\rangle\,. \tag{5.83}$$

Applying Pauli matrices to this state, we may calculate $\sigma^{\pm}\sigma^{\mp}\,|\psi(t)\rangle$, which in the Schrödinger picture yields time-dependent expectation values

$$\begin{aligned} \langle\sigma^+(t)\sigma^-(t)\rangle &= \cos^2\Omega t + (\delta/2\Omega)^2\sin^2\Omega t = \mathrm{i}E^<(t,t), \\ \langle\sigma^-(t)\sigma^+(t)\rangle &= (g/\Omega)^2\sin^2\Omega t = \mathrm{i}G^<(t,t). \end{aligned} \tag{5.84}$$

Evidently, these happen to agree with $E^{<}(t,t)$ and $G^{<}(t,t)$, respectively, even though Eqs. (5.34) are perturbative. Because the greater function $E^{>}(t,t')$ does not correspond to a physical operator in terms of Pauli matrices, we cannot find a direct comparison. We may, however, construct physical operator products that involve $E^{>}(t,t')$ after the projection. As we will show in more detail in 5.4.2, for physical two-time expectation values such as $\langle\sigma^{-}(t')\sigma^{+}(t)\rangle$, the projection technique gives the result

$$\begin{aligned}\langle\sigma^{-}(t')\sigma^{+}(t)\rangle &\equiv G^{<}(t,t')E^{>}(t,t')^{*} \\ &= \frac{\mathrm{e}^{\mathrm{i}\delta\tau}}{2}\left(g/\Omega\right)^{2}\left(\cos\Omega\tau-\cos 2\Omega T\right)\left(\cos\Omega\tau-\frac{\mathrm{i}\delta}{2\Omega}\sin\Omega\tau\right).\end{aligned} \tag{5.85}$$

To verify our numerical implementation of Eqs. (5.34), we present in Fig. 5.6 the absolute deviation of this expression from the numerical result obtained by our predictor-corrector method. As one can see, the error is small and goes down systematically for an increased number of steps.

For the exact solution of the Jaynes-Cummings model, a complication arises because the two-time structure of $\langle\sigma^{-}(t')\sigma^{+}(t)\rangle$ couples the subspace $\{|1\rangle|g\rangle, |0\rangle|e\rangle\}$ of $|\psi(t)\rangle$ to the adjacent subspace $\{|2\rangle|g\rangle, |1\rangle|e\rangle\}$. This means we have to calculate $\boldsymbol{U}_1(t'-t)\sigma^{+}|\psi(t)\rangle = -\mathrm{i}\left(g/\Omega\right)\sin\Omega t\,\boldsymbol{U}_1(t'-t)|1\rangle|e\rangle$, where

$$\boldsymbol{U}_1(t)|1\rangle|e\rangle = \left(\cos\beta_1 t+\frac{\mathrm{i}\delta}{2\beta_1}\sin\beta_1 t\right)|1\rangle|e\rangle-\mathrm{i}\frac{\sqrt{2}g}{\beta_1}\sin\beta_1 t\,|2\rangle|g\rangle. \tag{5.86}$$

Hence, we may evaluate

$$\begin{aligned}\langle\sigma^{-}(t')\sigma^{+}(t)\rangle &= \langle\psi(t')|\,\sigma^{-}U_1(t'-t)\sigma^{+}|\psi(t)\rangle \\ &= \left(g/\Omega\right)^{2}\sin\Omega t'\left(\cos\left(\beta_1(t-t')\right)-\frac{\mathrm{i}\delta}{2\beta_1}\sin\left(\beta_1(t-t')\right)\right)\sin\Omega t \\ &= \frac{1}{2}\left(g/\Omega\right)^{2}\left(\cos\Omega\tau-\cos 2\Omega T\right)\left(\cos\beta_1\tau-\frac{\mathrm{i}\delta}{2\beta_1}\sin\beta_1\tau\right).\end{aligned} \tag{5.87}$$

To compare this to our auxiliary-boson result, we have to rotate Eq. (5.85) to the photon frame, which removes the phase factor $\exp\left(\mathrm{i}\delta\tau\right)$. As is underlined by Fig. 5.7, Eq. (5.87) agrees with Eq. (5.85) only for small $\delta\tau$. This is, however, not surprising since Eqs. (5.34) are approximate to begin with and the ratio $g/\delta = 2^{-2}$ is relatively large in the present example. In the perturbative limit $g/\delta \to 0$, one may see that Eqs. (5.87) and (5.85) agree perfectly for all τ as $\beta_1 \to \Omega$. Another interesting limit is the resonant case $\delta \to 0$ where evidently $g/\delta \to \infty$, such that we are in effect in the non-perturbative regime. Then $\beta_1 \to \sqrt{2}\Omega$ and the two results only agree for $\tau = 0$. For all physical applications of our non-Markovian model, the ratio g/δ will indeed be very small, leading in turn to small photon numbers per molecule. Furthermore, we will be mostly interested in equal-time results, which for our current example agree with the exact expressions even though the spectral results from relative-time dynamics are only approximate. We continue this discussion in 5.4.2.

5.4.2 Open Jaynes-Cummings Model

In addition to the dynamics induced by H_{JC}, we introduce a cavity loss for the photon mode in the manner established in Eq. (2.15) of 2.1.3. From the corresponding master equation, one may derive the equations of motion as

$$\begin{aligned}
\partial_t \langle a^\dagger a\rangle &= -\kappa\langle a^\dagger a\rangle - \mathrm{i}g\left(\langle a^\dagger\sigma^-\rangle - \langle a\sigma^+\rangle\right),\\
\partial_t \langle \sigma^z\rangle &= 2\mathrm{i}g\left(\langle a^\dagger\sigma^-\rangle - \langle a\sigma^+\rangle\right),\\
\partial_t \langle a\sigma^+\rangle &= -\mathrm{i}\delta\langle a\sigma^+\rangle - \frac{\kappa}{2}\langle a\sigma^+\rangle - \mathrm{i}g\left(\langle a^\dagger a\sigma^z\rangle + \langle \sigma^+\sigma^-\rangle\right).
\end{aligned} \tag{5.88}$$

These are, however, not closed because of the occurrence of $\langle a^\dagger a\sigma^z\rangle$ in the last of Eqs. (5.88). In the photon-BEC literature, this term has been treated by means of the heuristic truncation $\langle a^\dagger a\sigma^z\rangle \approx \langle a^\dagger a\rangle\langle\sigma^z\rangle$ [19]. While this may work in certain parameter regimes, it is not a controlled approximation. This can have undesirable consequences, as exemplified by the negative particle numbers highlighted in Fig. 5.8, which indeed are not a numerical artifact. While this problem is mild for the parameters we have chosen here, it becomes more severe in other parameter regimes. In particular, a factor of M coming from a sum over many molecules in the equation for $\langle a^\dagger a\rangle$ can lead to strongly unphysical results. This is yet another manifestation of the difficulties involved in truncating the expectation-value hierarchy when phase coherence between photons and molecule(s) plays a role (cf. the introduction to this Chp.). As explained above, the auxiliary-boson technique provides a way out of this conundrum. In the present context, this can be appreciated from Fig. 5.9. The inset underlines that the unphysical negative particle numbers have been removed by the pseudo-particle method and that this correctly reproduces numerically exact results. Fig. 5.10 shows similar plots for an increased detuning parameter, which results in less photons and a slightly altered spectral function. Again, numerically exact results are captured well by the predictor-corrector scheme, even for a relatively small number of steps.

To calculate physical expectation values such as $\langle\sigma^z(t)\rangle = \langle\sigma^+(t)\sigma^-(t)\rangle - \langle\sigma^-(t)\sigma^+(t)\rangle$, we

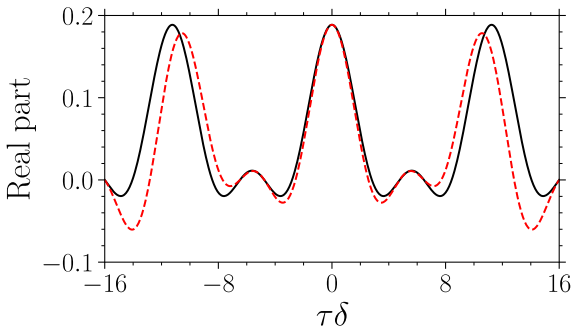

Figure 5.7: Comparison of relative-time dynamics. Dashed (red) line: the analytical solution (5.87) of the Jaynes-Cummings model for $\langle\sigma^-(t')\sigma^+(t)\rangle$; solid (black) line: the analytical solution (5.85) rotated to the photon frame. The times are $t = \frac{1}{2}(T_{\mathrm{max}} + \tau)$, $t' = \frac{1}{2}(T_{\mathrm{max}} - \tau)$ where $g/\delta = 2^{-2}$ and $T_{\mathrm{max}}\delta = 16.0$.

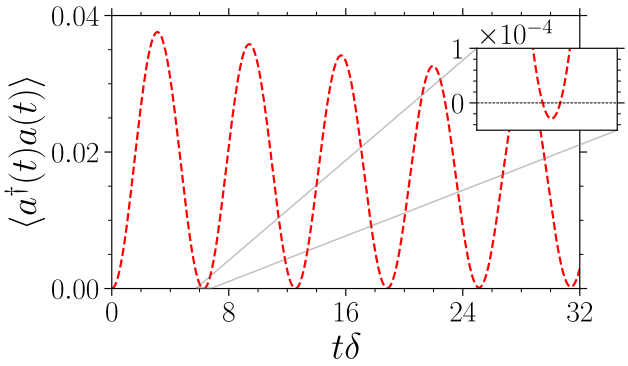

Figure 5.8: Solution of Eqs. (5.88) with truncation $\langle a^\dagger a\sigma^z\rangle \approx \langle a^\dagger a\rangle\langle\sigma^z\rangle$ for parameters $\kappa/\delta = 2^{-6}$, $g/\delta = 2\pi\cdot 2^{-6}$. The negative occupations are not a numerical artifact but result from the uncontrolled truncation.

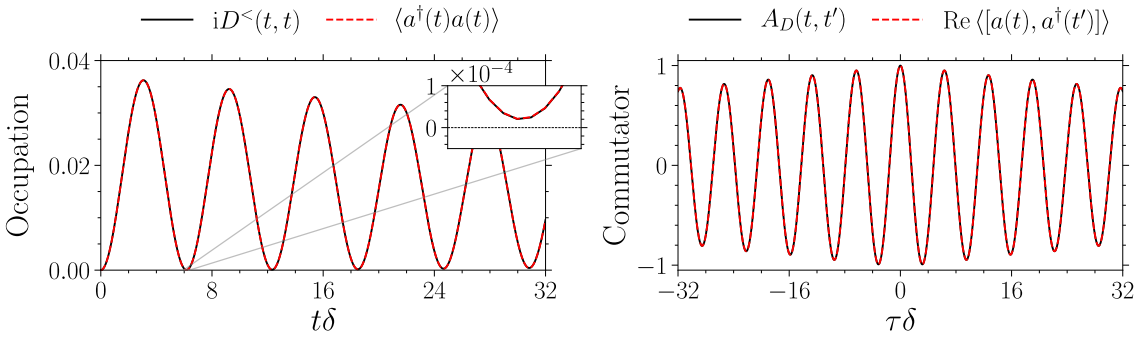

Figure 5.9: Solution of Eqs. (5.43) and (5.44) for parameters $\kappa/\delta = 2^{-6}$, $g/\delta = 2\pi\cdot 2^{-6}$. The (black) solid lines are based on the algorithm of Sec. 2.3. The (red) dashed lines are the benchmark results calculated with a numerically exact method from the corresponding von Neumann equation. Because of the good agreement, the lines overlap identically. The spectral function is defined as $A_D(t,t') = -\,\mathrm{Im}\left(D^>(t,t') - D^<(t,t')\right)$. In the right panel, the times are $t = (T_{\mathrm{max}} + \tau)/2$ and $t' = (T_{\mathrm{max}} - \tau)/2$, where $T_{\mathrm{max}}\delta = 32.0$. The results were calculated with a step size of $\delta \mathrm{d}t = 10^{-2}$ for a number of 2^{10} steps ($n_{\mathrm{ini}} = 3\cdot 2^6$).

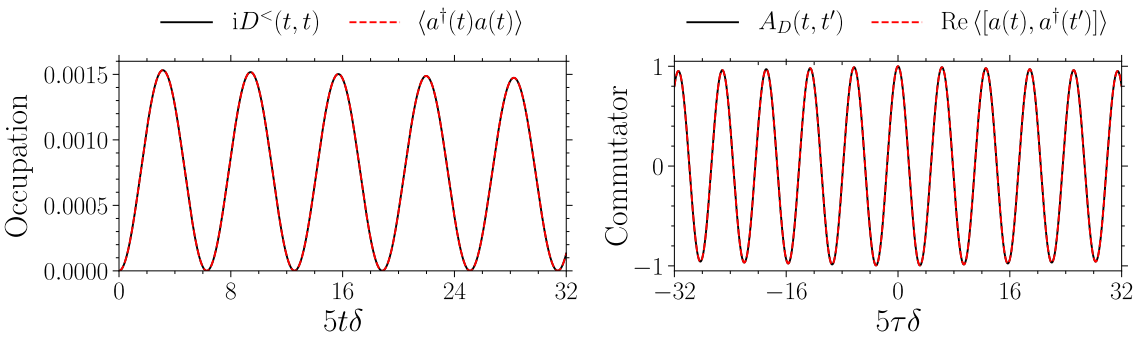

Figure 5.10: Solution of Eqs. (5.43) and (5.44) for the same parameters as in Fig. 5.9, yet with increased detuning 5δ. In the right panel, the times are again $t = (T_{\max} + \tau)/2$ and $t' = (T_{\max} - \tau)/2$, where now $5T_{\max}\delta = 32.0$. The results were calculated with a step size of $\delta \mathrm{d}t = 10^{-2}$ for a number of 2^{10} steps ($n_{\mathrm{ini}} = 3 \cdot 2^6$).

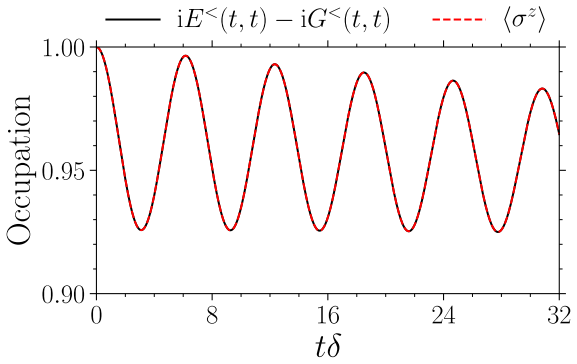

Figure 5.11: Equal-time occupation as given by the pseudo-particle lesser Green functions and the corresponding numerically exact time evolution of $\langle\sigma^z\rangle$. The parameters are those of Fig. (5.9).

have to apply the projection according to

$$\begin{aligned}
\langle\sigma^+(t')\sigma^-(t)\rangle &= \lim_{\zeta\to 0}\frac{1}{\langle\hat{Q}\rangle_\zeta}\langle d_e^\dagger(t')d_g(t')d_g^\dagger(t)d_e(t)\rangle_\zeta \\
&\overset{t'\geq t}{=} -\lim_{\zeta\to 0}\frac{1}{\zeta}\,\zeta E^<(t,t')G^>(t',t) = E^<(t,t')G^>(t,t')^*, \\
\langle\sigma^-(t')\sigma^+(t)\rangle &= \lim_{\zeta\to 0}\frac{1}{\langle\hat{Q}\rangle_\zeta}\langle d_g^\dagger(t')d_e(t')d_e^\dagger(t)d_g(t)\rangle_\zeta \\
&\overset{t'\geq t}{=} -\lim_{\zeta\to 0}\frac{1}{\zeta}\,\zeta G^<(t,t')E^>(t',t) = G^<(t,t')E^>(t,t')^*.
\end{aligned} \tag{5.89}$$

Since a product of a greater and a lesser pseudo-particle Green function is of order ζ, this yields the correct result. Note that arbitrary products of time-ordered Pauli matrices can be treated in the

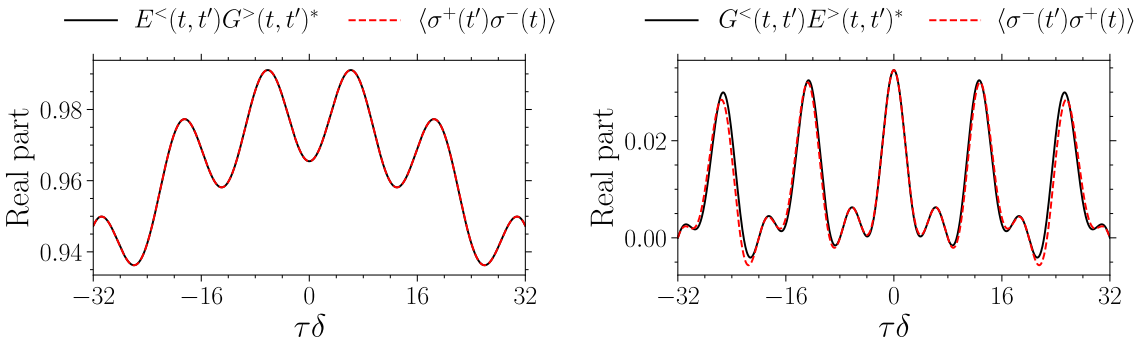

Figure 5.12: Relative-time dynamics of projected quantities for the parameters of Fig. 5.9. The solutions for the real parts of Eqs. (5.89) are shown. The results for $t' < t$ follow from symmetry. The deviations from the benchmark result are not due to numerical imprecision but follow from the limited validity of the perturbative expansion (cf. Fig. 5.13).

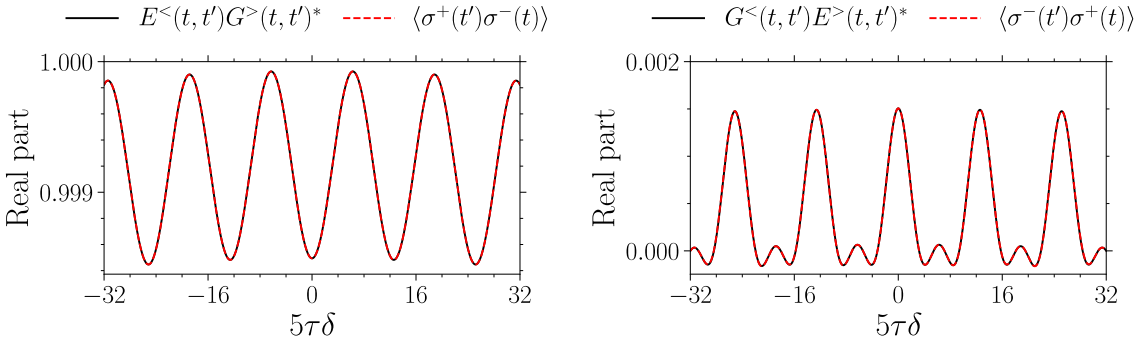

Figure 5.13: Relative-time dynamics of projected quantities for the parameters of Fig. 5.10. The solutions for the real parts of Eqs. (5.89) are shown. The deviations from the benchmark result in the right panel are hardly perceptible. The reason for this are the smaller occupation numbers, which also enter the criterion of validity of the loop expansion.

same way. For the equal-time average, we hence find the expected result

$$\langle\sigma^z(t)\rangle = \lim_{\zeta\to 0}\frac{1}{\zeta}\left(\zeta E^<(t,t)G^>(t,t)^* - \zeta G^<(t,t)E^>(t,t)^*\right) = \mathrm{i}E^<(t,t) - \mathrm{i}G^<(t,t), \quad (5.90)$$

which is plotted in Fig. 5.11. Further confirmation for the logic behind Eqs. (5.89) can be obtained by considering the dynamics in τ-direction, which is studied in Fig. 5.12. Again, we find good agreement between the predictor-corrector method and the solution of the master equation, except for the small deviations visible for large τ in the right panel of Fig. 5.12. To understand this, we also have to consider Fig. 5.13, which shows the same quantities but for the large detuning 5δ. This entails smaller occupation numbers for the photons (cf. Fig. 5.10). Looking back to Sec. 2.2, we understand that our perturbative expansion to two-loop order neglects higher-order terms that contain time integrals over products of powers of the coupling constant with Green functions. The validity of this approximation hence hinges on the magnitude of the neglected terms, to which the

Green functions contribute more for larger occupation numbers. Another contributing factor is the maximal time of integration: the magnitude of the neglected integrals can increase for larger integration domains, for which reason any such perturbative expansion should at some point start to deviate from exact results.[5] This is indeed what we witness in Fig. 5.12. That the deviations have disappeared in Fig. 5.13, even though the integration time has increased, confirms that the occupation numbers influence the perturbative validity independently. Most importantly, we can conclude that the deviations in Fig. 5.12 are not due to a failure of the auxiliary-boson method.

5.4.3 Fulfillment of the Operator Constraint

The way we employed the projection technique in Eqs. (5.89) brings our attention back to the operator constraint. In terms of the original Pauli matrices, it reads

$$\mathbb{1} = \hat{Q} = \sigma^+\sigma^- + \sigma^-\sigma^+. \tag{5.91}$$

To verify that it is indeed satisfied as an *operator* constraint[6], in principle one has to check the expectation values $\langle \hat{Q}^k \rangle$ for all values k. To illustrate, we inspect only the cases $k = 1, 2$. Time-ordering properly, we can write

$$\begin{aligned}
\langle \sigma^+(t^+)\sigma^-(t)\rangle + \langle \sigma^-(t^+)\sigma^+(t)\rangle &= \lim_{\zeta\to 0} \frac{1}{\langle \hat{Q}\rangle_\zeta}\Big[\langle \mathcal{T} d_e^\dagger(t^+) d_g(t^+) d_g^\dagger(t) d_e(t)\rangle \\
&\quad + \langle \mathcal{T} d_g^\dagger(t^+) d_e(t^+) d_e^\dagger(t) d_g(t)\rangle\Big] \\
&= \lim_{\zeta\to 0} \frac{1}{\langle \hat{Q}\rangle_\zeta}\Big[\langle \mathcal{T} d_e^\dagger(t^+) d_e(t)\rangle\langle \mathcal{T} d_g(t^+) d_g^\dagger(t)\rangle \\
&\quad + \langle \mathcal{T} d_g^\dagger(t^+) d_g(t)\rangle\langle \mathcal{T} d_e(t^+) d_e^\dagger(t)\rangle\Big] \\
&= -\left(E^<(t,t)G^>(t,t) + G^<(t,t)E^>(t,t)\right) \\
&= n_g + n_e = \langle \hat{Q}\rangle = 1,
\end{aligned} \tag{5.92}$$

where we have used that for pseudo-particles, $\mathrm{i}G^>(t,t) = \mathrm{i}E^>(t,t) = 1$. In the unconstrained field theory, on the contrary, one ends up with

$$\begin{aligned}
\langle \sigma^+(t^+)\sigma^-(t)\rangle + \langle \sigma^-(t^+)\sigma^+(t)\rangle &= -\left(E^<(t,t)G^>(t,t) + G^<(t,t)E^>(t,t)\right) \\
&= n_e\left(n_g+1\right) + n_g\left(n_e+1\right) \\
&= \left(1-n_g\right)\left(n_g+1\right) + n_g\left(1-n_g+1\right) \\
&= -2n_g^2 + 2n_g + 1 \geq 1,
\end{aligned} \tag{5.93}$$

[5] If this were not true, one could simply reduce the coupling constant to make the neglected terms smaller, while the necessary increase of integration time would not make them larger.

[6] To be distinguished from the expectation-value constraint $\langle \hat{Q}\rangle = 1$ which can be implemented easily via the initial conditions of any conserving approximation.

where the final inequality holds for $n_g \in [0,1]$. Thus, we understand that the projection technique is vital already on this level. For $k=2$, we have the more complicated expression

$$\begin{aligned}\langle \hat{Q}^2 \rangle &= \lim_{\zeta\to 0} \frac{1}{\langle \hat{Q} \rangle_\zeta} \left\langle \mathcal{T}\left[d_e^\dagger(t^{++}) d_e(t^+) + d_g^\dagger(t^{++}) d_g(t^+) \right] \left[d_e^\dagger(t) d_e(t^-) + d_g^\dagger(t) d_g(t^-) \right] \right\rangle \\ &= -\lim_{\zeta\to 0} \frac{1}{\langle \hat{Q} \rangle_\zeta} \Big[\zeta^2 E^<(t,t) E^<(t,t) + \zeta E^<(t,t) E^>(t,t) + \zeta^2 G^<(t,t) E^<(t,t) \\ &+ \zeta^2 G^<(t,t) E^<(t,t) + \zeta G^<(t,t) G^>(t,t) + \zeta^2 G^<(t,t) G^<(t,t) \Big] \\ &= n_g + n_e = \langle \hat{Q} \rangle = 1.\end{aligned}$$

Again, for the unconstrained field theory, one finds a different result which in this case is even strictly greater than one,

$$\langle \hat{Q}^2 \rangle = \left(n_e + n_g\right)^2 + n_e\left(n_e+1\right) + n_g\left(n_g+1\right) = 1 + 2\left(n_g^2 - n_g + 1\right) > 1. \tag{5.94}$$

Without attempting a rigorous proof of $\langle \hat{Q}^k \rangle = 1$ for all k, we can conclude that the auxiliary-boson method goes beyond approaches where the operator constraint is satisfied on average [33, 34].

5.4.4 Single-Mode Cavity Coupled to Four-Level System

To explore the behavior of our implementation of Eq. (5.56) in the presence of some vibrational substructure, we move on to the special case of a single dissipative cavity mode coupled to what essentially amounts to a four-level atom. We should emphasize that the auxiliary-boson field theory can in principle be used to describe an arbitrary multi-level atom, i.e. the Hamiltonian need not have the specific structure of Eq. (5.8). In particular, one could employ the technique to implement a proper spin algebra in terms of auxiliary bosons. The closest analogy to the four-level atom we are about to describe would be a spin-$3/2$. Moving back to bra-ket notation for the molecule, we have a Hamiltonian

$$\begin{aligned}H &= \omega_0 a^\dagger a - \Delta\,|g,0\rangle\langle g,0| + (\Omega-\Delta)\,|g,1\rangle\langle g,1| + \Delta\,|e,0\rangle\langle e,0| + (\Omega+\Delta)\,|e,1\rangle\langle e,1| \\ &+ \Omega\sqrt{S}\left(|e,0\rangle\langle e,1| - |g,0\rangle\langle g,1| + \text{h.c.}\right) + g\sum_{n=0,1}\left(a^\dagger\,|g,n\rangle\langle e,n| + \text{h.c.}\right),\end{aligned} \tag{5.95}$$

which is a special case of Eq. 5.8. For brevity, we also define the notation

$$J_{\sigma,\,n;\,\sigma',\,n'} := |\sigma\,,n\rangle\langle\sigma',n'| \tag{5.96}$$

for these operators. The Lindbladians of the vibrational relaxation then become

$$\begin{aligned}\mathcal{L}[J_{e,\,0;\,e,\,1}]\rho = \mathcal{L}\Big[\,|e,0\rangle\langle e,1|\,\Big]\rho &= |e,0\rangle\langle e,1|\,\rho\,|e,1\rangle\langle e,0| - \frac{1}{2}\left\{|e,1\rangle\langle e,0|\,|e,0\rangle\langle e,1|\,,\rho\right\} \\ &= |e,0\rangle\langle e,1|\,\rho\,|e,1\rangle\langle e,0| - \frac{1}{2}\left\{|e,1\rangle\langle e,1|\,,\rho\right\}\end{aligned} \tag{5.97}$$

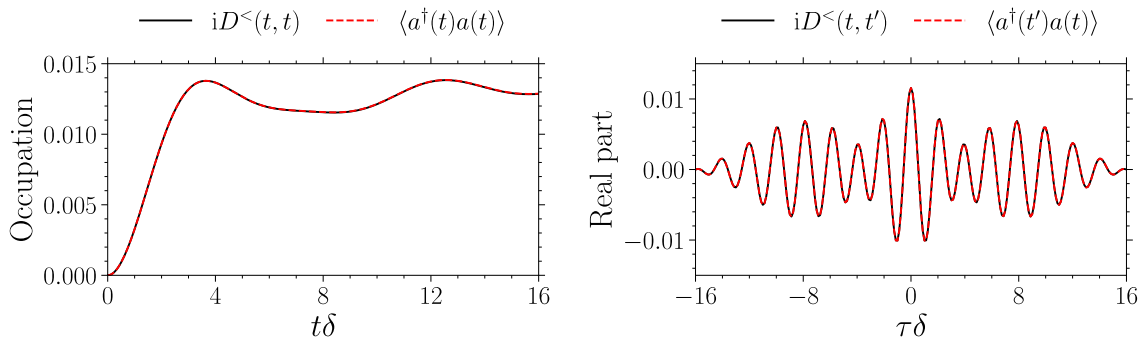

Figure 5.14: Solution of Eqs. (5.43) and (5.44) for parameters $\kappa/\delta = 0.1$, $g/\delta = 2\pi \cdot 0.01$, $\lambda/\delta = 0.05$, $\bar{N} = 1.0$, $\Omega/\delta = 0.1$, $S = 1.0$, $\Gamma_\uparrow/\delta = 0.1$, $\Gamma_\downarrow = \Gamma_\uparrow/20$. Initial conditions are given in Fig. 5.15. The (black) solid lines are based on the algorithm of Sec. 2.3. The (red) dashed lines are the benchmark results calculated with a numerically exact method from the corresponding von Neumann equation. Because of the good agreement, the lines overlap identically. In the right panel, the times are $t = (T_{\text{max}} + \tau)/2$ and $t' = (T_{\text{max}} - \tau)/2$, where $T_{\text{max}}\delta = 16$. The results were calculated with a step size of $\delta \mathrm{d}t = 2^{-4}$ for a number of 2^8 steps ($n_{\text{ini}} = 3 \cdot 2^6$).

and $\mathcal{L}[J_{e,1;\,e,0}]$, which are proportional to $\lambda(\bar{N}+1)$ and $\lambda\bar{N}$, respectively. We remark that the collapse of the matrix element in the anti-commutator is reproduced by the auxiliary-boson algebra when applying the operator constraint. Furthermore, we include the analogous operators $\Gamma_\uparrow\mathcal{L}[J_{e,n;\,g,n}]$ and $\Gamma_\downarrow\mathcal{L}[J_{g,n;\,e,n}]$ for $n = 0, 1$. Simulation results for this model are summarized in Figs. 5.14, 5.15 and 5.16. The pseudo-particle dynamics is dominated by the driven-dissipative processes. The cavity occupation relaxes toward a steady-state. The benchmark results were again obtained by solving the master equation directly with a standard library [156]. They agree very well with our multi-step solutions of the Kadanoff-Baym equations. Physical expectation values such as time-ordered products of molecular operators are projected according to the same rules as before. For instance,

$$\begin{aligned}
\langle \mathcal{T} J_{g,n;\,e,n}(t') J_{e,n;\,g,n}(t)\rangle &= \langle \mathcal{T} d^\dagger_{g,\,n}(t') d_{e,\,n}(t') d^\dagger_{e,\,n}(t) d_{g,\,n}(t)\rangle \\
&\overset{t'\geq t}{=} -G^<_{nn}(t,t')E^>_{nn}(t',t) = G^<_{nn}(t,t')E^>_{nn}(t,t')^*, \\
\langle \mathcal{T} J_{e,n;\,g,n}(t') J_{g,n;\,e,n}(t)\rangle &= \langle \mathcal{T} d^\dagger_{e,\,n}(t') d_{g,\,n}(t') d^\dagger_{g,\,n}(t) d_{e,\,n}(t)\rangle \\
&\overset{t'\geq t}{=} -E^<_{nn}(t,t')G^>_{nn}(t',t) = E^<_{nn}(t,t')G^>_{nn}(t,t')^*,
\end{aligned} \tag{5.98}$$

where $\mathcal{T}$ is the time-ordering operator. The corresponding results are presented in Fig. 5.16 and show excellent agreement. The principles used in Eq. (5.98) can be used to calculate arbitrarily long chains of molecular operators.

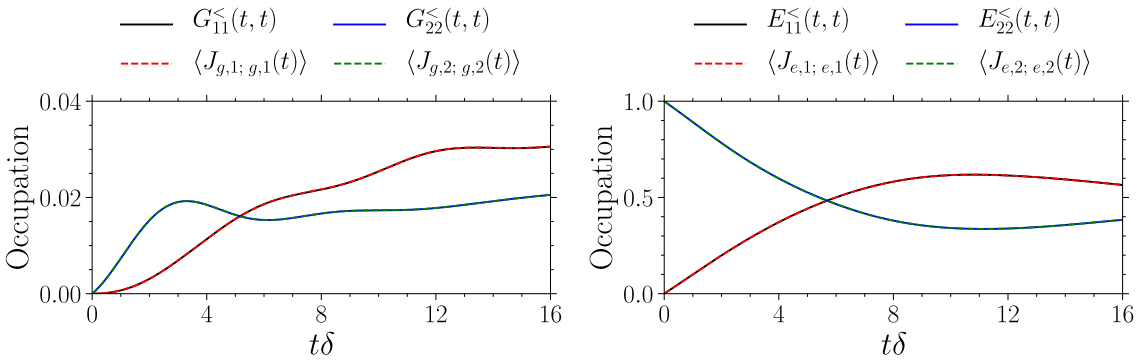

Figure 5.15: Equal-time pseudo-particle occupations for the same parameters as in Fig. 5.14. The initial conditions are $G^<_{nn}(0,0) = 0$ for $n = 0, 1$, $E^<_{00}(0,0) = 0$, $E^<_{11}(0,0) = -\mathrm{i}$ and an empty cavity. The operators $J_{g,\,0;\,g,\,0}$ etc. are defined in Eq. (5.96).

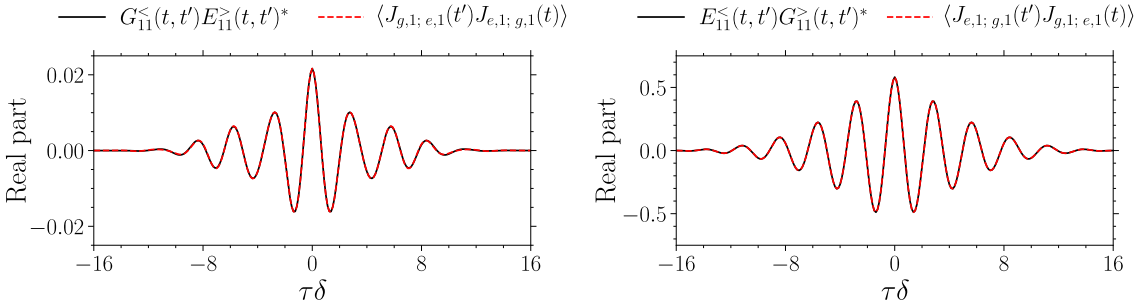

Figure 5.16: Relative-time dynamics of projected quantities for the parameters of Fig. 5.14. The solutions for the real parts of Eqs. (5.98) are shown for $n = 0$.

5.5 Memory Truncation

As mentioned in Sec. 2.3, solving the equations of motion for interacting systems[7] numerically on the two-time grid becomes computationally very expensive when the number of grid points needs to be large. This happens whenever the product of the fastest system frequency and the required final time is not small. In our case, there are both the usually fast molecular relaxation rate λ and the *a priori* much slower photon dynamics. Incidentally, waiting for stimulated emission to set in may take a long time.

Compared to numerically solving ordinary differential equations, the cubic instead of linear dependence on the number of grid points in the interacting case originates in the second temporal dimension and the summation of discretized time integrals. Loosely speaking, the Green functions in driven-dissipative systems will have a τ-dependence of the form $\exp(-\lambda\tau)$, where λ is a sum over terms proportional to all relevant drive and dissipation constants (comprising λ in particular). When λ is large, the two-time grid must have a fineness capable of resolving the exponential decay (or any fast coherent oscillations, for that matter). However, such a resolution will neither

[7] Here, "interacting" refers to anything *beyond* Hartree-Fock.

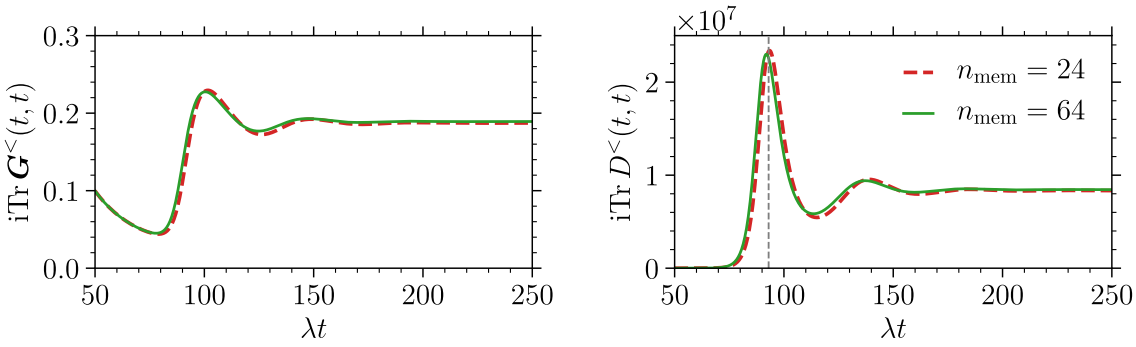

Figure 5.17: Forward dynamics of a single photon mode $k = 0$ for different memory truncations. Initial conditions and parameters are $\mathrm{Tr}\, D^<(0,0) = 0$, $\mathrm{i}G^<_{00}(0,0) = 1$, and $M = 10^9$, $g/\lambda = 4.5 \cdot 10^{-5}$, $\omega_0/\lambda = -1.0$, $\kappa/\lambda = 1.0$, $\Omega/\lambda = 1.0$, $S = 1.0$, $\bar{N} = 0.25$, $\Gamma_\uparrow/\lambda = 0.05$, $\Gamma_\downarrow = \Gamma_\uparrow/40$, and vibrational-state truncation at $n = 4$. Simulations calculated for 2^{13} steps up to a final time $\lambda T_{\mathrm{max}} = 512$ with memory times $\lambda\tau_{\mathrm{mem}} = \{1.5, 4.0\}$. The steady-state occupations are $\lim_{t\to\infty} \mathrm{i}\,\mathrm{Tr}\, D^<(t,t) = \{8.347 \cdot 10^6, 8.446 \cdot 10^6\}$, which means that the short-memory value deviates only by about 0.012.

be possible nor required in T-direction. One solution here would be to transform the equations of motion to Wigner coordinates and then to construct a grid with different spacings in the two orthogonal time directions. Yet there is an even simpler approach. Any integral over relatively fast decaying Green functions will be computable at sufficient precision over a small support that does not grow as the two-time grid expands towards its final size. In the same spirit, computing points far off the "time diagonal" $\tau = 0$ will be superfluous because they are negligible in the first place. This way, by truncating the number of steps we move away from the time diagonal, and by restricting the computation of the integrals to that same narrow "band", it is indeed possible to achieve a quasi-linear scaling in the number of grid points without losing substantial accuracy.

The quantitative consequences of different truncation parameters n_{mem} are studied in Figs. 5.17 and 5.18. Note that technically, n_{mem} is *not* the number of points included away from the diagonal moving in τ-direction, but rather moving in the vertical and horizontal directions t and t'. As one may understand from Fig. 5.18, a short-valued memory $n_{\mathrm{mem}} = 24$ results in a certain number of points inaccurately remaining zero. With a longer-valued memory $n_{\mathrm{mem}} = 64$, these points attain their proper values. However, looking to Fig. 5.17, we see that the influence of this inaccuracy is not even considerable (at least for similar parameters). Needless to say, computing all of the points and the full integrals for a grid of final size 2^{13} would be abominably expensive and yet bring no noticeable improvement.

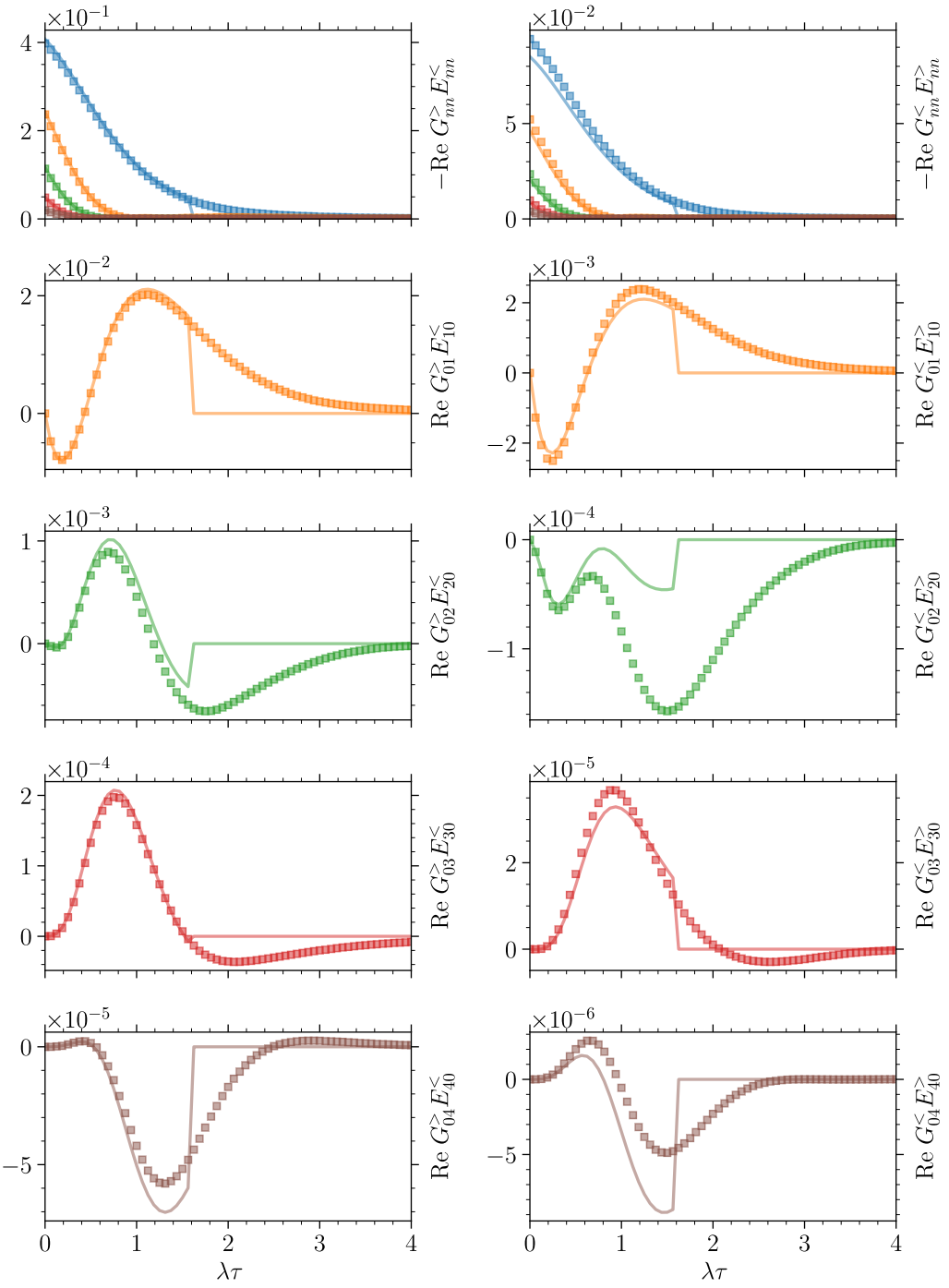

Figure 5.18: Influence of the memory truncation on the photon T-matrices. The initial conditions and parameters are identical to those of Fig. 5.17. The solid lines belong to the shorter memory time $\lambda\tau_{\mathrm{mem}} = 1.5$. The time arguments are $G^{\lessgtr}_{mn} E^{\gtrless}_{nm} = G^{\lessgtr}_{mn}(t, t-\tau) E^{\gtrless}_{nm}(t-\tau, t)$, where the center-of-mass time $T = t$ is indicated by the vertical dashed line in Fig. 5.17. The color code is explained in Fig. 5.20.

5.6 Markovian Limit & Photon-BEC Gross-Pitaevskii Equation

To establish a connection with Chp. 4 where the photon BEC was investigated by means of the rate equations (4.27a), it is very instructive to see how the fully non-Markovian equations of motion give rise to the rate equations in a certain form of *memoryless* limit, which is the topic of 5.6.1. In the same spirit, in 5.6.2 we will apply the auxiliary-boson technique to the master equation (4.26) from which the vibrational degrees of freedom have already been removed.

5.6.1 Derivation of the Rate Equations from the Non-Markovian Model

The forward dynamics of the photons is given by[8]

$$\partial_T \boldsymbol{D}^<(t,t) = -\mathrm{i}[\boldsymbol{h}_D, \boldsymbol{D}^<(t,t)] + Mg^2 \int_0^t \mathrm{d}\bar{t}\; I_D(t,\bar{t}), \tag{5.99}$$

where the memory integral kernel is now

$$\begin{aligned} I_D(t,\bar{t}) = {} & \mathrm{Tr}\left[\boldsymbol{E}^>(t,\bar{t})\boldsymbol{G}^<(\bar{t},t)\right]\boldsymbol{D}^<(\bar{t},t) + \mathrm{Tr}\left[\boldsymbol{G}^<(t,\bar{t})\boldsymbol{E}^>(\bar{t},t)\right]\boldsymbol{D}^<(t,\bar{t}) \\ & - \mathrm{Tr}\left[\boldsymbol{E}^<(t,\bar{t})\boldsymbol{G}^>(\bar{t},t)\right]\boldsymbol{D}^>(\bar{t},t) - \mathrm{Tr}\left[\boldsymbol{G}^>(t,\bar{t})\boldsymbol{E}^<(\bar{t},t)\right]\boldsymbol{D}^>(t,\bar{t}). \end{aligned} \tag{5.100}$$

The trace over the pseudo-particles involves all of the off-diagonal Green functions, i.e.

$$\int_{t_0}^t \mathrm{d}\bar{t}\; \mathrm{Tr}\left[\boldsymbol{E}^>(t,\bar{t})\boldsymbol{G}^<(\bar{t},t)\right]\boldsymbol{D}^<(\bar{t},t) = \int_0^t \mathrm{d}\bar{t} \sum_{m,n=0}^{\infty} E^>_{mn}(t,\bar{t})G^<_{nm}(\bar{t},t)\boldsymbol{D}^<(\bar{t},t). \tag{5.101}$$

Since the ground- and excited-state Hamiltonians differ,[9] there does not exist a simultaneous eigenbasis for the two, even though they have identical eigenvalues. Neither can the polaron transformation be employed to get rid of the off-diagonals because they come back into the problem via the then off-diagonal self-energies. Therefore, we do not apply any basis transformation to simplify the traces in Eq. (5.99).[10] When the vibrational states have a fast relaxation, or in other words are strongly broadened by collisions with the surrounding solvent, the dynamics of the pseudo-particles in τ direction is approximately stationary and independent of the dynamics in T direction. Additionally, the vibrational states can only have an overall forward evolution, which is to say that a quantum going either into the ground- or excited-state manifold will end up in vibrational state n with a fixed probability p_n, where $\sum_n p_n = 1$. This enables us to write, for instance,

$$G^<_{nm}(t,t') = G^<(t,t)\mathrm{e}^{-\Gamma_\uparrow \tau/2} g_{nm}(\tau), \tag{5.102}$$

[8] For this paragraph, we drop the explicit inclusion of the various driven-dissipative processes.

[9] They have hopping elements of opposite sign.

[10] In the following, one should also bear in mind that the off-diagonal greater functions are always zero at equal times whereas the diagonal ones are complex unity, i.e. $G^>_{mn}(t,t) = -\mathrm{i}\delta_{mn}$.

where $g_{nm}(\tau)$ encodes the relative-time dynamics of $G^<_{nm}(t,t')$ beyond the effect of $\Gamma_\uparrow$, that is, the vibrational frequencies and relaxation. It has the property $g_{nm}(0) = G^<_{nm}(t,t)/G^<(t,t)$, such that $g_{nn}(0) = p_n$. Note that the ground states are indeed not broadened by $\Gamma_\downarrow$. The corresponding expression for the excited states reads

$$E^<_{mn}(t,t') = E^<(t,t)\mathrm{e}^{-\Gamma_\downarrow \tau/2} e_{mn}(\tau), \tag{5.103}$$

where similarly $e_{nm}(0) = E^<_{nm}(t,t)/E^<(t,t)$. This allows us now to write the total number of excited molecules as

$$\langle M_\uparrow\rangle(t) = \mathrm{i}M\,\mathrm{Tr}\,\boldsymbol{E}^<(t,t) = \mathrm{i}M\sum_{n=0}^{\infty} E^<_{nn}(t,t) = \mathrm{i}ME^<(t,t), \tag{5.104}$$

and similarly for the ground state where

$$M - \langle M_\uparrow\rangle(t) = \mathrm{i}M\,\mathrm{Tr}\,\boldsymbol{G}^<(t,t) = \mathrm{i}M\sum_{n=0}^{\infty} G^<_{nn}(t,t) = \mathrm{i}MG^<(t,t), \tag{5.105}$$

such that the constraint $\hat{Q} = 1$ ensures total number conservation. Now, the stationarity assumption of the pseudo-particle τ dynamics assures that their greater functions do not have a T dependence ($E^>_{mn}(t,t') = E^>_{mn}(t-t')$ and analogously for $G^>_{mn}$). Finally, apart from rapidly oscillating phase factors, for small cavity loss the photon lesser Green functions can be considered constant over the narrow support of the highly dissipative greater functions around the equal-time diagonal. With this in mind, pulling out a factor of $\exp(-\Gamma_\downarrow\tau/2)$ from the greater function, we can combine the above approximations to write

$$\begin{aligned}
&Mg^2\int_0^t \mathrm{d}\bar{t}\;\mathrm{Tr}\left[\boldsymbol{E}^>(t,\bar{t})\boldsymbol{G}^<(\bar{t},t)\right] D^<_{kk}(\bar{t},t) \approx D^<_{kk}(t,t)MG^<(t,t)\sum_{m,n=0}^{\infty} g^2 \\
&\qquad\times\int_0^t \mathrm{d}\bar{t}\left\{\mathrm{e}^{\mathrm{i}\delta_k(t-\bar{t})}\mathrm{e}^{-\left(\Gamma_\uparrow+\Gamma_\downarrow\right)(t-\bar{t})/2}\left[\mathrm{e}^{\Gamma_\downarrow(t-\bar{t})/2}E^>_{mn}(t-\bar{t})g_{nm}(\bar{t}-t)\right]\right\} \\
&= -n_k(t)\left[M-\langle M_\uparrow\rangle(t)\right]\sum_{m,n=0}^{\infty} g^2\int_0^t \mathrm{d}\tau\;\mathrm{e}^{\mathrm{i}\delta_k\tau}\mathrm{e}^{-\left(\Gamma_\uparrow+\Gamma_\downarrow\right)\tau/2}\left[\mathrm{e}^{\Gamma_\downarrow\tau/2}E^>_{mn}(\tau)g_{nm}(-\tau)\right] \\
&= \mathrm{i}n_k(t)\left[M-\langle M_\uparrow\rangle(t)\right]g^2\int_0^t \mathrm{d}\tau\;\mathrm{e}^{\mathrm{i}\delta_k\tau}\mathrm{e}^{-\left(\Gamma_\uparrow+\Gamma_\downarrow\right)\tau/2}A(\tau) = \mathrm{i}K(\delta_k)n_k(t)\left[M-\langle M_\uparrow\rangle(t)\right],
\end{aligned}$$

where we have also pulled out the factor of $-\mathrm{i}$ from the greater function, $\boldsymbol{G}^<$ and $\boldsymbol{E}^>$ have each contributed a phase factor proportional to $\Delta/2$, and $\delta_k = \omega_k - \Delta$ as before. Evidently, we have introduced $A(\tau) := \mathrm{i}\mathrm{e}^{\Gamma_\downarrow\tau/2}E^>_{mn}(\tau)g_{nm}(-\tau)$ as well as

$$K(\delta) := g^2\int_0^t \mathrm{d}\tau\;\mathrm{e}^{\mathrm{i}\delta\tau}\mathrm{e}^{-\left(\Gamma_\uparrow+\Gamma_\downarrow\right)\tau/2}A(\tau), \tag{5.106}$$

which plays the same role as Eq. (4.20) defined in Chp. 4.1.4. The final term of Eq. (5.100) can be treated analogously, yielding

$$\begin{aligned}
&Mg^2 \int_0^t \mathrm{d}\bar{t}\ \mathrm{Tr}\left[\boldsymbol{G}^{>}(t,\bar{t})\boldsymbol{E}^{<}(\bar{t},t)\right] D^{>}_{kk}(t,\bar{t}) \\
&\approx -\left[n_k(t)+1\right]\langle M_\uparrow\rangle(t)\sum_{n=0}^{\infty} g^2 \int_0^t \mathrm{d}\tau\ \mathrm{e}^{-\mathrm{i}\delta_k\tau}\mathrm{e}^{-(\Gamma_\uparrow+\Gamma_\downarrow)\tau/2}\left[\mathrm{e}^{\Gamma_\uparrow\tau/2}G^{>}_{mn}(\tau)e_{nm}(-\tau)\right] \\
&= \mathrm{i}\left[n_k(t)+1\right]\langle M_\uparrow\rangle(t) g^2 \int_0^t \mathrm{d}\tau\ \mathrm{e}^{-\mathrm{i}\delta_k\tau}\mathrm{e}^{-(\Gamma_\uparrow+\Gamma_\downarrow)\tau/2}A(\tau) = \mathrm{i}K(-\delta_k)\left[n_k(t)+1\right]\langle M_\uparrow\rangle(t),
\end{aligned}$$

where we have used $\mathrm{e}^{\Gamma_\uparrow\tau/2}G^{>}_{mn}(\tau)e_{nm}(-\tau) = \mathrm{e}^{\Gamma_\downarrow\tau/2}E^{>}_{mn}(\tau)g_{nm}(-\tau)$. With the remaining terms from Eq. (5.100), we find in total that

$$\begin{aligned}
Mg^2 \int_0^t \mathrm{d}\bar{t}\, I_D(t,\bar{t}) \approx\ &\mathrm{i}\left[K(\delta_k)+K^*(\delta_k)\right] n_k(t)\left[M-\langle M_\uparrow\rangle(t)\right] \\
&-\mathrm{i}\left[K^*(-\delta_k)+K(-\delta_k)\right]\left[n_k(t)+1\right]\langle M_\uparrow\rangle(t) \\
=\ &2\mathrm{i}\,\mathrm{Re}\left[K(\delta_k)\right] n_k(t)\left[M-\langle M_\uparrow\rangle(t)\right] \\
&-2\mathrm{i}\,\mathrm{Re}\left[K(-\delta_k)\right]\left[n_k(t)+1\right]\langle M_\uparrow\rangle(t).
\end{aligned} \tag{5.107}$$

With $\partial_T D_{kk}(t,t) \equiv -\mathrm{i}\partial_t n_k(t)$, this reproduces the correct rate equation (4.29a) for the photons. The same analysis we have just performed can be repeated to obtain the rate equation for $\langle M_\uparrow\rangle(t)$ from the forward equation of motion of $\boldsymbol{E}^{<}$ (or for that matter $\boldsymbol{G}^{<}$), which we present for completeness,

$$\begin{aligned}
\partial_T \boldsymbol{G}^{<}(t,t) &= -\mathrm{i}[\boldsymbol{h}_G, \boldsymbol{G}^{<}(t,t)] + g^2 \int_0^t \mathrm{d}\bar{t}\, I(t,\bar{t}), \\
\partial_T \boldsymbol{E}^{<}(t,t) &= -\mathrm{i}[\boldsymbol{h}_E, \boldsymbol{E}^{<}(t,t)] - g^2 \int_0^t \mathrm{d}\bar{t}\, I(t,\bar{t}),
\end{aligned} \tag{5.108}$$

where the memory integral is given by

$$\begin{aligned}
I(t,\bar{t}) = &\boldsymbol{E}^{>}(t,\bar{t})\boldsymbol{G}^{<}(\bar{t},t)\,\mathrm{Tr}\,\boldsymbol{D}^{<}(\bar{t},t) \\
&+\boldsymbol{G}^{<}(t,\bar{t})\boldsymbol{E}^{>}(\bar{t},t)\,\mathrm{Tr}\,\boldsymbol{D}^{<}(t,\bar{t}) \\
&-\boldsymbol{E}^{<}(t,\bar{t})\boldsymbol{G}^{>}(\bar{t},t)\,\mathrm{Tr}\,\boldsymbol{D}^{>}(\bar{t},t) \\
&-\boldsymbol{G}^{>}(t,\bar{t})\boldsymbol{E}^{<}(\bar{t},t)\,\mathrm{Tr}\,\boldsymbol{D}^{>}(t,\bar{t}).
\end{aligned} \tag{5.109}$$

Figs. 5.19 and 5.20 illustrate how the assumptions leading up to Eq. (5.107) are reproduced naturally by the microscopic dynamics for according parameters. We may thus conclude that our model indeed constitutes a valid generalization of the existing treatments.

5.6.2 Application of Pseudo-Particles to the Master Equation

The discussion of the memoryless limit of our theory naturally leads us to ask if pseudo-particles can also be applied to the master equation (4.26)? This is essentially equivalent to investigating if summing over the vibrational states on the level of the Dyson equation yields the same results as performing the Born-Markov approximation in the framework of the density matrix. Clearly, the answer should be affirmative. Introducing the time-dependent fields $\phi(t)$, $\phi_\sigma(t)$, $\sigma = g,\, e$ for a single photon mode and pseudo-particles, respectively, and dropping $\Gamma_{\uparrow,\downarrow}$ for conciseness, we find the Schwinger-Keldysh actions

$$S_0^{\pm} = \int \mathrm{d}t \, \left\{ \phi_\pm^* \left[\mathrm{i}\partial_t - \delta \pm \mathrm{i}\kappa/2 \right] \phi_\pm + \phi_{g,\pm}^* \mathrm{i}\partial_t \phi_{g,\pm} + \phi_{e,\pm}^* \mathrm{i}\partial_t \phi_{e,\pm} \right\}, \tag{5.110}$$

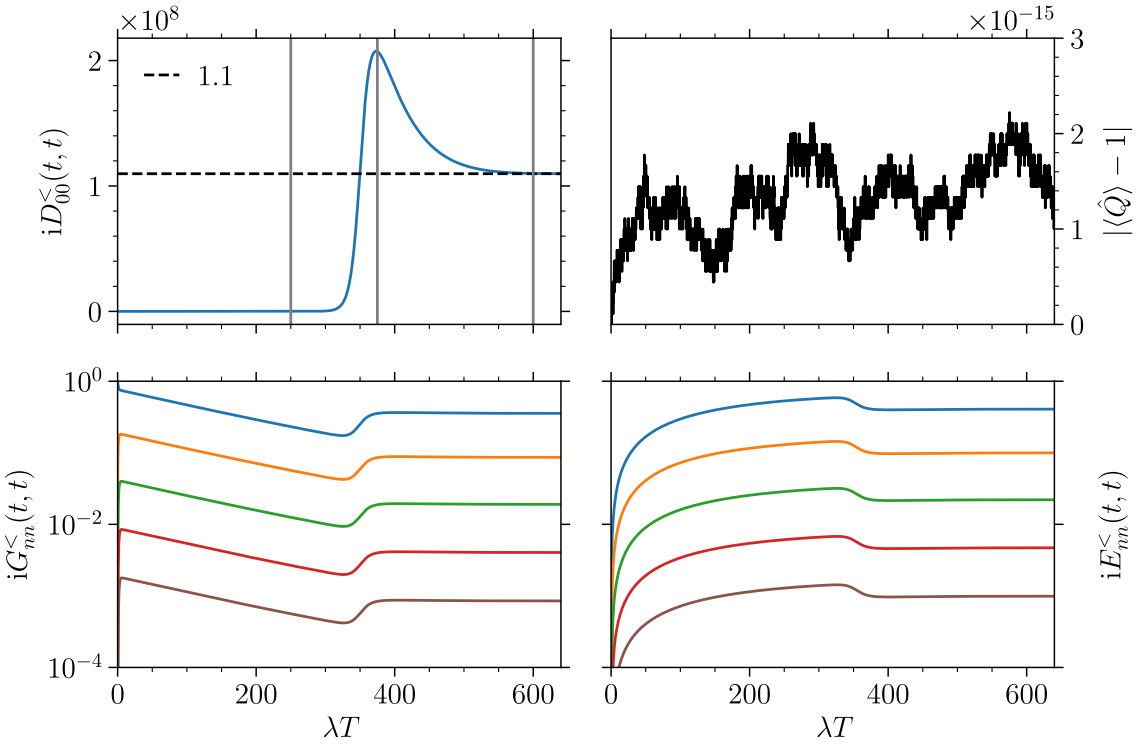

Figure 5.19: Forward dynamics of a single photon mode $k = 0$ with initial conditions $\mathrm{i}D^<_{00}(0,0) = 0$, $\mathrm{i}G^<_{00}(0,0) = 1$ (from which it follows via the operator constraint that all other vibrational states are unoccupied), and parameters $M = 10^9$, $g/\lambda = 9.0 \cdot 10^{-6}$, $\omega_0/\lambda = -0.2$, $\kappa/\lambda = 0.02$, $\Omega/\lambda = 0.2$, $S = 1.0$, $\bar{N} = 0.25$, $\Gamma_\uparrow/\lambda = 0.005$, $\Gamma_\downarrow = \Gamma_\uparrow/20$, and vibrational-state truncation at $n = 4$. Simulations calculated for 2^{12} steps up to a final time $\lambda T_{\mathrm{max}} = 640$ with a memory time of $\lambda\tau_{\mathrm{mem}} = 20.0$. The color code is explained in the caption of Fig. 5.20. The three vertical lines in the top left panel refer to the different center-of-mass times investigated also in Fig. 5.20. The average constraint $\langle \hat{Q} \rangle = 1$ is fulfilled to machine precision. The forward dynamics of the molecules indeed display the envelopes $G^<(t,t)$ and $E^<(t,t)$.

such that $S_0 = S_0^+ - S_0^- - \mathrm{i}\kappa \int \mathrm{d}t\ \phi_+\phi_-^*$. In the interacting part, for later use we also retain the thermally averaged coherent coupling g_β defined in 4.1.2 and hence obtain

$$\begin{aligned} S_{\mathrm{int}}^{\pm} = &-g_\beta \int \mathrm{d}t\ \left\{\phi_\pm^*\phi_{g,\pm}^*, \phi_{e,\pm} + \phi_\pm\phi_{g,\pm}, \phi_{e,\pm}^*\right\} \\ &\pm \mathrm{i}\frac{\Gamma^+}{2} \int \mathrm{d}t\ \phi_\pm^*(t)\phi_\pm(t^\mp)\phi_{g,\pm}^*(t)\phi_{g,\pm}(t^\mp)\phi_{e,\pm}(t)\phi_{e,\pm}^*(t^\mp) \\ &\pm \mathrm{i}\frac{\Gamma^-}{2} \int \mathrm{d}t\ \phi_\pm(t)\phi_\pm^*(t^\mp)\phi_{g,\pm}(t)\phi_{g,\pm}^*(t^\mp)\phi_{e,\pm}^*(t)\phi_{e,\pm}(t^\mp), \end{aligned} \tag{5.111}$$

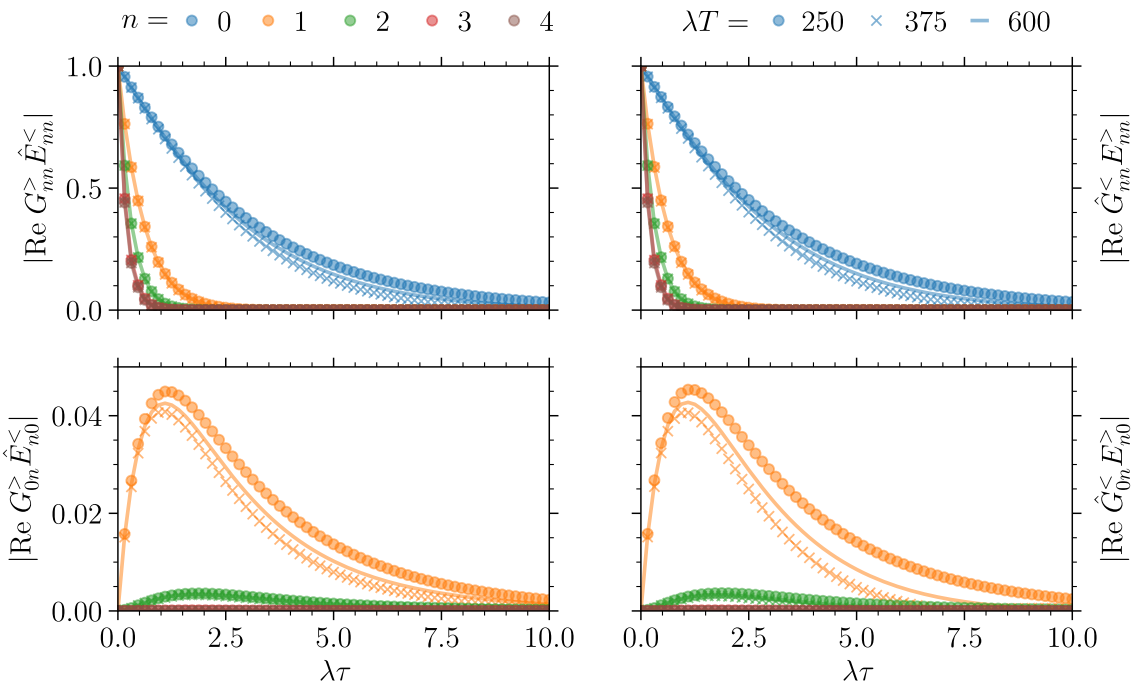

Figure 5.20: Relative-time dynamics of the quantities determining the emission and absorption spectrum for the same initial conditions and parameters as in Fig. 5.19. The time arguments are $G^{\lessgtr}_{mn}E^{\gtrless}_{nm} = G^{\lessgtr}_{mn}(t, t-\tau)E^{\gtrless}_{nm}(t-\tau, t)$. The hat notation signifies $\hat{G}^{<}_{mn} := G^{<}_{mn}(t, t-\tau)/G^{<}_{nn}(t, t)$, and $\hat{E}^{<}_{nm} := E^{<}_{nm}(t, t-\tau)/E^{<}_{nn}(t, t)$ (note that we have chosen this denominator instead of the envelopes simply for better visibility). Thus the functions which enter $A(\tau)$ are indeed found to be approximately T-independent. The slight variations that are visible can be further reduced with increasing λ. The center-of-mass times $\lambda T = \{250, 375, 600\}$ are marked by the vertical lines in the photon evolution shown in Fig. 5.19.

where we have time-ordered appropriately.[11] The total action then follows as

$$\begin{aligned} S &= S_0 + S_{\text{int}}^{+} - S_{\text{int}}^{-} \\ &\quad - \mathrm{i}\Gamma^{+} \int \mathrm{d}t\ \phi_{+}\phi_{e,+}^{*}\phi_{g,+}\phi_{-}^{*}\phi_{e,-}\phi_{g,-}^{*} \\ &\quad - \mathrm{i}\Gamma^{-} \int \mathrm{d}t\ \phi_{+}^{*}\phi_{g,+}^{*}\phi_{e,+}\phi_{-}\phi_{g,-}\phi_{e,-}^{*}. \end{aligned} \tag{5.112}$$

This is an interesting example of a physically arising vertex with *six* fields in total. In terms of the lengthy total field spinor

$$\begin{aligned} \boldsymbol{\phi} &= \left(\phi_{+}, \phi_{+}^{*}, \phi_{g,+}, \phi_{g,+}^{*}, \phi_{e,+}, \phi_{e,+}^{*}, \phi_{-}, \phi_{-}^{*}, \phi_{g,-}, \phi_{g,-}^{*}, \phi_{e,-}, \phi_{e,-}^{*}\right)^{T} \\ &= \left(\phi_1, \phi_2, \phi_3, \phi_4, \phi_5, \phi_6, \phi_7, \phi_8, \phi_9, \phi_{10}, \phi_{11}, \phi_{12}\right)^{T}, \end{aligned} \tag{5.113}$$

and with the condensate-fluctuation decomposition $\phi_{\pm} = \Phi + \delta\phi_{\pm}$,[12] we find

$$\begin{aligned} S_0 = \int \mathrm{d}t\ \{&\delta\phi_2(\mathrm{i}\partial_t - \delta + \mathrm{i}\kappa/2)\delta\phi_1 + \phi_4\mathrm{i}\partial_t\phi_3 + \phi_6\mathrm{i}\partial_t\phi_5 - \delta\phi_8(\mathrm{i}\partial_t - \delta - \mathrm{i}\kappa/2)\delta\phi_7 \\ &-\phi_{10}\mathrm{i}\partial_t\phi_9 - \phi_{12}\mathrm{i}\partial_t\phi_{11} - \mathrm{i}\kappa\delta\phi_1\delta\phi_8 - \tilde{g}\left[\Phi^{*}\phi_4\phi_5 + \Phi\phi_3\phi_6 - \Phi^{*}\phi_{10}\phi_{11} - \Phi\phi_9\phi_{12}\right]\}. \end{aligned} \tag{5.114}$$

The interacting part then summarizes as

$$\begin{aligned} S_{\text{int}} = &\frac{\mathrm{i}\Gamma^{+}}{2} \int \mathrm{d}t\ \left(|\Phi|^2 + \delta\phi_1(t^{-})\delta\phi_2(t)\right)\phi_3(t^{-})\phi_4(t)\phi_5(t)\phi_6(t^{-}) \\ &+ \frac{\mathrm{i}\Gamma^{-}}{2} \int \mathrm{d}t\ \left(|\Phi|^2 + \delta\phi_1(t)\delta\phi_2(t^{-})\right)\phi_3(t)\phi_4(t^{-})\phi_5(t^{-})\phi_6(t) \\ &+ \frac{\mathrm{i}\Gamma^{+}}{2} \int \mathrm{d}t\ \left(|\Phi|^2 + \delta\phi_7(t^{+})\delta\phi_8(t)\right)\phi_9(t^{+})\phi_{10}(t)\phi_{11}(t)\phi_{12}(t^{+}) \\ &+ \frac{\mathrm{i}\Gamma^{-}}{2} \int \mathrm{d}t\ \left(|\Phi|^2 + \delta\phi_7(t)\delta\phi_8(t^{+})\right)\phi_9(t)\phi_{10}(t^{+})\phi_{11}(t^{+})\phi_{12}(t) \\ &- \mathrm{i}\Gamma^{+} \int \mathrm{d}t\ \left(|\Phi|^2 + \delta\phi_1\delta\phi_8\right)\phi_3\phi_6\phi_{10}\phi_{11} \\ &- \mathrm{i}\Gamma^{-} \int \mathrm{d}t\ \left(|\Phi|^2 + \delta\phi_2\delta\phi_7\right)\phi_4\phi_5\phi_9\phi_{12}, \end{aligned} \tag{5.115}$$

[11] Details on how to do this can be found in Sec. 3.1 and App. C.

[12] Here we do not introduce a contour subscript for the classical field because we already know that it should to satisfy $\Phi_{+} = \Phi_{-}$.

which results in a contribution to the effective action that reads[13]

$$\begin{aligned}
W^{(2)}[\varphi, G] = &\frac{\mathrm{i}\Gamma^{+}}{2}\int \mathrm{d}t\ (-\mathrm{i}G_{12}(t^{-},t) + \mathrm{i}^2\left|\varphi^2\right|)\left[G_{34}(t^{-},t)G_{56}(t,t^{-}) + G_{36}G_{45}\right] \\
&+ \frac{\mathrm{i}\Gamma^{-}}{2}\int \mathrm{d}t\ (-\mathrm{i}G_{12}(t,t^{-}) + \mathrm{i}^2\left|\varphi^2\right|)\left[G_{34}(t,t^{-})G_{56}(t^{-},t) + G_{36}G_{45}\right] \\
&+ \frac{\mathrm{i}\Gamma^{+}}{2}\int \mathrm{d}t\ (-\mathrm{i}G_{78}(t^{+},t) + \mathrm{i}^2\left|\varphi^2\right|)\left[G_{9,10}(t^{+},t)G_{11,12}(t,t^{+}) + G_{9,12}G_{10,11}\right] \\
&+ \frac{\mathrm{i}\Gamma^{-}}{2}\int \mathrm{d}t\ (-\mathrm{i}G_{78}(t,t^{+}) + \mathrm{i}^2\left|\varphi^2\right|)\left[G_{9,10}(t,t^{+})G_{11,12}(t^{+},t) + G_{9,12}G_{10,11}\right] \\
&- \mathrm{i}\Gamma^{+}\int \mathrm{d}t\ (-\mathrm{i}G_{18} + \mathrm{i}^2|\varphi|^2)\left[G_{3,10}G_{6,11} + G_{36}G_{10,11}\right] \\
&- \mathrm{i}\Gamma^{-}\int \mathrm{d}t\ (-\mathrm{i}G_{27} + \mathrm{i}^2|\varphi|^2)\left[G_{49}G_{5,12} + G_{45}G_{9,12}\right].
\end{aligned} \tag{5.116}$$

For the photon Green functions, we then find equations of motion

$$\begin{aligned}
0 = &\Bigg\{ [\mathrm{i}\partial_t - \delta + \mathrm{i}\kappa/2] - \frac{\mathrm{i}\Gamma^{+}}{2}\left[G^{T}(t^{-},t)E^{T}(t,t^{-}) + \Delta^{T,\dagger}(t,t)\Delta^{T}(t,t)\right] \\
&- \frac{\mathrm{i}\Gamma^{-}}{2}\left[G^{T}(t,t^{-})E^{T}(t^{-},t) + \Delta^{T,\dagger}(t,t)\Delta^{T}(t,t)\right]\Bigg\} D^{<}(t,t') \\
&+ \mathrm{i}\Gamma^{-}\left[G^{>}(t,t)E^{<}(t,t) + \Delta^{T}(t,t)\Delta^{\tilde{T},\dagger}(t,t)\right] D^{\tilde{T}}(t,t'), \\
0 = &\Bigg\{ -[\mathrm{i}\partial_t - \delta - \mathrm{i}\kappa/2] - \frac{\mathrm{i}\Gamma^{+}}{2}\left[G^{\tilde{T}}(t^{+},t)E^{\tilde{T}}(t,t^{+}) + \Delta^{\tilde{T},\dagger}(t,t)\Delta^{\tilde{T}}(t,t)\right] \\
&- \frac{\mathrm{i}\Gamma^{-}}{2}\left[G^{\tilde{T}}(t,t^{+})E^{\tilde{T}}(t^{+},t) + \Delta^{\tilde{T},\dagger}(t,t)\Delta^{\tilde{T}}(t,t)\right]\Bigg\} D^{>}(t,t') \\
&- \Big\{\mathrm{i}\kappa - \mathrm{i}\Gamma^{+}\left[G^{<}(t,t)E^{>}(t,t) + \Delta^{T,\dagger}(t,t)\Delta^{\tilde{T}}(t,t)\right]\Big\} D^{T}(t,t'),
\end{aligned} \tag{5.117}$$

where we have introduced the new Green functions

$$\begin{aligned}
\Delta^{T}(t,t') &= -\mathrm{i}\langle \mathcal{T} d_e(t) d_g^{\dagger}(t')\rangle = -\mathrm{i}\langle \phi_{e,+}(t)\phi_{g,+}^{*}(t')\rangle, \\
\Delta^{T,\dagger}(t,t') &= -\mathrm{i}\langle \mathcal{T} d_g(t) d_e^{\dagger}(t')\rangle = -\mathrm{i}\langle \phi_{g,+}(t)\phi_{e,+}^{*}(t')\rangle.
\end{aligned} \tag{5.118}$$

and their corresponding anti-timed-ordered varieties. Their lesser and greater components obey $\Delta^{\lessgtr,\dagger}(t,t') = -[\Delta^{\lessgtr}(t',t)]^{\dagger}$. These functions are only relevant when a symmetry-broken solution

[13] Note that the additional factor (with $\hbar$ restored) from the expansion of $W^{(2)}$ is in this case $\mathrm{i}\hbar\cdot(-\mathrm{i}) \equiv 1$ because of the Lindbladian character of the interaction.

with a condensate amplitude $\varphi(t)$ is to be considered (in which case they are crucial). From their definition, we conclude they describe the coherence between the ground and excited states of the molecules. As usual for pseudo-particles, the greater function must have the important property

$$\Delta^{>}(t,t) = 0. \tag{5.119}$$

Below, we briefly come back to these functions; to verify the Markovian limit, we set $\varphi = 0$ and may hence discard them. For a very large number of molecules, the lesser function now obeys[14]

$$\begin{aligned}
(\mathrm{i}\partial_t - \delta + \mathrm{i}\kappa/2)\, D^{<}(t,t') &= M\left\{\frac{\mathrm{i}\Gamma^{+}}{2}G^{<}(t,t)E^{>}(t,t) + \frac{\mathrm{i}\Gamma^{-}}{2}G^{>}(t,t)E^{<}(t,t)\right\}D^{<}(t,t') \\
&\quad - \mathrm{i}M\Gamma^{-}G^{>}(t,t)E^{<}(t,t)D^{\tilde{T}}(t,t'), \\
\left(\mathrm{i}\partial_{t'} + \delta + \mathrm{i}\kappa/2\right) D^{<}(t,t') &= M\left\{\frac{\mathrm{i}\Gamma^{+}}{2}G^{<}(t,t)E^{>}(t,t) + \frac{\mathrm{i}\Gamma^{-}}{2}G^{>}(t,t)E^{<}(t,t)\right\}D^{<}(t,t') \\
&\quad - \mathrm{i}M\Gamma^{-}G^{>}(t,t)E^{<}(t,t)D^{T}(t,t'),
\end{aligned} \tag{5.120}$$

such that in the equal-time limit, we correctly obtain

$$\begin{aligned}
(\mathrm{i}\partial_T + \mathrm{i}\kappa)\, D^{<}(t,t) &= M\left[\Gamma^{+}G^{<}(t,t) + \Gamma^{-}E^{<}(t,t)\right] D^{<}(t,t') \\
&\quad - M\Gamma^{-}E^{<}(t,t)\left[D^{>}(t,t) + D^{<}(t,t)\right] \\
&= M\left[\Gamma^{+}G^{<}(t,t)D^{<}(t,t) - \Gamma^{-}E^{<}(t,t)D^{>}(t,t)\right].
\end{aligned} \tag{5.121}$$

This underlines once more the importance of properly taking care of the time-ordered Green functions. For the greater function, we have

$$\begin{aligned}
(\mathrm{i}\partial_t - \delta - \mathrm{i}\kappa/2)\, D^{>}(t,t') &= -M\left\{\frac{\mathrm{i}\Gamma^{+}}{2}G^{<}(t,t)E^{>}(t,t) + \frac{\mathrm{i}\Gamma^{-}}{2}G^{>}(t,t)E^{<}(t,t)\right\}D^{>}(t,t') \\
&\quad - \left\{\mathrm{i}\kappa - \mathrm{i}M\Gamma^{+}G^{<}(t,t)E^{>}(t,t)\right\}D^{T}(t,t'),
\end{aligned} \tag{5.122}$$

which in the equal-time limit dutifully produces the same result. The equations for $G^{<}(t,t)$ and $E^{<}(t,t)$ can also be calculated from S_0 and Eq. (5.116) in the established manner. The present results further substantiate the general validity of our approach.

[14] Here we have rather sweepingly repeated the resummation over many incoherent molecules described in 5.2.5. The influence of a single molecule would scale as $\mathcal{O}(\zeta)$ and hence drop out from the photon dynamics.

5.6.3 Gross-Pitaevskii Equation

Even though we are not going to investigate it in the remainder of this thesis, the proper Gross-Pitaevskii equation of the photon BEC is interesting in its own right and a novel result that we should present for completeness. Taking the derivative of the effective action with respect to $\varphi^*(t)$, we find

$$\begin{aligned} 0 &= (\mathrm{i}\partial_t - \delta + \mathrm{i}\kappa/2)\,\varphi(t) - \mathrm{i}g_\beta\left(\Delta^<(t,t) + \Delta^>(t,t)\right) \\ &\quad - \frac{\mathrm{i}\Gamma^+}{2}\varphi(t)\left[G^<(t,t)E^>(t,t) + \mathcal{O}(\zeta^2)\right] \\ &\quad - \frac{\mathrm{i}\Gamma^-}{2}\varphi(t)\left[G^>(t,t)E^<(t,t) + \mathcal{O}(\zeta^2)\right] \\ &\quad + \mathrm{i}\Gamma^-\varphi(t)\left[G^>(t,t)E^<(t,t) + \mathcal{O}(\zeta^2)\right]. \end{aligned} \tag{5.123}$$

With $G^>(t,t) = E^>(t,t) = -\mathrm{i}$ and $\Delta^>(t,t) = 0$, dropping the $\mathcal{O}(\zeta^2)$ contributions, and applying the same reasoning we have already used for the photon Green functions $D^{\lessgtr}$ when it comes to the resummation over many incoherent molecules,[15] this becomes

$$\mathrm{i}\partial_t\varphi(t) = (\delta - \mathrm{i}\kappa/2)\,\varphi(t) + \mathrm{i}Mg_\beta\Delta^<(t,t) + \frac{M}{2}\left[\Gamma^+G^<(t,t) - \Gamma^-E^<(t,t)\right]\varphi(t), \tag{5.124}$$

which needs to be complemented by equations for $E^<(t,t)$ and $\Delta^<(t,t)$. Deriving a fully space-dependent version of this equation will be left for future projects. Note that it is indeed inhomogeneous, a fact that one may anticipate from the structure of the g_β-vertex. While it is otherwise superficially linear in $\varphi(t)$, it is still, of course, a non-linear equation by virtue of the terms proportional to $\Gamma^\pm$. We can also appreciate that $\Delta^<$ is indeed crucial for non-trivial solutions to exist. As the last result of this section, consider the evolution of the excited-state lesser function,

$$\begin{aligned} \mathrm{i}\partial_t E^<(t,t') &= g_\beta\varphi(t)\Delta^{<,\dagger}(t,t') + \frac{\Gamma^-}{2}\left(\mathrm{i}D^>(t,t) + |\varphi(t)|^2\right)G^>(t,t)E^<(t,t') \\ &\quad - \Gamma^+\left(\mathrm{i}D^<(t,t) + |\varphi(t)|^2\right)G^<(t,t)E^T(t,t') \\ &\quad + \frac{1}{2}\left[\Gamma^+\left(\mathrm{i}D^<(t,t) + |\varphi(t)|^2\right) + \Gamma^-\left(\mathrm{i}D^>(t,t) + |\varphi(t)|^2\right)\right]\Delta^>(t,t)\Delta^{<,\dagger}(t,t') \\ &\quad - \Gamma^+\left(\mathrm{i}D^<(t,t) + |\varphi(t)|^2\right)\Delta^>(t,t)\Delta^{<,\dagger}(t,t') + O(\zeta^2) \\ &= g_\beta\varphi(t)\Delta^{<,\dagger}(t,t') + \frac{\Gamma^-}{2}\left(\mathrm{i}D^>(t,t) + |\varphi(t)|^2\right)G^>(t,t)E^<(t,t') \\ &\quad - \Gamma^+\left(\mathrm{i}D^<(t,t) + |\varphi(t)|^2\right)G^<(t,t)E^T(t,t'), \end{aligned} \tag{5.125}$$

[15] One should investigate this in more detail to see if there are subtleties involved (certainly when going over to a space-dependent condensate $\varphi(x,t)$).

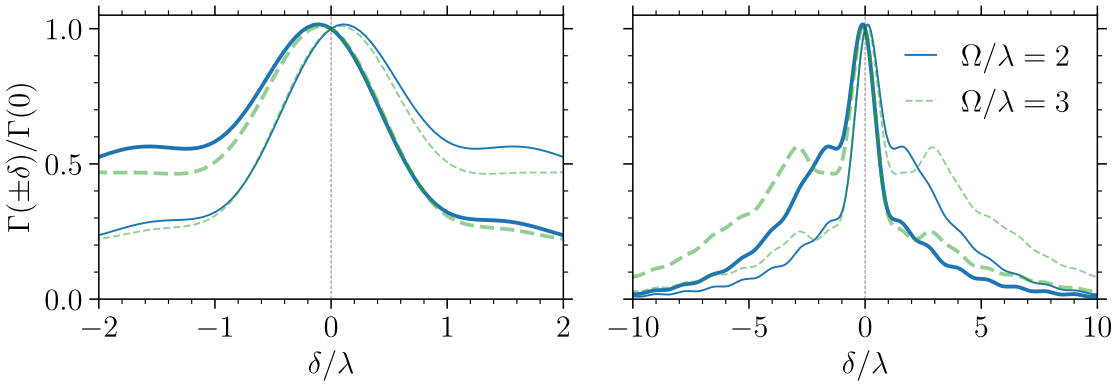

Figure 5.21: Microscopic steady-state emission (dashed line) and absorption (solid line) spectra $\Gamma^{\pm}(\delta)$ *without* the approximate assumptions $g_{nm}(t,t') = g_{nm}(\tau)$ and $e_{mn}(t,t') = e_{mn}(\tau)$ (cf. Eqs. (5.102) and (5.103)) for initial conditions $\mathrm{i}\,\mathrm{Tr}\,\boldsymbol{G}^{<}(0,0) = \mathrm{i}\,\mathrm{Tr}\,\boldsymbol{E}^{<}(0,0) = 1/2$, and parameters $g = 0$ (i.e. only the molecules are considered), $\Omega/\lambda = \{2,3\}$, $S = 0.25$, $\bar{N} = 0.25$, $\Gamma_{\uparrow} = \Gamma_{\downarrow} = 0$, and vibrational-state truncation at $n = 4$. At the zero-phonon line $\delta = 0$, the emission and absorption coefficient that would enter the rate equations have the same value $\lambda\Gamma(0) = g^2 \cdot \{1.298, 0.970\}$. Simulations calculated for 2^{11} steps up to a final time $\lambda T_{\mathrm{max}} = 16$ with a memory time of $\lambda\tau_{\mathrm{mem}} = 5.0$. The spectra are taken at "half time" $\lambda T = 8.0$.

which possesses the correct equal-time limit. The equation for $\Delta^{<}(t,t')$ follows analogously. As a final remark, consider that $\Delta^{<}(t,t) = -\mathrm{i}\langle d_g^{\dagger}(t) d_e(t)\rangle$ is connected to the "anomalous" expectation value $\langle\sigma^{-}(t)\rangle$, which is only non-zero when evaluated in a spin coherent state. These interesting perspectives will be considered elsewhere.

5.7 Molecular Spectra and Kennard-Stepanov Relation

This Sec. discusses the molecular spectra produced by our method when no simplifying assumptions are made. The resulting spectra should satisfy the Kennard-Stepanov relation (4.23) at least in the vicinity of the zero-phonon line $\delta = 0$. Technically, the emission and absorption curves are related to the photon T-matrices via

$$\begin{aligned}
\Gamma^{-}(\delta) &= -2g^2\,\mathrm{Re}\left[\mathrm{i}\,\mathrm{Tr}\,\boldsymbol{E}^{<}(t,t)\right]^{-1}\int_0^t \mathrm{d}(t-\bar{t})\;\mathrm{e}^{-\mathrm{i}\delta(t-\bar{t})}\mathrm{e}^{-(\Gamma_{\uparrow}+\Gamma_{\downarrow})(t-\bar{t})/2}\,\mathrm{Tr}\,\widetilde{\boldsymbol{G}}^{>}(t,\bar{t})\widetilde{\boldsymbol{E}}^{<}(\bar{t},t),\\
\Gamma^{+}(\delta) &= -2g^2\,\mathrm{Re}\left[\mathrm{i}\,\mathrm{Tr}\,\boldsymbol{G}^{<}(t,t)\right]^{-1}\int_0^t \mathrm{d}(t-\bar{t})\;\mathrm{e}^{-\mathrm{i}\delta(t-\bar{t})}\mathrm{e}^{-(\Gamma_{\uparrow}+\Gamma_{\downarrow})(t-\bar{t})/2}\,\mathrm{Tr}\,\widetilde{\boldsymbol{G}}^{<}(t,\bar{t})\widetilde{\boldsymbol{E}}^{>}(\bar{t},t),
\end{aligned} \tag{5.126}$$

where the tilde symbols indicate that we have pulled the exponential factors $\exp\left(\mathrm{i}\Delta(t-\bar{t})\right)$ and $\exp\left\{-\left(\Gamma_{\uparrow}+\Gamma_{\downarrow}\right)(t-\bar{t})/2\right\}$ out of the trace. Defining $K(\delta)$ in this way occurs with the idea in mind that it is the right-hand sides of Eq. (5.126) acting in lieu of Eq. (4.20) when the parameters are chosen such that the full pseudo-particle dynamics effectively recovers the rate equations.

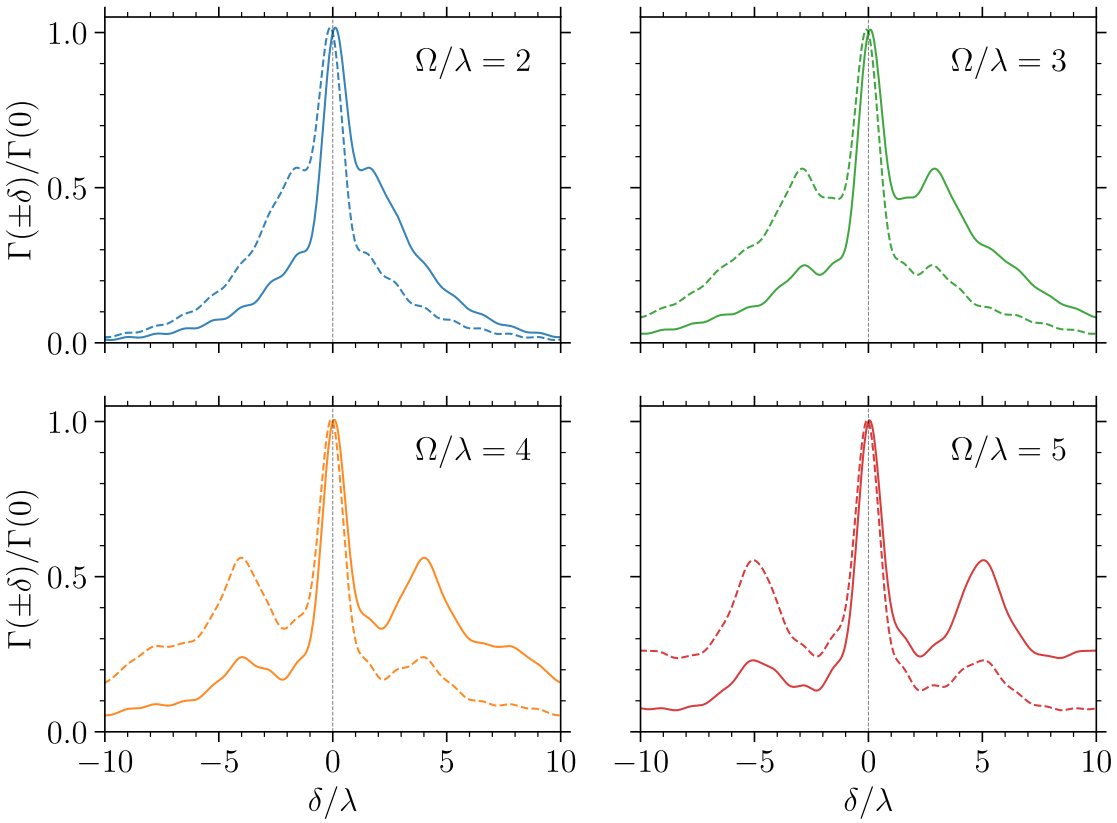

Figure 5.22: Microscopic steady-state emission and absorption spectra $\Gamma^{\pm}(\delta)$ for initial conditions $\mathrm{i}\,\mathrm{Tr}\,\boldsymbol{G}^{<}(0,0) = \mathrm{i}\,\mathrm{Tr}\,\boldsymbol{E}^{<}(0,0) = 1/2$, and parameters $g = 0$ (i.e. only the molecules are considered), $\Omega/\lambda = \{2,3,4,5\}$, $S = 0.25$, $\bar{N} = 0.25$, $\Gamma_{\uparrow} = \Gamma_{\downarrow} = 0$, and vibrational-state truncation at $n = 4$. At the zero-phonon line, we find $\lambda\Gamma(0) = g^2 \cdot \{1.298, 0.970, 0.833, 0.763\}$. Simulations done as in Fig. 5.21. Observe that the secondary peaks indeed appear at the correct location as specified by the respective value of the vibrational frequency Ω.

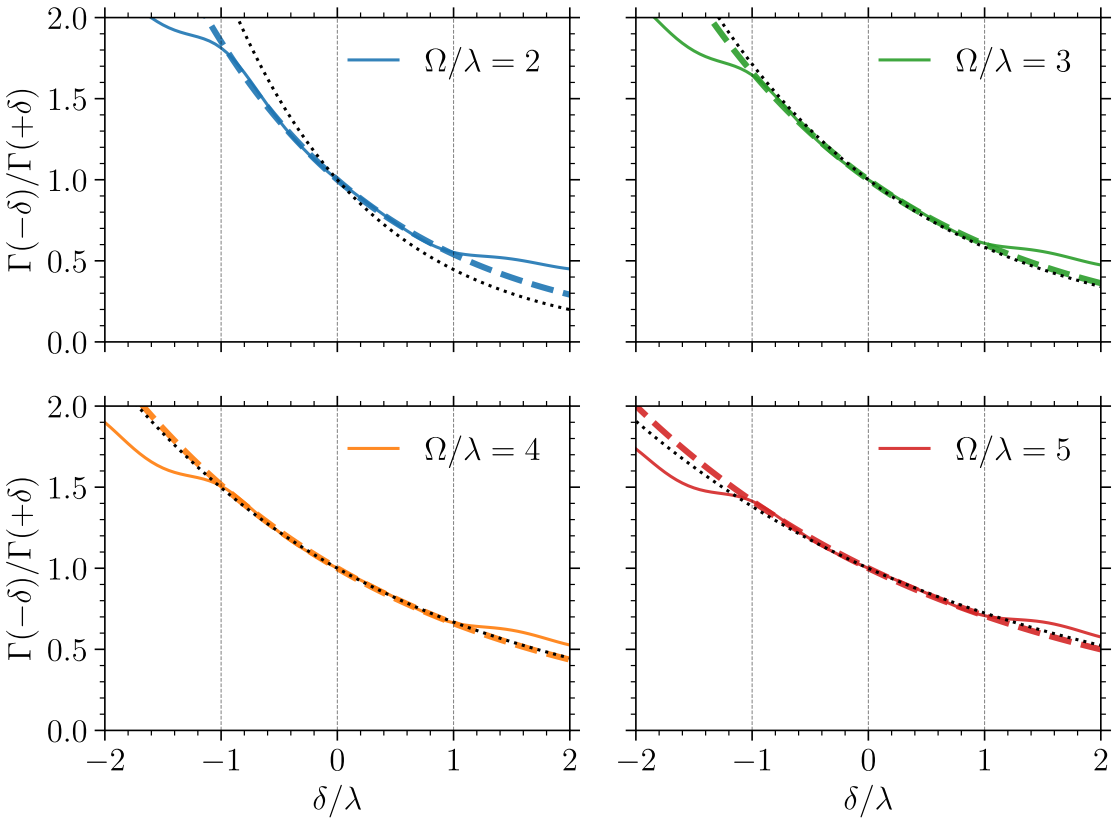

Figure 5.23: Ratio of steady-state emission and absorption spectra $\Gamma^{\pm}(\delta)$ as depicted in Fig. 5.22. The thick dashed lines show the best least-squares fit of the data to an exponential $\exp(-C \cdot \delta/\lambda)$ over the interval $\delta/\lambda \in [-1, 1]$, where the best fits for the constants are $C = \{0.616, 0.508, 0.415, 0.347\}$. The dotted (black) line shows the Kennard-Stepanov relation $\exp(-\hbar\delta/k_B T)$ for $T = 293$ K. Because of the thermal occupation $\bar{N} = 0.25$, the frequency scale is fixed implicitly to $\Omega \approx 62.2$ THz or $\hbar\Omega/k_B \approx 473$ K. A collection of photon modes placed inside the dashed vertical lines would attain a Bose-Einstein number distribution in the steady state.

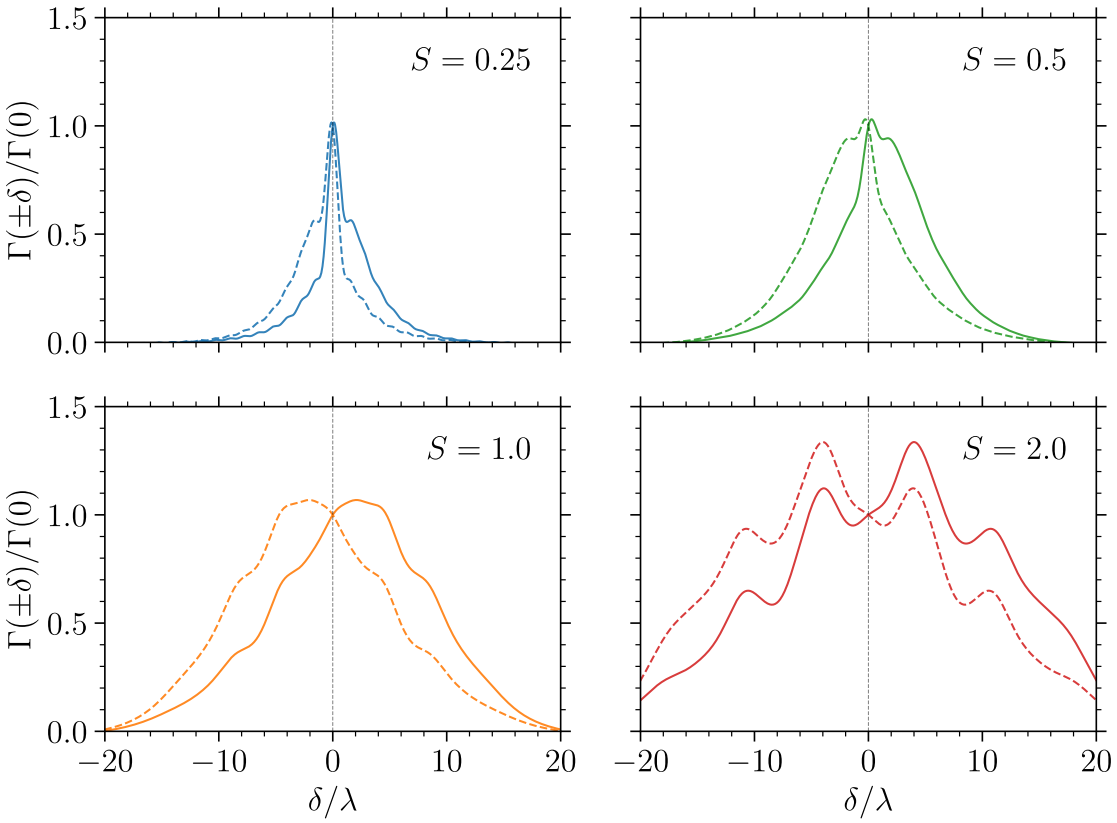

Figure 5.24: Steady-state emission (dashed line) and absorption (solid line) spectra $\Gamma^{\pm}(\delta)$ for initial conditions $\mathrm{i}\,\mathrm{Tr}\,\boldsymbol{G}^{<}(0,0) = \mathrm{i}\,\mathrm{Tr}\,\boldsymbol{E}^{<}(0,0) = 1/2$, and parameters $g = 0$ (i.e. only the molecules are considered), $\Omega/\lambda = 2$, $S = \{0.25, 0.5, 1.0, 2.0\}$, $\bar{N} = 0.25$, $\Gamma_{\uparrow} = \Gamma_{\downarrow} = 0$, and vibrational-state truncation at $n = 4$. At the zero-phonon line, we find $\lambda\Gamma(0) = g^2 \cdot \{1.298, 0.569, 0.300, 0.173\}$. Simulations done as in Fig. 5.21. The Huang-Rhys parameter S has a strong influence on the spectra. Note how the value at the zero-phonon line decreases with the increasing bandwidth.

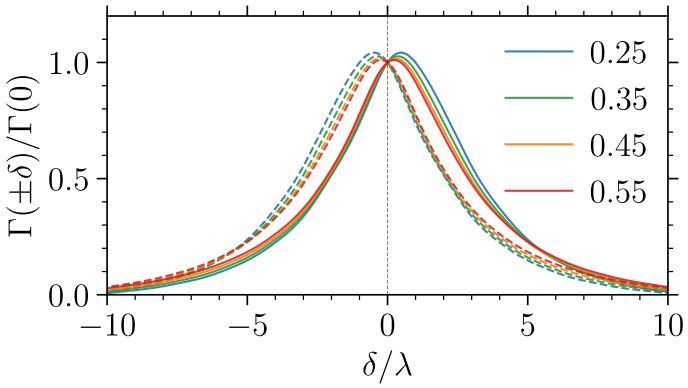

Figure 5.25: Microscopic steady-state emission and absorption spectra $\Gamma^{\pm}(\delta)$ for different values of $\bar{N} = \{0.25, 0.35, 0.45, 0.55\}$, initial conditions and $g = 0$ as above, $\Omega/\lambda = 1$, $S = 1$, $\Gamma_{\uparrow} = \Gamma_{\downarrow} = 0$, and vibrational-state truncation at $n = 4$. At the zero-phonon line, we find $\lambda\Gamma(0) = g^2 \cdot \{0.797, 0.786, 0.768, 0.745\}$. Simulations calculated for 2^{10} steps up to a final time $\lambda T_{\text{max}} = 16$ with a memory time of $\lambda\tau_{\text{mem}} = 3.5$. The spectra are taken at "half time" $\lambda T = 8.0$.

To investigate the spectra, we decouple the photons from the molecules by setting $g = 0$ and equally distribute the molecular population over the ground and excited manifolds. Moreover, we evolve the system such that it is in the steady state at "half-time", i.e in the center of the two-time square depicted in Fig. 2.3. This ensures that we have maximal time intervals at our disposal to compute the spectra. For vibrational frequencies on the order of 10 THz we know from Fig. 5.5 that the corresponding thermal occupation $\bar{N}$ will be low. In fact, one finds that a thermal occupation $\bar{N} = 0.25$ corresponds to a realistic vibrational frequency $\Omega \approx 62.2$ THz [17], which is equivalent to a temperature of $\hbar\Omega/k_B \approx 473$ K. Such a low value of $\bar{N}$ has the advantage that we do not have to include a very large number of vibrational states into the simulations. Truncation of these states at $n = 4$ (meaning that 5 states are included) is sufficient to produce physically realistic results. Fig. 5.21 compares two exemplary spectra for different ratios Ω/λ. In the right panel, the characteristic secondary peaks appear at the correct locations. The Kennard-Stepanov relation is in fact fulfilled around the zero-phonon line. Fig. 5.22 shows these two spectra again on a larger frequency interval, alongside with two more spectra at higher vibrational frequencies. For these four panels, Fig. 5.23 compares the ratios $\Gamma(-\delta)/\Gamma(+\delta)$ to the Kennard-Stepanov relation at $T = 293$ K. A least-squares fit on the interval $\delta \in [-1, 1]$ is used to determine the exponential constant. Within this interval around $\delta = 0$, the agreement is very good even four our relatively simple relaxation model. Placing a collection of photon modes inside this interval would hence result in these modes being thermally occupied according to a Bose-Einstein distribution. Outside the interval, the spectra do no longer satisfy the Kennard-Stepanov relation, which also holds true for the spectra of real dye molecules. Fig. 5.24 presents some more results for different Huang-Rhys parameters S, which as expected has a strong effect on the peak structure. Note that the height of the spectra decreases strongly with the growing width. Finally, in Fig. 5.25 we do not find a strong dependence of the spectra on $\bar{N}$. These results are very encouraging as regards the general ability of the auxiliary-boson method to describe the relevant physics.

$\lambda\Gamma^-(-1,0)$	$\lambda\Gamma^+(-1,0)$	c_1^-	c_1^+	c_2^-	c_2^+
$g^2 \cdot 0.7960$	$g^2 \cdot 0.5900$	-0.1200	-0.0480	0.0085	0.0010

Table 5.2: Fit parameters for modeling the dependence of emission and absorption on the external pumping according to Eq. (5.127).

One should not forget that the spectra presented here are calculated for $\Gamma_\uparrow = \Gamma_\downarrow = 0$. The additional broadening in Eq. (4.20) due to these processes is automatically included by the auxiliary-boson method if the two parameters are different from zero. When they are small compared to λ, this effect is not pronounced. From our method, it also becomes evident that in general κ will have a similar influence on the emission and absorption spectra.

5.8 Non-Markovian Corrections to the Phase-Diagram Boundary

This final part is devoted to answering the question brought up in the introduction to Chp. 5 and discussed in Fig. 5.1: Is the $g^{(2)}$ phase diagram bounded from above, and if so, does the system timescale κ influence the dynamics beyond the approximation provided by the rate equations (cf. Chp. 4)? The first part of the question regarding the upper boundary will be addressed on the basis of the rate equations. For the second part, the quantitative corrections due to the non-separable system-reservoir timescales, we employ the full capacity of the formalism developed above. Unlike Chp. 4 where we were restricted to a small region of the $g^{(2)}$ phase diagram for which the spectral influence of the external pumping could be neglected ($\Gamma_\uparrow \ll \lambda$ in the notation of our microscopic model), the full exploration of the diagram requires us to take into account the emission and absorption coefficients $\Gamma^\pm$ as functions of $\Gamma_\uparrow$.[16] This is the topic of the first part of the present Sec. in 5.8.1. Afterwards, we present the closed $g^{(2)}$ phase diagram in 5.8.2. This Sec. is then concluded by a discussion of the quantitative corrections following from the full microscopic model in 5.8.3.

5.8.1 Emission and Absorption Spectrum

The emission and absorption spectrum following from the auxiliary-boson field theory for the parameters given in Tab. 5.3 is presented in Fig. 5.26. The single photon mode $k = 0$ that we want to study in reference to Chp. 4 is indicated by the dashed vertical line at $\delta = 0$. The peak displaced toward the left (red detuning) corresponds to the emission, whereas the peak displaced toward the right (blue detuning) models the absorption coefficient.

In Fig. 5.26, the influence of the external pumping $\Gamma_\uparrow$ is not taken into account on purpose. For the study of the entire $g^{(2)}$ phase diagram, however, this is no longer acceptable. The additional broadening due to the exponential factor $\mathrm{e}^{-\Gamma_\uparrow \tau/2}$ in Eq. (4.20) needs to be incorporated when computing the spectra from the photon T-matrices. Therefore, we treat the coefficients as functions

[16] While we do not neglect $\Gamma_\downarrow$, this parameter is kept constant and hence never goes into a regime where its influence on the spectra becomes noticeable compared to that of λ.

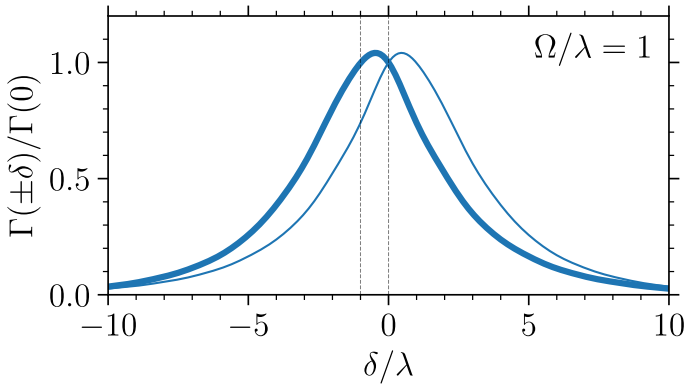

Figure 5.26: Steady-state emission (thick line) and absorption (thin line) spectra $\Gamma^{\pm}(\delta)$ as calculated from the steady-state photon T-matrix for initial conditions $\mathrm{i}\,\mathrm{Tr}\,\boldsymbol{G}^{<}(0,0) = \mathrm{i}\,\mathrm{Tr}\,\boldsymbol{E}^{<}(0,0) = 1/2$, parameters $S = 1.00$, $\bar{N} = 0.25$, $\Gamma_{\uparrow} = \Gamma_{\downarrow} = 0$, vibrational-state truncation at $n = 4$, and $\lambda\Gamma(0) = g^2 \cdot 0.798$. The thick line corresponds to the emission coefficient $\Gamma(-\delta)$. Simulations calculated for 2^{11} steps up to a final time of $\lambda T_{\mathrm{max}} = 16$ with memory time $\lambda\tau_{\mathrm{mem}} = 4.0$ ($n_{\mathrm{mem}} = 512$).

of both the detuning and the pumping by letting $\Gamma^{\pm} = \Gamma^{\pm}(\delta, \Gamma_{\uparrow})$.[17] Then the broadening effect of the pumping on emission and absorption at the location of the photon mode $k = 0$ can be modeled via the functions

$$\lambda\Gamma^{\pm}(\delta = -1, \Gamma_{\uparrow}) = g^2 \left(c_1^{\pm}\Gamma_{\uparrow}/\lambda + c_2^{\pm} \left(\Gamma_{\uparrow}/\lambda\right)^2 \right) + \lambda\Gamma^{\pm}(-1, 0), \tag{5.127}$$

where for the present system parameters the constants take the values given in Tab. 5.2. These constants can be obtained from fits to the numerically determined $\Gamma^{\pm}(\delta, \Gamma_{\uparrow})$. As expected, the broadening results in a *decrease* of $\Gamma^{\pm}$ as the pumping $\Gamma_{\uparrow}$ is ramped up. We emphasize again that this effect is included in the auxiliary-boson field theory by default, while within the framework of Chp. 4 it has to be taken into account by explicitly adjusting $\Gamma^{\pm}$. For larger values of $\Gamma_{\uparrow}/\lambda$, it turns out to have a non-trivial influence on the position of the boundary of the $g^{(2)}$.

5.8.2 Boundary of the Phase Diagram

With Eq. (5.127) at our disposal, we may compute the full boundary of the $g^{(2)}$ phase diagram along the lines of paragraph 4.2.11, where now emission and absorption also change along the $\Gamma_{\uparrow}$-axis. The result is presented in Fig. 5.27 (a): the phase diagram is indeed bounded instead of open. Note that neglecting Eq. (5.127) would entail a larger oscillating region with the phase boundary extending almost up to $\Gamma_{\uparrow}/\lambda = 1.0$, while the qualitative shape of the oscillating region would not change much.

Although not visible on the large scale of the full diagram, the lower "tip" does in fact not reach all the way down to the origin $\kappa = \Gamma_{\uparrow} = 0$, for which reason it is possible to circumvent the oscillating region when going from the "equilibrium" area at very weak external pumping and

[17] Note that we use the notation $\Gamma^{\pm}(\delta) \equiv \Gamma(\pm\delta)$.

cavity loss to the strongly driven case toward the right (cf. lower panel of Fig. 5.27 (a)).

Evidently, the upper boundary of the oscillating region lies in a parameter regime where the system timescale κ is comparable to the vibrational relaxation rate λ. For this reason, the boundary drawn according to the rate equations of Chp. 4 cannot be relied upon, which is why we compare the steep (red) dashed line with the results from the microscopic auxiliary-boson field theory in the subsequent paragraph 5.8.3.

The remaining three straight lines drawn across the phase diagram correspond to the transverse sections investigated in Figs. 5.27 (c) – (d). Note that these results are also calculated from the rate equations and hence ignore any corrections arising from the system timescale κ. Their qualitative features are still expected to be modeled accurately by the rate equations and highlight a number of physically interesting points: (i) The seemingly unintuitive collapse in photon population visible in Fig. 5.27 (c) for *increasing* $\Gamma_\uparrow$, while κ is held constant, follows from the change in $\Gamma^\pm$ as functions of $\Gamma_\uparrow$. As one could expect, the photon mode is quite sensitive to these parameters. For broader emission and absorption peaks, the ratio Γ^+/Γ^- known from the Kennard-Stepanov relation gradually approaches unity.

(ii) The condensation or decondensation transitions [5] are always accompanied by a critical slowing down of the system in the sense that one of the relaxation rates τ^{-1} goes to zero rapidly, which can be interpreted as an indication of a phase transition also out of equilibrium [157]. Furthermore, the molecule excitations become fully saturated (this cannot be discerned very well in Figs. 5.27 (c) – (d)), which can also be thought of as triggering the collapse in photon occupation in the first place.

(iii) The behavior of the second-order coherence $g^{(2)}$ needs to be considered separately from the occupation of the photon mode. The transition in the second-order coherence can but does not have to coincide with the condensation or decondensation transition. However, if one passes through the oscillating zone, the decondensation transition must occur *after* the change from oscillating to bi-exponential $g^{(2)}$ behavior because the decondensation transition is accompanied by a diverging relaxation time. Yet a single relaxation rate in the system can never approach zero since a zero relaxation rate is only possible when the square root in Eq. (4.69) becomes real and cancels the term in front. Thus we find that out of equilibrium, there is a more sensitive mechanism at work in the temporal second-order coherence that may antecede the decondensation phase transition.

5.8.3 Quantitative Corrections to the Boundary

In this paragraph, we turn to a comparison of the steep, (red) dashed path $\kappa(\Gamma_\uparrow) = 20\,\Gamma_\uparrow$ drawn in Fig. 5.27 with the corresponding results following from the fully non-Markovian microscopic dynamics. Instead of obtaining the steady-state occupation analytically from the rate equations of Chp. 4 and calculating the eigenvalues of the matrix in Eq. (4.69), we now have to solve the integro-differential equations derived from our field-theoretic considerations. Therefore, we resort to computing the density response of the photon mode to an external perturbation rather than the actual second-order coherence. By the quantum regression theorem which we derived in 4.2.5, these two approaches are equivalent, i.e. we could have adopted the same procedure to be used here also for extracting the frequency and relaxation rate of the second-order coherence from the rate equations. The initial conditions for the numerical simulations are as follows. We start with an

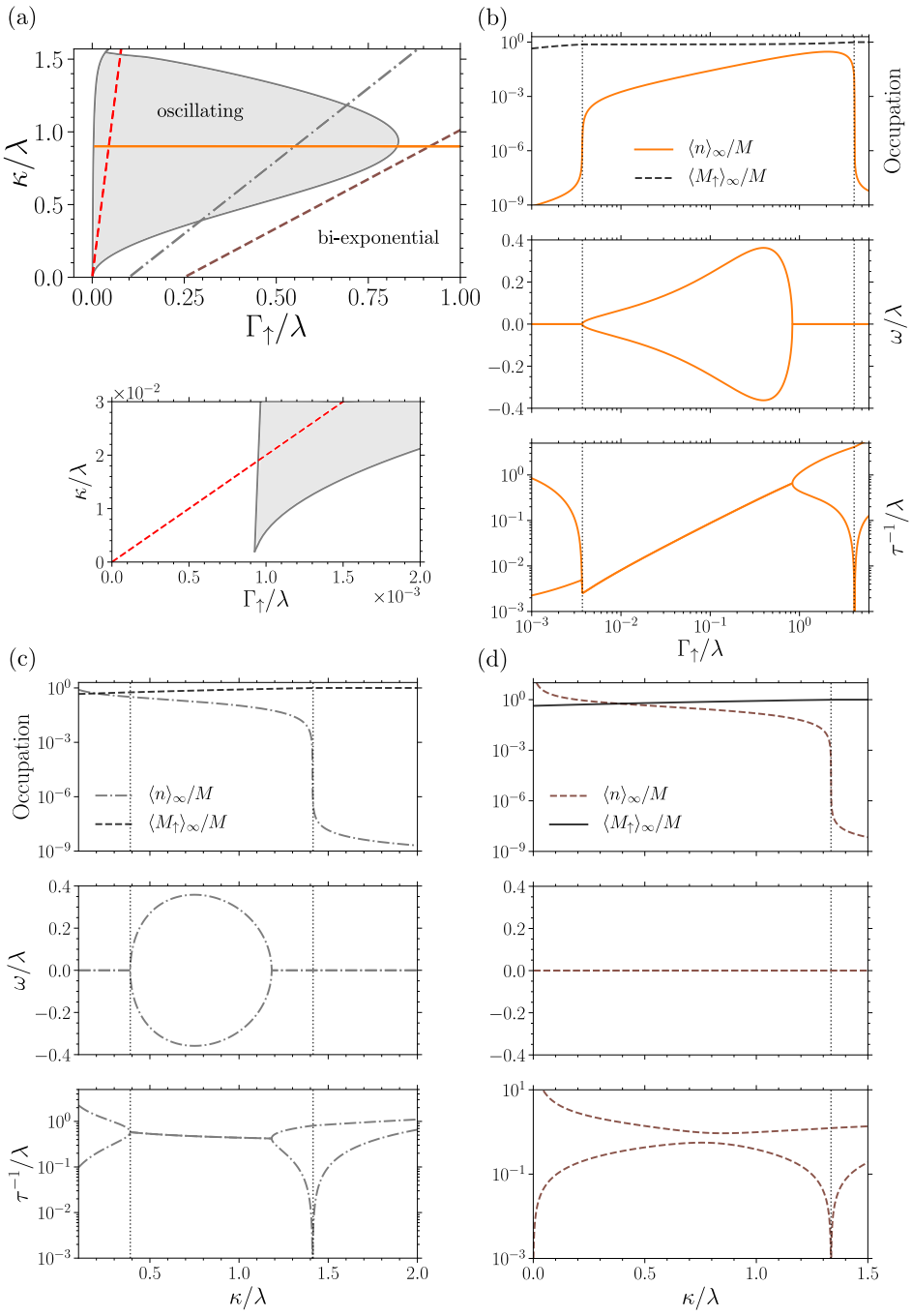

Figure 5.27: (a) The closed $g^{(2)}$ phase diagram for $M = 10^9$ as computed from the model of Chp. 4 with the steady-state occupations, $g^{(2)}$ frequency ω and relaxation rate τ^{-1} presented for the paths parameterized by (b) $\kappa(\Gamma_\uparrow) = 0.9\lambda$, (c) $\kappa(\Gamma_\uparrow) = 2.00\,(\Gamma_\uparrow - 0.10\lambda)$ and (d) $\kappa(\Gamma_\uparrow) = 1.35\,(\Gamma_\uparrow - 0.25\lambda)$. The parameters $\Gamma^\pm$ are analyzed in 5.8.1. For the figure discussion, s. paragraph 5.8.2. The (red) dashed line corresponds to $\kappa = 20\,\Gamma_\uparrow$ and is separately compared to the auxiliary-boson method in Fig. 5.30.

M	g/λ	δ/λ	Ω/λ	S	$\bar{N}$	$\Gamma_\uparrow/\kappa$	$\Gamma_\downarrow/\lambda$
10^9	$4.5 \cdot 10^{-5}$	-1.0	1.0	1.0	0.25	0.05	$1.25 \cdot 10^{-3}$

Table 5.3: Overview of the generic system parameters employed for the final results. The cavity loss κ is excluded because it serves as a control parameter. Note that the external pumping $\Gamma_\uparrow$ is given in units of κ, i.e. their ratio is held fixed. For the diagrammatics to be accurate, the photo-molecular coupling g should be small enough that the product of g^2 and the photon number is also small.

empty cavity and all molecules in the total ground state, which can be expressed in terms of Green functions as $D^<(0,0) = 0$, where we dropped the subscript $k = 0$ and $D^>(0,0)$ follows from the commutator, $G^<_{mn}(0,0) = -\mathrm{i}\delta_{00}$ and $E^<_{mn}(0,0) = 0$. Remember that the greater functions $G^>_{mn}(0,0) = E^>_{mn}(0,0) = -\mathrm{i}\delta_{mn}$ are fixed automatically by the projection. The system is then evolved until it reaches the steady state. The set of generic parameters used for the simulations is summarized in Tab. 5.3. The results to be presented do not depend strongly on the precise values of the various parameters.

A number of exemplary trajectories of the photon occupation $\langle n\rangle(t) = \mathrm{i}D^<(t,t)$ are shown in the inset of Fig. 5.28. Depending on the value of κ, the attainment of the steady state requires a different amount of time. As expected, the critical slowing down indicated by a diverging relaxation time also bears on the approach to the steady state which becomes very slow. After reaching the steady state, a weak, short Gaussian pulse is added to the constant external drive, such that the functional form of the total external pumping reads

$$\Gamma_\uparrow(t) = \Gamma_\uparrow \left(1 + A \exp\left\{ -\frac{(t-t_P)^2}{2\sigma_P^2} \right\} \right), \tag{5.128}$$

where t_P varies with the attainment of the steady state, and $A = 10^{-2}$, $\lambda\sigma_P = 1/2$. The density responses in the main panel of Fig. 5.28 show the evolution of the photon occupation following the Gaussian pulse (5.128), where the points $t = 0$ of the four trajectories in Fig. 5.28 correspond to the respective maxima of the $\langle n\rangle(t)$ curves after t_P. For the examples depicted in Fig. 5.28, it is evident that the first two cases with smaller κ show an oscillating response, while the other two cases with larger κ do not. Close to the upper boundary of the $g^{(2)}$ phase diagram in Fig. 5.27, however, this difference is no longer obvious, of course, such that the determination of the boundary demands for a quantitatively accurate criterion to group the trajectories into "oscillating" vs. "bi-exponential". The frequency ω and decay rate τ of the density responses can be extracted well by least-squares fitting the ansatz functions

$$\begin{aligned} f_{\text{osc}}(t) &= \mathrm{e}^{-t/\tau} \left(f(0)\cos\omega t + C \sin\omega t \right), \\ f_{\text{bi-exp}}(t) &= \frac{f(0)}{2} \left(\mathrm{e}^{-t/\tau_1} + \mathrm{e}^{-t/\tau_2} \right) + C \left(\mathrm{e}^{-t/\tau_1} - \mathrm{e}^{-t/\tau_2} \right) \end{aligned} \tag{5.129}$$

to the simulation data. The quality of the fit is can then be estimated by the standard error, which in turn determines whether the response is classified as damped-oscillating or bi-exponentially

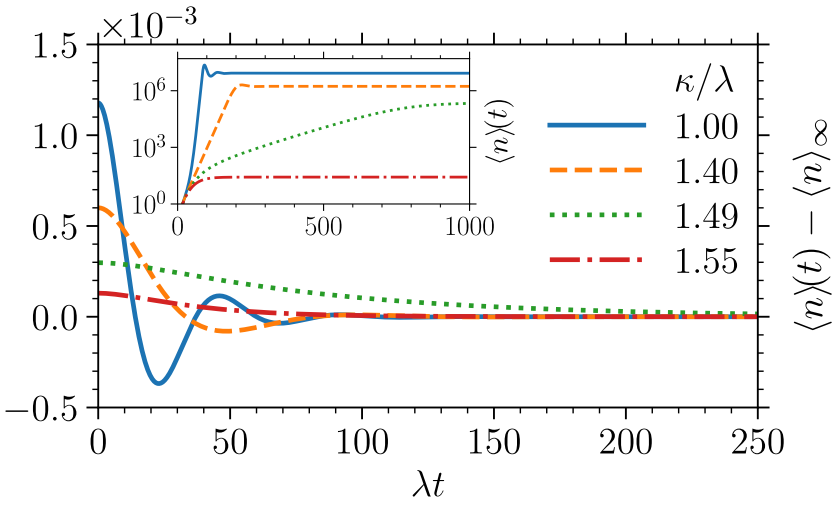

Figure 5.28: *(Main panel)* Density response $\langle n\rangle(t) - \langle n\rangle_\infty$ after the pump pulse Eq. 5.128 and *(inset)* approach to the steady state $\langle n\rangle_\infty = \lim_{t\to\infty} \mathrm{i}D^<(t,t)$ for initial conditions and parameters $\mathrm{Tr}\, D^<(0,0) = 0$, $\mathrm{i}G^<_{00}(0,0) = 1$, $M = 10^9$, $g/\lambda = 4.5\cdot 10^{-5}$, $\delta/\lambda = -1.00$, $\Omega/\lambda = 1.00$, $S = 1$, $\bar{N} = 0.25$, $\Gamma_\uparrow/\kappa = 0.05$, $\Gamma_\downarrow/\lambda = 1.25\cdot 10^{-3}$, vibrational-state truncation at $n = 4$, a temporal resolution of $\lambda \mathrm{d}t = 2^{-4}$ and memory time $\lambda\tau_{\mathrm{mem}} = 4.0$. We have verified the convergence of our simulations by varying both $\mathrm{d}t$ and τ_{mem}.

relaxing. An illustration of the fitting procedure for the two points directly next to the upper boundary of the phase diagram is given in Fig. 5.29 and Tabs. 5.4, 5.5. One can see that even for these two points on either side of the boundary, the fit classification is always unique. To ensure that the data are not fitted even better by a single exponential decay, the corresponding best fits are also presented in Fig. 5.29. Because they are evidently worse than either of the functions in Eq. (5.129), their standard errors are excluded from Tabs. 5.4, 5.5. Due to the slowing down of the dynamics between $\kappa/\lambda = 1.475$ and $\kappa/\lambda = 1.480$ (cf. Fig. 5.29), the numerical solution of the Kadanoff-Baym equations becomes very expensive and does not allow for an arbitrarily close approach of the transition.

Going over to our final results in Fig. 5.30, one can see that we still resolve the phase transition well enough to clearly differentiate it from the one predicted by the rate equations (s. the right inset of Fig. 5.30 (c)). While qualitatively similar, the latter happens for a larger value of κ/λ compared to the microscopic result. These quantitative corrections we observe for large κ/λ confirm our insight about the non-separable system-reservoir timescales and that the photon condensate requires a treatment beyond the rate equations in certain parameter regimes. The upper boundary of the $g^{(2)}$ phase diagram is indeed modified by taking into account the effect of the cavity loss. Physically, this can be understood from the additional broadening of the emission and absorption spectrum effected by the cavity loss κ.

Although the difference between the two theoretical methods is not particularly pronounced for the parameters of Tab. 5.3, one can envisage situations where the upper boundary of the $g^{(2)}$ phase diagram lies at even larger values of the system-reservoir ratio κ/λ, in which case one

κ/λ	$s(\tau)$	$s(\omega)$	$s(C)$
1.475	$1.01 \cdot 10^{-8}$	$1.08 \cdot 10^{-8}$	$1.29 \cdot 10^{-9}$
1.480	$2.35 \cdot 10^{-5}$	$1.18 \cdot 10^{-3}$	$1.61 \cdot 10^{-1}$

Table 5.4: Standard errors for the damped-oscillating ansatz.

κ/λ	$s(\tau_1)$	$s(\tau_2)$	$s(C)$
1.475	$2.84 \cdot 10^{-3}$	$2.93 \cdot 10^{-3}$	$2.85 \cdot 10^{-1}$
1.480	$4.02 \cdot 10^{-9}$	$1.45 \cdot 10^{-8}$	$4.42 \cdot 10^{-10}$

Table 5.5: Standard errors for the bi-exponentially decaying ansatz.

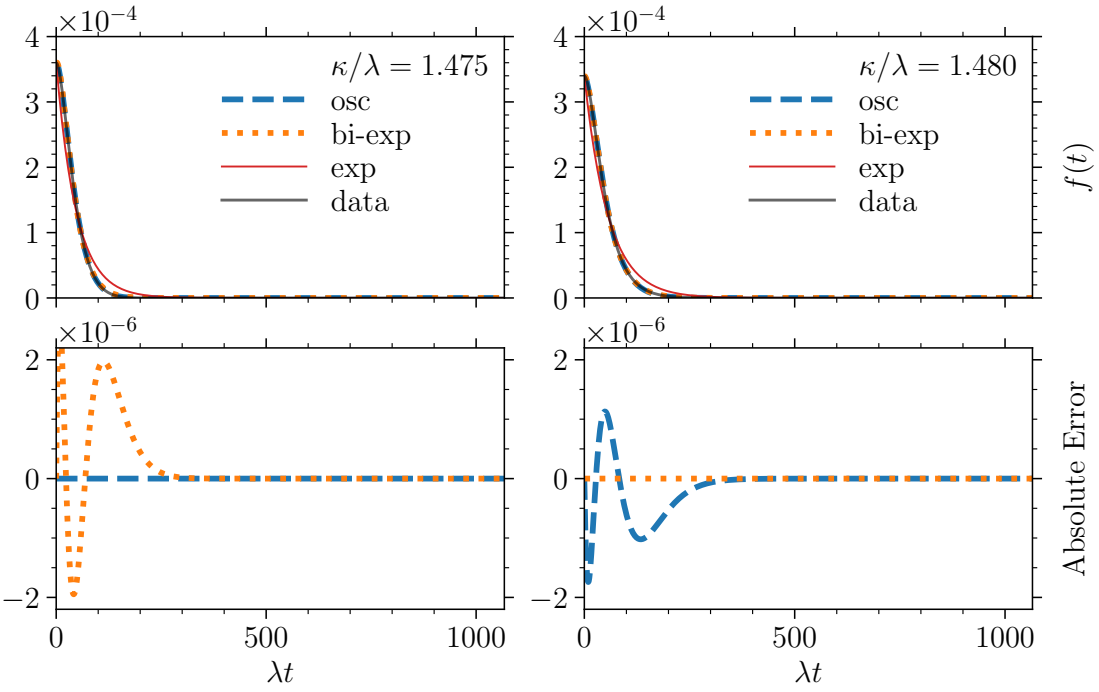

Figure 5.29: Comparison of the fits directly to the left and right of the transition at large κ. *(Upper panels)* Data and best fits for several different ansatz functions. A uni-exponential decay is also fitted to underline that it is not a possible best fit, as can indeed be judged by eye. *(Lower panels)* The absolute error (difference of data and fit) for the two viable options f_{osc} and $f_{\text{bi-exp}}$.

would expect the rate equations to strongly misquantify the crossover to the bi-exponential region. The same holds for the phase transition in the photon occupation accompanied by the diverging relaxation time.

The quantitative reliability of our non-Markovian microscopic theory stems mainly from two factors. The first and weaker one is that it seems reasonable to expect the kind of deviation that we find numerically given our physical understanding of the molecular spectrum. The second and more important factor is that for small κ/λ, the insets of Fig. 5.30 show that the auxiliary-boson field theory agrees very well with the rate equations,[18] which serves as an independent validation of our analytical and numerical methods. Considering the far greater complexity of both the analytical derivation described in Secs. 5.1 – 5.3 and the numerical methods of Sec. 2.3, the agreement with the much simpler methods in the expected parameter regime is in fact a strong indicator of the correctness of the entire scheme. Before concluding this Chp. we should point out again that the full non-equilibrium auxiliary field theory (developed here for the first time in the context of open systems) is not restricted to applications to photon condensation but also has the potential to yield interesting results in fields such as exciton-polaritons or even strongly correlated electrons where, of course, the auxiliary bosons would be joined by auxiliary fermions.

[18] Clearly, the $g^{(2)}$ oscillation frequency in Fig. 5.30 (b) is most sensitive to our corrections and departs from the rate-equation result quite early. This can be understood in broad terms by again considering the square root in Eq. (4.69), which tells us that oscillation frequency essentially traces out a half ellipse of a certain eccentricity. When the latter changes due to our quantitative corrections, the entire shape of the curve must be affected.

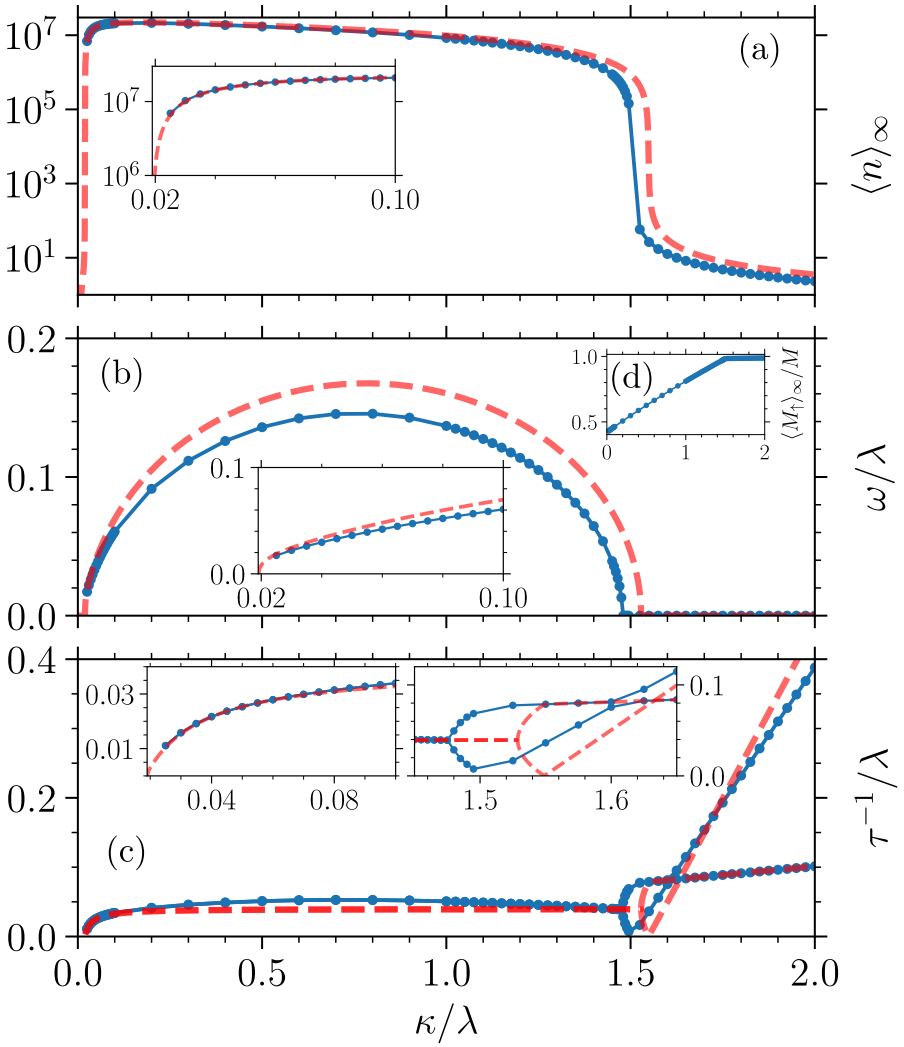

Figure 5.30: Comparsion of the pseudo-particle dynamics with the rate equations. (a) Steady-state photon number $\langle n\rangle_\infty$, (b) density-response frequency ω, and (c) relaxation rate τ^{-1} as functions of the cavity loss κ. The inset (d) shows the saturation of the steady-state molecular excitation $\langle M_\uparrow\rangle_\infty = \lim_{t\to\infty} \mathrm{i}\,\mathrm{Tr}\,\boldsymbol{E}^<(t,t)$. The ratio $\kappa/\Gamma_\uparrow = 20$ is held constant and the remaining parameters take the values summarized in Tab. 5.3. The (red) dashed lines (s. also Fig. 5.27) show the rate-equation results for parameters $\Gamma^\pm$ as discussed in 5.8.1.

Conclusion

This thesis presented an overall perspective on a variety of methods to describe non-equilibrium quantum systems. The position of photon condensates between quantum optics and condensed matter made them an ideal object of study to also understand in detail how these different methods are *connected*. We developed the Schwinger-Keldysh formalism in its full scope as it applies to open systems, going beyond mean-field descriptions by including self-consistently resummed propagators. A still larger perspective opened up when we compared these methods to classical stochastic processes, which are often neglected in the context of condensed-matter physics yet indispensable for building a proper understanding of many physical and formal details. Furthermore, we discussed the implementation of an efficient method to solve equations of Kadanoff-Baym type and showed how to apply these techniques to classical Brownian motion, which serves as a bridge between separate fields of study. For the future, this marks a starting point when applying non-equilibrium field theory to non-Markovian and multiplicative classical stochastic systems, which can be difficult to treat by other means.

In Chp. 3, we presented a summary of our detailed analysis of two of the trap geometries employed in cold-atom BEC experiments and their influence on the dynamical stability of such systems. In the course of this, we also provided a comprehensive review of the frequently used two-mode approximation in App. C, including the mean-field stability analysis which, to the author's knowledge, so far lacks from the literature.

We began our investigation of the photon BEC as it is driven away from equilibrium in Chp. 4, and gave a detailed description of the time-dependent second-order correlation by rederiving the phenomenologically established rate equations from the microscopic Hamiltonian and then applying quantum regression. The driven-dissipative character of the system induced non-Hermitian dynamics, which led to the appearance of exceptional points in the spectrum of the intensity-intensity correlations. Notably, our calculations matched the experimental findings, which confirmed that intensity fluctuations are more sensitive to deviations from equilibrium than the stationary occupation spectrum. These results provide an important building block to understanding the properties of the photon BEC in steady-state operation where it essentially acts as a fluctuating light source. Moreover, it is of practical relevance that second-order correlations can be used to determine the system parameters accurately. In the future, lattice systems of coupled dye microcavities may lead to the appearance of novel driven-dissipative phases of light.

Chp. 5 was devoted to developing a generalized model of the photon BEC that allows for a genuinely non-Markovian description beyond the previously given frequency-dependent emission and absorption. In Sec. 5.2 we gave an independent derivation of the pseudo-particle method in non-equilibrium, making it more accessible as a technique for future research. In particular, we

applied pseudo-particles with a faithfully enforced operator constraint for the first time to open systems, and thus proved that the technique also works for Lindblad operators where superficially there seemed to be an ambiguity (cf. Sec. 5.3). The photon BEC Gross-Pitaevskii equation derived in 5.6.3 is a novel result that has lead to an already on-going project with the aim of describing vortex formation in ring-shaped lattices.

Another research topic to be addressed is the inclusion of multiple cavity modes beyond the ground state. While both our theoretical derivations and the numerical methods already cover this case, it was not investigated in this thesis because it is not relevant for the dynamics of the ground mode. Since our microscopic model is able to produce emission and absorption spectra satisfying the Kennard-Stepanov relation, we can be confident that it is also capable of dynamically generating a Bose-Einstein distribution for modes near the zero-phonon line. The auxiliary-boson technique then allows one to study the effect of non-Markovianity on the equilibration of the cavity spectrum.

A closely related idea concerns the introduction of a symmetry-broken order parameter into the fully non-Markovian model, that is, to combine the technique used to derive the photon-BEC Gross-Pitaevskii equation from the master equation of Chp. 4 with the established field-theory treatment of the fully microscopic master equation of Sec. 5.3. Although not necessary from the perspective of having a valid approximation, this would yield access to the phase of the photon condensate and the effect of incoherent excitations.

One of the motivations for an extension of the existing description of photon condensates was the possibility to realize very rapid Josephson oscillations in double-well potentials experimentally. It seems natural to implement a model of this set-up with our formalism and to study in detail its physical behavior as the Josephson frequency is increased until it competes with the reservoir relaxation.

As touched upon briefly in paragraph 5.2.5, there are only a few discussions of the four-particle-irreducible (4PI) effective action [94, 158]. To the author's knowledge, actual applications of the technique to the dynamics of open systems do not exist. Even though it is certainly very challenging to formulate the equations, let alone to integrate them numerically, it would be rather interesting from a field-theory perspective to better understand the role played by vertex corrections in non-equilibrium problems. A related question regards the feasibility of the auxiliary field theory as generated via the fugacity scaling in the context of a two-impurity problem. Independent of the numerical solvability of such 4PI approaches, one could investigate if the technique succeeds at all in providing a consistent set of equations that implements the two-impurity operator constraint faithfully.

Bibliography

[1] F. P. Schäfer, *Dye lasers*, vol. 1, Springer Science & Business Media, 2013 (cit. on pp. vii, 9).

[2] J. Klaers, J. Schmitt, F. Vewinger and M. Weitz, *Bose–Einstein condensation of photons in an optical microcavity*, Nature **468** (2010) 545 (cit. on pp. vii, 9).

[3] J. Klaers, J. Schmitt, T. Damm, F. Vewinger and M. Weitz, *Statistical physics of Bose-Einstein-condensed light in a dye microcavity*, Phys. Rev. Lett. **108** (2012) 160403 (cit. on pp. vii, 99).

[4] J. Schmitt, T. Damm, D. Dung, F. Vewinger, J. Klaers and M. Weitz, *Observation of grand-canonical number statistics in a photon Bose-Einstein condensate*, Phys. Rev. Lett. **112** (2014) 030401 (cit. on pp. vii, 99).

[5] H. J. Hesten, R. A. Nyman and F. Mintert, *Decondensation in Nonequilibrium Photonic Condensates: When Less Is More*, Phys. Rev. Lett. **120** (2018) 040601 (cit. on pp. vii, 157).

[6] B. T. Walker, L. C. Flatten, H. J. Hesten, F. Mintert, D. Hunger, A. A. Trichet, J. M. Smith and R. A. Nyman, *Driven-dissipative non-equilibrium Bose–Einstein condensation of less than ten photons*, Nature Physics **14** (2018) 1173 (cit. on p. vii).

[7] J. Keeling and S. Kéna-Cohen, *Bose–Einstein Condensation of Exciton-Polaritons in Organic Microcavities*, Annual Review of Physical Chemistry **71** (2020) (cit. on p. vii).

[8] M. Ramezani, A. Halpin, S. Wang, M. Berghuis and J. G. Rivas, *Ultrafast Dynamics of Nonequilibrium Organic Exciton–Polariton Condensates*, Nano Lett. **19** (2019) 8590 (cit. on p. vii).

[9] T. K. Hakala, A. J. Moilanen, A. I. Väkeväinen, R. Guo, J.-P. Martikainen, K. S. Daskalakis, H. T. Rekola, A. Julku et al., *Bose–Einstein condensation in a plasmonic lattice*, Nature Physics **14** (2018) 739 (cit. on p. vii).

[10] C. Clear, R. C. Schofield, K. D. Major, J. Iles-Smith, A. S. Clark and D. P. McCutcheon, *Phonon-Induced Optical Dephasing in Single Organic Molecules*, Phys. Rev. Lett. **124** (2020) (cit. on p. vii).

[11] L. M. Sieberer, M. Buchhold and S. Diehl,
Keldysh field theory for driven open quantum systems,
Reports on Progress in Physics **79** (2016) 096001 (cit. on pp. vii, 8, 29, 31, 34, 109).

[12] C. Kurtscheid, D. Dung, E. Busley, F. Vewinger, A. Rosch and M. Weitz,
Thermally condensing photons into a coherently split state of light,
Science **366** (2019) 894 (cit. on pp. vii, 104).

[13] I. De Vega and D. Alonso, *Dynamics of non-Markovian open quantum systems*,
Rev. Mod. Phys. **89** (2017) 015001 (cit. on p. vii).

[14] J. del Pino, F. A. Schröder, A. W. Chin, J. Feist and F. J. Garcia-Vidal,
Tensor network simulation of non-Markovian dynamics in organic polaritons,
Phys. Rev. Lett. **121** (2018) 227401 (cit. on p. vii).

[15] M. Marthaler, Y. Utsumi, D. S. Golubev, A. Shnirman and G. Schön,
Lasing without inversion in circuit quantum electrodynamics, Phys. Rev. Lett. (2011),
arXiv: 1012.3557 (cit. on pp. vii, 72, 73, 78, 79).

[16] P. Kirton and J. Keeling, *Nonequilibrium model of photon condensation*,
Phys. Rev. Lett. (2013), arXiv: 1303.3459
(cit. on pp. vii, 12, 72–75, 78, 79, 98, 103, 104).

[17] P. Kirton and J. Keeling,
Thermalization and breakdown of thermalization in photon condensates,
Phys. Rev. A **91** (2015) (cit. on pp. vii, 72, 73, 79, 81, 82, 85, 90, 93, 104, 154).

[18] J. Keeling and P. Kirton,
Spatial dynamics, thermalization, and gain clamping in a photon condensate,
Phys. Rev. A **93** (2016) 1, arXiv: 1506.00280 (cit. on pp. vii, 77, 104, 105).

[19] M. Radonjić, W. Kopylov, A. Balaž and A. Pelster,
Interplay of coherent and dissipative dynamics in condensates of light,
New J. Phys. **20** (2018) (cit. on pp. vii, 73–75, 105, 131).

[20] J. Lebreuilly, A. Chiocchetta and I. Carusotto,
Pseudothermalization in driven-dissipative non-Markovian open quantum systems,
Phys. Rev. A **97** (2018) 033603 (cit. on p. vii).

[21] A. A. Abrikosov,
Electron scattering on magnetic impurities in metals and anomalous resistivity effects,
Physics Physique Fizika **2** (1965) 5 (cit. on pp. vii, 105).

[22] P. W. Anderson, *Localized magnetic states in metals*, Phys. Rev. **124** (1961) 41
(cit. on pp. viii, 105).

[23] S. Barnes, *New method for the Anderson model*, J. Phys. F **6** (1976) 1375
(cit. on pp. viii, 105).

[24] S. Barnes, *New method for the Anderson model. II. The U= 0 limit*,
J. Phys. F **7** (1977) 2637 (cit. on pp. viii, 105).

[25] N. E. Bickers, *Review of Techniques in the large-N expansion for dilute magnetic alloys*, **59** (1987) (cit. on pp. viii, 105).

[26] P. Coleman, *New approach to the mixed-valence problem*, Phys. Rev. B **29** (1984) 3035 (cit. on pp. viii, 105, 108).

[27] J. Kroha and P. Wölfle, *Fermi and non-fermi liquid behavior in quantum impurity systems: Conserving slave boson theory*, Acta Phys. Pol. B **29** (1998) 3781 (cit. on pp. viii, 105).

[28] D. C. Langreth and P. Nordlander, *Derivation of a master equation for charge-transfer processes in atom-surface collisions*, Phys. Rev. B **43** (1991) (cit. on pp. viii, 105).

[29] N. S. Wingreen and Y. Meir, *Anderson model out of equilibrium: Noncrossing-approximation approach to transport through a quantum dot*, Phys. Rev. B **49** (1994) 11040, arXiv: arXiv:1011.1669v3 (cit. on pp. viii, 105).

[30] M. H. Hettler, J. Kroha and S. Hershfield, *Nonequilibrium dynamics of the Anderson impurity model*, Phys. Rev. B **58** (1998) 5649 (cit. on p. viii).

[31] J. Kroha and A. Zawadowski, *Nonequilibrium quasiparticle distribution induced by Kondo defects*, Phys. Rev. Lett. **88** (2002) 176803 (cit. on pp. viii, 105).

[32] M. Eckstein and P. Werner, *Nonequilibrium dynamical mean-field calculations based on the noncrossing approximation and its generalizations*, Phys. Rev. B - Condens. Matter Mater. Phys. **82** (2010) 1, arXiv: 1005.1872 (cit. on pp. viii, 36, 105, 109).

[33] A. Schuckert, A. Piñeiro Orioli and J. Berges, *Nonequilibrium quantum spin dynamics from two-particle irreducible functional integral techniques in the Schwinger boson representation*, Phys. Rev. B **98** (2018) 1, arXiv: arXiv:1806.02347v1 (cit. on pp. viii, 52, 117, 136).

[34] J. S. Bernier, D. Poletti and C. Kollath, *Dissipative quantum dynamics of fermions in optical lattices: A slave-spin approach*, Phys. Rev. B **90** (2014) 1 (cit. on pp. viii, 136).

[35] T. Lappe, A. Posazhennikova and J. Kroha, *Fluctuation damping of isolated, oscillating Bose-Einstein condensates*, Phys. Rev. A **98** (2018) 023626 (cit. on pp. ix, 63, 70, 217).

[36] F. E. Ozturk, T. Lappe, G. Hellmann, J. Schmitt, J. Klaers, F. Vewinger, J. Kroha and M. Weitz, *Fluctuation dynamics of an open photon Bose-Einstein condensate*, Phys. Rev. A **100** (2019) 043803 (cit. on pp. ix, 72, 98, 101).

[37] F. E. Ozturk, T. Lappe, G. Hellmann, J. Schmitt, J. Klaers, F. Vewinger, J. Kroha and M. Weitz, "Observation of a Non-Hermitian Phase Transition in an Optical Quantum Gas", submitted (cit. on pp. ix, 98).

[38] T. Lappe, M. Kajan, F. Meirinhos and J. Kroha,
"Non-Markovian Dynamics of Open Photon Condensates", in preparation (cit. on p. x).

[39] M. H. Anderson, J. R. Ensher, M. R. Matthews, C. E. Wieman and E. A. Cornell,
Observation of Bose-Einstein condensation in a dilute atomic vapor,
Science **269** (1995) 198 (cit. on pp. 1, 7, 55).

[40] A. Bach, *Boltzmann's probability distribution of 1877*,
Archive for History of Exact Sciences (1990) 1 (cit. on pp. 2, 3).

[41] A. Pais, *Subtle is the Lord: The Science and the Life of Albert Einstein: The Science and the Life of Albert Einstein*, Oxford University Press, USA, 1982 (cit. on p. 2).

[42] A. Einstein, *Quantentheorie des einatomigen idealen Gases*, **6** (1924) 261 (cit. on p. 2).

[43] A. Einstein, *Quantentheorie des Einatomigen Gases, 2*,
Sitzungsberichte der Preuss. Akad. der Wissenschaften **3** (1925) (cit. on p. 2).

[44] Y. De Decker, *Stochastic thermodynamics based on an Einstein-Boltzmann definition of fluctuating entropy*, Phys. Rev. E **99** (2019) 1 (cit. on p. 2).

[45] H. Touchette, *The large deviation approach to statistical mechanics*,
Physics Reports **478** (2009) 1 (cit. on p. 2).

[46] K. Von Meyenn, *Eine Entdeckung von ganz außerordentlicher Tragweite: Schrödingers Briefwechsel zur Wellenmechanik und zum Katzenparadoxon*, Springer, 2011
(cit. on pp. 3, 4).

[47] A. Bach, H. Blank and H. Francke,
Bose-Einstein statistics derived from the statistics of classical particles,
Lett. Al Nuovo Cim. Ser. 2 **43** (1985) 195 (cit. on pp. 3, 4).

[48] A. Bach,
Indistinguishability or distinguishability of the particles of Maxwell-Boltzmann statistics,
Phys. Lett. A **125** (1987) 447 (cit. on p. 3).

[49] R. H. Swendsen, *The ambiguity of "distinguishability" in statistical mechanics*,
Am. J. Phys. **83** (2015) 545 (cit. on p. 3).

[50] M. Sigrist, *Statistical Physics*, 2014 (cit. on pp. 4, 8).

[51] P. C. Hohenberg, *Existence of long-range order in one and two dimensions*,
Phys. Rev. **158** (1967) 383 (cit. on p. 7).

[52] V. Bagnato and D. Kleppner,
Bose-Einstein condensation in low-dimensional traps Vanderlei,
Phys. Rev. A **44** (1991) 7439 (cit. on p. 8).

[53] J. Klaers, *The thermalization, condensation and flickering of photons*,
J. Phys. B At. Mol. Opt. Phys. **47** (2014) 243001 (cit. on pp. 8, 9, 11–13, 104).

[54] C. W. Gardiner et al., *Handbook of stochastic methods*, vol. 3, Springer Berlin, 1985
(cit. on pp. 14, 185, 188).

[55] P. Hänggi, *Path integral solutions for non-Markovian processes*, Zeitschrift für Physik B Condensed Matter **75** (1989) 275 (cit. on pp. 16, 17).

[56] A. Kamenev, *Field Theory of Non-Equilibrium Systems*, Cambridge University Press, 2011, ISBN: 9780521760829 (cit. on pp. 16, 18, 29, 31, 35, 109, 110).

[57] L. F. Cugliandolo, V. Lecomte and F. Van Wijland, *Building a path-integral calculus*, arXiv preprint (2018), arXiv: 1806.09486 (cit. on p. 16).

[58] N. G. van Kampen, *Stochastic Processes in Physics and Chemistry (Third Edition)*, 2007 (cit. on pp. 16, 19, 185).

[59] C. W. Gardiner and P. Zoller, *Quantum noise: a handbook of Markovian and non-Markovian quantum stochastic methods with applications to quantum optics*, vol. 56, Springer Science & Business Media, 2004 (cit. on pp. 21, 22, 24, 26, 186, 189).

[60] G. W. Ford, J. T. Lewis and R. F. Oconnell, *Quantum Langevin equation*, Phys. Rev. A **37** (1988) 4419, arXiv: 1912.12063 (cit. on p. 21).

[61] J. Rammer, *Quantum field theory of non-equilibrium states*, vol. 22, Cambridge University Press Cambridge, 2007 (cit. on pp. 22, 23, 30, 180, 208).

[62] H. Bruus and K. Flensberg, *Many-body quantum theory in condensed matter physics: an introduction*, Oxford university press, 2004 (cit. on p. 23).

[63] L. I. Plimak, M. K. Olsen, M. Fleischhauer and M. J. Collett, *Beyond the Fokker-Planck equation: Stochastic simulation of complete Wigner representation for the optical parametric oscillator*, Europhys. Lett. **56** (2001) 372, arXiv: 0108128 [quant-ph] (cit. on p. 26).

[64] L. I. Plimak, M. Fleischhauer, M. K. Olsen and M. J. Collett, *Quantum-field-theoretical techniques for stochastic representation of quantum problems*, (2001) 1, arXiv: 0102483 [cond-mat] (cit. on p. 26).

[65] P. D. Drummond, *Higher-order stochastic differential equations and the positive Wigner function*, Phys. Rev. A **96** (2017) 1 (cit. on p. 26).

[66] A. Gilchrist, C. W. Gardiner and P. D. Drummond, *Positive P representation: Application and validity*, Phys. Rev. A **55** (1997) 3014 (cit. on pp. 26, 189).

[67] P. Deuar and P. D. Drummond, *Gauge [Formula Presented] representations for quantum-dynamical problems: Removal of boundary terms*, Phys. Rev. A **66** (2002) 16, arXiv: 0203025 [quant-ph] (cit. on pp. 26, 189).

[68] C. W. G. P. D. Drummond, *Generalised P-representations in quantum optics*, J. Phys. A. (1980) (cit. on pp. 26, 189).

[69] L. E. Rosales-Zárate and P. D. Drummond,
Probabilistic Q-function distributions in fermionic phase-space, New J. Phys. **17** (2015) 1 (cit. on p. 26).

[70] P. D. Drummond and M. D. Reid, *Q-functions as models of physical reality*, () 1, arXiv: arXiv:1909.01798v1 (cit. on p. 26).

[71] J. Schwinger, *Brownian motion of a quantum oscillator*,
Journal of Mathematical Physics **2** (1961) 407 (cit. on pp. 29, 31, 34).

[72] L. V. Keldysh, *Diagram technique for nonequilibrium processes*, JETP **20** (1964) 1080 (cit. on pp. 29, 35).

[73] P. C. Martin and J. Schwinger, *Theory of many-particle systems. I*,
Phys. Rev. **115** (1959) 1342 (cit. on pp. 29, 79).

[74] R. Kubo, *The fluctuation-dissipation theorem*, Reports Prog. Phys. **29** (1966) 255 (cit. on p. 29).

[75] J. Berges, *Introduction to Nonequilibrium Quantum Field Theory*, (2004), arXiv: 0409233 [hep-ph] (cit. on pp. 29, 37).

[76] J. Berges, *Nonequilibrium Quantum Fields: From Cold Atoms to Cosmology*, (2015), arXiv: 1503.02907 (cit. on pp. 29, 32, 37, 48, 52, 107).

[77] K. Chou, Z. Su, B. Hao and L. Yu,
Equilibrium and Nonequilibrium Formalisms Made Unified, Phys. Rep. **118** (1985) 1 (cit. on pp. 29, 31).

[78] A. Altland and B. D. Simons, *Condensed matter field theory*,
Cambridge university press, 2010 (cit. on pp. 30, 31, 109).

[79] E. A. Calzetta and B.-L. B. Hu, *Nonequilibrium quantum field theory*,
Nonequilibrium Quantum Field Theory, by Esteban A. Calzetta, Bei-Lok B. Hu, Cambridge, UK: Cambridge University Press, 2008 (2008) (cit. on pp. 30, 37, 108).

[80] G. Stefanucci and R. Van Leeuwen,
Nonequilibrium many-body theory of quantum systems: a modern introduction,
Cambridge University Press, 2013 (cit. on pp. 30, 33, 36, 48).

[81] T. Gasenzer, J. Berges, M. G. Schmidt and M. Seco,
Nonperturbative dynamical many-body theory of a Bose-Einstein condensate,
Phys. Rev. A **72** (2005) 1, arXiv: 0507480 [cond-mat] (cit. on pp. 30, 65, 211).

[82] J. Berges and T. Gasenzer,
Quantum versus classical statistical dynamics of an ultracold Bose gas,
Phys. Rev. A **76** (2007), arXiv: 0703163 [cond-mat] (cit. on pp. 30, 36, 58).

[83] L. M. Sieberer, S. D. Huber, E. Altman and S. Diehl, *Nonequilibrium functional renormalization for driven-dissipative Bose-Einstein condensation*,
Phys. Rev. B **89** (2014) 1, arXiv: 1309.7027 (cit. on p. 30).

[84] X. Busch, I. Carusotto and R. Parentani,
Spectrum and entanglement of phonons in quantum fluids of light,
Phys. Rev. A **89** (2014) 1, arXiv: arXiv:1311.3507v1 (cit. on p. 30).

[85] P. C. Martin, E. D. Siggia and H. A. Rose, *Statistical dynamics of classical systems*,
Phys. Rev. A **8** (1973) 423, arXiv: arXiv:1011.1669v3 (cit. on pp. 30, 35).

[86] H.-K. Janssen, *On a Lagrangean for classical field dynamics and renormalization group calculations of dynamical critical properties*,
Zeitschrift für Physik B Condensed Matter **23** (1976) 377 (cit. on pp. 30, 36).

[87] C. De Dominicis and L. Peliti, *Field-theory renormalization and critical dynamics above T c: Helium, antiferromagnets, and liquid-gas systems*, Phys. Rev. B **18** (1978) 353
(cit. on pp. 30, 36).

[88] V. V. Khoze and J. Reiness,
Review of the semiclassical formalism for multiparticle production at high energies,
Phys. Rep. **822** (2019) 1, arXiv: 1810.01722 (cit. on p. 30).

[89] R. El-Ganainy, K. G. Makris, M. Khajavikhan, Z. H. Musslimani, S. Rotter and D. N. Christodoulides, *Non-Hermitian physics and PT symmetry*, Nat. Phys. **14** (2018) 11
(cit. on p. 34).

[90] *Effective action for composite operators*, Phys. Rev. D **10** (1974) 2428
(cit. on pp. 36, 183).

[91] A. N. Vasiliev, *Functional methods in quantum field theory and statistical physics*,
Routledge, 2019 (cit. on p. 36).

[92] G. Baym and L. P. Kadanoff, *Conservation laws and correlation functions*,
Phys. Rev. **124** (1961) 287 (cit. on p. 36).

[93] J. Rammer, *Quantum transport theory*, CRC Press, 2018 (cit. on p. 37).

[94] M. Carrington, The European Physical Journal C **35** (2004) 383 (cit. on pp. 37, 42, 166).

[95] M. E. Carrington and E. Kovalchuk, *Towards next-to-leading order transport coefficients from the four-particle irreducible effective action*, Phys. Rev. D **81** (2010) 1
(cit. on pp. 37, 117).

[96] M. E. Carrington and Y. Guo, *Techniques for n-particle irreducible effective theories*,
Phys. Rev. D **83** (2011) 1 (cit. on p. 37).

[97] M. E. Carrington and Y. Guo,
New method to calculate the n-particle irreducible effective action,
Phys. Rev. D **85** (2012) 1 (cit. on p. 37).

[98] M. E. Carrington, B. A. Meggison and D. Pickering,
2PI effective action at four loop order in ϕ4 theory, Phys. Rev. D **94** (2016) 1,
arXiv: 1603.02085 (cit. on p. 37).

[99] M. E. Carrington, S. A. Friesen, C. D. Phillips and D. Pickering,
Renormalization of the 4PI effective action using the functional renormalization group,
Phys. Rev. D **99** (2019) 74002, arXiv: 1901.00840 (cit. on pp. 37, 117).

[100] K. Balzer, *Solving the two-time Kadanoff-Baym equations. Application to model atoms and molecules*, PhD thesis: Christian-Albrechts Universität Kiel, 2011 (cit. on pp. 48, 50).

[101] K. Balzer and M. Bonitz,
Nonequilibrium Green's Functions Approach to Inhomogeneous Systems, Springer, 2012 (cit. on p. 48).

[102] A. Stan, N. E. Dahlen and R. van Leeuwen,
Time propagation of the Kadanoff-Baym equations for inhomogeneous systems,
J. Chem. Phys. **130** (2009), arXiv: 0906.1704 (cit. on pp. 48, 50).

[103] N. E. Dahlen and R. Van Leeuwen, *Solving the Kadanoff-Baym equations for inhomogeneous systems: Application to atoms and molecules*, Phys. Rev. Lett. **98** (2007) 2, arXiv: 0703411 [cond-mat] (cit. on p. 48).

[104] M. A. Sentef, A. F. Kemper, A. Georges and C. Kollath,
Theory of light-enhanced phonon-mediated superconductivity, Phys. Rev. B **93** (2016) 1, arXiv: 1505.07575 (cit. on pp. 48, 52).

[105] N. Schluenzen, J.-P. Joost and M. Bonitz,
Achieving the Ultimate Scaling Limit for Nonequilibrium Green Functions Simulations, Phys. Rev. Lett. **124** (2019) 76601, arXiv: 1909.11489 (cit. on pp. 48, 52).

[106] S. Bock, A. Liluashvili and T. Gasenzer, *Buildup of the Kondo effect from real-time effective action for the Anderson impurity model*, Phys. Rev. B **94** (2016) 1, arXiv: 1512.06127 (cit. on pp. 50–52).

[107] K. B. Davis, M.-O. Mewes, M. R. Andrews, N. J. van Druten, D. S. Durfee, D. Kurn and W. Ketterle, *Bose-Einstein condensation in a gas of sodium atoms*,
Phys. Rev. Lett. **75** (1995) 3969 (cit. on p. 55).

[108] A. Posazhennikova, M. Trujillo-Martinez and J. Kroha, *Thermalization of Isolated Bose-Einstein Condensates by Dynamical Heat Bath Generation*,
Annalen der Physik **1700124** (2017) 1 (cit. on pp. 55, 63).

[109] D. W. Snoke and S. M. Girvin, *Dynamics of phase coherence onset in Bose condensates of photons by incoherent phonon emission*, J. Low Temp. Phys. **171** (2013) 1
(cit. on pp. 55, 56, 62).

[110] D. W. Snoke, G. Liu and S. M. Girvin,
The basis of the Second Law of thermodynamics in quantum field theory,
Ann. Phys. (N. Y). **327** (2012) 1825, arXiv: 1112.3009 (cit. on pp. 55, 62).

[111] J. R. Anglin, *Cold, Dilute, Trapped Bosons as an Open Quantum System*,
Phys. Rev. Lett. **79** (1997) 6, arXiv: 9611008v1 [arXiv:quant-ph] (cit. on p. 56).

[112] N. P. Proukakis and B. Jackson,
Finite Temperature Models of Bose-Einstein Condensation, (2008), arXiv: 0810.0210
(cit. on p. 56).

[113] A. M. Rey, B. L. Hu, E. Calzetta, A. Roura and C. W. Clark, *Nonequilibrium dynamics of optical-lattice-loaded Bose-Einstein-condensate atoms: Beyond the Hartree-Fock-Bogoliubov approximation*, Phys. Rev. A **69** (2004) (cit. on pp. 63, 203).

[114] A. Posazhennikova, M. Trujillo-Martinez and J. Kroha, *Inflationary Quasiparticle Creation and Thermalization Dynamics in Coupled Bose-Einstein Condensates*, Phys. Rev. Lett. **116** (2016) 225304 (cit. on pp. 63, 66).

[115] M. Albiez, R. Gati, J. Fölling, S. Hunsmann, M. Cristiani and M. K. Oberthaler, *Direct observation of tunneling and nonlinear self-trapping in a single bosonic josephson junction*, Phys. Rev. Lett. **95** (2005) 1 (cit. on pp. 63, 64, 67, 70, 216).

[116] L. J. LeBlanc, A. B. Bardon, J. McKeever, M. H. T. Extavour, D. Jervis, J. H. Thywissen, F. Piazza and A. Smerzi, *Dynamics of a tunable superfluid junction*, Phys. Rev. Lett. **106** (2011) 25302 (cit. on pp. 63, 64, 67, 69, 70, 216).

[117] L. Leblanc, *Exploring many-body physics with ultracold atoms*, PhD thesis, 2010 (cit. on pp. 63, 216).

[118] B. Josephson, *Possible new effect in superconducting tunneling*, Phys. Lett. **1** (1962) 251 (cit. on p. 64).

[119] J. Javanainen, *Oscillatory exchange of atoms between traps containing Bose condensates*, Phys. Rev. Lett. **57** (1986) 3164 (cit. on p. 64).

[120] S. Levy, E. Lahoud, I. Shomroni and J. Steinhauer, *The a.c. and d.c. Josephson effects in a Bose–Einstein condensate*, Nature **449** (2007) 579 (cit. on p. 64).

[121] G. J. Milburn, J. Corney, E. M. Wright and D. F. Walls, *Quantum dynamics of an atomic Bose-Einstein condensate in a double-well potential*, Phys. Rev. A **55** (1997) 4318 (cit. on p. 64).

[122] A. Smerzi, S. Fantoni, S. Giovanazzi and S. R. Shenoy, *Quantum Coherent Atomic Tunneling between Two Trapped Bose-Einstein Condensates*, Phys. Rev. Lett. **79** (1997) 4950 (cit. on pp. 64, 195, 200, 202).

[123] J. Ruostekoski and D. F. Walls, *Bose-Einstein condensate in a double-well potential as an open quantum system*, Phys. Rev. A **58** (1998) R50, arXiv: `9803298 [cond-mat]` (cit. on pp. 64, 216).

[124] S. Raghavan, A. Smerzi, S. Fantoni and S. R. Shenoy, *Coherent oscillations between two weakly coupled Bose-Einstein condensates: Josephson effects, [Formula Presented] oscillations, and macroscopic quantum self-trapping*, Phys. Rev. A **59** (1999) 620 (cit. on p. 64).

[125] S. Raghavan, A. Smerzi and V. M. Kenkre, *Transitions in coherent oscillations between two trapped Bose-Einstein condensates*, Phys. Rev. A **60** (1999) R1787 (cit. on pp. 64, 216).

[126] I. Marino, S. Raghavan, S. Fantoni, S. R. Shenoy and a. Smerzi, *Bose-condensate tunneling dynamics: Momentum-shortened pendulum with damping*, Phys. Rev. A **60** (1999) 487 (cit. on p. 64).

[127] J. Williams, R. Walser, J. Cooper, E. Cornell and M. Holland, *Nonlinear Josephson-type oscillations of a driven, two-component Bose-Einstein condensate*, Phys. Rev. A **59** (1999) R31 (cit. on p. 64).

[128] D. Gordon and C. M. Savage, *Creating Macroscopic Superpositions with Bose-Einstein Condensates*, Phys. Rev. A **59** (1999) 4623 (cit. on p. 64).

[129] S. Giovanazzi, A. Smerzi and S. Fantoni, *Josephson effects in dilute bose-einstein condensates*, Phys. Rev. Lett. **84** (2000) 4521 (cit. on p. 64).

[130] A. Vardi and J. R. Anglin, *Bose-Einstein condensates beyond mean field theory: quantum backreaction as decoherence*, Phys. Rev. Lett. **86** (2001) 568 (cit. on pp. 64, 195).

[131] J. R. Anglin and A. Vardi, *Dynamics of a two-mode Bose-Einstein condensate beyond mean-field theory*, Phys. Rev. A **64** (2001) 9 (cit. on pp. 64, 69).

[132] L. P. Pitaevskii and S. Stringari, *Thermal vs quantum decoherence in double well trapped bose-einstein condensates*, Phys. Rev. Lett. **87** (2001) 180402–1–180402 (cit. on p. 64).

[133] A. Micheli, D. Jaksch, J. I. Cirac and P. Zoller, *Many-particle entanglement in two-component Bose-Einstein condensates*, Phys. Rev. A **67** (2003) 11 (cit. on p. 64).

[134] K. W. Mahmud, H. Perry and W. P. Reinhardt, *Quantum phase-space picture of Bose-Einstein condensates in a double well*, Phys. Rev. A **71** (2005) 1 (cit. on pp. 64, 216).

[135] D. Ananikian and T. Bergeman, *Gross-Pitaevskii equation for Bose particles in a double-well potential: Two-mode models and beyond*, Phys. Rev. A **73** (2006) 13604 (cit. on pp. 64, 65).

[136] G. Spagnolli, G. Semeghini, L. Masi, G. Ferioli, A. Trenkwalder, S. Coop, M. Landini, L. Pezzè et al., *Crossing over from Attractive to Repulsive Interactions in a Tunneling Bosonic Josephson Junction*, Phys. Rev. Lett. **118** (2017) 1, arXiv: arXiv:1703.02370v1 (cit. on p. 64).

[137] E. M. Graefe, H. J. Korsch and D. Witthaut, *Mean-field dynamics of a Bose-Einstein condensate in a time-dependent triple-well trap: Nonlinear eigenstates, Landau-Zener models, and stimulated Raman adiabatic passage*, Phys. Rev. A **73** (2006) 1 (cit. on p. 65).

[138] A. Griffin, T. Nikuni and E. Zaremba, *Bose-condensed gases at finite temperatures*, Cambridge University Press, 2009 (cit. on pp. 65, 202).

[139] J. M. Vogels, C. C. Tsai, R. S. Freeland, S. J. J. M. F. Kokkelmans, B. J. Verhaar and D. J. Heinzen,
Prediction of Feshbach resonances in collisions of ultracold rubidium atoms,
Phys. Rev. A **56** (1997) R1067 (cit. on p. 66).

[140] E. G. van Kempen, S. J. Kokkelmans, D. J. Heinzen and B. J. Verhaar, *Interisotope determination of ultracold rubidium interactions from three high-precision experiments*,
Phys. Rev. Lett. **88** (2002) 932011 (cit. on p. 66).

[141] G. Guennebaud, B. Jacob et al., *Eigen*, URl: http://eigen. tuxfamily. org (2010)
(cit. on p. 67).

[142] R. Geus, *The Jacobi-Davidson algorithm for solving large sparse symmetric eigenvalue problems with application to the design of accelerator cavities*, Dissertation (2002)
(cit. on p. 67).

[143] S. Mukamel, *Principles of nonlinear optical spectroscopy*, vol. 6,
Oxford university press New York, 1995 (cit. on p. 72).

[144] H. Schoeller and G. Schön, *Mesoscopic quantum transport: Resonant tunneling in the presence of a strong Coulomb interaction*, Phys. Rev. B **50** (1994) 18436 (cit. on p. 78).

[145] R. Kubo, *Statistical-mechanical theory of irreversible processes. I. General theory and simple applications to magnetic and conduction problems*,
Journal of the Physical Society of Japan **12** (1957) 570 (cit. on p. 79).

[146] H. J. Carmichael,
Statistical methods in quantum optics 1: master equations and Fokker-Planck equations,
Springer Science & Business Media, 2013 (cit. on p. 91).

[147] W. Heiss, *The physics of exceptional points*,
Journal of Physics A: Mathematical and Theoretical **45** (2012) 444016
(cit. on pp. 97, 217).

[148] J. Barroso, A. Costela, I. Garcıa-Moreno and R. Sastre, *Wavelength dependence of the nonlinear absorption properties of laser dyes in solid and liquid solutions*,
Chem. Phys. **238** (1998) 257 (cit. on p. 99).

[149] A. H. Steinbach, J. M. Martinis and M. H. Devoret,
Observation of hot-electron shot noise in a metallic resistor,
Phys. Rev. Lett. **76** (1996) 3806 (cit. on p. 101).

[150] D. Dung, C. Kurtscheid, T. Damm, J. Schmitt, F. Vewinger, M. Weitz and J. Klaers,
Variable potentials for thermalized light and coupled condensates,
Nature Photonics **11** (2017) 565 (cit. on p. 104).

[151] A. W. De Leeuw, H. T. C. Stoof and R. A. Duine, *Schwinger-Keldysh theory for Bose-Einstein condensation of photons in a dye-filled optical microcavity*,
Phys. Rev. A (2013), arXiv: 1306.5107 (cit. on p. 105).

[152] J. A. Ćwik, *Organic polaritons: modelling the effect of vibrational dressing*,
PhD thesis: University of St Andrews, 2015 (cit. on p. 105).

[153] R. Juárez-Amaro, A. Zúñiga-Segundo and H. M. Moya-Cessa, *Several ways to solve the Jaynes-Cummings model*, Appl. Math. Inf. Sci. **9** (2015) 299 (cit. on pp. 126, 129).

[154] P. Linz, *Analytical and numerical methods for Volterra equations*, vol. 7, Siam, 1985 (cit. on p. 127).

[155] G. Arfken and H. Weber, *Sturm- Liouville theory—Orthogonal functions*, Mathematical Methods for Physicists (2005) 621 (cit. on p. 128).

[156] J. R. Johansson, P. D. Nation and F. Nori, *QuTiP: An open-source Python framework for the dynamics of open quantum systems*, Computer Physics Communications **183** (2012) 1760 (cit. on p. 137).

[157] B. T. Walker, H. J. Hesten, H. S. Dhar, R. A. Nyman and F. Mintert, *Noncritical slowing down of photonic condensation*, Phys. Rev. Lett. **123** (2019) 203602 (cit. on p. 157).

[158] J. Berges, *N-particle irreducible effective action techniques for gauge theories*, Phys. Rev. D **70** (2004) 105010 (cit. on p. 166).

[159] V. I. Arnol'd, *Mathematical methods of classical mechanics*, vol. 60, Springer, 2013 (cit. on p. 199).

APPENDIX A

Functions & Functionals

A.1 Green Functions

Given the plethora of Green functions being in use, a summary of their respective definitions and relations is desirable. For the rest of this section, we will refer to them as *components*. The most commonplace are the *retarded* and *advanced* components

$$G^R(t,t') := -\mathrm{i}\theta(t-t')\langle[a(t),a^\dagger(t')]\rangle, \tag{A.1a}$$
$$G^A(t,t') := \quad \mathrm{i}\theta(t'-t)\langle[a(t),a^\dagger(t')]\rangle. \tag{A.1b}$$

Directly related are two different ways of defining the *spectral function*,

$$\rho(t,t') := \mathrm{i}\langle[a(t),a^\dagger(t')]\rangle, \tag{A.2a}$$
$$A(t,t') := -\mathrm{i}\rho(t,t'). \tag{A.2b}$$

The statistical information is usually summarized in either the *statistical function*

$$F(t,t') := \frac{1}{2}\langle\{a(t),a^\dagger(t')\}\rangle \tag{A.3}$$

or the *Keldysh* component

$$G^K(t,t') := -2\mathrm{i}F(t,t'). \tag{A.4}$$

Evidently, all of these functions are defined in terms of expectation values of the commutator and anti-commutator,

$$\langle[a(t),a^\dagger(t')]\rangle = \langle a(t)a^\dagger(t')\rangle - \langle a^\dagger(t')a(t)\rangle$$
$$\langle\{a(t),a^\dagger(t')\}\rangle = \langle a(t)a^\dagger(t')\rangle + \langle a^\dagger(t')a(t)\rangle.$$

This naturally leads us to consider the *greater* and *lesser* components

$$G^{>}(t,t') := -\mathrm{i}\langle a(t)a^{\dagger}(t')\rangle, \tag{A.5a}$$
$$G^{<}(t,t') := -\mathrm{i}\langle a^{\dagger}(t')a(t)\rangle, \tag{A.5b}$$

which are given primacy in this thesis. The *time-ordered* and *anti-time-ordered* components are defined via these as

$$G^{T}(t,t') := -\mathrm{i}\left\langle T\left(a(t)a^{\dagger}(t')\right)\right\rangle = \theta(t-t')G^{>}(t,t') + \theta(t'-t)G^{<}(t,t'), \tag{A.6a}$$
$$G^{\tilde{T}}(t,t') := -\mathrm{i}\left\langle \tilde{T}\left(a(t)a^{\dagger}(t')\right)\right\rangle = \theta(t-t')G^{<}(t,t') + \theta(t'-t)G^{>}(t,t'). \tag{A.6b}$$

It is possible to encounter the alternative notation

$$\begin{pmatrix} G^{++} & G^{+-} \\ G^{-+} & G^{--} \end{pmatrix} = \begin{pmatrix} G^{T} & G^{<} \\ G^{>} & G^{\tilde{T}} \end{pmatrix}. \tag{A.7}$$

Coming to some important identities, we note

$$G^{T}(t,t') + G^{\tilde{T}}(t,t') - \left(G^{>}(t,t') + G^{<}(t,t')\right) = 0, \tag{A.8}$$

from which the Keldysh representation is constructed. Furthermore, observe

$$G^{R}(t,t') = -\theta(t-t')\left(G^{<}(t,t') - G^{>}(t,t')\right) = -\theta(t-t')\rho(t,t'), \tag{A.9a}$$
$$G^{A}(t,t') = \quad \theta(t'-t)\left(G^{<}(t,t') - G^{>}(t,t')\right) = \quad \theta(t'-t)\rho(t,t'), \tag{A.9b}$$

which also implies that [61]

$$\rho(t,t') = G^{<}(t,t') - G^{>}(t,t') = G^{A}(t,t') - G^{R}(t,t'), \tag{A.10}$$

Similarly, we find

$$F(t,t') = \frac{\mathrm{i}}{2}\left(G^{<}(t,t') + G^{>}(t,t')\right). \tag{A.11}$$

Two frequently used equal-time identities are

$$\begin{aligned} G^{A}(t,t) - G^{R}(t,t) &= \mathrm{i}, \\ G^{A}(t,t) + G^{R}(t,t) &= 0, \end{aligned} \tag{A.12}$$

although technically these should never appear.

A.2 Gaussian Integration

In a notation that relates to the main body of this thesis, the quadratic Gaussian integral is

$$\begin{aligned} I_{\text{Gauss}} &= \int \mathrm{d}^d\varphi \exp\left\{\mathrm{i}S[\boldsymbol{\varphi}]\right\} \\ &= \int \mathrm{d}^d\varphi \exp\left\{\frac{\mathrm{i}}{2}\boldsymbol{\varphi}^T\left(\partial^2 S[\boldsymbol{\varphi}]\right)\boldsymbol{\varphi}\right\} \\ &= \int \mathrm{d}^d\varphi \exp\left\{-\frac{1}{2}\boldsymbol{\varphi}^T\boldsymbol{G}_0^{-1}\boldsymbol{\varphi}\right\} \\ &= (2\pi)^{d/2}\left(\det \boldsymbol{G}_0^{-1}\right)^{-1/2}, \end{aligned} \tag{A.13}$$

with $\boldsymbol{G}_0^{-1} = -\mathrm{i}\partial^2 S[\boldsymbol{\varphi}]$ and the Hessian matrix

$$\partial^2 S[\boldsymbol{\varphi}] = \begin{pmatrix} \frac{\delta^2 S[\boldsymbol{\varphi}]}{\delta\varphi_1^2} & \cdots & \frac{\delta^2 S[\boldsymbol{\varphi}]}{\delta\varphi_1\delta\varphi_d} \\ \vdots & \ddots & \vdots \\ \frac{\delta^2 S[\boldsymbol{\varphi}]}{\delta\varphi_d\delta\varphi_1} & \cdots & \frac{\delta^2 S[\boldsymbol{\varphi}]}{\delta\varphi_d^2} \end{pmatrix}. \tag{A.14}$$

Furthermore, we have

$$\int \mathrm{d}^d\varphi \exp\left\{-\frac{1}{2}\boldsymbol{\varphi}^T\boldsymbol{G}_0^{-1}\boldsymbol{\varphi} + \boldsymbol{j}^T\boldsymbol{\varphi}\right\} = (2\pi)^{d/2}\left(\det \boldsymbol{G}_0^{-1}\right)^{-1/2}\exp\left\{\frac{1}{2}\boldsymbol{j}^T\boldsymbol{G}_0\,\boldsymbol{j}\right\}, \tag{A.15}$$

which proves immediately that

$$\begin{aligned} \langle\varphi_\alpha\varphi_\beta\rangle &= (2\pi)^{-d/2}\left(\det \boldsymbol{G}_0^{-1}\right)^{1/2}\int \mathrm{d}^d\varphi\ \varphi_\alpha\varphi_\beta \exp\left\{-\frac{1}{2}\boldsymbol{\varphi}^T\boldsymbol{G}_0^{-1}\boldsymbol{\varphi}\right\} \\ &= (2\pi)^{-d/2}\left(\det \boldsymbol{G}_0^{-1}\right)^{1/2}\left[\frac{\delta^2}{\delta j_\alpha \delta j_\beta}\int \mathrm{d}^d\varphi\ \exp\left\{-\frac{1}{2}\boldsymbol{\varphi}^T\boldsymbol{G}_0^{-1}\boldsymbol{\varphi} + \boldsymbol{j}^T\boldsymbol{\varphi}\right\}\right]_{\boldsymbol{j}=0} \\ &= \left[\frac{\delta^2}{\delta j_\alpha \delta j_\beta}\exp\left\{\frac{1}{2}\boldsymbol{j}^T\boldsymbol{G}_0\,\boldsymbol{j}\right\}\right]_{\boldsymbol{j}=0} \\ &= (\boldsymbol{G}_0)_{\alpha\beta} = \mathrm{i}G_{\alpha\beta}, \end{aligned} \tag{A.16}$$

assuming that $\boldsymbol{G}_0$ is symmetric. Finally, we state the important identity

$$-\mathrm{i}\ln I_{\text{Gauss}} = \text{const.} + \frac{\mathrm{i}}{2}\mathrm{Tr}\ln \boldsymbol{G}_0^{-1}. \tag{A.17}$$

A.3 Functional Differentiation

In this section, we summarize a few useful functional differential identities. For the matrix logarithm, one finds

$$\begin{aligned}(\ln \boldsymbol{A}(x))' &= \boldsymbol{T}\,\mathrm{diag}(\lambda_i^{-1}(x))\,\mathrm{diag}(\lambda_i'(x))\boldsymbol{T}^{-1} \\ &= \boldsymbol{T}\boldsymbol{D}^{-1}\boldsymbol{T}^{-1}\boldsymbol{T}\,\mathrm{diag}(\lambda_i'(x))\boldsymbol{T}^{-1} = \boldsymbol{A}^{-1}\boldsymbol{A}'.\end{aligned} \tag{A.18}$$

Furthermore, one may write $0 = \big(\boldsymbol{A}(x)\boldsymbol{A}^{-1}(x)\big)' = \boldsymbol{A}'(x)\boldsymbol{A}^{-1}(x) + \boldsymbol{A}(x)\big(\boldsymbol{A}^{-1}(x)\big)'$, from which it follows that

$$\big(\boldsymbol{A}^{-1}(x)\big)' = -\boldsymbol{A}^{-1}(x)\boldsymbol{A}'(x)\boldsymbol{A}^{-1}(x). \tag{A.19}$$

A related result important for the 2PI effective action reads

$$\begin{aligned}\frac{\delta}{\delta G_{ji}}\,\mathrm{Tr}\ln \boldsymbol{G}^{-1} &= \mathrm{Tr}\,\frac{\delta \boldsymbol{G}^{-1}}{\delta G_{ji}}\frac{\delta}{\delta \boldsymbol{G}^{-1}}\ln \boldsymbol{G}^{-1} \\ &= \mathrm{Tr}\,\boldsymbol{G}\frac{\delta \boldsymbol{G}^{-1}}{\delta G_{ji}} = -\,\mathrm{Tr}\,\boldsymbol{G}\boldsymbol{G}^{-1}\frac{\delta \boldsymbol{G}}{\delta G_{ji}}\boldsymbol{G}^{-1} \\ &= -G^{-1}_{ab}\frac{\delta G_{ba}}{\delta G_{ji}} = -G^{-1}_{ab}\delta_{ai}\delta_{bj} = -G^{-1}_{ij},\end{aligned} \tag{A.20}$$

where we have switched to summation convention in the last line. In the presence of time-ordered fields, one should also be aware of

$$\begin{aligned}\frac{\delta}{\delta\phi(t)\delta\hat{\phi}^*(t')}\int \mathrm{d}s\;\hat{\phi}^*(s^\pm)\phi(s) &= \frac{\delta}{\delta\phi(t)}\phi(t'^\mp) = \delta(t^\pm - t'), \\ \frac{\delta}{\delta\hat{\phi}^*(t)\delta\phi(t')}\int \mathrm{d}s\;\hat{\phi}^*(s^\pm)\phi(s) &= \frac{\delta}{\delta\hat{\phi}(t)}\hat{\phi}^*(t'^\pm) = \delta(t^\mp - t').\end{aligned} \tag{A.21}$$

A.4 Effective Action

In the framework of the 1PI effective action $\Gamma = \Gamma[\varphi]$, for the two-point function

$$G(x,y) = -\frac{\delta^2 W[j,K]}{\delta j(x)\delta j(y)} \tag{A.22}$$

there holds the well-known identity

$$\int \mathrm{d}z\;\frac{\delta^2\Gamma[\varphi]}{\delta\varphi(x)\delta\varphi(z)}G(z,y) = \delta(x-y). \tag{A.23}$$

It can be proved by noticing that the adjoint Legendre-transform relations $\delta W[j,K]/\delta j(x) = \varphi(x)$ and $j(x) = -\delta\Gamma[\varphi]/\delta\varphi(x)$ imply

$$G^{-1}(x,y) = -\left(\frac{\delta\varphi(x)}{\delta j(y)}\right)^{-1} = -\frac{\delta j(y)}{\delta\varphi(x)} = \frac{\delta^2\Gamma[\varphi]}{\delta\varphi(x)\delta\varphi(y)}, \tag{A.24}$$

where the inverse is understood in the functional sense. An obvious question to ask is: What constitutes the equivalent identity for the 2PI effective action $\Gamma = \Gamma[\varphi, G]$? The answer can be found without proof in a footnote of Ref. [90] and reads

$$-\frac{1}{\hbar}\begin{pmatrix} W_{jj} & W_{jK} \\ W_{Kj} & W_{KK}\end{pmatrix}\begin{pmatrix} \hbar\Gamma_{\varphi\varphi} - 2\Gamma_G - 4\varphi\Gamma_{\varphi G} + 4\varphi^2\Gamma_{GG}/\hbar & 2\hbar\Gamma_{\varphi G} - 4\varphi\Gamma_{GG}/\hbar \\ 2\hbar\Gamma_{\varphi G} - 4\varphi\Gamma_{GG}/\hbar & 4\Gamma_{GG}/\hbar\end{pmatrix} = \mathbb{1}, \tag{A.25}$$

where we have resorted to writing functional derivatives as subscripts. To prove this identity, we employ the *implicit-function theorem*. As a reminder, consider the standard example of a function $f : \mathbb{R}^2 \to \mathbb{R}$, where $f(x,y) = x^2 + y^2 - 1$. This implicitly defines a function $y : \mathbb{R} \to \mathbb{R}$. The theorem now allows one to calculate the derivative of $y(x)$ without knowing its functional form explicitly. Specifically, in this case

$$y_x(x) = -\big(f_y(x,y(x))\big)^{-1} f_x(x,y(x)) = -\frac{x}{y(x)}, \tag{A.26}$$

which from $y(x) = \pm\sqrt{1-x^2}$ can be seen to give the correct answer. To prove Eq. (A.25), we need the theorem in the form

$$\begin{pmatrix} x_u & x_v \\ y_u & y_v\end{pmatrix} = -\begin{pmatrix} f_{xx} & f_{xy} \\ f_{yx} & f_{yy}\end{pmatrix}^{-1}\begin{pmatrix} S_u & S_v \\ T_u & T_v\end{pmatrix}, \tag{A.27}$$

where the functions $x,\ y : \mathbb{R}^2 \to \mathbb{R}$ are defined implicitly via

$$\begin{aligned} S(x,y,u,v) &= f_x(x,y) - u, \\ T(x,y,u,v) &= f_y(x,y) - \frac{1}{2}\left(u^2 + cv\right), \end{aligned} \tag{A.28}$$

where c is a constant. To make the connection with Eq. (A.25), note the correspondences $x \leftrightarrow j$, $y \leftrightarrow K$, $u \leftrightarrow \varphi$ and $v \leftrightarrow G$. The functions S and T are defined according to the double Legendre transform used in the 2PI effective action,

$$f(u,v) = f(x(u,v),y(u,v)) - ux(u,v) - \frac{1}{2}\left(u^2 + cv\right)y(u,v). \tag{A.29}$$

The inverse relations are

$$\begin{aligned} f_u(u,v) &= -x - yu, \\ f_v(u,v) &= -cy/2. \end{aligned} \tag{A.30}$$

To make another connection, the Legendre transform familiar from classical mechanics and the 1PI effective action would read

$$f(u,y) = ux(u) - f(x(u),y). \tag{A.31}$$

Note also that $f(u,v)$ corresponds to $\Gamma[\varphi,G]$, while its adjoint $f(x,y)$, for which we use the same function symbol, corresponds to $W[j,K]$. Eq. (A.27) is equivalent to

$$\begin{pmatrix} x_u & x_v \\ y_u & y_v \end{pmatrix} \begin{pmatrix} -1 & 0 \\ -u & -c/2 \end{pmatrix}^{-1} = -\begin{pmatrix} f_{xx} & f_{xy} \\ f_{yx} & f_{yy} \end{pmatrix}^{-1}, \tag{A.32}$$

in which we still have to determine the derivatives on the left-hand side. From (A.30), we know

$$\begin{aligned} f_{uu} &= -\left(x_u + y + uy_u\right), \\ f_{uv} &= -\left(x_v + uy_v\right) = -cy_u/2, \\ f_{vv} &= -cy_v/2, \end{aligned} \tag{A.33}$$

which can be solved for $x_{u,v}$ and $y_{u,v}$ to yield

$$\begin{aligned} x_u &= 2uf_{uv}/c - f_{uu} + 2f_v/c, \\ x_v &= 2uf_{vv}/c - f_{uv}, \\ y_u &= -2f_{uv}/c, \\ y_v &= -2f_{vv}/c. \end{aligned} \tag{A.34}$$

where in solving for $x_{u,v}$, we have inserted y and y_v from the second equation in (A.30), respectively. Feeding these back into the left-hand side of Eq. (A.32), we obtain

$$\begin{aligned} \frac{1}{c}\begin{pmatrix} x_u & x_v \\ y_u & y_v \end{pmatrix} \begin{pmatrix} -c & 0 \\ 2u & -2 \end{pmatrix} &= \frac{1}{c}\begin{pmatrix} -cx_u + 2ux_v & -2x_v \\ -cy_u + 2uy_v & -2y_v \end{pmatrix} \\ &= \frac{1}{c}\begin{pmatrix} cf_{uu} - 2f_v - 4uf_{uv} + 4u^2 f_{vv}/c & 2f_{uv} - 4uf_{vv}/c \\ 2f_{uv} - 4uf_{vv}/c & 4f_{vv}/c \end{pmatrix}, \end{aligned} \tag{A.35}$$

which, *eo ipso*, proves Eq. (A.25) if we set $c = \hbar$ and use the above correspondences.[1] Mathematically, the essence of this procedure is that we have expressed the inverse Hessian matrix via the Legendre-transformed quantities.

[1] Be aware that this convention does not conform to the Legendre transform used in Sec. 2.2 where $c = \mathrm{i}\hbar$.

APPENDIX B

Stochastic Calculus

B.1 Multivariate Fokker-Planck and Langevin Equations

The multivariate stochastic differential equation (SDE)

$$\mathrm{d}\boldsymbol{x} = \boldsymbol{A}(\boldsymbol{x},t)\mathrm{d}t + \boldsymbol{B}(\boldsymbol{x},t)\mathrm{d}\boldsymbol{W}(t) \tag{B.1}$$

is equivalent to the Fokker-Planck equation [54, 58]

$$\dot{P}(\boldsymbol{x},t) = -\sum_i \partial_i \left[A_i(\boldsymbol{x},t)P(\boldsymbol{x},t)\right] + \frac{1}{2}\sum_{i,j}\partial_i\partial_j\left\{\left[\boldsymbol{B}(\boldsymbol{x},t)\boldsymbol{B}^{\mathrm{T}}(\boldsymbol{x},t)\right]_{ij}P(\boldsymbol{x},t)\right\}. \tag{B.2}$$

The Fokker-Planck equation (1.92),

$$\dot{\mathcal{W}}\left(\alpha,\alpha^*\right) = \left[\left(\mathrm{i}\omega_0 + \frac{\lambda}{2}\right)\frac{\partial}{\partial\alpha}\alpha - \left(\mathrm{i}\omega_0 - \frac{\lambda}{2}\right)\frac{\partial}{\partial\alpha^*}\alpha^* + \frac{\lambda}{2}\frac{\partial^2}{\partial\alpha\partial\alpha^*}\right]\mathcal{W}\left(\alpha,\alpha^*\right), \tag{B.3}$$

then has a diffusion matrix

$$\boldsymbol{B}(\boldsymbol{\alpha},t)\boldsymbol{B}^T(\boldsymbol{\alpha},t) = \begin{pmatrix} 0 & \lambda/2 \\ \lambda/2 & 0 \end{pmatrix}. \tag{B.4}$$

Possible solutions for $\boldsymbol{B}$ are therefore

$$\boldsymbol{B} = \sqrt{\lambda/2}\,\frac{1}{\sqrt{2}}\begin{pmatrix} 1 & \pm\mathrm{i} \\ 1 & \mp\mathrm{i} \end{pmatrix}. \tag{B.5}$$

Accordingly, its SDE is

$$\begin{aligned} \mathrm{d}\alpha &= -\left(\mathrm{i}\omega_0 + \lambda/2\right)\alpha\,\mathrm{d}t + \boldsymbol{B}\left(\mathrm{d}W_1, \mathrm{d}W_2\right)^T \\ &= -\left(\mathrm{i}\omega_0 + \lambda/2\right)\alpha\,\mathrm{d}t + \sqrt{\lambda/2}\,\frac{\mathrm{d}W_1 \pm \mathrm{i}\,\mathrm{d}W_2}{\sqrt{2}}. \end{aligned} \tag{B.6}$$

With $\alpha = q + \mathrm{i}p$, this turns into the pair of equations

$$\begin{aligned} \mathrm{d}q &= \quad (\omega_0 p - \lambda q/2)\,\mathrm{d}t + \sqrt{\lambda/2}\,\mathrm{d}W_1/\sqrt{2}, \\ \mathrm{d}p &= -(\omega_0 q + \lambda p/2)\,\mathrm{d}t \pm \sqrt{\lambda/2}\,\mathrm{d}W_2/\sqrt{2}. \end{aligned} \tag{B.7}$$

From Eq. (B.2), this is equivalent to a Fokker-Planck equation

$$\dot{\mathcal{W}}(q,p) = \left[\omega_0\left(\frac{\partial}{\partial p}q - \frac{\partial}{\partial q}p\right) + \frac{\lambda}{2}\left(\frac{\partial}{\partial q}q + \frac{\partial}{\partial p}p\right) + \frac{\lambda}{4}\left(\frac{1}{2}\frac{\partial^2}{\partial q^2} + \frac{1}{2}\frac{\partial^2}{\partial p^2}\right)\right]\mathcal{W}(q,p)\,.$$

Note that the factors of $1/2$ in the diffusive part are accidentally missing from Eq. (6.2.5) of [59] (they are present in an older version of the book).

B.2 Polar Coordinates

B.2.1 Fokker-Planck Equation

Turning back to equations (1.92) and (B.3), we would like to be able to perform the substitution $\alpha = r\mathrm{e}^{\mathrm{i}\varphi}$, where the corresponding Jacobian determinant reads

$$\det \mathcal{J} = \left|\begin{pmatrix} \mathrm{e}^{\mathrm{i}\varphi} & \mathrm{i}r\mathrm{e}^{\mathrm{i}\varphi} \\ \mathrm{e}^{-\mathrm{i}\varphi} & -\mathrm{i}r\mathrm{e}^{-\mathrm{i}\varphi} \end{pmatrix}\right| = -2\mathrm{i}r. \tag{B.8}$$

The distribution transforms as $\mathcal{W}(\alpha,\alpha^*) = |\det\mathcal{J}|^{-1}\,\mathcal{W}(r,\varphi) = \mathcal{W}(r,\varphi)/2r$. From

$$\frac{\partial}{\partial\alpha}f(\alpha,\alpha^*) = \frac{\mathrm{d}}{\mathrm{d}\alpha}f(r(\alpha,\alpha^*),\varphi(\alpha,\alpha^*)) = \frac{\partial f}{\partial r}\frac{\partial r}{\partial\alpha} + \frac{\partial f}{\partial\varphi}\frac{\partial\varphi}{\partial\alpha}, \tag{B.9}$$

we find with $2\partial r/\partial\alpha = \sqrt{\alpha^*/\alpha} = \mathrm{e}^{-\mathrm{i}\varphi}$ and $2\mathrm{i}\partial\varphi/\partial\alpha = 1/\alpha = \mathrm{e}^{-\mathrm{i}\varphi}/r$ that

$$\frac{\partial f(\alpha,\alpha^*)}{\partial\alpha} = \frac{\mathrm{e}^{-\mathrm{i}\varphi}}{2}\left[\frac{\partial f(r,\varphi)}{\partial r} + \frac{1}{\mathrm{i}r}\frac{\partial f(r,\varphi)}{\partial\varphi}\right]. \tag{B.10}$$

Hence, we may calculate

$$\frac{\partial}{\partial\alpha}\alpha = \frac{1}{2}\left[\frac{\partial}{\partial r}r - \mathrm{i}\mathrm{e}^{-\mathrm{i}\varphi}\frac{\partial}{\partial\varphi}\mathrm{e}^{\mathrm{i}\varphi}\right], \tag{B.11}$$

and

$$\begin{aligned} \frac{\partial}{\partial\alpha}\alpha + \frac{\partial}{\partial\alpha^*}\alpha^* &= \frac{\partial}{\partial r}r + 1 = \frac{1}{r}\frac{\partial}{\partial r}r^2, \\ \frac{\partial}{\partial\alpha}\alpha - \frac{\partial}{\partial\alpha^*}\alpha^* &= -\mathrm{i}\frac{\partial}{\partial\varphi}. \end{aligned} \tag{B.12}$$

For the diffusion term, we need

$$\frac{\partial^2}{\partial\alpha\partial\alpha^*} = \frac{1}{4}\left[\frac{1}{r}\frac{\partial}{\partial r}r\frac{\partial}{\partial r} + \frac{1}{r^2}\frac{\partial^2}{\partial\varphi^2}\right]. \tag{B.13}$$

The Fokker-Planck equation of the Wigner distribution in polar coordinates finally reads

$$\dot{\mathcal{W}}(r,\varphi) = \omega_0\frac{\partial}{\partial\varphi}\mathcal{W}(r,\varphi) + \frac{\lambda}{2}\frac{\partial}{\partial r}r\mathcal{W}(r,\varphi) + \frac{\lambda}{4}\left[\frac{1}{2}\frac{\partial}{\partial r}r\frac{\partial}{\partial r}\frac{1}{r} + \frac{1}{2}\frac{1}{r^2}\frac{\partial^2}{\partial\varphi^2}\right]\mathcal{W}(r,\varphi). \tag{B.14}$$

To make this physically intuitive, we should make the further substitution $r = \sqrt{N}$, which implies $\mathcal{W}(r,\varphi) = 2\sqrt{N}\mathcal{W}(N,\varphi)$. Furthermore, we have $\partial/\partial r = 2\sqrt{N}\partial/\partial N$. As a function of the particle number, the Wigner distribution then obeys

$$\dot{\mathcal{W}}(N,\varphi) = \left[\omega_0\frac{\partial}{\partial\varphi} + \lambda\frac{\partial}{\partial N}\left(N - 1/2\right)\right]\mathcal{W}(N,\varphi) + \frac{\lambda}{2}\left[\frac{\partial^2}{\partial N^2}N + \frac{1}{4N}\frac{\partial^2}{\partial\varphi^2}\right]\mathcal{W}(N,\varphi),$$

in which the loss manifestly does not act on the vacuum fluctuations. The SDE for phase and particle number can be read off and become

$$\begin{aligned}\mathrm{d}\varphi &= -\omega_0\mathrm{d}t + \frac{1}{2}\sqrt{\lambda/N}\mathrm{d}W_\varphi,\\ \mathrm{d}N &= -\lambda\left(N - 1/2\right)\mathrm{d}t + \sqrt{\lambda N}\mathrm{d}W_N,\end{aligned} \tag{B.15}$$

where we have introduced the independent Wiener processes W_φ and W_N, respectively. This nicely underlines how it is possible for a lossy Bose field to have both a well-defined particle number *and* phase. If $N \gg 1$, then phase fluctuations are evidently suppressed. Yet in this case, certainly $N \gg \sqrt{N}$ holds almost as well, such that particle-number fluctuations may also be neglected.

B.2.2 Itô Calculus

It is instructive to repeat the change of variables directly on the level of the SDE by means of the *Itô calculus*. Writing Eq. (B.6) and its adjoint as

$$\begin{aligned}\mathrm{d}\alpha &= -\left(\mathrm{i}\omega_0 + \lambda/2\right)\alpha\ \mathrm{d}t + \sqrt{\lambda/2}\,\mathrm{d}W_\alpha,\\ \mathrm{d}\alpha^* &= \left(\mathrm{i}\omega_0 - \lambda/2\right)\alpha^*\mathrm{d}t + \sqrt{\lambda/2}\,\mathrm{d}W_\alpha^*,\end{aligned} \tag{B.16}$$

we apply Itô's lemma to the functions $\varphi(\alpha,\alpha^*) = -\mathrm{i}(\ln\alpha - \ln\alpha^*)/2$ and $N(\alpha,\alpha^*) = \alpha^*\alpha$, i.e.

$$\begin{aligned}
\mathrm{d}\varphi &= \frac{1}{2\mathrm{i}}\left\{\frac{\mathrm{d}\alpha}{\alpha} - \frac{\mathrm{d}\alpha^*}{\alpha^*} - \frac{1}{2}\left[\left(\frac{\mathrm{d}\alpha}{\alpha}\right)^2 - \left(\frac{\mathrm{d}\alpha^*}{\alpha^*}\right)^2\right]\right\} \\
&= \frac{1}{2\mathrm{i}}\Big[-2\mathrm{i}\omega_0\mathrm{d}t + \sqrt{\lambda/2N}\left(\mathrm{e}^{-\mathrm{i}\varphi}\mathrm{d}W_\alpha - \mathrm{e}^{\mathrm{i}\varphi}\mathrm{d}W_\alpha^*\right) \\
&\quad - (\lambda/4N)\left(\left(\mathrm{e}^{-\mathrm{i}\varphi}\mathrm{d}W_\alpha\right)^2 - \left(\mathrm{e}^{\mathrm{i}\varphi}\mathrm{d}W_\alpha^*\right)^2\right)\mathrm{d}t\Big], \\
\mathrm{d}N &= \alpha^*\mathrm{d}\alpha + \alpha\mathrm{d}\alpha^* + \mathrm{d}\alpha\mathrm{d}\alpha^* \\
&= -\lambda N\mathrm{d}t + \sqrt{\lambda N/2}\left(\mathrm{e}^{-\mathrm{i}\varphi}\mathrm{d}W_\alpha + \mathrm{e}^{\mathrm{i}\varphi}\mathrm{d}W_\alpha^*\right) + \lambda\mathrm{d}t/2,
\end{aligned} \tag{B.17}$$

where from the second-order terms of the Taylor expansion we have only kept $\mathrm{d}W_\alpha^2 \sim \mathrm{d}t$ and dropped both $\mathrm{d}t\mathrm{d}W_\alpha \sim \mathrm{d}t^{3/2}$ and $\mathrm{d}t^2$. The Wiener processes

$$\begin{aligned}
W_\varphi &= \frac{1}{\sqrt{2}\mathrm{i}}\left(\mathrm{e}^{-\mathrm{i}\varphi}\mathrm{d}W_\alpha - \mathrm{e}^{\mathrm{i}\varphi}\mathrm{d}W_\alpha^*\right) = \sqrt{2}\,\mathrm{Im}\left[\mathrm{e}^{-\mathrm{i}\varphi}\mathrm{d}W_\alpha\right] \\
&= \cos\varphi\,\mathrm{d}W_2 - \sin\varphi\,\mathrm{d}W_1, \\
W_N &= \frac{1}{\sqrt{2}}\left(\mathrm{e}^{-\mathrm{i}\varphi}\mathrm{d}W_\alpha + \mathrm{e}^{\mathrm{i}\varphi}\mathrm{d}W_\alpha^*\right) = \sqrt{2}\,\mathrm{Re}\left[\mathrm{e}^{-\mathrm{i}\varphi}\mathrm{d}W_\alpha\right] \\
&= \cos\varphi\,\mathrm{d}W_1 + \sin\varphi\,\mathrm{d}W_2
\end{aligned} \tag{B.18}$$

are connected to $W_{1,2}$ by an orthogonal transformation and may be considered as independent [54]. Therefore, we can also write $\sqrt{2}\mathrm{e}^{-\mathrm{i}\varphi}\mathrm{d}W_\alpha = \mathrm{d}W_N + \mathrm{i}\mathrm{d}W_\varphi$ and conclude

$$\mathrm{Im}\left[\left(\mathrm{e}^{-\mathrm{i}\varphi}\mathrm{d}W_\alpha\right)^2\right] = \mathrm{d}W_N\mathrm{d}W_\varphi = 0. \tag{B.19}$$

Using all of this on Eqs. (B.17), we have

$$\begin{aligned}
\mathrm{d}\varphi &= -\omega_0\mathrm{d}t + \frac{1}{2}\sqrt{\lambda/N}\mathrm{d}W_\varphi, \\
\mathrm{d}N &= -\lambda N\mathrm{d}t + \sqrt{\lambda N}\mathrm{d}W_N + \lambda\mathrm{d}t/2,
\end{aligned} \tag{B.20}$$

which is identical to Eqs. (B.15).

B.3 Positive P Representation

This section is devoted to a few applications of the positive P representation [66–68]. It allows one to map even interacting Bose systems to proper Fokker-Planck equations. As was remarked in the introduction (cf. 1.5.4), this is not possible, for instance, by means of the Wigner representation. Now the *complex* P operator-phase-space correspondences are

$$\begin{aligned} a\rho &\longleftarrow \alpha P(\boldsymbol{\alpha}), \\ a^\dagger\rho &\longleftarrow (\beta - \partial/\partial\alpha)P(\boldsymbol{\alpha}), \\ \rho a^\dagger &\longleftarrow \beta P(\boldsymbol{\alpha}), \\ \rho a &\longleftarrow (\alpha - \partial/\partial\beta)P(\boldsymbol{\alpha}), \end{aligned} \tag{B.21}$$

where $\boldsymbol{\alpha} = (\alpha, \alpha^*, \beta, \beta^*)^T$. When applying these rules sequentially, one finds, e.g.

$$\left[\rho a^\dagger\right] a = (\alpha - \partial/\partial\beta)\left[\beta P(\boldsymbol{\alpha})\right] = \left(\alpha\beta - \frac{\partial}{\partial\beta}\beta\right) P(\boldsymbol{\alpha}). \tag{B.22}$$

The jump terms require a moment's reflection to see that

$$\begin{aligned} a^\dagger\rho a &= (\beta - \partial/\partial\alpha)(\alpha - \partial/\partial\beta)P(\boldsymbol{\alpha}) \\ &= \left\{\alpha\beta - \frac{\partial}{\partial\alpha}\alpha - \beta\frac{\partial}{\partial\beta} + \frac{\partial^2}{\partial\alpha\partial\beta}\right\} P(\boldsymbol{\alpha}) \\ &= \left\{\alpha\beta - \alpha\frac{\partial}{\partial\alpha} - \frac{\partial}{\partial\beta}\beta + \frac{\partial^2}{\partial\alpha\partial\beta}\right\} P(\boldsymbol{\alpha}) \\ &= (\alpha - \partial/\partial\beta)(\beta - \partial/\partial\alpha)P(\boldsymbol{\alpha}). \end{aligned} \tag{B.23}$$

Upon using the analyticity of the projection operator $\Lambda(\boldsymbol{\alpha})$ [59] and with $\alpha = \alpha_x + \mathrm{i}\alpha_y$, we may replace the derivatives in (B.21) according to

$$\frac{\partial}{\partial\alpha} = \frac{\partial}{\partial\alpha_x} = -\mathrm{i}\frac{\partial}{\partial\alpha_y}, \tag{B.24}$$

and analogously for β, which then yields the correspondences of the *positive* P representation.

B.3.1 Driven-Dissipative Single-Mode Cavity

As a first application, we take the standard driven-dissipative, single-mode master equation

$$\dot\rho = -\mathrm{i}\omega_0[a^\dagger a, \rho] + \frac{\gamma}{2}\left\{\left(\bar N + 1\right)\mathcal{L}[a] + \bar N\mathcal{L}[a^\dagger]\right\}\rho. \tag{B.25}$$

We then find a Fokker-Planck equation

$$\begin{aligned}\dot{P} = &-\mathrm{i}\omega_0 \left(-\frac{\partial}{\partial\alpha}\alpha + \frac{\partial}{\partial\beta}\beta\right) P + \frac{\gamma}{2}\left(\bar{N}+1\right)\left(2\alpha\beta - \alpha\beta + \frac{\partial}{\partial\alpha}\alpha - \alpha\beta + \frac{\partial}{\partial\beta}\beta\right) P \\ &+ \frac{\gamma}{2}\bar{N}\left[2\left(\alpha\beta - \frac{\partial}{\partial\alpha}\alpha - \beta\frac{\partial}{\partial\beta} + \frac{\partial^2}{\partial\alpha\partial\beta}\right) - \alpha\beta + \alpha\frac{\partial}{\partial\alpha} - \alpha\beta + \beta\frac{\partial}{\partial\beta}\right] P.\end{aligned} \tag{B.26}$$

Bringing the drift terms into standard form (derivatives to the left of variables) and collecting terms, we obtain the much simpler form

$$\begin{aligned}\dot{P} = &-\mathrm{i}\omega_0 \left(-\frac{\partial}{\partial\alpha}\alpha + \frac{\partial}{\partial\beta}\beta\right) P \\ &+ \frac{\gamma}{2}\left(\frac{\partial}{\partial\alpha}\alpha + \frac{\partial}{\partial\beta}\beta\right) P + \gamma\bar{N}\frac{\partial^2}{\partial\alpha\partial\beta}P.\end{aligned} \tag{B.27}$$

This is not a valid Fokker-Planck equation, though, because we are lacking the "diagonal" diffusion terms $\partial^2/\partial\alpha^2$, $\partial^2/\partial\beta^2$. Fortunately, having the positive P representation at our disposal, we can resort to a trick to solve this problem and write[1]

$$\begin{aligned}\frac{\partial^2}{\partial\alpha\partial\beta} &= c\left(\frac{\partial^2}{\partial\alpha^2} - \frac{\partial^2}{\partial\alpha^2} + \frac{\partial^2}{\partial\beta^2} - \frac{\partial^2}{\partial\beta^2}\right) + \frac{\partial^2}{\partial\alpha\partial\beta} \\ &= c\left(\frac{\partial^2}{\partial\alpha_x^2} + \frac{\partial^2}{\partial\alpha_y^2} + \frac{\partial^2}{\partial\beta_x^2} + \frac{\partial^2}{\partial\beta_y^2}\right) + \frac{1}{2}\left(\frac{\partial^2}{\partial\alpha_x\partial\beta_x} - \frac{\partial^2}{\partial\alpha_y\partial\beta_y}\right),\end{aligned} \tag{B.28}$$

where c is an arbitrary constant, which we set to $c = 1/4$ for simplicity. Then the diffusion matrix from B.1 is

$$\boldsymbol{B}(\boldsymbol{\alpha})\boldsymbol{B}^T(\boldsymbol{\alpha}) = \frac{\gamma\bar{N}}{2}\begin{pmatrix}\boldsymbol{B}_x\boldsymbol{B}_x^T & \boldsymbol{B}_x\boldsymbol{B}_y^T \\ \boldsymbol{B}_y\boldsymbol{B}_x^T & \boldsymbol{B}_y\boldsymbol{B}_y^T\end{pmatrix} = \frac{\gamma\bar{N}}{2}\begin{pmatrix}1 & 1 & 0 & 0 \\ 1 & 1 & 0 & 0 \\ 0 & 0 & 1 & -1 \\ 0 & 0 & -1 & 1\end{pmatrix}, \tag{B.29}$$

where now $\boldsymbol{\alpha} = (\alpha_x, \beta_x, \alpha_y, \beta_y)^T$. The matrices $\boldsymbol{B}_{x,y}$ are found to be

$$\begin{aligned}\boldsymbol{B}_x &= \sqrt{\gamma\bar{N}/2}\begin{pmatrix}1 & 0 \\ 1 & 0\end{pmatrix}, \\ \boldsymbol{B}_y &= \sqrt{\gamma\bar{N}/2}\begin{pmatrix}0 & 1 \\ 0 & -1\end{pmatrix}.\end{aligned} \tag{B.30}$$

[1] Note the connection to the Cauchy-Riemann equations $0 = \left(\partial_x + \mathrm{i}\partial_y\right)\left(u(x,y) + \mathrm{i}v(x,y)\right) = \partial_x u(x,y) - \partial_y v(x,y) + \mathrm{i}\left(\partial_y u(x,y) + \partial_x v(x,y)\right)$ for an analytic function $f(x+\mathrm{i}y) = u(x,y) + \mathrm{i}v(x,y)$.

The stochastic differential equations equivalent to Eq. (B.25) then follow as

$$\mathrm{d}\boldsymbol{\alpha} = \left[-\mathrm{i}\omega_0 \,\mathrm{diag}\,(1,-1,1,-1) - \frac{\gamma}{2}\,\mathrm{diag}\,(1,1,1,1)\right]\boldsymbol{\alpha}\,\mathrm{d}t + \begin{pmatrix}\boldsymbol{B}_x & \mathbf{0}\\ \boldsymbol{B}_y & \mathbf{0}\end{pmatrix}\mathrm{d}\boldsymbol{W}, \tag{B.31}$$

with the vector-valued Wiener-process $\mathrm{d}\boldsymbol{W} = (\mathrm{d}W_1, \mathrm{d}W_2, \mathrm{d}W_1, \mathrm{d}W_2)^T$. Note that while the phase-space dimension does indeed double, only two independent Wiener processes are required (as for the Sudarshan-Glauber P representation).

B.3.2 Interactions

We are in a position to consider an actual interaction term in the Hamiltonian. The obvious choice is $H = Ua^\dagger a^\dagger aa/2$. Then we need the correspondences

$$\begin{aligned} a^\dagger a^\dagger aa\rho &\longleftarrow (\beta - \partial_\alpha)^2\,\alpha^2 P(\boldsymbol{\alpha}),\\ \rho a^\dagger a^\dagger aa &\longleftarrow \left(\alpha - \partial_\beta\right)^2\beta^2 P(\boldsymbol{\alpha}). \end{aligned} \tag{B.32}$$

Instead of the von Neumann equation, there now holds

$$\begin{aligned} \dot{P}(\boldsymbol{\alpha}) &= -\frac{\mathrm{i}U}{2}\left(-2\partial_\alpha\alpha^2\beta + \partial_\alpha^2\alpha^2 + 2\partial_\beta\beta^2\alpha - \partial_\beta^2\beta^2\right)P(\boldsymbol{\alpha})\\ &= -\hat{F}(\boldsymbol{\alpha})P(\boldsymbol{\alpha}) - \frac{\mathrm{i}U}{2}\left(\partial_\alpha^2\alpha^2 - \partial_\beta^2\beta^2\right)P(\boldsymbol{\alpha}), \end{aligned} \tag{B.33}$$

where we have introduced the drift operator $\hat{F}(\boldsymbol{\alpha}) = -\mathrm{i}U\left(\partial_\alpha\alpha^2\beta - \partial_\beta\beta^2\alpha\right)$. Since $-\mathrm{i}\alpha^2 = 2\alpha_x\alpha_y - \mathrm{i}(\alpha_x^2 - \alpha_y^2)$, for each of these terms we have to evaluate ∂_α^2 in such a way as to produce a proper Fokker-Planck equation. That is to say

$$\partial_\alpha^2\left(-\mathrm{i}\alpha^2\right) = \left(\partial_{\alpha_x}^2 - \partial_{\alpha_y}^2\right)\alpha_x\alpha_y - \partial_{\alpha_x}\partial_{\alpha_y}\left(\alpha_x^2 - \alpha_y^2\right) \tag{B.34}$$

does *not* give a proper result because the corresponding determinant is strictly negative. However, by writing

$$\begin{aligned} \partial_\alpha^2\left(-\mathrm{i}\alpha^2\right) &= \frac{1}{2}\partial_\alpha^2\left[\left(\alpha_x+\alpha_y\right)^2 - \left(\alpha_x-\alpha_y\right)^2\right] - \partial_{\alpha_x}\partial_{\alpha_y}\left(\alpha_x^2-\alpha_y^2\right)\\ &= \frac{1}{2}\left[\partial_{\alpha_x}^2\left(\alpha_x+\alpha_y\right)^2 + \partial_{\alpha_y}^2\left(\alpha_x-\alpha_y\right)^2 - 2\partial_{\alpha_x}\partial_{\alpha_y}\left(\alpha_x^2-\alpha_y^2\right)\right] \end{aligned} \tag{B.35}$$

we may cure this problem. For β, we find similarly that

$$\partial_\beta^2\mathrm{i}\beta^2 = \frac{1}{2}\left[\partial_{\beta_x}^2\left(\beta_x-\beta_y\right)^2 + \partial_{\beta_y}^2\left(\beta_x+\beta_y\right)^2 + 2\partial_{\beta_x}\partial_{\beta_y}\left(\beta_x^2-\beta_y^2\right)\right]. \tag{B.36}$$

In total, we construct a diffusion matrix

$$\boldsymbol{B}(\boldsymbol{\alpha})\boldsymbol{B}^T(\boldsymbol{\alpha}) = \frac{U}{2}\begin{pmatrix} (\alpha_x+\alpha_y)^2 & 0 & -\alpha_x^2+\alpha_y^2 & 0 \\ 0 & (\beta_x-\beta_y)^2 & 0 & \beta_x^2-\beta_y^2 \\ -\alpha_x^2+\alpha_y^2 & 0 & (\alpha_x-\alpha_y)^2 & 0 \\ 0 & \beta_x^2-\beta_y^2 & 0 & (\beta_x+\beta_y)^2 \end{pmatrix}, \tag{B.37}$$

which has eigenvalues $\{0, 0, U(\alpha_x^2+\alpha_y^2), U(\beta_x^2+\beta_y^2)\}$ and is hence positive *semidefinite*. The matrices needed for the construction of the vector SDE become

$$\begin{aligned} \boldsymbol{B}_x &= \sqrt{U/2}\begin{pmatrix} \alpha_x+\alpha_y & 0 \\ 0 & \beta_x-\beta_y \end{pmatrix}, \\ \boldsymbol{B}_y &= \sqrt{U/2}\begin{pmatrix} \alpha_y-\alpha_x & 0 \\ 0 & \beta_x+\beta_y \end{pmatrix}. \end{aligned} \tag{B.38}$$

These are, of course, not unique. They entail the purely real equations

$$\begin{aligned} \mathrm{d}\alpha_x &= U\left(\alpha_x^2\beta_y + 2\alpha_x\alpha_y\beta_x - \alpha_y^2\beta_y\right)\mathrm{d}t + \sqrt{U/2}\left(\alpha_x+\alpha_y\right)\mathrm{d}W_1, \\ \mathrm{d}\beta_x &= -U\left(\beta_x^2\alpha_y + 2\beta_x\beta_y\alpha_x - \beta_y^2\alpha_y\right)\mathrm{d}t + \sqrt{U/2}\left(\beta_x-\beta_y\right)\mathrm{d}W_2, \\ \mathrm{d}\alpha_y &= U\left(\alpha_y^2\beta_x + 2\alpha_x\alpha_y\beta_y - \alpha_x^2\beta_x\right)\mathrm{d}t + \sqrt{U/2}\left(\alpha_x-\alpha_y\right)\mathrm{d}W_1, \\ \mathrm{d}\beta_y &= -U\left(\beta_y^2\alpha_x + 2\beta_x\beta_y\alpha_y - \beta_x^2\alpha_x\right)\mathrm{d}t + \sqrt{U/2}\left(\beta_x+\beta_y\right)\mathrm{d}W_2, \end{aligned} \tag{B.39}$$

where while going from $\alpha_{x,\,y}$ to $\beta_{x,\,y}$, in the drift terms we have interchanged α and β and flipped the signs. Obviously, the strength of the noise depends on the interaction U. Moreover, the noise is *multiplicative* instead of additive as for the non-interacting problem above, which unfortunately makes strongly interacting systems as hard to simulate as ever. Naturally, what these equations also lack is a physical interpretation.

B.4 Transfer-Matrix Derivation of the Fokker-Planck Equation

The two-dimensional probability density of subsection 1.4.3 is

$$f(z,\Delta x) = \exp\left\{-\varepsilon D\left[z^2 - \frac{\mathrm{i}z\Delta x}{\varepsilon D}\right]\right\} = \exp\left\{-\frac{\Delta x^2}{4\varepsilon D} - \varepsilon D\left(z - \frac{\mathrm{i}\Delta x}{2\varepsilon D}\right)^2\right\}. \tag{B.40}$$

The normalization is fixed by

$$1 = \frac{1}{2\pi}\int \mathrm{d}z\;\mathrm{d}\Delta x f(z,\Delta x). \tag{B.41}$$

For the first moments, we then have $\langle \Delta x \rangle = 0$ and

$$\langle z \rangle = \frac{1}{2\pi} \int \mathrm{d}z \, \mathrm{d}\Delta x \, z \, f(z, \Delta x) = \frac{1}{2\pi} \int \mathrm{d}\tilde{z} \, \mathrm{d}\Delta x \left(\tilde{z} + \frac{\mathrm{i}\Delta x}{2\varepsilon D} \right) f(\tilde{z} + \mathrm{i}\Delta x / 2\varepsilon D, \Delta x) = 0. \tag{B.42}$$

The second moments are

$$\begin{aligned} \langle \Delta x^2 \rangle &= 2\varepsilon D, \\ \langle z^2 \rangle &= \frac{1}{2\pi} \int \mathrm{d}\tilde{z} \, \mathrm{d}\Delta x \left(\tilde{z}^2 - \frac{\Delta x^2}{(2\varepsilon D)^2} + \frac{\mathrm{i}\tilde{z}\Delta x}{\varepsilon D} \right) f(\tilde{z} + \mathrm{i}\Delta x / 2\varepsilon D, \Delta x) \\ &= \frac{1}{2\varepsilon D} - \frac{2\varepsilon D}{(2\varepsilon D)^2}, \\ \langle z \Delta x \rangle &= \mathrm{i}. \end{aligned} \tag{B.43}$$

A number of trivial higher moments read $\langle z^2 \Delta x \rangle = \langle z \Delta x^2 \rangle = \langle z^2 \Delta x^3 \rangle = \langle z^4 \Delta x^2 \rangle = \langle z^4 \Delta x^3 \rangle = 0$. For the remainder, we find

$$\begin{aligned} \langle z^2 \Delta x^2 \rangle &= \langle \tilde{z}^2 \Delta x^2 \rangle - \frac{1}{(2\varepsilon D)^2} \langle \Delta x^4 \rangle + \frac{\mathrm{i}}{\varepsilon D} \langle \tilde{z} \Delta x^3 \rangle \\ &= \langle \tilde{z}^2 \rangle \langle \Delta x^2 \rangle - \frac{1}{(2\varepsilon D)^2} \cdot 3 \cdot \langle \Delta x^2 \rangle^2 \\ &= \frac{1}{2\varepsilon D} 2\varepsilon D - \frac{1}{(2\varepsilon D)^2} \cdot 3 \cdot (2\varepsilon D)^2 = -2, \end{aligned} \tag{B.44}$$

and $\langle z \Delta x^3 \rangle = 6\mathrm{i}\varepsilon D$, $\langle z^2 \Delta x^4 \rangle = -24\varepsilon D$, $\langle z^4 \Delta x^4 \rangle = 24$. With all of these moments evaluated, the transition probability obeys the equation

$$\begin{aligned} p = p &+ \underbrace{\langle \Delta x^2 \rangle}_{2\varepsilon D(x)} \frac{p''}{2} - \varepsilon \dot{p} + \mathrm{i}\varepsilon \underbrace{\langle z \Delta x \rangle}_{\mathrm{i}} (A(x)p' + A'(x)p) \\ &+ \mathrm{i}\varepsilon A'(x) \frac{p''}{2} \underbrace{\langle z \Delta x^3 \rangle}_{6\mathrm{i}\varepsilon D(x)} - \mathrm{i}\varepsilon^2 A'(x) \dot{p} \langle z \Delta x \rangle - \varepsilon D'(x) p' \underbrace{\langle z^2 \Delta x^2 \rangle}_{-2} \\ &- \frac{1}{2}\varepsilon^2 A^2(x) \frac{p''}{2} \langle z^2 \Delta x^2 \rangle + \frac{1}{2}\varepsilon^2 D'^2(x) \frac{p''}{2} \underbrace{\langle z^4 \Delta x^4 \rangle}_{24} \\ &- \varepsilon \frac{D''(x)}{2} p \langle z^2 \Delta x^2 \rangle - \varepsilon \frac{D''(x)}{2} \frac{p''}{2} \underbrace{\langle z^2 \Delta x^4 \rangle}_{-24\varepsilon D(x)} + \varepsilon^2 \frac{D''(x)}{2} \dot{p} \langle z^2 \Delta x^2 \rangle . \end{aligned} \tag{B.45}$$

APPENDIX C

Bosonic Double-Well Systems

This App. contains additional material related to Sec. 3.2. The two-mode approximation is investigated in some detail, including the mean-field equations and the beyond-mean-field treatment, where the latter is derived both from quantum field theory and in the Heisenberg picture. The relation between the two approaches is discussed. We also comment on the subject of the decay of macroscopic quantum self-trapping (MQST). Next, the stability analysis for an exemplary three-mode approximation is performed, which reveals two exceptional points as a control parameter is tuned.

C.1 Two-Mode Approximation

As explained in the main text, the two-mode approximation is the "standard model" of ultracold Bose gases in double-well potentials. The starting point for our discussion is Ref. [122], where MQST is derived. However, Ref. [122] does not analyze the stability of the mean-field, which is an important shortcoming since, as we will show in C.1.8, MQST can only occur in the presence of hyperbolic fixed points. The effect is, therefore, inherently unstable. Our analysis of the mean-field stability was inspired by Ref. [130], although the following analysis is not explicitly performed there.

A remark on units: Throughout this App., we set $\hbar = 1$. In all plots and tables to be shown, frequencies are understood to be measured in units of $|J|$, whereas time is measured in units of $|J|^{-1}$. The initial conditions for numerical simulations are always such that all quasiparticle Green functions vanish at $t = 0$ (apart from the vacuum contribution to the greater functions, of course).

C.1.1 Mean-Field Equations

In two-mode approximation, the mean-field or *Gross-Pitaevskii* equations for the classical field amplitudes $\Phi_{1,2}(t)$ read

$$\mathrm{i}\partial_t \Phi_1 = (\varepsilon_1 - \mu)\,\Phi_1 + J\Phi_2 + U\,|\Phi_1|^2\,\Phi_1, \tag{C.1a}$$
$$\mathrm{i}\partial_t \Phi_2 = (\varepsilon_2 - \mu)\,\Phi_2 + J\Phi_1 + U\,|\Phi_2|^2\,\Phi_2. \tag{C.1b}$$

Unless they are explicitly included, in the following we will always set $\varepsilon_1 = \varepsilon_2 = 0$. To derive semi-classical equations of motion for the two condensates, we begin by letting

$$\Phi_\alpha(t) = \sqrt{N_\alpha(t)}e^{i\varphi_\alpha(t)}, \tag{C.2a}$$
$$\Phi_{\alpha,\,c}(t) = \sqrt{2N_\alpha(t)}e^{i\varphi_{\alpha,\,c}(t)}, \tag{C.2b}$$

for $\alpha = 1, 2$, where $\Phi_{\alpha,\,c}$ is the *Keldysh* classical field, which is not identical to Φ_α.[1] Using the representation (C.2a) in Eq. (C.1a) gives

$$\frac{\mathrm{i}\dot{N}_1}{2\sqrt{N_1}}\mathrm{e}^{\mathrm{i}\varphi_1} - \dot{\varphi}_1\sqrt{N_1}\mathrm{e}^{\mathrm{i}\varphi_1} = -\mu\sqrt{N_1}\mathrm{e}^{\mathrm{i}\varphi_1} + J\sqrt{N_2}\mathrm{e}^{\mathrm{i}\varphi_2} + UN_1\sqrt{N_1}\mathrm{e}^{\mathrm{i}\varphi_1}. \tag{C.3}$$

Multiplying by $\Phi_1^* = \sqrt{N_1}\mathrm{e}^{-\mathrm{i}\varphi_1}$, we have

$$\frac{\mathrm{i}\dot{N}_1}{2} - N_1\dot{\varphi}_1 = -\mu N_1 + J\sqrt{N_1N_2}\mathrm{e}^{\mathrm{i}\varphi} + UN_1^2. \tag{C.4}$$

Separating real and imaginary parts by adding to (subtracting from) Eq. (C.4) its complex conjugate, one finds the sought-for semi-classical equations of motion for the condensate occupation and phase,

$$\dot{N}_1 = 2J\sqrt{N_1N_2}\sin\varphi, \tag{C.5a}$$
$$\dot{\varphi}_1 = \mu - J\frac{\sqrt{N_1N_2}}{N_1}\cos\varphi - UN_1. \tag{C.5b}$$

With the definitions

$$N = N_1 + N_2, \tag{C.6a}$$
$$z = \frac{N_1 - N_2}{N_1 + N_2}, \tag{C.6b}$$
$$\varphi = \varphi_2 - \varphi_1, \tag{C.6c}$$
$$\Theta = \varphi_1 + \varphi_2, \tag{C.6d}$$

[1] The factor of two will be explained below.

where z is the so-called *population imbalance*, these two equations transform into

$$\frac{\dot{N}}{2}(1+z) + \frac{N}{2}\dot{z} = NJ\sqrt{1-z^2}\sin\varphi, \tag{C.7a}$$

$$\frac{\dot{\Theta}-\dot{\varphi}}{2} = \mu - J\frac{\sqrt{1-z^2}}{1+z}\cos\varphi - \frac{NU}{2}(1+z)\,. \tag{C.7b}$$

From the equations for N_2 and φ_2, one furthermore obtains

$$\frac{\dot{N}}{2}(1-z) - \frac{N}{2}\dot{z} = -NJ\sqrt{1-z^2}\sin\varphi, \tag{C.8a}$$

$$\frac{\dot{\Theta}+\dot{\varphi}}{2} = \mu - J\frac{\sqrt{1-z^2}}{1-z}\cos\varphi - \frac{NU}{2}(1-z)\,. \tag{C.8b}$$

Combining these four to find equations for the variables of the representation (C.6) yields finally

$$\dot{N} = 0, \tag{C.9a}$$

$$\dot{z} = 2J\sqrt{1-z^2}\sin\varphi, \tag{C.9b}$$

$$\dot{\varphi} = NUz - 2Jz\frac{\cos\varphi}{\sqrt{1-z^2}}, \tag{C.9c}$$

$$\dot{\Theta} = 2\mu - NU - 2J\frac{\cos\varphi}{\sqrt{1-z^2}}, \tag{C.9d}$$

with $J < 0$. The interpretation of the first and last of these equations is straightforward: the total number of particles in the condensate is properly conserved, and the equation for the total phase Θ dutifully decouples. Hence, the dynamics is controlled only by the two equations in the middle, and the classical phase space reduces to two dimensions.

C.1.2 Fixed Points

To perform the stability analysis of the mean-field, we first need to find the fixed points of the equations of motion. For this purpose, it is useful to define the dimensionless quantity $\Lambda = NU/2|J| > 0$. As one may see immediately from Eqs. (C.9), an infinite set of fixed points is given by the phase-space vector $\mathbf{v}^* = (z^*, \varphi^*)^T = (0, m\pi)^T$, $m \in \mathbb{Z}$. For non-zero z, we find from (C.9c)

$$\frac{NU}{2\,|J|} = \mp\frac{1}{\sqrt{1-z^2}}, \tag{C.10}$$

which is equivalent to $\mp\Lambda^{-1} = \sqrt{1-z^2}$, depending on m even or odd. As $0 \leq |z| \leq 1$, one must choose the positive sign (setting $\varphi^* = \pi$ or odd multiples of π) and fix $\Lambda > 1$, which is the same as to say that there are no additional fixed points if $(0, \pi)$ is elliptic (s. C.1.3). With this, one obtains

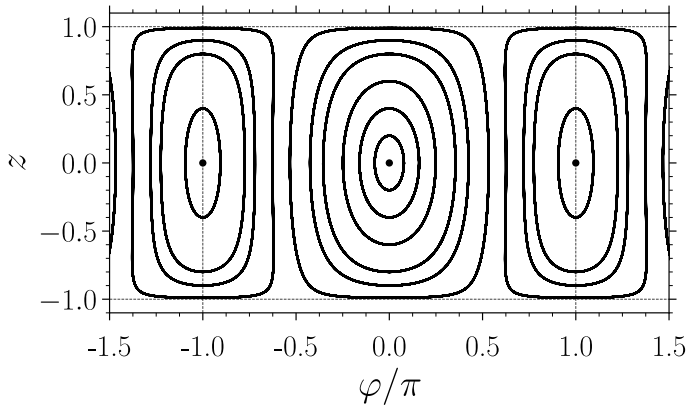

Figure C.1: Portrait of the phase space for $\Lambda = 0.5$. The three elliptic fixed points $(0, m\pi)$, $m = 0, \pm 1$ are indicated by black dots. For relative phase $\varphi(0) = m \cdot 2\pi$, the initial imbalances were chosen as $z(0) = 0.2, 0.4, 0.6, 0.8, 0.9, 0.99$. Accordingly, for $\varphi(0) = m \cdot \pi$, trajectories for $z(0) = 0.4, 0.8, 0.9, 0.99$ are shown.

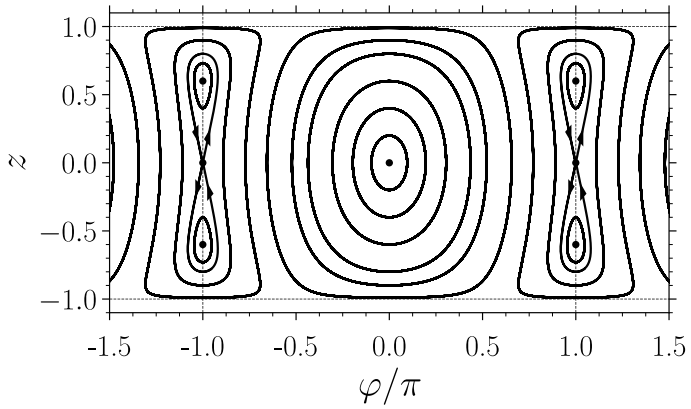

Figure C.2: Portrait of the phase space for $\Lambda = 1.25$. The two fixed points at $(0, \pm\pi)$ have become hyperbolic, as indicated by the black arrows. In agreement with classical mechanics, this entails the emergence of four new elliptic fixed points $(z_\pi^*, \pm\pi)$. For relative phase $\varphi(0) = m \cdot 2\pi$, the initial imbalances were chosen as $z(0) = 0.2, 0.4, 0.6, z_{\text{crit}}, 0.9, 0.99$. Accordingly, for $\varphi(0) = m \cdot \pi$, trajectories for $z(0) = -0.4, 0.4, z_{\text{crit}}, 0.9, 0.99$ are shown. The parameter z_{crit} is defined in C.1.4.

further fixed points at

$$z_\pi^* = \pm\sqrt{1 - \frac{1}{\Lambda^2}}. \tag{C.11}$$

For the relative phase φ at even multiples of π, one does not obtain fixed points for $z \neq 0$.

C.1.3 Stability Analysis

Moving to the stability analysis of the discovered fixed points, we note that the Jacobian of the two relevant equations of motion is

$$\mathcal{J}(z^*,\varphi^*) = \begin{pmatrix} \frac{2|J|z^*\sin(\varphi^*)}{\sqrt{1-(z^*)^2}} & -2|J|\sqrt{1-(z^*)^2}\cos(\varphi^*) \\ NU + \frac{2|J|\cos(\varphi^*)}{\left(1-(z^*)^2\right)^{3/2}} & \frac{2|J|z^*\sin(\varphi^*)}{\sqrt{1-(z^*)^2}} \end{pmatrix}. \tag{C.12}$$

Because of periodicity, the discussion may be limited to $m = 0, \pm 1$. For the point $(0,0)$, the Jacobian evaluates to

$$\mathcal{J}(0,0) = \begin{pmatrix} 0 & -2|J| \\ NU + 2|J| & 0 \end{pmatrix}, \tag{C.13}$$

which can be seen to result always in purely imaginary eigenvalues (for repulsive interaction $U < 0$). As a next step, we consider the fixed points $(0, \pm\pi)$. Evaluating the Jacobian there, we obtain

$$\mathcal{J}(0,\pm\pi) = \begin{pmatrix} 0 & 2|J| \\ NU - 2|J| & 0 \end{pmatrix}. \tag{C.14}$$

This has a characteristic polynomial $\lambda^2 = 2|J|(NU - 2|J|) = 4|J|^2(\Lambda - 1)$. Therefore, we find that these fixed points change from elliptic to hyperbolic depending on the ratio $\Lambda = NU/2|J|$,

$$\lambda = \begin{cases} \pm 2\mathrm{i}|J|\sqrt{|\Lambda - 1|}, & \Lambda < 1, \\ \pm 2|J|\sqrt{\Lambda - 1}, & \Lambda > 1. \end{cases} \tag{C.15}$$

As $\Lambda \nearrow 1$, the pair of complex eigenvalues go to zero, $|\lambda| \to 0$. This is an instance of *critical slowing down*. Above the transition point $\Lambda = 1$, there is a pair of purely real eigenvalues, while the oscillation frequency has become "soft". The presence of a positive real eigenvalue makes the fixed points *unstable* in this regime. For the remaining fixed points $z_\pi^* = \pm\sqrt{1 - 1/\Lambda^2}$, we find

$$\det\left(\mathcal{J}(z_\pi^*,\pm\pi) - \lambda\mathbb{1}\right) = \lambda^2 - \frac{2|J|}{\Lambda}\left(NU - 2|J|\Lambda^3\right) \tag{C.16}$$

and thus the purely imaginary eigenvalues $\lambda_\pi = \pm 2|J|\sqrt{1-\Lambda^2}$. This is in agreement with a well-known fact from classical mechanics: "the number of extrema minus the number of saddle-points" is conserved for dynamical systems [159]. Thus we find three elliptic points for $\Lambda < 1$, yet five elliptic and two hyperbolic points for $\Lambda > 1$. Potraits of the phase space for various values of Λ are shown in Figs. C.1, C.2 and C.3.

The same analysis we have just performed on the semi-classical equations of motion (C.9) may also be done in terms of the complex classical fields Φ_α. To study the points $(0, \pm\pi)$, one

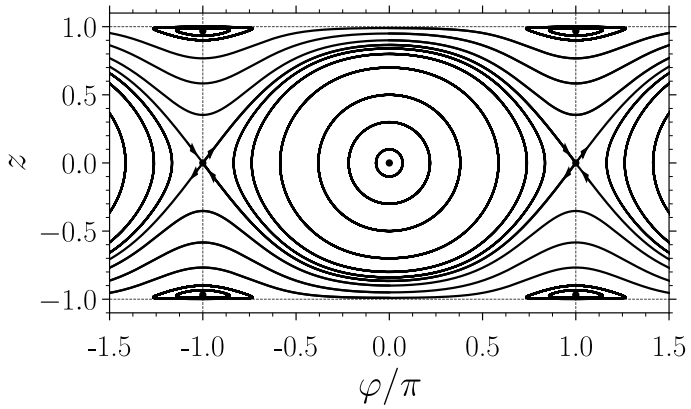

Figure C.3: Portrait of the phase space. The characteristic parameter is $\Lambda = 4.0$. This is the phase portrait usually shown in connection with the two-mode approximation [122]. For $\varphi(0) = m \cdot 2\pi$, the displayed initial imbalances are $z(0) = 0.1, 0.3, 0.5, 0.7, 0.8, 0.84, z_{\text{crit}}, \pm 0.9, \pm 0.95, \pm 0.99$. The parameter z_{crit} is defined in C.1.4. For $\varphi(0) = m \cdot \pi$, we have chosen $z(0) = \pm 0.9, \pm 0.99$. The curve connecting the pair of hyperbolic fixed points is called a *separatrix*. The trajectories for which $z(t) \lesseqgtr 0$ at all times correspond to MQST for monotonously increasing $\varphi(t)$ and to π-oscillations for bounded $\varphi(t)$.

possibility is to set $\Phi_1 = \sqrt{N/2} = -\Phi_2$. From the original Eqs. (C.1), one then obtains the chemical potential as

$$\mu = \frac{1}{2}\left(NU + 2\left|J\right|\right) = \left|J\right|\left(1 + \Lambda\right). \tag{C.17}$$

The Jacobian will be accordingly

$$\mathcal{J}(\Phi_{1,2}, \Phi_{1,2}^*) = -\mathrm{i}\begin{pmatrix} 2U\left|\Phi_1\right|^2 - \mu & U\Phi_1^2 & -\left|J\right| & 0 \\ -U\left(\Phi_1^*\right)^2 & -2U\left|\Phi_1\right|^2 + \mu & 0 & \left|J\right| \\ -\left|J\right| & 0 & 2U\left|\Phi_2\right|^2 - \mu & U\Phi_2^2 \\ 0 & \left|J\right| & -U\left(\Phi_2^*\right)^2 & -2U\left|\Phi_2\right|^2 + \mu \end{pmatrix}, \tag{C.18}$$

where we have to evaluate the fields as $\Phi_{1,2} = \pm\sqrt{N/2}$. The four eigenvalues of this matrix are then $\pm 2\mathrm{i}\left|J\right|\sqrt{1-\Lambda}$ and ± 0, which is the same as the result of Eq. (C.15).

C.1.4 Mechanical Analogy

In mean-field, the system possesses a mechanical analogy [122] that is worth being explained briefly. Remember from classical mechanics that the Hamiltonian for a "mathematical pendulum" (that is, before assuming Hooke's law) reads

$$H = \frac{p_\vartheta^2}{2ml^2} + mgl(1 - \cos\vartheta) \equiv \frac{p_\vartheta^2}{2ml^2} - mgl\cos\vartheta, \tag{C.19}$$

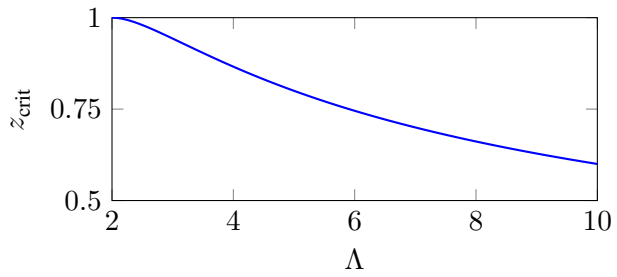

Figure C.4: The critical population imbalance z_{crit} for $\varphi(0) = 0$ as a function of Λ. For $\Lambda = 2$, one finds $z_{\text{crit}} = 1$. MQST may only occur for $\Lambda > 2$. For $1 < \Lambda < 2$, the only trajectories with $z(t) > 0$ for all t belong to the type of π-oscillations shown in Fig. C.2.

with $p_\vartheta = ml^2\dot{\vartheta}$. The mathematical pendulum has orbits circulating the phase-space origin for energies $-g/l < H/ml^2 < g/l$. For energies $g/l > H/ml^2$, the pendulum has enough kinetic energy to "topple over" and keep going round in circles.

Now if we identify the canonically conjugate variables $(\dot{\vartheta}, \vartheta)$ with (z, φ), and replace the fixed length l of the pendulum in the potential term according to $l \to l\sqrt{1-z^2}$, we end up with a Hamiltonian similar to the one corresponding to the mean-field equations,

$$\begin{aligned} H &= \frac{NU}{2}z^2 - 2|J|\sqrt{1-z^2}\cos\varphi \\ &= 2|J|\left(\frac{\Lambda}{2}z^2 - \sqrt{1-z^2}\cos\varphi\right). \end{aligned} \tag{C.20}$$

which can be interpreted as the Hamiltonian of a pendulum the length of which decreases with the rotation velocity (or angular momentum).

Since the system is closed, the total energy must be conserved. If the trajectory is to pass through either of the points $(z, \varphi) = (0, \pm\pi)$, we can conclude that $H = 2|J|$. The two points $(0, \pm\pi)$ are fixed points of the system. For $\Lambda > 2$, the system has a separatrix connecting these two points with $(z_{\text{crit}}, 0)$, where $z_{\text{crit}} = \pm 2\sqrt{\Lambda - 1}/\Lambda$ such that

$$\begin{aligned} \sqrt{1-z_{\text{crit}}^2} &= \frac{2}{\Lambda}\sqrt{\left(\frac{\Lambda}{2}-1\right)^2} = 1 - \frac{2}{\Lambda}, \\ \frac{\Lambda}{2}z^2 &= \frac{2}{\Lambda}(\Lambda - 1) = 2 - \frac{2}{\Lambda}. \end{aligned} \tag{C.21}$$

For the initial point $(z_{\text{crit}}, 0)$, where the phase difference is zero and hence $\cos\varphi(0) = +1$, we then have correctly that $H = 2\,|J|$. If $|z(0)| > |z_{\text{crit}}|$, the solution cannot cross $z = 0$ for all times, which gives rise to MQST. Moreover, non-trivial critical values only exist for $\Lambda > 1$. For arbitrary

$\varphi(0)$, the critical imbalance is given via [122]

$$\Lambda_c = 2\left(\frac{\sqrt{1-z_{\text{crit}}^2}\cos\varphi(0)+1}{z_{\text{crit}}^2}\right), \tag{C.22}$$

which also defines a critical interaction strength via parameter Λ_c for an initial imbalance $z(0) \equiv z_{\text{crit}}$. The critical population imbalance as a function of Λ is plotted in Fig. C.4.

C.1.5 Bogoliubov Quasiparticles (Heisenberg Equation)

The previous stability analysis is equivalent to studying the Bogoliubov quasiparticles of the Bose-Hubbard dimer defined by the Hamiltonian

$$H = \varepsilon_1 a_1^\dagger a_1 + \varepsilon_2 a_2^\dagger a_2 + J\left(a_1^\dagger a_2 + a_2^\dagger a_1\right) + \frac{U}{2}\left(a_1^\dagger a_1^\dagger a_1 a_1 + a_2^\dagger a_2^\dagger a_2 a_2\right), \tag{C.23}$$

which gives rise to the Heisenberg equations

$$\mathrm{i}\partial_t a_1 = \varepsilon_1 a_1 + J a_2 + U a_1^\dagger a_1 a_1, \tag{C.24a}$$
$$\mathrm{i}\partial_t a_2 = \varepsilon_2 a_2 + J a_1 + U a_2^\dagger a_2 a_2. \tag{C.24b}$$

Similar to the treatment of Ref. [138], by letting $a_\alpha = \mathrm{e}^{-\mathrm{i}\mu t}(\varphi_\alpha + \delta a_\alpha)$, Eqs. (C.24) can be written

$$\begin{aligned}\mathrm{i}\partial_t(\varphi_1+\delta a_1) = [\varepsilon_1-\mu](\varphi_1+\delta a_1) + J(\varphi_2+\delta a_2) + U\Big\{&|\varphi_1|^2\varphi_1 + 2|\varphi_1|^2\delta a_1 \\ &+ \varphi_1^2\delta a_1^\dagger + 2\varphi_1\delta a_1^\dagger\delta a_1 + \varphi_1^*\delta a_1\delta a_1 + \delta a_1^\dagger\delta a_1\delta a_1\Big\},\end{aligned} \tag{C.25a}$$

and analogously for the second mode. Taking the average and using $\langle\delta a_\alpha\rangle = 0$ gives the "modified" Gross-Pitaevskii equation

$$\mathrm{i}\partial_t\varphi_1 = [\varepsilon_1-\mu]\varphi_1 + J\varphi_2 + U\left\{|\varphi_1|^2\varphi_1 + 2\varphi_1\langle\delta a_1^\dagger\delta a_1\rangle + \varphi_1^*\langle\delta a_1\delta a_1\rangle + \langle\delta a_1^\dagger\delta a_1\delta a_1\rangle\right\}. \tag{C.26a}$$

N	Λ	J	$z(0)$	$\varphi(0)$
5000	$0.5, 0.95, 1.05, 1.25, 4.00$	-1	0.01	π

Table C.1: Parameters for the two-mode examples shown in Figs. C.5, C.6, C.7, C.8 and C.9.

Keeping only the lowest moments $\varphi_\alpha \equiv \Phi_\alpha$, we recover the original Eqs. (C.1). The Heisenberg equations for the fluctuations can be found as follows. Eq. (C.25a) may be written as

$$\begin{aligned}
\mathrm{i}\partial_t\left(\varphi_1+\delta a_1\right) &= \left[\varepsilon_1-\mu\right]\varphi_1 + J\varphi_2 + U\left|\varphi_1\right|^2\varphi_1 \\
&\quad + U\Big\{2\varphi_1\langle\delta a_1^\dagger\delta a_1\rangle + \varphi_1^*\langle\delta a_1\delta a_1\rangle + \langle\delta a_1^\dagger\delta a_1\delta a_1\rangle\Big\} \\
&\quad + \left[\varepsilon_1-\mu\right]\delta a_1 + J\delta a_2 + U\left\{2\left|\varphi_1\right|^2\delta a_1 + \varphi_1^2\delta a_1^\dagger\right\} \\
&\quad + U\Big\{2\varphi_1\left[\delta a_1^\dagger\delta a_1 - \langle\delta a_1^\dagger\delta a_1\rangle\right] + \varphi_1^*\left[\delta a_1\delta a_1 - \langle\delta a_1\delta a_1\rangle\right] \\
&\quad + \left[\delta a_1^\dagger\delta a_1\delta a_1 - \langle\delta a_1^\dagger\delta a_1\delta a_1\rangle\right]\Big\},
\end{aligned} \tag{C.27}$$

where we have constructively added and subtracted the three terms appearing in the first and last curly brackets. Using Eq. (C.26a), we come out with

$$\begin{aligned}
\mathrm{i}\partial_t\delta a_1 &= \left[\varepsilon_1-\mu\right]\delta a_1 + J\delta a_2 + U\left\{2\left|\varphi_1\right|^2\delta a_1 + \varphi_1^2\delta a_1^\dagger\right\} \\
&\quad + U\Big\{2\varphi_1\left[\delta a_1^\dagger\delta a_1 - \langle\delta a_1^\dagger\delta a_1\rangle\right] + \varphi_1^*\left[\delta a_1\delta a_1 - \langle\delta a_1\delta a_1\rangle\right] \\
&\quad + \left[\delta a_1^\dagger\delta a_1\delta a_1 - \langle\delta a_1^\dagger\delta a_1\delta a_1\rangle\right]\Big\}.
\end{aligned} \tag{C.28}$$

If we linearize this result by keeping only contributions from the first line, we readily see that the full system with $\boldsymbol{\delta} := (\delta a_1, \delta a_1^\dagger, \delta a_2, \delta a_2^\dagger)^T$ can be written in terms of the Jacobian used in Eq. (C.18) as

$$\partial_t\boldsymbol{\delta} = \mathcal{J}(\varphi_{1,2}, \varphi_{1,2}^*)\boldsymbol{\delta}. \tag{C.29}$$

These quadratic fluctuations around the saddle-point defined by the Gross-Pitaevskii equations (C.1) will remain small in the vicinity of the elliptic fixed points found above. Close to one of the hyperbolic fixed points, however, they will increase sharply due to the presence of the positive real eigenvalue. Physically, this stems from the fact that exciting these "long-wavelength" fluctuations does not cost any energy once the frequency has gone to zero. At this point, the mean-field approximation breaks down, as does the approximation including the quadratic fluctuations. Some improvement may be achieved by taking the next step of approximation, which is via the Hartree-Fock-Bogoliubov (HFB) equations. For very early times, and as long as fluctuations are still small, these are expected to model the system well. For large fluctuations and/or long evolution times, they will deviate from the exact result. As mentioned, including diagrams beyond Hartree-Fock will capture non-Markovian effects (e.g. damping of oscillations), where certain caveats such as overdamping are discussed in Ref. [113]. In the following, we are going to derive the HFB equations in two-mode approximation from the 2PI effective action. Simulations of these equations for the parameters listed in Tab. C.1 are plotted in Figs. C.5, C.6, C.7, C.8 and C.9.

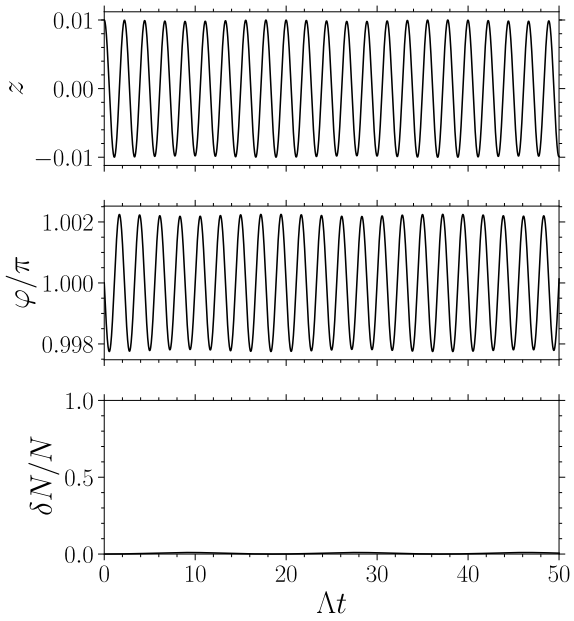

Figure C.5: Population imbalance $z(t)$, relative phase $\varphi(t)$ and total fraction of fluctuations $\delta N(t)/N$ (defined in Eq. (C.54)) for $\Lambda = 0.5$, $z(0) = 0.01$, $\varphi(0) = \pi$, $N = 5000$, $J = -1$. The initial population imbalance is small in order to start in the "linear regime". The fraction of fluctuations is negligible.

C.1.6 Hartree-Fock-Bogoliubov Equations from 2PI Effective Action

The HFB equations are going to be derived in "Schwinger" representation, that is, in terms of greater and lesser Green functions. A fully rigorous derivation of these self-consistent equations has to follow along the same lines as the loop expansion detailed in the Introduction. Here, we are going to pass over many of the details and rather emphasize from a practical perspective how the diagrammatic expansion may be constructed. The starting point for the field-theoretic derivation are the actions

$$S_{\pm} = \int \mathrm{d}\bar{t} \left\{ \sum_{\alpha} \phi^*_{\alpha,\pm}(\bar{t}) \mathrm{i}\partial_{\bar{t}} \phi_{\alpha,\pm}(\bar{t}) - J\left(\phi^*_{1,\pm}(\bar{t})\phi_{2,\pm}(\bar{t}) + \text{c.c.}\right) \right.$$
$$\left. - \frac{U}{2} \sum_{\alpha} \phi^*_{\alpha,\pm}(\bar{t})\phi^*_{\alpha,\pm}(\bar{t})\phi_{\alpha,\pm}(\bar{t}_{\mp})\phi_{\alpha,\pm}(\bar{t}_{\mp}) \right\},$$

where $\bar{t}_{\mp}$ is earlier (later) on the contour than $\bar{t}$. The corresponding non-equilibrium action is $S = S_+ - S_-$. To facilitate the application of perturbation theory, we introduce the following generalized field spinor:

$$\boldsymbol{\phi} = \left(\phi_{1,+}, \phi^*_{1,+}, \phi_{2,+}, \phi^*_{2,+}, \phi_{1,-}, \phi^*_{1,-}, \phi_{2,-}, \phi^*_{2,-}\right)^T = \left(\phi_1, ..., \phi_8\right)^T . \tag{C.30}$$

The ordering defined here is, of course, conventional. This gives

$$\begin{aligned} S[\boldsymbol{\phi}] = \frac{1}{2}\int \mathrm{d}\bar{t}\, \Big\{ &\Big(\phi_2 \mathrm{i}\partial_{\bar{t}}\phi_1 - \phi_1 \mathrm{i}\partial_{\bar{t}}\phi_2 + \phi_4 \mathrm{i}\partial_{\bar{t}}\phi_3 - \phi_3 \mathrm{i}\partial_{\bar{t}}\phi_4\Big) - 2J\Big(\phi_2\phi_3 + \phi_1\phi_4\Big) \\ &- U\Big(\phi_1^2(\bar{t}_-)\phi_2^2(\bar{t}) + \phi_3^2(\bar{t}_-)\phi_4^2(\bar{t})\Big)\Big\} \\ -\frac{1}{2}\int \mathrm{d}\bar{t}\, \Big\{ &\Big(\phi_6 \mathrm{i}\partial_{\bar{t}}\phi_5 - \phi_5 \mathrm{i}\partial_{\bar{t}}\phi_6 + \phi_8 \mathrm{i}\partial_{\bar{t}}\phi_7 - \phi_7 \mathrm{i}\partial_{\bar{t}}\phi_8\Big) - 2J\Big(\phi_6\phi_7 + \phi_5\phi_8\Big) \\ &- U\Big(\phi_5^2(\bar{t}_+)\phi_6^2(\bar{t}) + \phi_7^2(\bar{t}_+)\phi_8^2(\bar{t})\Big)\Big\}. \end{aligned} \tag{C.31}$$

For the HFB approximation, we decompose the spinor field as $\boldsymbol{\phi} = \boldsymbol{\varphi} + \delta\boldsymbol{\phi}$ and keep only the terms quadratic or quartic in the fluctuations (have in mind that terms linear in the fluctuations cancel during the construction of the 2PI effective action). This results in an effective action (which we denote slightly inconsistently by S instead of Γ)

$$\begin{aligned} S_{\mathrm{HFB}}[\boldsymbol{\varphi},\, \delta\boldsymbol{\phi}] &= S[\boldsymbol{\varphi}] + S[\delta\boldsymbol{\phi}] \\ -\frac{U}{2}\int \mathrm{d}\bar{t}\, \Big\{ &\Big(\varphi_1^2(\bar{t}_-)\delta\phi_2^2(\bar{t}) + 4\varphi_1(\bar{t}_-)\varphi_2(\bar{t})\delta\phi_1(\bar{t}_-)\delta\phi_2(\bar{t}) + \varphi_2^2(\bar{t})\delta\phi_1^2(\bar{t}_-)\Big) \\ &+ \Big(\varphi_3^2(\bar{t}_-)\delta\phi_4^2(\bar{t}) + 4\varphi_3(\bar{t}_-)\varphi_4(\bar{t})\delta\phi_3(\bar{t}_-)\delta\phi_4(\bar{t}) + \varphi_4^2(\bar{t})\delta\phi_3^2(\bar{t}_-)\Big) \\ &- \Big(\varphi_5^2(\bar{t}_+)\delta\phi_6^2(\bar{t}) + 4\varphi_5(\bar{t}_+)\varphi_6(\bar{t})\delta\phi_5(\bar{t}_+)\delta\phi_6(\bar{t}) + \varphi_6^2(\bar{t})\delta\phi_5^2(\bar{t}_+)\Big) \\ &- \Big(\varphi_7^2(\bar{t}_+)\delta\phi_8^2(\bar{t}) + 4\varphi_7(\bar{t}_+)\varphi_8(\bar{t})\delta\phi_7(\bar{t}_+)\delta\phi_8(\bar{t}) + \varphi_8^2(\bar{t})\delta\phi_7^2(\bar{t}_+)\Big)\Big\}. \end{aligned} \tag{C.32}$$

This means we have as an inverse Green function

$$\boldsymbol{G}_0^{-1}(t,t') = \delta(t-t')\begin{pmatrix} G_{0,++}^{-1}(t) & 0 \\ 0 & G_{0,--}^{-1}(t) \end{pmatrix}, \tag{C.33}$$

with

$$G_{0,++}^{-1}(t) = \begin{pmatrix} -U\varphi_2^2 & -\mathrm{i}\partial_t - 2U\varphi_1\varphi_2 & 0 & -J \\ \mathrm{i}\partial_t - 2U\varphi_1\varphi_2 & -U\varphi_1^2 & -J & 0 \\ 0 & -J & -U\varphi_4^2 & -\mathrm{i}\partial_t - 2U\varphi_3\varphi_4 \\ -J & 0 & \mathrm{i}\partial_t - 2U\varphi_3\varphi_4 & -U\varphi_3^2 \end{pmatrix}$$

and $G_{0,--}^{-1}$ being defined analogously. We still have to take care of the quartic fluctuation terms in the action. As usual, this is done by using the Gaussian property when converting expectation values of interaction terms in the cumulant-generating function into products of second moments. Here, this essentially amounts to replacing

$$\delta\phi_k^2(t)\delta\phi_l^2(t') \to 2\langle\delta\phi_k(t)\delta\phi_l(t')\rangle\langle\delta\phi_k(t)\delta\phi_l(t')\rangle + \langle\delta\phi_k(t)\delta\phi_k(t)\rangle\langle\delta\phi_l(t')\delta\phi_l(t')\rangle. \tag{C.34}$$

When converting the second moments into Green functions, one has to be careful to symmetrize correctly. For instance,

$$\begin{aligned}\delta\phi_2^2(t)\delta\phi_1^2(t_-) &\to 2\langle\delta\phi_2(t)\delta\phi_1(t_-)\rangle^2 + \langle\delta\phi_2^2(t)\rangle\langle\delta\phi_1^2(t_-)\rangle \\ &= -\left[2\left(\frac{G_{12}(t_-,t)+G_{21}(t,t_-)}{2}\right)^2 + G_{11}(t,t)G_{22}(t,t)\right],\end{aligned} \tag{C.35}$$

where the Green functions in spinor space are given by $G_{kl}(t,t') = -\mathrm{i}\langle\delta\phi_k(t)\delta\phi_l(t')\rangle$. The (anomalous) Schwinger Green functions are defined as

$$G^{\lessgtr}_{\alpha\beta}(t,t') = -\mathrm{i}\langle\delta\phi_{\alpha,\pm}(t)\delta\phi^*_{\beta,\mp}(t')\rangle, \tag{C.36a}$$

$$G^{T/\tilde{T}}_{\alpha\beta}(t,t') = -\mathrm{i}\langle\delta\phi_{\alpha,+/-}(t)\delta\phi^*_{\beta,+/-}(t')\rangle, \tag{C.36b}$$

$$g^{\lessgtr}_{\alpha\beta}(t,t') = -\mathrm{i}\langle\delta\phi_{\alpha,\pm}(t)\delta\phi_{\beta,\mp}(t')\rangle, \tag{C.36c}$$

$$g^{T/\tilde{T}}_{\alpha\beta}(t,t') = -\mathrm{i}\langle\delta\phi_{\alpha,+/-}(t)\delta\phi_{\beta,+/-}(t')\rangle, \tag{C.36d}$$

This gives, for example,

$$\begin{aligned}G^{<}_{11}(t,t') &= G_{16}(t,t'),\\ G^{>}_{11}(t,t') &= G_{52}(t,t'),\\ G^{T}_{11}(t,t') &= G_{12}(t,t'),\\ G^{\tilde{T}}_{11}(t,t') &= G_{56}(t,t'),\end{aligned}$$

as well as $g^{<}_{11}(t,t') = G_{15}(t,t') = g^{>}_{11}(t',t)$ (pay attention to the time arguments). Accordingly, one may find the self-energies as

$$\boldsymbol{\Sigma}(t,t') = \delta(t-t')\begin{pmatrix}\Sigma_{++}(t) & 0\\ 0 & \Sigma_{--}(t)\end{pmatrix}, \tag{C.37}$$

with[2]

$$\Sigma_{++}(t) = \mathrm{i}U\begin{pmatrix}G_{22}(t,t) & 2G_{12}(t_-,t) & 0 & 0\\ 2G_{12}(t_-,t) & G_{11}(t,t) & 0 & 0\\ 0 & 0 & G_{44}(t,t) & 2G_{34}(t_-,t)\\ 0 & 0 & 2G_{34}(t_-,t) & G_{33}(t,t)\end{pmatrix}. \tag{C.38}$$

[2] Making use of $G_{12}(t_-,t) + G_{21}(t,t_-) = 2G_{12}(t_-,t)$ and so forth.

The self-energy $\Sigma_{--}(t)$ follows from $\Sigma_{++}(t)$ through increasing all Green-function indices by four. As an equation of motion, in the present approximation we have

$$\left[\begin{pmatrix} G^{-1}_{0,++}(t) & 0 \\ 0 & G^{-1}_{0,--}(t) \end{pmatrix} - \begin{pmatrix} \Sigma_{++}(t) & 0 \\ 0 & \Sigma_{--}(t) \end{pmatrix}\right] \boldsymbol{G}(t,t') = \delta(t-t')\mathbb{1}. \tag{C.39}$$

The matrix

$$\boldsymbol{G}(t,t') = \begin{pmatrix} G_{++}(t,t') & G_{+-}(t,t') \\ G_{-+}(t,t') & G_{--}(t,t') \end{pmatrix} \tag{C.40}$$

is defined in components as $\left(\boldsymbol{G}(t,t')\right)_{kk'} := G_{kk'}(t,t')$. Thus the Dyson equation on the plus-contour reads

$$0 = \left[G^{-1}_{0,++}(t) - \Sigma_{++}\right] G_{+-}, \tag{C.41}$$

and in components

$$\begin{aligned} 0 = &\begin{pmatrix} -U\varphi_2^2 & -i\partial_t - 2U\varphi_1\varphi_2 \\ i\partial_t - 2U\varphi_1\varphi_2 & -U\varphi_1^2 \end{pmatrix} \begin{pmatrix} G_{15} & G_{16} \\ G_{25} & G_{26} \end{pmatrix} + \begin{pmatrix} 0 & -J \\ -J & 0 \end{pmatrix} \begin{pmatrix} G_{35} & G_{36} \\ G_{45} & G_{46} \end{pmatrix} \\ &- \mathrm{i}U \begin{pmatrix} G_{22}(t,t) & 2G_{12}(t_-,t) \\ 2G_{12}(t_-,t) & G_{11}(t,t) \end{pmatrix} \begin{pmatrix} G_{15} & G_{16} \\ G_{25} & G_{26} \end{pmatrix}. \end{aligned} \tag{C.42}$$

By taking the lower-right component of the resulting 2×2 matrix, we find

$$0 = (i\partial_t - 2U\varphi_1\varphi_2)\, G_{16} - U\varphi_1^2 G_{26} - JG_{36} - \mathrm{i}U\left[(G_{12}(t_-,t) + G_{21}(t,t_-))\, G_{16} + G_{11}G_{26}\right]. \tag{C.43}$$

Along the very same lines, on the minus contour we have the Dyson equations

$$0 = \left[G^{-1}_{0,--}(t) - \Sigma_{--}\right] G_{-+}, \tag{C.44}$$

which becomes in components

$$\begin{aligned} 0 = &\begin{pmatrix} -U\varphi_6^2 & -i\partial_t - 2U\varphi_5\varphi_6 \\ i\partial_t - 2U\varphi_5\varphi_6 & -U\varphi_5^2 \end{pmatrix} \begin{pmatrix} G_{51} & G_{52} \\ G_{61} & G_{62} \end{pmatrix} + \begin{pmatrix} 0 & -J \\ -J & 0 \end{pmatrix} \begin{pmatrix} G_{71} & G_{72} \\ G_{81} & G_{82} \end{pmatrix} \\ &- \mathrm{i}U \begin{pmatrix} G_{66}(t,t) & 2G_{56}(t_+,t) \\ 2G_{56}(t_+,t) & G_{55}(t,t) \end{pmatrix} \begin{pmatrix} G_{51} & G_{52} \\ G_{61} & G_{62} \end{pmatrix}. \end{aligned} \tag{C.45}$$

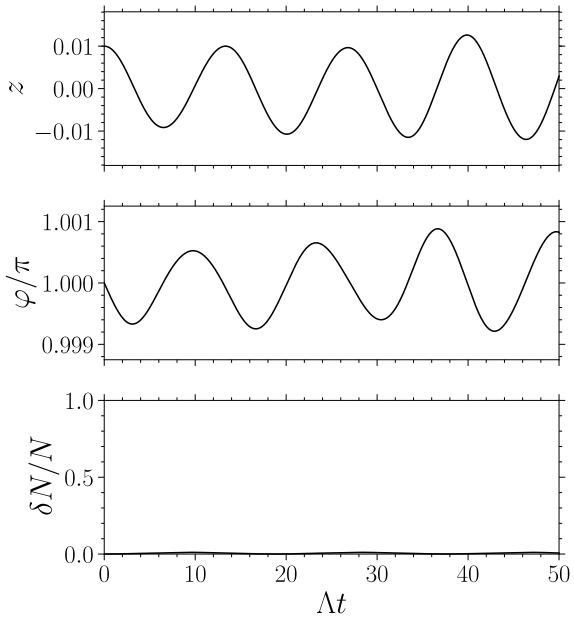

Figure C.6: Population imbalance $z(t)$, relative phase $\varphi(t)$ and total fraction of fluctuations $\delta N(t)/N$ for $\Lambda = 0.95$, $z(0) = 0.01$, $\varphi(0) = \pi$, $N = 5000$, $J = -1$. The slowing down of the oscillation frequency is clearly visible. Since $\Lambda < 1$, the fraction of fluctuations is still negligible.

Taking the lower-right component, we have

$$0 = (i\partial_t - 2U\varphi_5\varphi_6)\, G_{52} - U\varphi_5^2 G_{62} - JG_{72} - \mathrm{i}U\left[(G_{56}(t_+,t) + G_{65}(t,t_+))\, G_{52} + G_{55}G_{62}\right]. \tag{C.46}$$

Eqs. (C.43) and (C.46) can now be translated back into the familiar "RAK" representation [61]. Subsequently, the equal-time limit needs to be taken. The classical fields are translated easily, since $\varphi_{\alpha,\pm} = (\varphi_{\alpha,c} \pm \varphi_{\alpha,q})/\sqrt{2} = \varphi_{\alpha,c}/\sqrt{2}$. The Green functions are translated according to the transformation belonging to the above field spinor. One obtains

$$\begin{aligned}
0 &= \left(i\partial_t - U\left|\varphi_{1,c}\right|^2\right) G^<_{11}(t,t') + \frac{U}{2}\left(\varphi_{1,c}\right)^2 g^<_{11}(t,t')^* - JG^<_{21}(t,t') \\
&\quad - \mathrm{i}U\Big[2\underbrace{G^T_{11}(t_-,t)}_{=G^<_{11}(t,t)} G^<_{11}(t,t') - \underbrace{g^T_{11}(t,t)}_{=g^<_{11}(t,t)} g^<_{11}(t,t')^*\Big], \\
0 &= \left(i\partial_t - U\left|\varphi_{1,c}\right|^2\right) G^>_{11}(t,t') + \frac{U}{2}\left(\varphi_{1,c}\right)^2 g^>_{11}(t,t')^* - JG^>_{21}(t,t') \\
&\quad - \mathrm{i}U\Big[2\underbrace{G^{\tilde{T}}_{11}(t_+,t)}_{=G^<_{11}(t,t)} G^>_{11}(t,t') - \underbrace{g^{\tilde{T}}_{11}(t,t)}_{=g^>_{11}(t,t)} g^>_{11}(t,t')^*\Big],
\end{aligned} \tag{C.47}$$

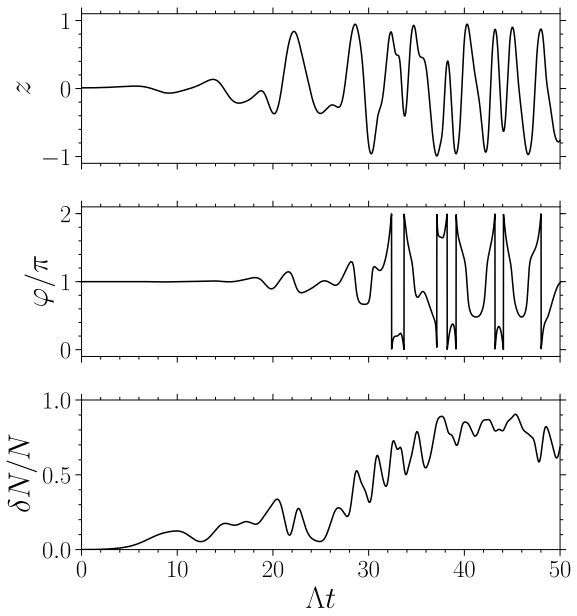

Figure C.7: Population imbalance $z(t)$, relative phase $\varphi(t)$ and total fraction of fluctuations $\delta N(t)/N$ for $\Lambda = 1.05$, $z(0) = 0.01$, $\varphi(0) = \pi$, $N = 5000$, $J = -1$. The fraction of fluctuation increases strongly as we enter the unstable regime $\Lambda > 1$. This in turn causes uncontrolled oscillations of large amplitude in the population imbalance. Note that this is not expected to reproduce the exact solution beyond very early times.

where we have used $G_{26}(t,t') = -\mathrm{i}\langle\delta\phi_2(t)\delta\phi_6(t')\rangle = -\mathrm{i}\langle\delta\phi^*_{1,+}(t)\delta\phi^*_{1,-}(t')\rangle = -\left[g^<_{11}(t,t')\right]^*$. For anomalous (anti-) time-ordered Green functions like $g_{11}^{T/\tilde{T}}(t,t)$, one does not have to keep track of time-ordering. The conjugate equations after switching t and t' read

$$\begin{aligned}
0 &= \left(-i\partial_{t'} - U\left|\varphi_{1,c}(t')\right|^2\right) G^<_{11}(t,t') - \frac{U}{2}\left(\varphi^*_{1,c}(t')\right)^2 g^<_{11}(t,t') - JG^<_{12}(t,t') \\
&\quad - \mathrm{i}U\left(2G^<_{11}(t',t')G^<_{11}(t,t') - g^<_{11}(t',t')^* g^<_{11}(t,t')\right), \\
0 &= \left(-i\partial_{t'} - U\left|\varphi_{1,c}(t')\right|^2\right) G^>_{11}(t,t') - \frac{U}{2}\left(\varphi^*_{1,c}(t')\right)^2 g^>_{11}(t,t') - JG^>_{12}(t,t') \\
&\quad - \mathrm{i}U\left[2G^<_{11}(t',t')G^>_{11}(t,t') - g^>_{11}(t',t')^* g^>_{11}(t,t')\right],
\end{aligned} \tag{C.48}$$

where we employed the identities $G^{\lessgtr}_{\alpha\beta}(t,t')^\dagger = -G^{\lessgtr}_{\beta\alpha}(t',t)$. Combining the $i\partial_t$ and $i\partial_{t'}$ equations by subtraction and then taking $t' \to t$ yields

$$\begin{aligned}
0 &= i\partial_t G^<_{11}(t,t) + \frac{U}{2}\left[\left(\varphi_{1,c}\right)^2 g^<_{11}(t,t)^* + \left(\varphi^*_{1,c}\right)^2 g^<_{11}(t,t)\right] - J\left(G^<_{21}(t,t) - G^<_{12}(t,t)\right), \\
0 &= i\partial_t G^>_{11}(t,t) + \frac{U}{2}\left[\left(\varphi_{1,c}\right)^2 g^>_{11}(t,t)^* + \left(\varphi^*_{1,c}\right)^2 g^>_{11}(t,t)\right] - J\left(G^>_{21}(t,t) - G^>_{12}(t,t)\right).
\end{aligned}$$

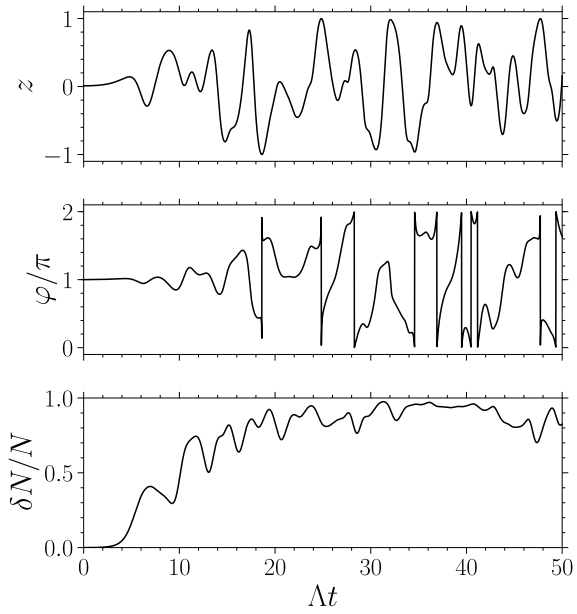

Figure C.8: Population imbalance $z(t)$, relative phase $\varphi(t)$ and total fraction of fluctuations $\delta N(t)/N$ for $\Lambda = 1.25$, $z(0) = 0.01$, $\varphi(0) = \pi$, $N = 5000$, $J = -1$. The situation is similar to Fig. C.7.

Adding these two gives finally

$$0 = i\partial_t G^K_{11}(t,t) + \frac{U}{2}\left[\left(\varphi_{1,c}\right)^2 g^K_{11}(t,t)^* + \left(\varphi^*_{1,c}\right)^2 g^K_{11}(t,t)\right] + J\left(G^K_{12}(t,t) + G^K_{12}(t,t)^*\right),$$

where $G^K_{21}(t,t) = -G^K_{12}(t,t)^*$ was applied. Next, we look at the lower-left components of Eqs. (C.42) and (C.45). These read

$$0 = \left(i\partial_t - U\varphi_1\varphi_2\right) G_{15} - \frac{U}{2}\varphi_1^2 G_{25} - JG_{35} - \mathrm{i}U\left[\left(G_{12}(t_-,t) + G_{21}(t,t_-)\right) G_{15} + G_{11}G_{25}\right], \tag{C.49a}$$

$$0 = \left(i\partial_t - U\varphi_5\varphi_6\right) G_{51} - \frac{U}{2}\varphi_5^2 G_{61} - JG_{71} - \mathrm{i}U\left[\left(G_{56}(t_+,t) + G_{65}(t,t_+)\right) G_{51} + G_{55}G_{61}\right]. \tag{C.49b}$$

Translating back to physical notation, we obtain

$$\begin{aligned} 0 = {} & \left(i\partial_t - U\left|\varphi_{1,c}\right|^2\right) g^<_{11}(t,t') - \frac{U}{2}\left(\varphi_{1,c}\right)^2 G^>_{11}(t',t) - Jg^>_{21}(t',t) \\ & - \mathrm{i}U\left(2G^<_{11}(t,t)g^<_{11}(t,t') + g^>_{11}(t,t)G^>_{11}(t',t)\right), \end{aligned} \tag{C.50a}$$

$$\begin{aligned} 0 = {} & \left(i\partial_t - U\left|\varphi_{1,c}\right|^2\right) g^>_{11}(t,t') - \frac{U}{2}\left(\varphi_{1,c}\right)^2 G^<_{11}(t',t) - Jg^<_{21}(t,t') \\ & - \mathrm{i}U\left(2G^<_{11}(t,t)g^>_{11}(t,t') + g^<_{11}(t,t)G^<_{11}(t',t)\right). \end{aligned} \tag{C.50b}$$

With $g_{11}^{<}(t,t') = g_{11}^{>}(t',t)$ and switching t and t', these are equivalent to

$$\begin{aligned} 0 = &\left(i\partial_{t'} - U\left|\varphi_{1,c}(t')\right|^2\right) g_{11}^{>}(t,t') - \frac{U}{2}\left(\varphi_{1,c}(t')\right)^2 G_{11}^{>}(t,t') - J g_{21}^{>}(t,t') \\ &- \mathrm{i}U\left(2G_{11}^{<}(t',t')g_{11}^{>}(t,t') + g_{11}^{<}(t',t')G_{11}^{>}(t,t')\right), \end{aligned} \tag{C.51a}$$

$$\begin{aligned} 0 = &\left(i\partial_{t'} - U\left|\varphi_{1,c}(t')\right|^2\right) g_{11}^{<}(t,t') - \frac{U}{2}\left(\varphi_{1,c}(t')\right)^2 G_{11}^{<}(t,t') - J g_{21}^{<}(t',t) \\ &- \mathrm{i}U\left(2G_{11}^{<}(t',t')g_{11}^{<}(t,t') + g_{11}^{>}(t',t')G_{11}^{<}(t,t')\right). \end{aligned} \tag{C.51b}$$

Adding Eqs. (C.50a) and (C.51b), and Eqs. (C.50b) and (C.51a), after again taking $t' \to t$ we arrive at

$$\begin{aligned} 0 = &\left(i\partial_t - 2U\left|\varphi_{1,c}\right|^2\right) g_{11}^{<}(t,t) - \frac{U}{2}\left(\varphi_{1,c}\right)^2 G_{11}^{K}(t,t) - J g_{21}^{K}(t,t) \\ &- \mathrm{i}U\left(4G_{11}^{<}(t,t)g_{11}^{<}(t,t) + g_{11}^{>}(t,t)G_{11}^{K}(t,t)\right), \end{aligned} \tag{C.52a}$$

$$\begin{aligned} 0 = &\left(i\partial_t - 2U\left|\varphi_{1,c}\right|^2\right) g_{11}^{>}(t,t) - \frac{U}{2}\left(\varphi_{1,c}\right)^2 G_{11}^{K}(t,t) - J g_{21}^{K}(t,t) \\ &- \mathrm{i}U\left(4G_{11}^{<}(t,t)g_{11}^{>}(t,t) + g_{11}^{<}(t,t)G_{11}^{K}(t,t)\right). \end{aligned} \tag{C.52b}$$

As a last step, adding these two equations produces

$$\begin{aligned} 0 = &\left(i\partial_t - 2U\left|\varphi_{1,c}\right|^2\right) g_{11}^{K}(t,t) - U\left(\varphi_{1,c}\right)^2 G_{11}^{K}(t,t) - 2J g_{21}^{K}(t,t) \\ &- \mathrm{i}U\left(4G_{11}^{<}(t,t)g_{11}^{K}(t,t) + g_{11}^{K}(t,t)G_{11}^{K}(t,t)\right). \end{aligned} \tag{C.53}$$

To fully convert this equation into the Keldysh or "RAK" representation, we have to replace two of the lesser functions in the first term of the second line by greater functions, i.e. $4G_{11}^{<}(t,t) \longleftarrow 2G_{11}^{K}(t,t)$. The technical reason for this is that the Keldysh representation corresponds to Wigner-Weyl or symmetric operator ordering [81] which diagrammatically leads to additional vacuum terms when evaluating loops. As we show below, these additional terms coming from the appearance of the equal-time greater functions can be absorbed into the overall chemical potential and hence do not have physical consequences.

The explicit procedure we have just carried out will not be repeated here for all of the other Green-function equations required to fully specify the dynamical problem. The results will simply be stated in the next paragraph.

C.1.7 Equivalence of Heisenberg Picture and Keldysh Representation

After stating the remaining HFB equations as derived from the 2PI effective action, we will go through the instructive exercise of explicitly comparing them with the corresponding Heisenberg equations. This will both confirm the correctness of our field-theory derivation and shed light on some minor differences between the two approaches that one should keep in mind. With the

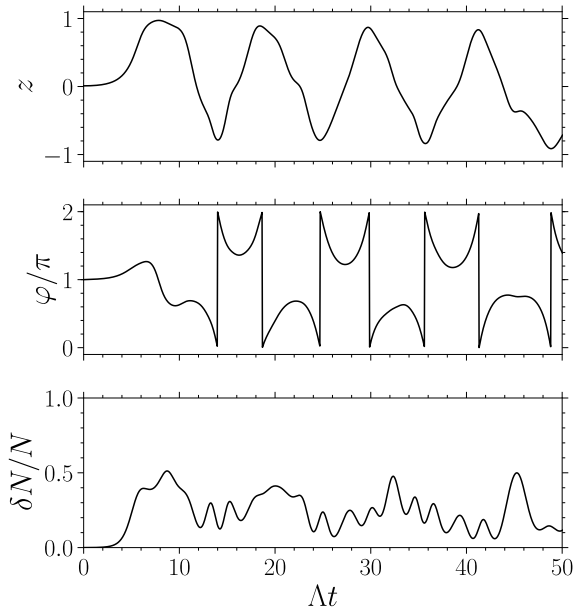

Figure C.9: Population imbalance $z(t)$, relative phase $\varphi(t)$ and total fraction of fluctuations $\delta N(t)/N$ for $\Lambda = 4.00$, $z(0) = 0.01$, $\varphi(0) = \pi$, $N = 5000$, $J = -1$. Interestingly, for even larger values of Λ one enters a new regime where fluctuations start to become smaller again. We have not investigated this phenomenon any further, however.

identifications $G^K_{\alpha\alpha} = -\mathrm{i}F_\alpha = -\mathrm{i}\,(2\delta N_\alpha + 1)$,[3] $G^K_{12} = G_{12}$, and $g^K_{\alpha\beta} = g_{\alpha\beta}$. The total fraction of fluctuations shown in the third panels of Figs. C.5, C.6, C.7, C.8 and C.9 is defined via

$$\delta N(t) = \delta N_1(t) + \delta N_2(t). \tag{C.54}$$

From C.1.6, the equal-time HFB equations in two-mode approximation are then as follows. For the condensate amplitudes, there holds

$$\mathrm{i}\partial_t \varphi_{1,c} = \varepsilon_1 \varphi_{1,c} + J\varphi_{2,c} + UF_1\varphi_{1,c} + \frac{U}{2}\left(\left|\varphi_{1,c}\right|^2 \varphi_{1,c} + \mathrm{i}g_{11}\varphi^*_{1,c}\right), \tag{C.55a}$$

$$\mathrm{i}\partial_t \varphi_{2,c} = \varepsilon_2 \varphi_{2,c} + J\varphi_{1,c} + UF_2\varphi_{2,c} + \frac{U}{2}\left(\left|\varphi_{2,c}\right|^2 \varphi_{2,c} + \mathrm{i}g_{22}\varphi^*_{2,c}\right), \tag{C.55b}$$

[3] This assignment of the symbol F_α is not strictly consistent with the definition of the *statistical* function elsewhere in this thesis.

and for the fluctuation Green functions,

$$\partial_t F_1 = -J\left(G_{12} + G_{12}^*\right) - \frac{U}{2}\left(\left(\varphi_{1,c}^*\right)^2 g_{11} + \left(\varphi_{1,c}\right)^2 g_{11}^*\right), \tag{C.56a}$$

$$\partial_t F_2 = +J\left(G_{12} + G_{12}^*\right) - \frac{U}{2}\left(\left(\varphi_{2,c}^*\right)^2 g_{22} + \left(\varphi_{2,c}\right)^2 g_{22}^*\right), \tag{C.56b}$$

$$\begin{aligned}\partial_t G_{12} = &-\mathrm{i}\left(\varepsilon_1 - \varepsilon_2\right) G_{12} + J\left(F_1 - F_2\right) - \mathrm{i}U\left(F_1 - F_2 + \left|\varphi_{1,c}\right|^2 - \left|\varphi_{2,c}\right|^2\right) G_{12} \\ &+ \frac{U}{2}\left\{\left[\mathrm{i}\left(\varphi_{2,c}^*\right)^2 + g_{22}^*\right] g_{12} + \left[\mathrm{i}\varphi_{1,c}^2 - g_{11}\right] g_{12}^*\right\},\end{aligned} \tag{C.56c}$$

$$\mathrm{i}\partial_t g_{11} = 2\varepsilon_1 g_{11} + 2J g_{12} + U\left\{\left[g_{11} - \mathrm{i}\varphi_{1,c}^2\right] F_1 + 2\left[\left|\varphi_{1,c}\right|^2 + F_1\right] g_{11}\right\}, \tag{C.56d}$$

$$\mathrm{i}\partial_t g_{22} = 2\varepsilon_2 g_{22} + 2J g_{12} + U\left\{\left[g_{22} - \mathrm{i}\varphi_{2,c}^2\right] F_2 + 2\left[\left|\varphi_{2,c}\right|^2 + F_2\right] g_{22}\right\},$$

$$\begin{aligned}\partial_t g_{12} = &-\mathrm{i}\left(\varepsilon_1 + \varepsilon_2\right) g_{12} - \mathrm{i}J\left(g_{11} + g_{22}\right) - \mathrm{i}U\left(F_1 + F_2 + \left|\varphi_{1,c}\right|^2 + \left|\varphi_{2,c}\right|^2\right) g_{12} \\ &+ \frac{U}{2}\left\{\left[\mathrm{i}\varphi_{1,c}^2 - g_{11}\right] G_{12}^* - \left[\mathrm{i}\varphi_{2,c}^2 - g_{22}\right] G_{12}\right\}.\end{aligned} \tag{C.56e}$$

For consistency, we will now check that these equations agree with the results one obtains from the Heisenberg equations of motion. As a first step, compare Eqs. (C.26a) and (C.55a):

$$\mathrm{i}\partial_t \varphi_1 = \left[\varepsilon_1 - \mu\right]\varphi_1 + J\varphi_2 + U\left(\left|\varphi_1\right|^2 \varphi_1 + 2\varphi_1\langle\delta a_1^\dagger \delta a_1\rangle + \varphi_1^*\langle\delta a_1 \delta a_1\rangle\right),$$

$$\mathrm{i}\partial_t \varphi_{1,c} = \varepsilon_1 \varphi_{1,c} + J\varphi_{2,c} + \frac{U}{2}\left(\left|\varphi_{1,c}\right|^2 \varphi_{1,c} + 2\varphi_{1,c} F_1 + \mathrm{i}\varphi_{1,c}^* g_{11}\right),$$

where we have dropped the contribution of the third cumulant $\langle\delta a_1^\dagger \delta a_1 \delta a_1\rangle$ from Eq. (C.26a), as this corresponds to the HFB approximation. Setting $\varphi_{\alpha,c} = \sqrt{2}\mathrm{e}^{-\mathrm{i}\tilde{\mu}t}\varphi_\alpha$, and $\varphi_\alpha = \sqrt{N_\alpha}\mathrm{e}^{\mathrm{i}\varphi_\alpha}$ (note that to avoid introducing even more notation, we use the same symbols N_α and φ_α in the polar decomposition of the corrected saddle-point φ_α as we did above for the classical saddle-point Φ_α), we find from Eq. (C.55a) that

$$\mathrm{i}\partial_t \varphi_1 = \left[\varepsilon_1 - \tilde{\mu}\right]\varphi_1 + J\varphi_2 + U\left(\left|\varphi_1\right|^2 \varphi_1 + \varphi_1 F_1 + \frac{\mathrm{i}}{2}\varphi_1^* \mathrm{e}^{2\mathrm{i}\tilde{\mu}t} g_{11}\right).$$

For the anomalous Green function we identify $g_{11} = -2\mathrm{i}\mathrm{e}^{-2\mathrm{i}\tilde{\mu}t}\langle\delta a_1 \delta a_1\rangle$.[4] Similarly, we have $F_1 = 2\langle\delta a_1^\dagger \delta a_1\rangle + 1$. This establishes the equivalence of Eqs. (C.26a) and (C.55a) except for the zero-point contribution in the definition of the "statistical" function F_1. This is the reason we have chosen a different chemical potential $\tilde{\mu}$ for the Keldysh approach. By setting $\tilde{\mu} = \mu + U$, Eqs. (C.26a) and (C.55a) become identical. To understand this better, we can consider the equations for

[4] The factor of two in this identity again stems from the fact that the Keldysh representation corresponds symmetric operator ordering; the "Keldysh" Green function G^K, however, is defined *without* a factor of $1/2$.

the condensate phases in the two approaches:

$$\begin{aligned}-\dot{\varphi}_1 &= \varepsilon_1 - \mu + J\sqrt{N_2/N_1}\cos\varphi + N_1 U \\ &\quad + \frac{1}{2}N_1 U\left[\mathrm{e}^{-2\mathrm{i}\varphi_1}\langle\delta a_1\delta a_1\rangle + \mathrm{e}^{2\mathrm{i}\varphi_1}\langle\delta a_1^\dagger\delta a_1^\dagger\rangle\right] + 2U\langle\delta a_1^\dagger\delta a_1\rangle,\end{aligned} \tag{C.57a}$$

$$\begin{aligned}-\dot{\varphi}_{1,\,c} &= \varepsilon_1 - \tilde{\mu} + J\sqrt{N_2/N_1}\cos\varphi_c + N_1 U \\ &\quad + \frac{\mathrm{i}}{4}N_1 U\left[\mathrm{e}^{-2\mathrm{i}\varphi_{1,\,c}}g_{11} + \mathrm{e}^{2\mathrm{i}\varphi_{1,\,c}}g_{11}^*\right] + UF_1,\end{aligned} \tag{C.57b}$$

where $\varphi_c = \varphi_{2,\,c} - \varphi_{1,\,c}$. As before, there appears the vacuum contribution from F_1 which can be absorbed into the chemical potential $\tilde{\mu}$. Of course, the difference in chemical potential, which acts as a total phase factor, cannot have a physical effect. This can also be understood from the dynamical equations for the condensate. The physical degrees of freedom are N_1, N_2 and $\varphi = \varphi_2 - \varphi_1$ (both occupation numbers are needed since the condensate now couples to the non-condensate particles, such that the condensate number is no longer conserved on its own). In both equations for N_α, the contribution from the F_α term vanishes, whereas in the equation for φ, only the difference $(F_1 - F_2)$ appears, such that the zero-point contribution cancels exactly. It remains to be shown that none of the HFB equations (C.56) depends on the total phase $\Theta = \varphi_1 + \varphi_2$. From the Heisenberg equation (C.28), one may calculate the equations of motion for the second cumulants by using, for example, $\mathrm{i}\partial_t\delta a_1^\dagger\delta a_1 = (\mathrm{i}\partial_t\delta a_1^\dagger)\delta a_1 + \delta a_1^\dagger\mathrm{i}\partial_t\delta a_1$. In this way, one finds

$$\mathrm{i}\partial_t\langle\delta a_1^\dagger\delta a_1\rangle = J\left(\langle\delta a_1^\dagger\delta a_2\rangle - \langle\delta a_2^\dagger\delta a_1\rangle\right) + U\left\{\varphi_1^2\langle\delta a_1^\dagger\delta a_1^\dagger\rangle - \left(\varphi_1^*\right)^2\langle\delta a_1\delta a_1\rangle\right\}, \tag{C.58a}$$

$$\begin{aligned}\mathrm{i}\partial_t\langle\delta a_1\delta a_2^\dagger\rangle &= \left[\varepsilon_1 - \varepsilon_2\right]\langle\delta a_1\delta a_2^\dagger\rangle - J\left(\langle\delta a_1^\dagger\delta a_1\rangle - \langle\delta a_2^\dagger\delta a_2\rangle\right) \\ &\quad + U\left\{2\left[|\varphi_1|^2 - |\varphi_2|^2\right]\langle\delta a_1\delta a_2^\dagger\rangle - \left(\varphi_2^*\right)^2\langle\delta a_1\delta a_2\rangle + \varphi_1^2\langle\delta a_1^\dagger\delta a_2^\dagger\rangle\right. \\ &\quad \left. - \langle\delta a_1\delta a_2^\dagger\delta a_2^\dagger\delta a_2\rangle + \langle\delta a_1^\dagger\delta a_1\delta a_1\delta a_2^\dagger\rangle\right\},\end{aligned} \tag{C.58b}$$

$$\begin{aligned}\mathrm{i}\partial_t\langle\delta a_1\delta a_1\rangle &= 2\left[\varepsilon_1 - \mu\right]\langle\delta a_1\delta a_1\rangle + 2J\langle\delta a_1\delta a_2\rangle \\ &\quad + U\left\{4\left|\varphi_1\right|^2\langle\delta a_1\delta a_1\rangle + \varphi_1^2\left[2\langle\delta a_1^\dagger\delta a_1\rangle + 1\right]\right. \\ &\quad \left. + \langle\delta a_1\delta a_1^\dagger\delta a_1\delta a_1\rangle + \langle\delta a_1^\dagger\delta a_1\delta a_1\delta a_1\rangle\right\},\end{aligned} \tag{C.58c}$$

$$\begin{aligned}\mathrm{i}\partial_t\langle\delta a_2\delta a_2\rangle &= 2\left[\varepsilon_2 - \mu\right]\langle\delta a_2\delta a_2\rangle + 2J\langle\delta a_2\delta a_1\rangle \\ &\quad + U\left\{4\left|\varphi_2\right|^2\langle\delta a_2\delta a_2\rangle + \varphi_2^2\left[2\langle\delta a_2^\dagger\delta a_2\rangle + 1\right]\right. \\ &\quad \left. + \langle\delta a_2\delta a_2^\dagger\delta a_2\delta a_2\rangle + \langle\delta a_2^\dagger\delta a_2\delta a_2\delta a_2\rangle\right\},\end{aligned} \tag{C.58d}$$

$$\begin{aligned}\mathrm{i}\partial_t\langle\delta a_1\delta a_2\rangle &= \left[\varepsilon_1 + \varepsilon_2 - 2\mu\right]\langle\delta a_1\delta a_2\rangle + J\left(\langle\delta a_1\delta a_1\rangle + \langle\delta a_2\delta a_2\rangle\right) \\ &\quad + U\left\{2\left[|\varphi_1|^2 + |\varphi_2|^2\right]\langle\delta a_1\delta a_2\rangle + \varphi_1^2\langle\delta a_1^\dagger\delta a_2\rangle + \varphi_2^2\langle\delta a_1\delta a_2^\dagger\rangle\right. \\ &\quad \left. + \langle\delta a_1\delta a_2^\dagger\delta a_2\delta a_2\rangle + \langle\delta a_1^\dagger\delta a_1\delta a_1\delta a_2\rangle\right\},\end{aligned} \tag{C.58e}$$

where, again, we have dropped the contributions from the third cumulants. It is easy to see that the first two of Eqs. (C.56) agree with the first two of Eqs. (C.58) upon identifying $G_{12} = -2\mathrm{i}\langle\delta a_1 \delta a_2^\dagger\rangle$.

Next we have to compare the equations for $\langle\delta a_1 \delta a_2^\dagger\rangle$ and G_{12}. Then the quartic expectation values in Eqs. (C.58) have to be decomposed. This is essentially achieved by using the Gaussian expectation-value identity

$$\mathrm{E}\left[X_i^2 X_m X_n\right] = \sigma_{ii}\sigma_{mn} + 2\sigma_{in}\sigma_{im}. \tag{C.59}$$

The analogous expressions for the normal-ordered Heisenberg operators are in this case

$$\langle\delta a_1 \delta a_2^\dagger \delta a_2^\dagger \delta a_2\rangle = \langle\delta a_1 \delta a_2\rangle\langle\delta a_2^\dagger \delta a_2^\dagger\rangle + 2\langle\delta a_1 \delta a_2^\dagger\rangle\langle\delta a_2^\dagger \delta a_2\rangle, \tag{C.60}$$

$$\langle\delta a_1^\dagger \delta a_1 \delta a_1 \delta a_2^\dagger\rangle = \langle\delta a_1 \delta a_1\rangle\langle\delta a_1^\dagger \delta a_2^\dagger\rangle + 2\langle\delta a_1^\dagger \delta a_1\rangle\langle\delta a_1 \delta a_2^\dagger\rangle. \tag{C.61}$$

Together with $g_{12} = -2\mathrm{i}\mathrm{e}^{-2\mathrm{i}\tilde{\mu}t}\langle\delta a_1 \delta a_2\rangle$, one can then verify that the third of Eqs. (C.56) agrees with the third of Eqs. (C.58). Next, we move to the comparison of the equations for g_{11} and $\langle\delta a_1 \delta a_1\rangle$ in Eq. (C.56d) and (C.58c), respectively. To repeat, they read

$$\begin{aligned}
\mathrm{i}\partial_t g_{11} &= 2\varepsilon_1 g_{11} + 2J g_{12} + U\left\{-\mathrm{i}\varphi_{1,c}^2 F_1 + 2\left|\varphi_{1,c}\right|^2 g_{11} + 3F_1 g_{11}\right\}, \\
\mathrm{i}\partial_t\langle\delta a_1 \delta a_1\rangle &= 2\left[\varepsilon_1 - \mu\right]\langle\delta a_1 \delta a_1\rangle + 2J\langle\delta a_1 \delta a_2\rangle \\
&\quad + U\left\{4\left|\varphi_1\right|^2\langle\delta a_1 \delta a_1\rangle + \varphi_1^2\left[2\langle\delta a_1^\dagger \delta a_1\rangle + 1\right] + \langle\delta a_1 \delta a_1\rangle + 2\langle\delta a_1^\dagger \delta a_1 \delta a_1 \delta a_1\rangle\right\}.
\end{aligned}$$

With the Gaussian decomposition

$$2\langle\delta a_1^\dagger \delta a_1 \delta a_1 \delta a_1\rangle = 6\langle\delta a_1^\dagger \delta a_1\rangle\langle\delta a_1 \delta a_1\rangle, \tag{C.62}$$

one comes out with an expression for the right-hand side of Eq. (C.58c) that seemingly lacks a term $2U\langle\delta a_1 \delta a_1\rangle$ relative to the Green-function result in Eq. (C.56d), from where one obtains

$$3F_1 g_{11} = 2g_{11} + g_{11} + 6\langle\delta a_1^\dagger \delta a_1\rangle g_{11}. \tag{C.63}$$

This will be corrected for by the tilded chemical potential coming from

$$\mathrm{i}\partial_t g_{11} = \mathrm{i}\partial_t\left(-2\mathrm{i}\mathrm{e}^{-2\mathrm{i}\tilde{\mu}t}\langle\delta a_1 \delta a_1\rangle\right) = -2\mathrm{i}\mathrm{e}^{-2\mathrm{i}\tilde{\mu}t}\left(\mathrm{i}\partial_t\langle\delta a_1 \delta a_1\rangle + 2\tilde{\mu}\langle\delta a_1 \delta a_1\rangle\right). \tag{C.64}$$

By symmetry, what we have just shown also follows for $\langle\delta a_2 \delta a_2\rangle$ and g_{22}. The field-theoretic equation for g_{12} may be verified in a similar manner. As a further comment, consider that the dependence on the bare phases φ_α, $\varphi_{\alpha,c}$ has to be an artifact and could be removed by replacing $\langle\delta a_\alpha \delta a_\alpha\rangle \leftarrow \mathrm{e}^{2\mathrm{i}\varphi_\alpha}\langle\delta a_\alpha \delta a_\alpha\rangle$, $g_{\alpha\alpha} \leftarrow \mathrm{e}^{2\mathrm{i}\varphi_{\alpha,c}} g_{\alpha\alpha}$ and so forth. Note also that by removing these phase factors, one sees that the HFB equations do not depend on the total condensate phase Θ.

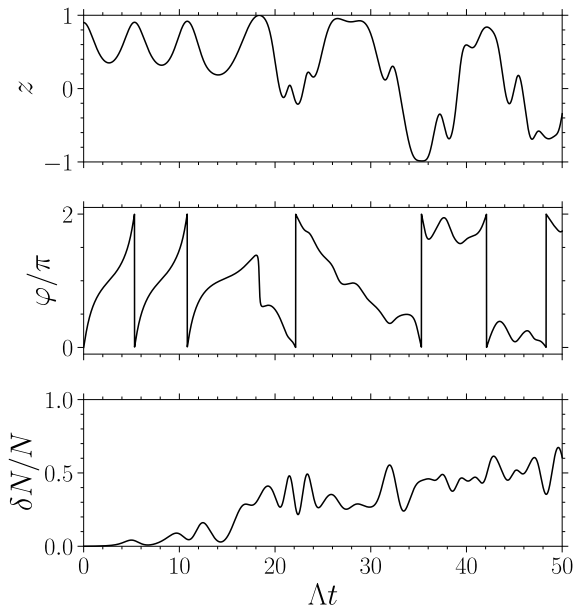

Figure C.10: Decay of self-trapping for $\Lambda = 4.00$, $z(0) = 0.9$, $\varphi(0) = 0$, $N = 5000$, $J = -1$. Explanations are given in the text.

C.1.8 Decay of Macroscopic Quantum Self-Trapping

The decay of MQST was predicted in Ref. [123]. For further discussion, see also [125]. In Ref. [117] related to experiment B, this phenomenon was observed, yet not connected to the aforementioned references. As we have seen, the instability of MQST can be understood analytically from the unavoidable presence of hyperbolic fixed points in the phase space: the system will have a purely real, positive eigenvalue whenever it is self-trapped. This is because the separatrix enabling the appearance of MQST only occurs for $\Lambda > 2$ (s. Fig. C.3). The related effect of π-oscillations [134] can already happen for $\Lambda > 1$ when the initial relative phase $\varphi(0)$ is around the two hyperbolic fixed points $(0, \pm\pi)$, as can be seen from Fig. C.2. A simulation of the decaying MQST via the HFB equations is shown in Fig. C.10. Because $z(0) = 0.9$ is above the critical imbalance for $\Lambda = 4.0$ (cf. Fig. C.4), the system is initially in the self-trapped state. As the fluctuations grow, at early times the self-trapped amplitude decays slowly in a manner very similar to the observed data from Ref. [117]. With the presence of a large amount of fluctuations for $\Lambda t > 20$, the state begins to disintegrate. We have to keep in mind, however, that this is also the point around which the HFB approximation should not be trusted any longer.

C.2 Three-Mode Approximation

In neither of the experiments under consideration [115, 116] in 3.2, the Josephson frequency goes to zero. Hence, critical slowing down of the Josephson oscillations cannot be the explanation of the observed damping. To capture the physics beyond a single frequency going soft, it is necessary

to include more than two modes into the description. In this section, we will study the effect of adding a third mode to the problem. The fully realistic description of the experiments in question requires more than three modes.

The following Gross-Pitaevskii equations were written down in consideration of the interaction parameters that are typical for the type of traps employed in experiments A and B (cf. Ref. [35]). Beyond the local interaction U encountered previously, this includes an effective Josephson coupling J' between the two modes localized in either well, an interaction K describing the coupling between either of the localized modes and the third mode, and finally an interaction R that couples these modes asymmetrically. As a result, the equations for the classical mean-fields become

$$\begin{aligned}
[\mathrm{i}\partial_t - \mu]\,\Phi_{1,c} &= J\Phi_{2,c} + \frac{1}{2}U\left|\Phi_{1,c}\right|^2\Phi_{1,c} + K\left[\Phi_{1,c}\left|\Phi_{3,c}\right|^2 + \frac{1}{2}\Phi_{1,c}^*\Phi_{3,c}^2\right] \\
&\quad + R\left[\left|\Phi_{1,c}\right|^2\Phi_{3,c} + \frac{1}{2}\Phi_{1,c}^2\Phi_{3,c}^*\right] \\
&\quad + J'\left[\left(\left|\Phi_{1,c}\right|^2 + \frac{1}{2}\left|\Phi_{2,c}\right|^2\right)\Phi_{2,c} + \frac{1}{2}\Phi_{1,c}^2\Phi_{2,c}^*\right], \\
[\mathrm{i}\partial_t - \mu]\,\Phi_{2,c} &= J\Phi_{1,c} + \frac{1}{2}U\left|\Phi_{2,c}\right|^2\Phi_{2,c} + K\left[\Phi_{2,c}\left|\Phi_{3,c}\right|^2 + \frac{1}{2}\Phi_{2,c}^*\Phi_{3,c}^2\right] \\
&\quad - R\left[\left|\Phi_{2,c}\right|^2\Phi_{3,c} + \frac{1}{2}\Phi_{2,c}^2\Phi_{3,c}^*\right] \\
&\quad + J'\left[\left(\left|\Phi_{2,c}\right|^2 + \frac{1}{2}\left|\Phi_{1,c}\right|^2\right)\Phi_{1,c} + \frac{1}{2}\Phi_{2,c}^2\Phi_{1,c}^*\right], \\
[\mathrm{i}\partial_t - \mu]\,\Phi_{3,c} &= \varepsilon_3\Phi_{3,c} + \frac{1}{2}U_3\left|\Phi_{3,c}\right|^2\Phi_{3,c} \\
&\quad + K\left[\left(\left|\Phi_{2,c}\right|^2 + \left|\Phi_{1,c}\right|^2\right)\Phi_{3,c} + \frac{1}{2}\left(\Phi_{1,c}^2 + \Phi_{2,c}^2\right)\Phi_{3,c}^*\right] \\
&\quad + \frac{R}{2}\left[\left|\Phi_{1,c}\right|^2\Phi_{1,c} - \left|\Phi_{2,c}\right|^2\Phi_{2,c}\right].
\end{aligned} \tag{C.65}$$

For these equations, we are going to perform a systematic stability analysis around the experimentally relevant fixed point in terms of the single-particle energy ε_3 of the third mode, which we take as a control parameter. In this way, we will see how the bare energy of the third mode can be used to tune an experiment in and out of the regime of stable oscillations between the modes localized in the two wells. Interestingly, this will reveal an *exceptional point* in the spectrum [147].

C.2.1 Stability Analysis

It is not instructive to attempt a full stability analysis of the dynamical system described by Eqs. (C.65). For two modes, the effective dimension of the phase space turns out to be two because of number conservation and gauge invariance. With three modes, we have six degrees of freedom and two conservation laws, resulting in a four-dimensional effective phase space. Experimentally,

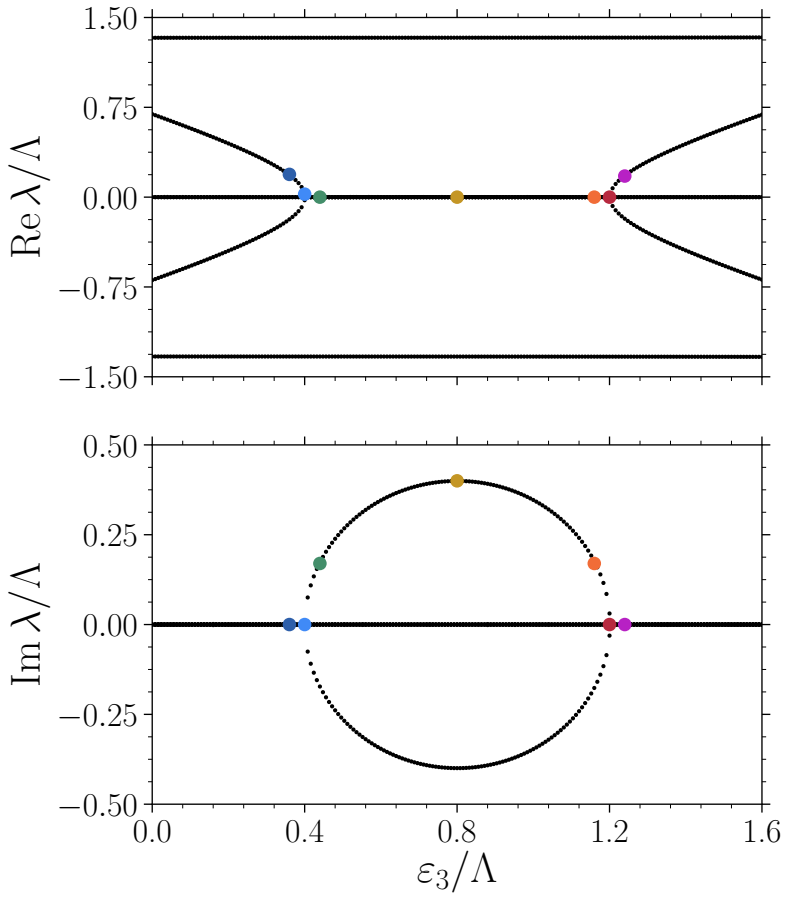

Figure C.11: Eigenvalue spectrum from the stability analysis of the Gross-Pitaevskii equations (C.65) around the fixed point (C.66) as the control parameter ε_3 is increased. The characteristic parameter is $\Lambda = 1250$. The upper panel shows the real parts corresponding to the frequencies present in the system. The lower panel shows the imaginary parts. The negative branch amounts to a damping of the oscillations, while the positive branch indicates an instability. As the real parts go to (depart from) zero, the respective imaginary parts depart from (go to) zero. These points are marked by the second (light blue) dot and next to last (red) dot. This behavior is typical for exceptional points where a conjugate pair of complex eigenvalues turns into two different purely real eigenvalues.

J	U	J'	U_3	K	R
-1.00	1.00	-0.05	0.50	0.10	0.01

Table C.2: Interaction parameters for the three-mode Gross-Piatevskii equations (C.65).

however, only a very restricted subset of this space is relevant. Both experiments can be considered as perturbations from a fixed point where $N_1^* = N_2^* = N/2$, $N_3^* = 0$, where N is accordingly the total number of particles.[5] Furthermore, the initial phase differences between any of the modes can be assumed to be zero. This suggests setting $\varphi_{1,c}^* = \varphi_{2,c}^* = \varphi_{3,c}^* = 0$ without loss of experimental applicability. As one appreciates immediately, these conditions provide a solution to the fixed-point condition arising from the last of Eqs. (C.65). With a chemical potential $\mu = -\left[J + N\left(U + 4J'\right)/2\right]$, the same holds for the first two equations. By studying the eigenvalues of the Jacobian of Eqs. (C.65) around the fixed point

$$\mathbf{v}^* = \left(N_1^*, N_2^*, N_3^*, \varphi_{1,c}^*, \varphi_{2,c}^*, \varphi_{3,c}^*\right)^T \tag{C.66}$$

as a function of ε_3, we will gain insights into the effect of the third mode on the dynamics of the Bose-Josephson junction. The three-mode analogue of the two-mode Jacobian (C.18) will also have two trivial eigenvalues ± 0. Since its explicit form is lengthy and little instructive, we directly go over to discussing the remaining four eigenvalues as functions of the control parameter ε_3, which are shown in Fig. C.11. The parameters used throughout the analysis are summarized in Tab. C.2.[6] The most striking feature is the appearance of two exceptional points as one of the two frequencies present in the system first becomes soft (or "massless") and subsequently regains a finite "mass". As this happens, the system develops both a damping and an instability. Beyond that, there is always a stable frequency (the two straight lines in the upper panel) that corresponds to the effective Josephson frequency $\tilde{\omega}_J$.[7] Thus we find that both a finite Josephson frequency and the excitation of quasiparticles through a soft mode are possible in a three-mode system. The (colored) dots in Fig. C.11 correspond from left to right to the values of ε_3 given in Tab. C.3.

To illustrate the behavior of the system as ε_3 is increased across both exceptional points, first consider the time evolution of the population imbalance shown in Fig. C.12, where ε_3 now increases from top to bottom and the system is slightly displaced from the fixed point (C.66). The fast frequency $\tilde{\omega}_J$ is present in all panels, although it is hardly discernible in the fifth (orange). The first two panels show nicely how the slower frequency gradually softens. The instability of the system becomes clear from the panels in the middle. One should keep in mind that the eigenvectors of the Jacobian are superpositions of the standard basis belonging to the original variables. They are also non-orthogonal because the Jacobian is non-Hermitian. This means that weakly displacing the third amplitude, for instance, can still result in both eigenfrequencies being excited because the vector corresponding to a displacement of Φ_3 and Φ_3^*

[5] $N = 5000$ throughout this section.

[6] In relation to the overlap integrals introduced in subsection 3.2.2, these parameters are $U = U_{1111} = U_{2222}$, $U_3 = U_{3333}$, $J' = U_{1112} = U_{1222}$, $K = 2U_{1133} = 2U_{2233}$, $R = U_{1113} = -U_{2223}$.

[7] The bare Josephson frequency is always $2|J|$.

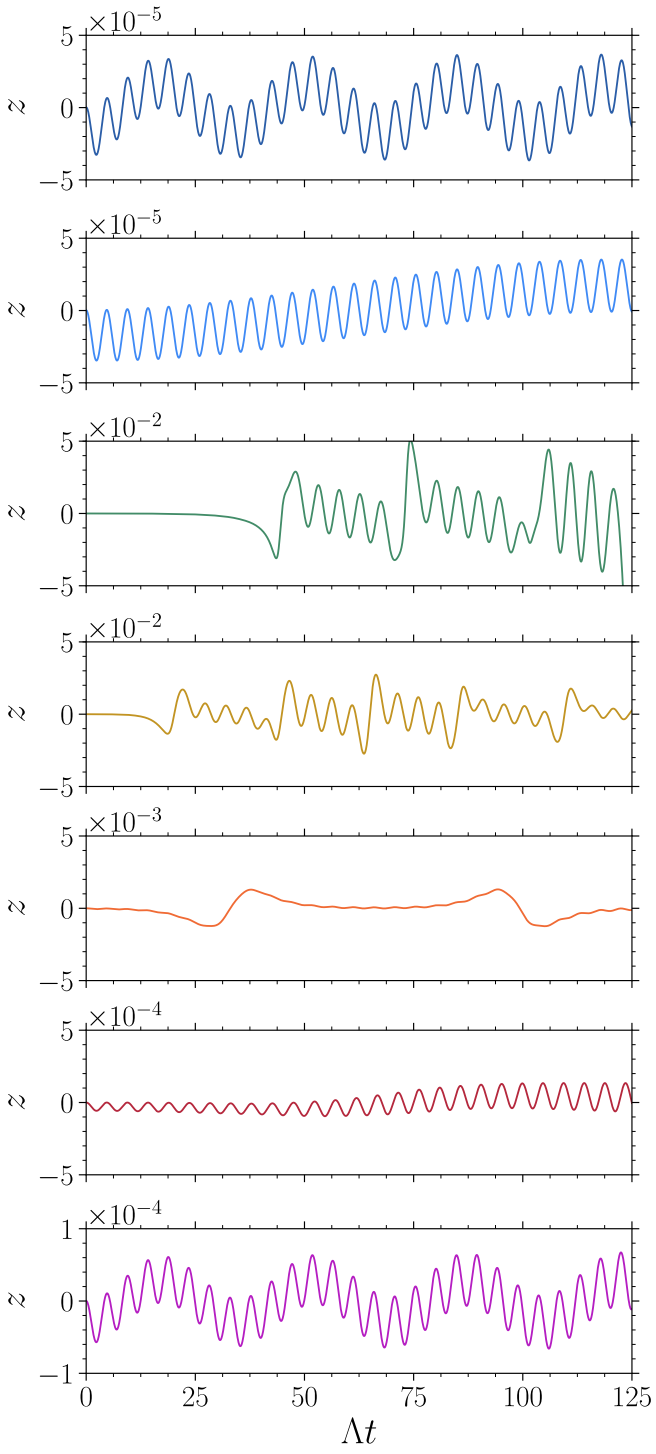

Figure C.12: Mean-field $z(t)$ from Eqs. (C.65) for different values of ε_3 (s. Tab. C.3). The initial conditions are $N_1(0) = 2500$, $N_2(0) = 2500 - 10^{-3}$, $N_3(0) = 10^{-3}$, $\Phi_{k,\,c}(0) = \sqrt{2N_k}$.

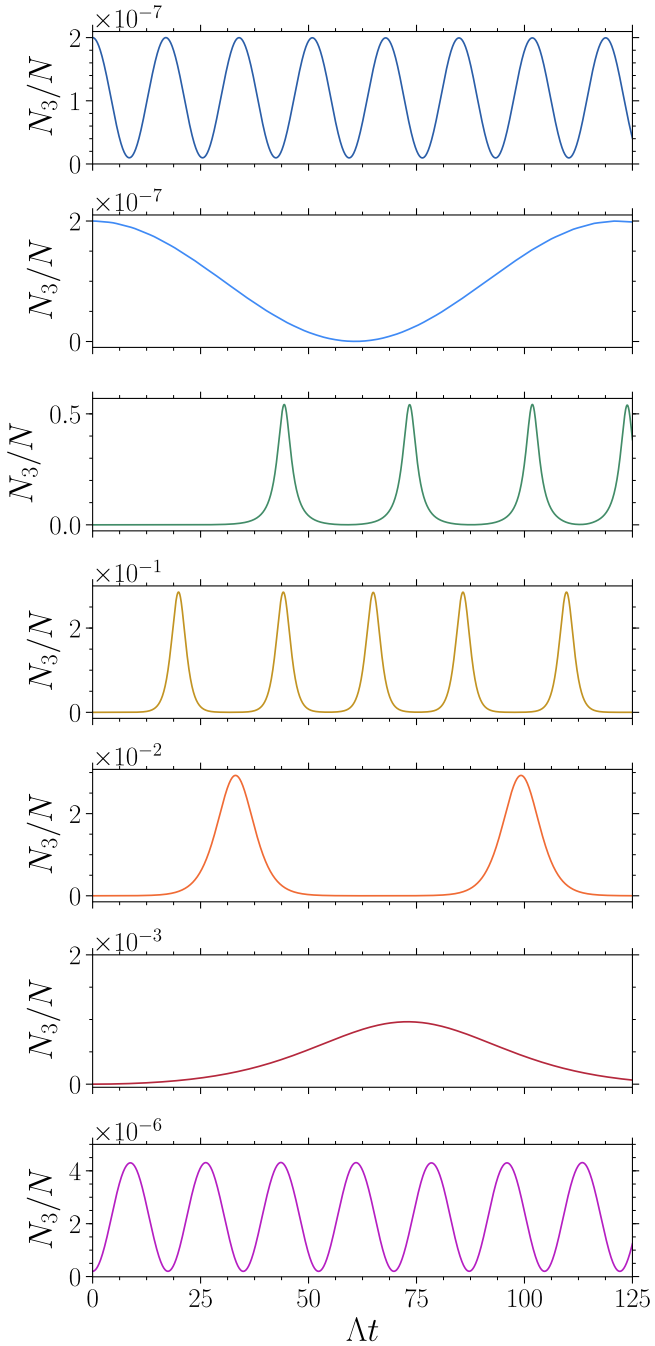

Figure C.13: Mean-field $N_3(t)$ from Eqs. (C.65) for different values of ε_3 (s. Tab. C.3), with initial conditions identical to Fig. C.12.

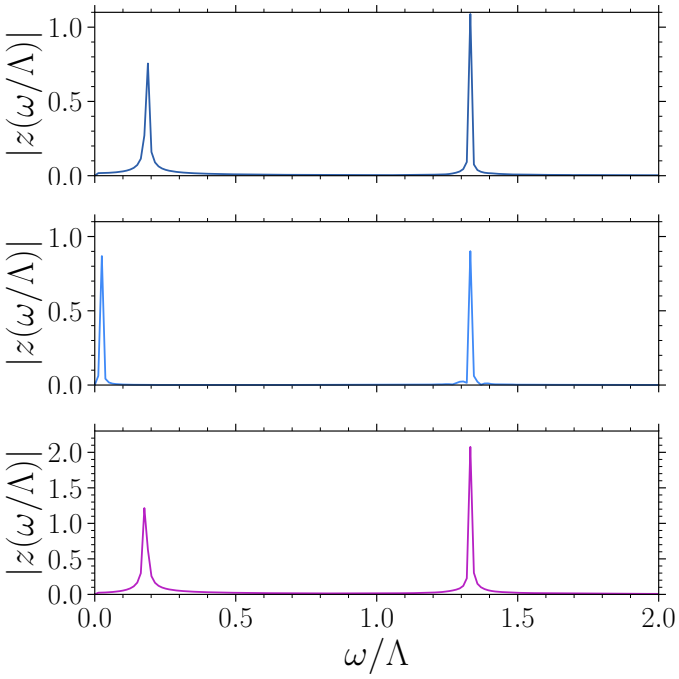

Figure C.14: Normalized fast Fourier transforms (FFT) within the oscillating regimes. The final time for the FFT was taken at $\Lambda t = 500$. The right peaks correspond to the effective Josephson frequency $\tilde{\omega}_J/\Lambda = 1.3336$.

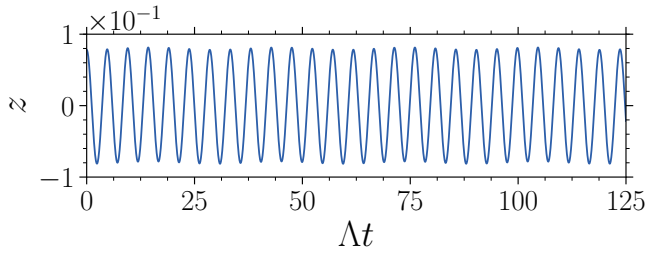

Figure C.15: The second frequency is not visible for larger initial population imbalance, $N_1(0) = 2500+190$, $N_2(0) = 2500 - 200$, $N_3(0) = 10$ (all other parameters as in Fig. C.12).

may have an overlap with both. Since the eigenvectors change as ε_3 is increased, the unaltered initial conditions always correspond to different superpositions of eigenvectors. This becomes especially apparent in Fig. C.13, where the largest occupation N_3 of the third mode does not correspond does the "most unstable" panel in the middle (yellow). It is also important to notice that $N_3(t)$ is negligible when the system is stable. Another thing that comes to mind upon closer comparison of Figs. C.12 and C.13 is that $N_3(t)$ oscillates at *twice* the value of the softening frequency, which is not the case for the population imbalance (this is most easily apprehended from

Color	Dark blue	Light blue	Green	Yellow	Orange	Red	Purple
$\varepsilon_3/\left\|J\right\|$	450	500	550	1000	1450	1500	1550

Table C.3: Single-particle eigenenergies of the third mode and associated color code corresponding to the plots shown from *top* to *bottom* in Figs. C.12, C.13 and C.16.

the second (light blue) panel). The stability analysis is, of course, valid only for the condensate *amplitudes*. The question is then: why do $\left|\Phi_{1,2}\right|^2$ oscillate at the same frequency as $\Phi_{1,2}$, while $\left|\Phi_3\right|^2$ oscillates at double the frequency as Φ_3? The answer is rather simple: the third mode oscillates around zero, which is the reason why squaring it doubles the frequency according to $(\mathrm{e}^{\mathrm{i}\omega t})^2 = \mathrm{e}^{2\mathrm{i}\omega t}$. The other two modes, however, have a large offset, such that squaring there amounts to $(\sqrt{n} + \mathrm{e}^{\mathrm{i}\omega t})^2 = N + 2\sqrt{N}\mathrm{e}^{\mathrm{i}\omega t} + \mathrm{e}^{2\mathrm{i}\omega t} \approx N + 2\sqrt{N}\mathrm{e}^{\mathrm{i}\omega t}$. This means that really only the frequencies from the stability analysis are present in the dynamics of the amplitudes, as it should be. The softening and "hardening" of the second frequency can also be seen from the Fourier transforms of the imbalance trajectories shown in Fig. C.14. While the Josephson frequency stays put, the slow frequency first moves to the left and then back to the right. Interestingly, from Fig. C.15 we learn that the second frequency is not discernible when the initial population imbalance is chosen much larger. Of course, for values on this order of magnitude, the perturbation from the steady-state can no longer be considered "small" and the stability analysis, therefore, does not apply well.

In the hyperbolic regime, the mean-field behavior changes drastically as soon as fluctuations are included. As for the two-mode approximation, we do not investigate quadratic fluctuations but immediately move to the HFB extension of the Gross-Pitaevskii equations (C.65). Their derivation is analogous to the one given in subsection C.1.6. Since they are lengthy and do not contain any structural information beyond that defined by Eqs. (C.65), we will not show them here. Instead we directly move to an inspection of the total number of fluctuations, which is given by

$$\delta N(t) = \frac{\mathrm{i}}{2}\left(G^K_{11} + G^K_{22} + G^K_{33}\right) - \frac{3}{2}. \tag{C.67}$$

The results from the HFB simulations with the same parameters as before are shown in Fig. C.16. As one can see, their magnitude is aligned with that of $N_3(t)$ for the mean-field case.

For completeness, in Fig. C.17 we also show an example of the dynamics following a large initial population imbalance when HFB corrections are included. Evidently, the fast oscillations at the effective Josephson frequency are retained for a few cycles before the instability fully sets in.

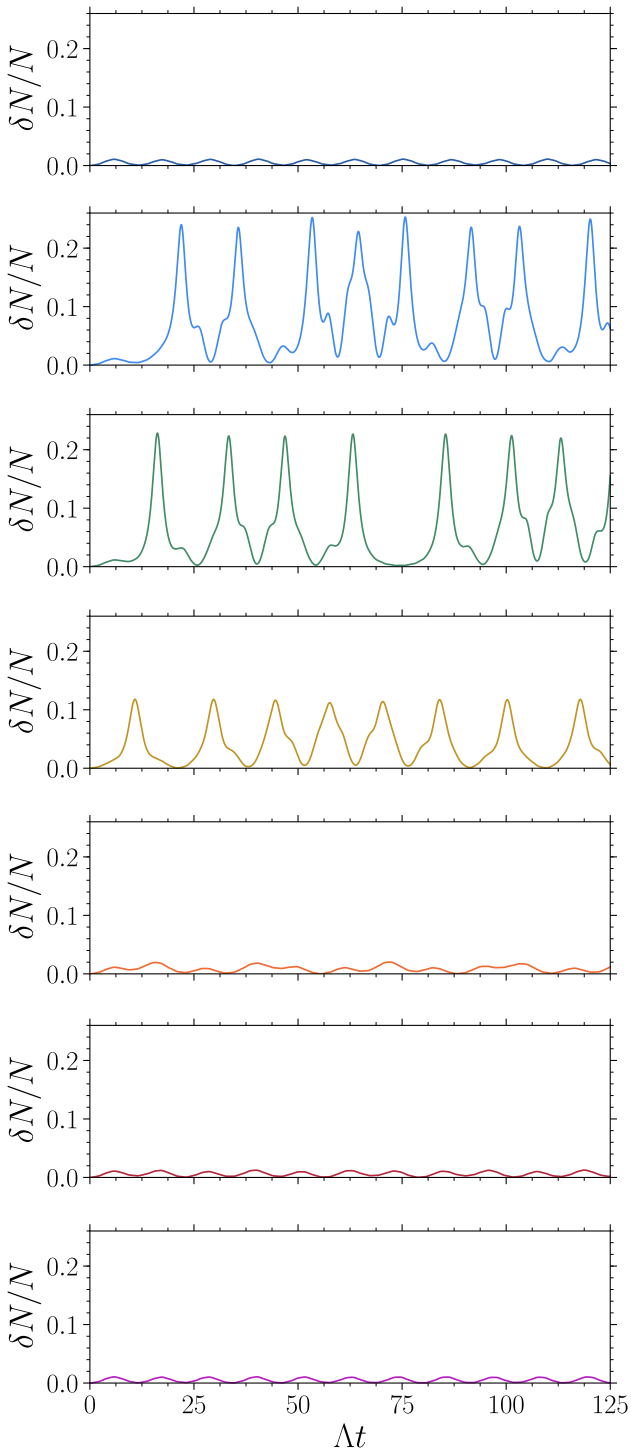

Figure C.16: Fluctuations $\delta N(t)/N$ defined via Eq. (C.67), as obtained from the HFB extension of Eqs. (C.65) with $N_1(0) = N_2(0) = 2500$, $N_3(0) = 0$, $\Phi_{k,c}(0) = \sqrt{2N_k}$ and parameters as in Fig. C.12.

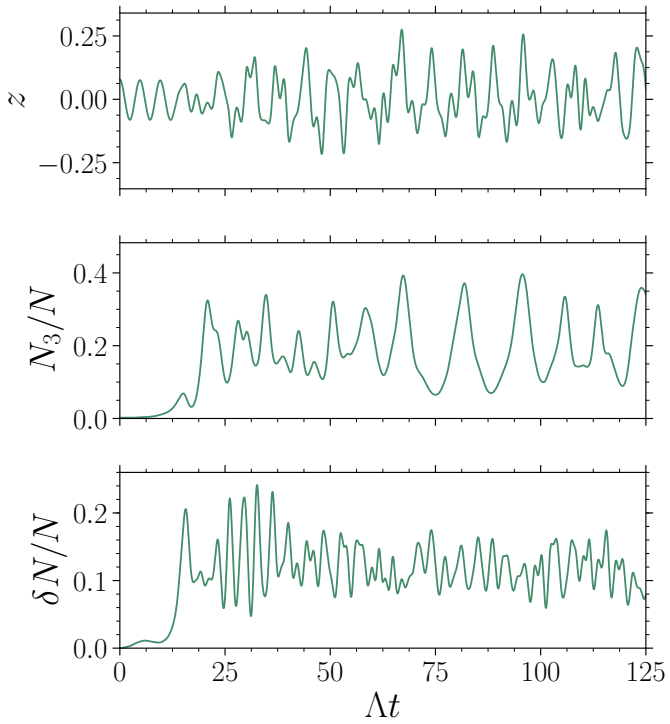

Figure C.17: Unstable regime for a larger initial population imbalance given by $N_1(0) = 2500 + 190$, $N_2(0) = 2500 - 200$, $N_3(0) = 10$ (all other parameters as in Fig. C.16).

List of Figures

List of Tables